SEICHES IN COASTAL BAYS

by

LICHEN WANG

A THESIS SUBMITTED IN PARTIAL FULFILMENT OF

THE REQUIREMENTS FOR THE DEGREE OF

MASTER OF SCIENCE

in

THE FACULTY OF GRADUATE STUDIES

Department of Oceanography

We accept this thesis as conforming

to the required standard

THE UNIVERSITY OF BRITISH COLUMBIA

December 1984

In presenting this thesis in partial fulfilment of the requirements for an advanced degree at the The University of British Columbia, I agree that the Library shall make it freely available for reference and study. I further agree that permission for extensive copying of this thesis for scholarly purposes may be granted by the Head of my Department or by his or her representatives. It is understood that copying or publication of this thesis for financial gain shall not be allowed without my written permission.

Department of Oceanography

The University of British Columbia
2075 Wesbrook Place
Vancouver, Canada
V6T 1W5

Date: December 1984

ABSTRACT

Resonant water waves in closed or semi-closed fluid systems are referred to as "seiches". Literature on this topic in recent years can be found in this thesis.

This research is based on wave data in three coastal bays at the southern coast of Vancouver Island opening to Juan de Fuca Strait. Preliminary aim is to look for the nature and cause of the observed wave motions of these bays. Time series analysis and numerical modeling are performed to reveal seiche nature and develop a method to predict frequency response of bays with arbitrary shapes and variable depths. The method is evaluated through its application in the three coastal bays. Results of spectral analysis and numerical model agree well.

The possible energy sources of observed seiches are discussed. Edge waves were the major source of observed seiches. The strongest seiches observed were attributed to Proudman coupling between pressure waves and water waves. Oceanic internal tides may contribute energy to a fortnightly pattern of seiche activity.

ACKNOWLEDGEMENT

Among all the people who helped this thesis project, I wish, in particular, to acknowledge my supervisor, Dr. P.H. LeBlond, for his enthusiastic encouragement and knowledgeable guidance throughout the development of this thesis. He offered me most important data to look into exciting sources of the observed seiches, and was very patient to correct my preliminary drafts. My deep gratitute also goes to Dr. R.E. Thomson who generously provided all the data he had concerning this research.

I would like to take this opportunity to express my heartfelt thanks to my teachers Drs. R.W. Burling, L.A. Mysak, S. Pond and W.J. Emery for their considerate helpfulness and seemingly infinite patience, which introduced me into the promising field of oceanography. Drs. Burling, Pond and Thomson read my preliminary drafts and gave me helpful directions. I highly appreciate the Oceanography community at UBC whose members' scientific zeal enourages me to devote myself to Ocean sciences.

I have been feeling indebted to my friend Mr. D.K. Lee and medical doctor of UBC hospital Ms. R. Ree for their selfless assistance during my two years study.

Finally, I would never forget the unending moral support from my father Prof. Bin-hua Wang and my *fiancée* Miss Yu-de Pan.

Table of Contents

List of Figures

List of Tables

I. INTRODUCTION

Water waves with exceptionally large amplitudes and well defined frequencies have often been observed, especially in closed or semi-closed water bodies, such as lakes, coastal bays etc.. The cause of these periodical oscillations is attributed to the resonant function of the fluid systems. These waves are refered to "seiche".

"Seiche" is a French word to describe this natural phenomenon. In recent publications "Abiki", a Japanese word with similar meaning, also appears in the oceanographic literature. Oceanic countries with numerous coastal bays, inlets, fjords, estuaries and straits are facing the challenges from the ocean. The creation of these words reflected the interest in this phenomenon.

In early this century this phenomenon was observed mostly in lakes and compared with the theoretically computed resonant periods by different methods. But there was not as much literature on this subject as on some other topics of physical oceanography. Within the past two decades this topic has attracted more scientists' attention and is studied by means of spectral analysis, analytical models and numerical models. But there are still many features for oceanographers to explore.

This thesis starts from a review of seiche study. Due to the lack of seiche review in recent years this review includes as many important papers as possible. The review includes a discussion of seiche reports, research methods

and energy sources, and will serve as a guide and a source of comparisons for this thesis research.

Sea surface oscillations from three coastal bays on the north shore of Juan de Fuca Strait, British Columbia, are analysed. The different procedures to remove low frequency components are discussed. Spectral analysis reveals seiche activities in these three bays, some of them having significant energy. Further attempts are undertaken to study the stronger seiches and the relation between seiches occuring and different tidal levels. The coherences of these data between every pair of bays throw light on the common energy source of observed seiches.

In order to study the wave response characteristics, a numerical model is developed. This model works in the frequency domain to test the frequency response of the bays with arbitrary shapes and variable depths. The model-predicted resonant periods agree well with the result of spectral analysis. Some features revealed by the model are the same as those revealed by the real wave spectra.

This research uses seismic, wave and meteorological data to explore the possible energy sources of the observed seiches. Travelling edge waves along Juan de Fuca Strait are studied by different theories. The result of the edge wave numerical model seems to be acceptable. It is difficult to verify this result, because there are no wave data available in the Strait. At last a preliminary conclusion as to the energy source is reached, it generally attributes the source

of the observed seiches to edge waves in the Strait, and the source of the strongest seiches observed to travelling barometric waves, which excited edge waves in the Strait through air-sea coupling, therefore the seiches inside bays were excited by edge waves passing by their mouths. Internal waves may be other exciting source, which is discussed and supported by available data.

II. A BRIEF REVIEW OF SEICHE STUDIES

This review is organized in three parts. The first part is a description of observed seiches reported all over the world from early 1960's until the end of last year. The second part is about theories and methods used in seiche studies. The third part describes the possible sources of seiche energy according to different researchers' opinion. In each part the material are mentioned chronologically.

A. EXAMPLES OF OBSERVED SEICHE ACTIVITY

Defant (1961) gave a brief survey of observed seiches in various lakes, including the striking data of Bergsten (1926) who observed a uninodal, one-dimensional seiche in Lake Vättern, Sweden.

Waves with large amplitude inside harbours were frequently reported to cause considerable damage, such as breaking anchors, destroying coastal projects, etc., even after constructing breakwaters. Many harbours with narrow entrances are limited in their usefulness not so much by the penetrating sea swell as by surging associated with harbour resonances. This phenomenon was refered to by Miles and Munk (1961) as a *harbour paradox*, that is, the wave agitation of resonance within the harbour may increase when the opening decreases, thus causing a narrowing of the harbour mouth to diminish the protection from seiching.

Olsen and Hwang (1971) reported ocean waves having periods between four minutes and about one hour, which were

measured simultaneously at several locations inside Keauhou Bay, Hawaii and at two deep-water stations approximately 4 km offshore. Barber and Taylor (1977) reported the measured data on the distribution of current in Lennox Passage, which indicated the self-oscillation of Chedabucto Bay, in eastern Canada. Lemon *et al* (1979) reported seiche motions observed with a bottom-mounted pressure gauge in Port San Juan, western Canada.

Besides the seiches in closed basins such as lakes, and half closed basins such as harbours, which are commonly observed, Petrusevics *et al* (1979) reported observations of a continental shelf seiche off south-west Australia, even though the near shore topography of the continental shelf does not form a closed basin, nor does it have a single side fully open to a deep ocean.

Wübber and Krauss (1979) verified the results of their numerical model by comparison with tide gauge records all along the Baltic coast and found that eigen-oscillations play a major role in the Baltic Sea. Their spectral analysis did not show any preference for special peaks. A wide variety of periods seems to be possible. Orlić (1980) reported an exceptional sea-level oscillation in Vela Luka, a small town on the island of Korčula, Yugoslavia, in the morning of June 21,1978. The peak amplitudes of sea level changes were evaluated at about 3 meters, while the period was equal to some 15 minutes; the oscillation lasted for three hours. At the same time as well as before and after

the date mentioned similar sea-level changes occurred in a few other places in the Adriatic. Great damage was reported to have been caused by the phenomenon. Fais and Michelato (1980) reported on free oscillations of Cagliari Gulf, which is a semi-enclosed basin located at the southern end of Sardinia, Italy, with periods of 73.1, 35.3, 23.2 and 18.9 minutes. To study the internal seiche, Dyer (1981) spectrally analyzed the salinity fluctuations at an STD near the halocline in Southampton Water, England. The predominant energy-containing periods had values of 7-9 and 3.5-4.5 minutes. His calculated wavelengths of the standing wave agree well with echo-sounding surveys of the elevation of the halocline. By careful visual inspection of the sea level records at the tidal station of Genoa, which is located in the inner part of the Ligurian Sea, Papa (1981) reported a nontidal oscillation with a mean period of about 2.6 hours and amplitude fluctuations from a few millimeters to some centimeters. The records cover the interval Oct. 1977 to March 1978 with sampling rate of 30 minutes. The spectral analysis revealed that two peaks, 3.36 hours and 2.56 hours, showed up above the background noise. Ben-Menahem and Vered (1982) Fourier analysed the mareograms at Haifa Bay, Israel, which revealed a sharp line spectrum with fundamental peaks at periods near 54 minutes. Lanyon *et al* (1982) collected data relevant to shelf waves and bay seiches with periods between 10-60 minutes both from the open ocean and from the beach groundwater wells at South Beach, Wollongong,

Australia. Giese *et al* (1982) reported coastal seiches at Magueyes Island, Puerto Rico, in distinct fortnightly groups with maximum seiche activity following new and full moon by 7 days. The result they presented were drawn from a many-faceted study which had spanned 14 years.

In the study of bay seiches at South Beach, Australia, Lanyon *et al* (1982) adopted data obtained both from the open ocean and beach groundwater wells. They followed Waddell's conclusion (1976) that the beach front acts as a low-pass filter, damping high-frequency waves and allowing low-frequency waves to be propagated onto the groundwater surface. The observed oscillations with periods between 10 to 60 minutes were refered to shelf waves and bay seiches.

In the early 1980's the Japanese carried out synoptic studies of the seiche activity, stimulated by a disastrous seiche which occured in Nagasaki Bay on March 31, 1979. The seiche was the largest one in the history of tidal observations in Nagasaki Bay. The maximum amplitude of the seiche observed at Matsugae Quay, located at the middle part of the bay, was 278 cm and the period was about 35 minutes, while it was 478 cm at the mouth of the Urakami-river located at the northern end of the bay (Akamatsu, 1982). The large seiches in Nagasaki Bay are most frequently observed in winter (Hibiya and Kajiura, 1982).

Besides the research work mentioned above, Isozaki (1979) reported observed seiches in Habu-harbor on Sept. 17, 1976 and Oct. 8, 1977. Kosuge and Saito (1981) examined the

natural modes of harbour oscillations and effects of man-made structures on the oscillation in Shimizu Harbour. They compared maregrams from three locations in the harbour, recorded before and after the breakwaters' construction, and found that in this case the "*harbour paradox*" did not play any important role. After the construction of the two breakwaters, the amplitudes of the oscillations are decreased by one-half, although the periods of the natural oscillations remain almost about the same. Nakamura and Serizawa (1983) studied the local climate of shelf-seiches on the basis of maregrams at Susami where the sea level variation with 12 minutes of period was significant through a year.

B. THEORY AND METHOD OF SEICHE STUDY

Early seiche theories were systematically described by Defant (1961). Afterwards Rao (1966) gave a brief survey about this topic which made numerous attempts to solve Helmholtz's equation for the barotropic mode in a rectangular basin of constant depth.

After the "*harbour paradox*" theory was advanced by Miles and Munk in the early 1960's, the development of coastal survey and projection is bound to be followed by an active scientific investigation, which challenges physical oceanographers into this research field to develop different methods in seiche study.

Analytical studies of seiche motions have only been carried out in special cases. Clarke (1968) applied the Galerkin method to the one-dimensional flow problem. Afterwards he extended the method in order to treat the two-dimensional flow problem in a basin whose surface shape is rectangular and whose depth is arbitrary although subject to the linear theory. Johns and Hamzah (1969) solved the seiche motion problem in a curved lake, and found that the periods of the first two modes are not effectively changed in comparison with those for a straight lake having a length equal to that of the median line along the curved lake. Based on the solution of a singular integral equation, Hwang and Tuck (1970) developed a theory for calculating oscillations of harbours of constant depth and arbitrary shape. Lee (1971) investigated both theoretically and experimentally the wave-induced oscillations in harbours of constant depth but arbitrary shape in the horizontal plane connected to the open-sea. He developed a theory called the "arbitrary-shape harbour" theory to solve Helmholtz' equation for arbitrary-shaped harbours by applying Green's identity formula and choosing the Hankel function of the first kind and zeroth order. Olsen and Hwang's (1971) numerical evaluation of their theory could account for most of the amplification factors observed in Keauhou Bay, Hawaii, which were as high as 10^3 (in power spectral density) at selected frequencies.

Miles (1971) constructed an equivalent electrical circuit, which contains a radiation impedance and a harbour impedance, to simulate the response of a harbour as a Helmholtz resonator. Garrett (1975) extended the harbour theory of Miles to take into account the tidal forces and provided a better description of reality. In his paper Garrett focused his attention on the properties of the forced oscillation in the gulf induced by the tidal forcing. Afterwards Garrett's theory was developed by Pierini (1981) so that its formalism includes the free oscilations (seiches) of the gulf.

Meanwhile, progress has come about through the development of the growth of digital computing machines and techniques for the presentation and analysis of information. The improved methods are approaching an engineering level of predictability. Therefore we confine this review to recent years' work, mainly in late 1970's and early 1980's and with emphasis on numerical modeling.

For the large-scale numerical study of the world oceans, Platzman (1975) calculated the normal modes for a homogeneous ocean occupying a connected domain consisting of the North Atlantic, South Atlantic and Indian Oceans. Based on the Lanczos process and with a grid of 675 six-degree Mercator squares, Platzman found 26 gravity modes with periods from 8 to 67 hours. The North Atlantic co-oscillates with the South Atlantic at a period of about 42 hours, and has strong resonances at 23, 21, 14.4, 12.8, 8.6 and 8.3

hours.

Barber and Taylor (1977) employed maximum entropy (ME) method (Ulrych and Bishop, 1975) to analyze the current fluctuations in Chedabucto Bay, eastern Canada. The result agreed fairly well with the spectrum of the output of their time-dependent numerical model.

Mattioli and Tinti (1978) numerically investigated the response of a rectangular large-mouthed harbour to exciting monochromatic plane waves, particularly to waves with rays not orthogonal to the straight coastline. In their further work (1979) they concluded that the reliability of the results obtained from an integral approach is strongly dependent on how the kernels are discretized, especially if rather complicated geometries are involved.

Following the analysis of edge waves over an exponential bathymetric profile presented by Ball (1967), Lemon *et al* (1979) constructed a theoretical model of oscillations in a rectangular basin with an exponential depth profile.

Isozaki (1979) estimated the resonant period of Habu-harbor by Merian's formula (LeBlond and Mysak, 1978. p.293), finding that the result was not consistent with the observed predominant period of 10.5 minutes. So he examined some characteristics of the bay water oscillations by means of a numerical model and obtained periods of 10.5, 2.4 and 1.4 minutes for the uni-, bi-, and tri-nodal oscillations. It was confirmed from theoretical considerations that the

seiches of that harbor would be explained by the coupled oscillation of the system of the harbor part and the canal part.

Wübber and Krauss (1979) constructed a numerical model to study the eigen-response of the Baltic Sea. The calculations took into account the bathymetry and shape of the Baltic and the earth's rotation, but no friction terms, though the authors knew that it is essential for an accurate spectral determination of the eigenfunctions. The seiches were produced by a forcing function which acted on the water body during an initial time. The resulting oscillations after the force was switched off were analyzed at each grid point and displayed in form of co-range and co-tidal lines. It was shown that the eigenoscillations of the Baltic Sea were strongly modified by the Coriolis force. Rotation converts all modes into positive amphidromic waves; only the interior parts of the Gulfs and of the Western Baltic exhibited standing waves. The periods of the oscillations were reduced by the earth's rotation, when they were longer than the inertial period.

Fais and Michelato's two-dimensional model (1980) resulted in the confirmation of the periods of the first two longitudinal modes and the first two transversal modes, which had been identified with the four main resonant periods of the observed data in the Gulf of Cagliari, Italy.

Orlić (1980) used the Proudman's equations to analyze the source of seiches in the Adriatic. But he suggested that

a hydrodynamical numerical model would be needed, since the existing analytic solutions could not be satisfactorily applied to the basins in the Adriatic.

Gotlib and Kagan (1980) calculated the corresponding pairs of resonance period and amplification factor in the Atlantic, Indian and Pacific Oceans.

Papa (1981) employed the leap-frog scheme (Sündermann, 1966) to simulate numerically the water movement of the Ligurian Sea, in association with a regime of southeasterly winds. The result agreed well with the observed data. Afterwards (1983) his model revealed a 5.7 hour period seiche which was identified in the observed data.

Miles (1981) studied free and forced oscillations in a basin connected through a narrow canal to either the open sea or a second basin. The resulting model yields a Hamiltonian pair of phase-plane equations for the free oscillations, which are integrated in terms of elliptic functions. The corresponding model for forced oscillations that are limited by radiation damping yields a generalization of Duffing's equation for an oscillator with a soft spring, the solution of which is obtained as an expansion in the amplitude of the fundamental term in a Fourier expansion. Ben-Menahem and Vered (1982) simplified the configuration of Haifa Bay as a semi-elliptic embayment with a semi-paraboloidal bathymetric profile and solved the shallow water equations in this domain to get the eigenperiods of the bay.

Hibiya and Kajiura(1982) carried out a numerical study of seiches in Nagasaki bay with the shallow water equations of motion and continuity including the effect on sea level of the atmospheric pressure deviation. Akamatsu (1982) adopted more accurate equations including the effects of bottom friction and wind stress on sea surface. Odamaki *et al* (1983) developed a numerical model to study the water movement in a large sea area. They added terms to represent the Coriolis force, non-linear and turbulent viscous effects.

In summary, along with the development of computer techniques numerical modelling has replaced the traditional analytical method, and therefore the complication of topography is no longer the leading obstacle to studying seiche motions in real bays.

C. THE EXCITING SOURCES OF SEICHES

In the opinion of Miles and Munk (1961), which is supported by many documented instances, the surges following the passage of an atmospheric pressure jump and a sudden shift in the winds appear to have been responsible for many seiche excitations. Random variations, which occur at all times in the normal and tangential stresses on the water surface, also contribute to the surging. Of incidental interest is the excitation of the normal modes by movements of the harbour bottom associated with the arrival of earthquake waves. Seiches can also be excited through the

harbour entrance. If there is a broad spectrum of waves exterior to the harbour, then those particular frequencies that correspond to the resonant frequencies will excite the interior resonances; in some localities the spectrum is even peaked at frequencies typical of harbour seiches. More frequently seiches are generated by long waves reaching the coast from the open sea (Miles, 1974). Such seiche-producing long waves can be generated by distant meteorological disturbances at the sea surface (Munk, 1962, pp647-663) and by seismic disturbances at the sea bed (Matuzawa *et al*, 1933).

Heaps and Ramsbottom (1966) did an interesting study of wind-generated internal seiches in Lake Windermere, England. Olsen and Hwang (1971) suggested that shelf resonance and edge-wave effects seemed to play a significant and interesting role for periods somewhat longer than the fundamental bay resonance period. Bowers (1977) showed theoretically that the natural oscillations of a harbour could be excited directly, without breaking of the primary wave system, by set-down beneath wave groups, which is a long-period disturbance travelling towards the shore line at the group velocity.

After studying the continental shelf seiches of south-west Australia, Petrusevics *et al* (1979) concluded that long ocean waves are the most probable source of seiche excitation, because during high seiche activity there were no other apparent sources of excitation, such as significant

changes in wind, or in barometric pressure, and no local seismic activity. Similar conclusions were made by Munk (1962) for other continental shelves.

Wübber and Krauss (1979) suggested that the development of seiches of the entire Baltic Sea requires large-scale meteorological forcing.

Isozaki (1979) attributed the seiches in Habu-harbor on Sept.17, 1976 and Oct.8, 1977 to the swells from Typhoon No.7619 and Typhoon No.7714 respectively.

Fais and Michelato's study of seiches in the Gulf of Cagliari (1980) suggested that seiche stimulation is mainly associated with the instability lines or meteorological fronts crossing the gulf at speeds close to the speeds of long waves on the gulf. Transversal seiches generally occur following the passage of atmospheric perturbations moving eastward or northeastward across the gulf, while longitudinal seiches are usually generated by perturbations passing northward or northwestward over the gulf.

Orlić (1980) studied the source of the seiches in the Adriatic. He gave an explanation connected with a forced progressive wave in the sea, instead of a free wave, as the seiche-exciting source. A gravity wave in the atmosphere caused a forced progressive wave in the sea, through the acting of the atmospheric pressure over the sea. The forced wave was of small amplitude until it met a basin whose position and configuration are suitable for an occurrence of the Proudman resonance, i.e. until the velocity of the

atmospheric disturbance (and the forced progressive wave) became equal to the velocity of the long wave in the sea.

Dyer (1982) considered that the lateral internal seiching in Southampton Water was produced by interaction of the surface seiche with the shallow side of the estuary. Interaction of a current with a sill could produce internal seiching if the waves were continually reflected. This has been experimentally observed at tidal frequencies in Oslo fjord and explained by a linear mechanism by Stigebrandt (1976). A non-linear mechanism has been explored by Blackford (1978).

Papa (1981) discussed the hypothesis of southeasterly winds as the forcing mechanism of the oscillation revealed at tide gauges in Ligurian Sea.

Ben-Menahem and Vered (1982) concluded that the dominant source of the seiches at Haifa Bay is meteorological and the coastal seiches may be both free and forced. The analytical study showed that the shape and size of the resonating water body is dependent to some degree on the direction and intensity of the exciting meteorological front.

Giese *et al* (1982) suggested that some internal waves were generated by tides in the southeastern Caribbean Sea and they were responsible for exciting the fortnightly groups of coastal seiches at Magueyes Island, Puerto Rico. To support their hypothesis they analysed the characteristics of coastal seiching at Puerto Princesa on

Palawan Island in the Philippines and indicated that the seiching was excited by the Sulu Sea internal waves. Apel *et al* (1980) observed the generation of these internal waves by strong tides in Sulu Sea.

Hibiya and Kajiura's numerical model (1982) confirmed that the exceptionally large range of oscillations in Nagasaki Bay was indeed produced by a pressure disturbance travelling eastward with an averaged speed of about 110 kmh^{-1}. It was concluded that the exciting mechanism was due to the leading part of shallow water waves induced by the atmospheric pressure disturbance being amplified over a broad continental shelf because of near-resonant coupling. After leaving this continental shelf region, the amplified water wave converged into the shelf region. A train of waves thus formed with a period of about 35 minutes entered Nagasaki Bay and was resonantly amplified at periods of 36 minutes and 23 minutes which are the eigen-periods of the Bay. Besides the resonance, the combined effects of shoaling and reflection inside Nagasaki Bay also enhanced the amplification. Akamatsu's analysis (1982) led to the conclusion that this seiche may be due to the severe barometric pressure jump associated with the cold air front. After examining the response of Nagasaki Bay to the forcing at the mouth of the Bay by means of a two-dimensional numerical model, it was considered reasonable that the seiches of Nagasaki Bay were caused by the resonance to the long waves due to the barometric pressure jump. Using a

similar numerical model, Odamaki *et al* (1983) confirmed the results above. They summed up the exciting procedure as three essential processes: air-sea coupling, refraction and reflection of the incident water wave by topographic effects in shelf and the amplification by the harbour resonance. Furthermore it was indicated that the most important process was the second, i.e. the water waves incident onto shelf generated the local oscillation systems by reflection and refraction, and caused the seiches in the adjoining bay or port.

Summing up the above researches, seiches may result from direct disturbances by meteorological forces at the surface of a coastal bay. More frequently they are generated by long waves reaching the coast from the open sea. Such seiche-producing long waves can be generated by distant meteorological disturbances at the sea surface. The mechanism of the latter is more complicated. In some cases internal waves may be the cause of the seiche excitation. Sea bottom movements are considered as an incidental source too.

III. SPECTRAL ANALYSIS OF SEA SURFACE FLUCTUATIONS IN COASTAL BAYS

This Chapter analyses the sea surface oscillation data in Pedder Bay, Becher Bay and Port San Juan on the north shore of Juan de Fuca Strait. The result identifies seiche activities, even very strong at times. The strong seiches and the influence of tidal phase are studied in more detail in the final sections of this chapter.

A. SYNOPTIC DESCRIPTION OF PHYSICAL OCEANOGRAPHY IN JUAN DE FUCA STRAIT

Juan de Fuca Strait is a long narrow submarine valley. Port San Juan near the Pacific entrance is the only major fjord-like opening along the north coast. Becher Bay and Pedder Bay are small bays at the eastern end of the strait near Race Rocks (Figure 1).

Water temperatures throughout the Strait remain colder than 12°C at depths of more than 10 meters. Salinity increases from top to bottom and from east to west. The wind patterns will be mentioned in chapter 6.

Since direct measurements of wind waves have not been made in the Strait, empirical relationships are relied upon to estimate their height distributions. Fully developed sea in the Strait can attain significant wave heights of 1.5 m, or most probable maximum heights of 2.7 m, for a 10 m/s wind that blows for at least 10 hours over a fetch of 140 km. (Thomson, 1981).

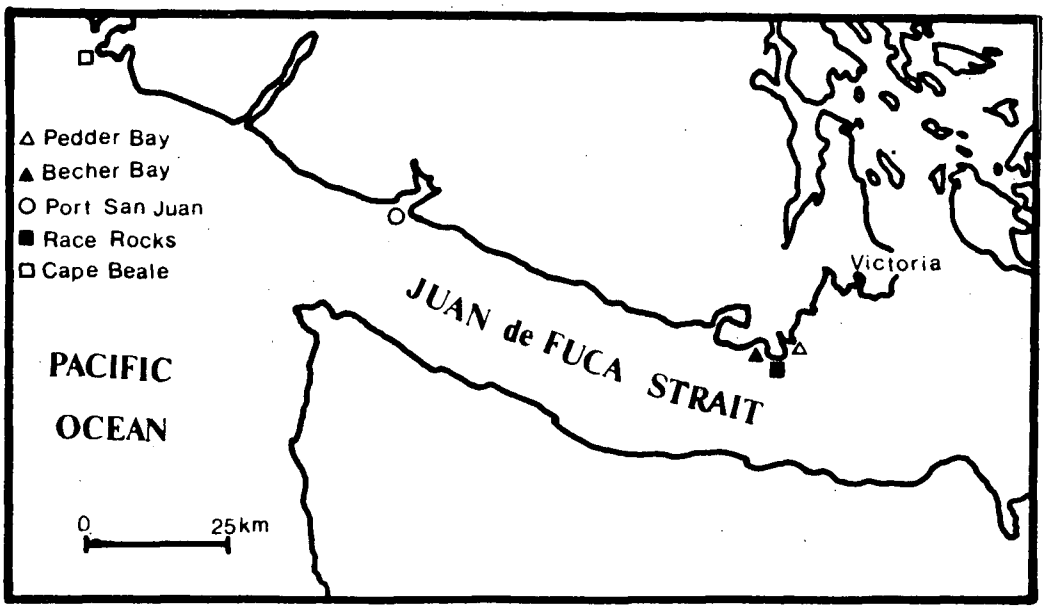

Figure 1 Map of Juan de Fuca Strait including the coastal bays in this research.

The oceanic tide travels northward along the west coast of North America and enters the Strait as a long progressive wave whose speed and range vary eastward as a result of changes in the depth and geometry of the Strait. The semidiurnal wave component (M_2 tide) and the diurnal wave component (K_1 tide) are the two main constituents. Tides, freshwater runoff, winds and along-channel atmospheric pressure differences are major factors affecting currents in the Strait. The current distributions from numerical modeling by Crean (1983) give a detailed illustration.

B. THE SEA SURFACE FLUCTUATION DATA

The data of sea surface fluctuation adopted in this research were obtained from Dr. R.E.Thomson, of the Institute of Ocean Sciences (IOS), Sidney , B.C. These data

were measured with pressure gauges. The gauges in Pedder Bay and Becher Bay were model 2A, manufactured by Aanderaa Instruments Ltd., the gauge in Port San Juan was model 12A, manufactured by Applied Micro System Ltd.. Original data were digitized and stored on a computer tape. Part of data were filtered by 7th order Butterworth digital filter with a cut off period of two hours which is described in the following section. Table 1 gives a simple description of these data:

Table 1 Original Data of Sea Surface Fluctuations

bays	date interval	pre. gauge positions	sampling rate	unfiltered data points	filtered data points
Ped. *set 1*	Jan. 15 Jan. 26 1980	N 48°20.3' W123°33.1' grid #161	2 min.	8490	0
Bec. *set 1*	Jan. 15 Jan. 26 1980	N 48°20.1' W123°36.0' grid #175	2 min.	8439	8435
San. *set 1*	Jan. 15 Jan. 26 1980	N 48°33.7' W124°24.8' grid #187	2 min.	7933	7933
Ped. *set 2*	Jan. 27 Feb. 20 1980	N 48°20.3' W123°33.1' grid #161	2 min.	17475	17000
Bec. *set 2*	Jan. 27 Feb. 20 1980	N 48°20.1' W123°36.0' grid #175	2 min.	17444	17000
San. *set 2*	Jan. 27 Feb. 20 1980	N 48°33.7' W124°24.8' grid #187	2 min.	17304	17000

where the grid #'s denote the corresponding positions in the numerical model grids.

C. REMOVAL OF TIDAL COMPONENTS

Our interest in this research is to study the high frequency sea surface oscillation with the range of periods from several minutes to about one hour. Before analysing the data to investigate the seiche properties one must remove the low frequency tidal constituents. There are many methods to reach this goal.

The widely adopted procedure is to subtract the predicted tidal components from time series data. If the amplitudes and phases of all the constituents of the tide are available, the sea surface variation associated with tidal stage can be calculated from the formula

$$h = H_0 + \Sigma\, fH\cos[at+(V_0+u)-k]$$

where

Σ is the summation sign for all the tidal constituents

h = the tide height at time t

H_0 = the mean water height above datum

H = the amplitude of a tidal constituent

f = a factor reducing the mean amplitude H to the year prediction

a = the angular frequency of the constituent of amplitude H

t = the time measured from starting point of

predictions

(V_0+u) = the value of equilibrium argument of the constituent of amplitude H when t=0 , at Greenwich

k = the phase of the constituent with respect to Greenwich (in the Canadian System)

The maximum tidal level and it's corresponding time in Juan de Fuca Strait can be found in Canadian Tide and Current Tables (1980).

Considering the filter function of the coastal bays and the adjacent sea area to tidal waves, the predicted tides at a specified point of a bay may be distorted at other points, such as the positions where the pressure gauges were installed, so after subtracting the predicted tides, there still remains a residual. Even though the parameters of tidal constituents are adopted at the position where the data for analysis were measured, this method still could not remove all the low frequency components. An example could be found in Lemon's thesis (1975).

The simplest way to remove tides and other low frequency components is to fit a curve to the low frequency part of the measured time series in the sense of least square differences. If the data set has only one extremum in low frequency component, a polynomial fit is sufficient. If there are two or more extrema, the spline fit need to be invoked. I chose one piece of time series to demonstrate this method. The selected time series is half a tidal cycle

from Port San Juan first data set, and includes 256 data points with the first point measured at 10:51 Jan. 18 , 1980. The 10th order polynomial curve fitted to this time series is the optimum polynomial curve under 16th order in the sense of least square differences which was selected automatically by the computer subroutine OLSF (described in "UBC Curve", computing Center, UBC). Figure 2 shows the time series and the fitting curve. They coincide pretty well with each other. Figure 3 shows the difference between original time series and the fitting curve, it is obvious that low frequency components have been removed. Figure 4 shows the spectral density of the filtered data which was calculated by Fast Fourier Transformation. The spectrum revealed that most of the energy is concentrated within the frequency band centered at frequencies 0.03 and 0.075 cycle per minute, with corresponding periods of 33 and 13.3 minutes. Figure 5 shows the phases of the Fourier coefficients which looks like pretty random. The Butterworth filtered data at same time interval were processed by Fast Fourier Transformation for comparison purpose. Both of these spectral density curves are shown in Figure 6. These two curves give quite the same spectra and reveal quite the same seiche phenomenon. It could be concluded that the filters perform their effective function to eliminate the tidal effect. The interesting point to be mentioned here is the difference of the two curves at lowest frequency band. The polynomial filter performs better function in reducing the lowest

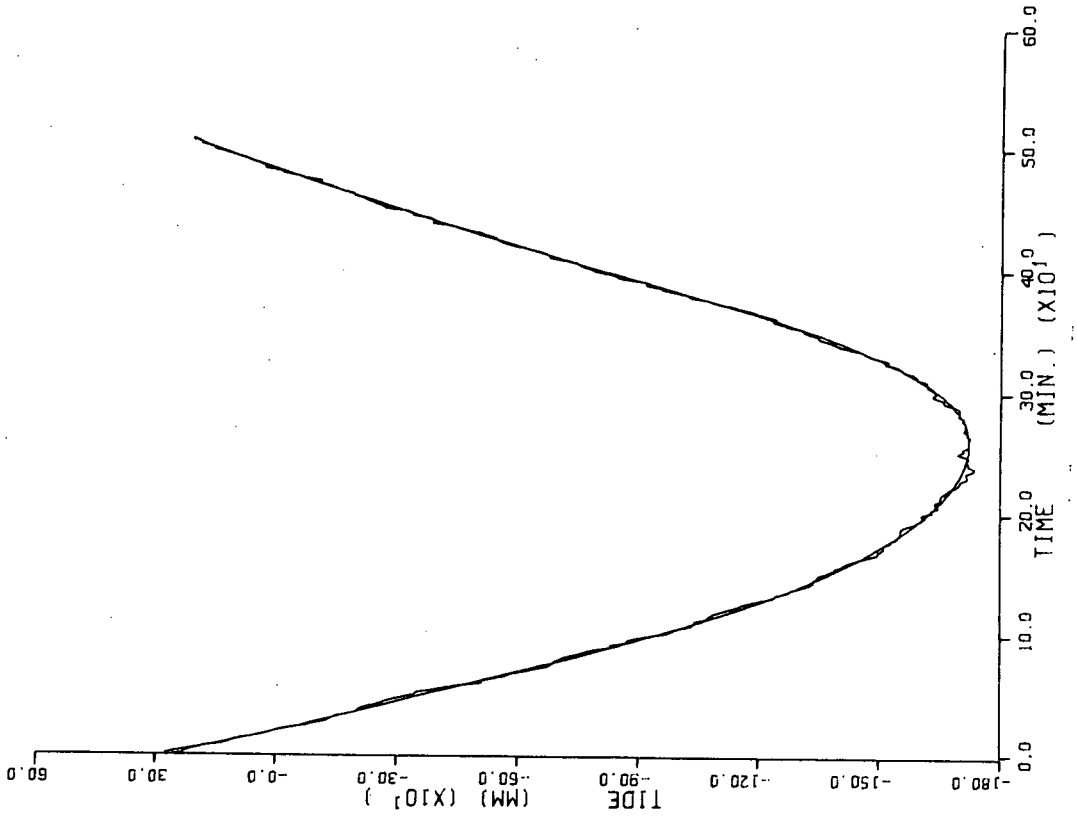

Figure 2 An example of polynomial curve fitting.

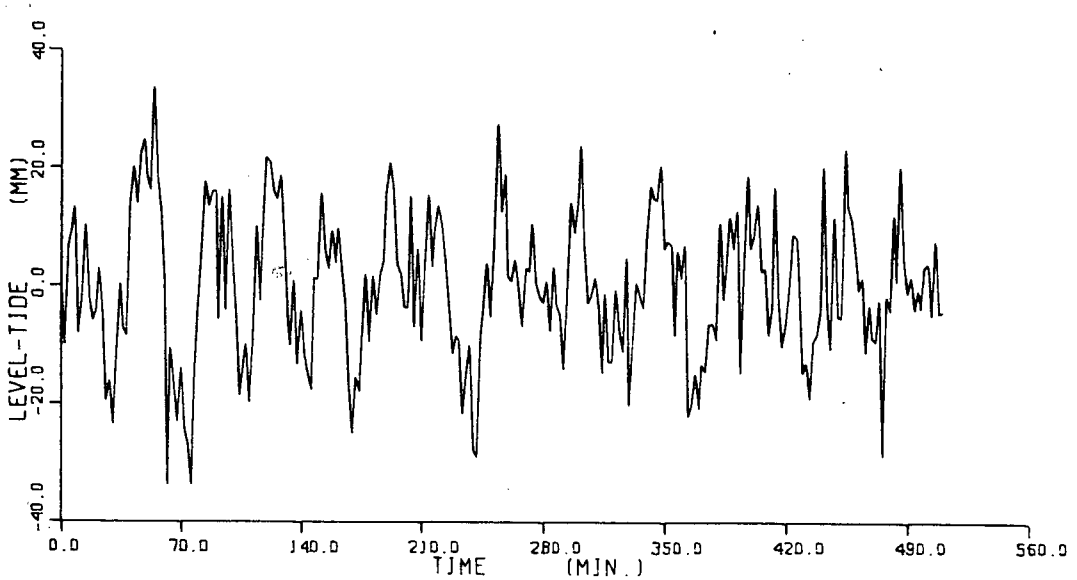

Figure 3 Polynomial filtered sea surface oscillation.

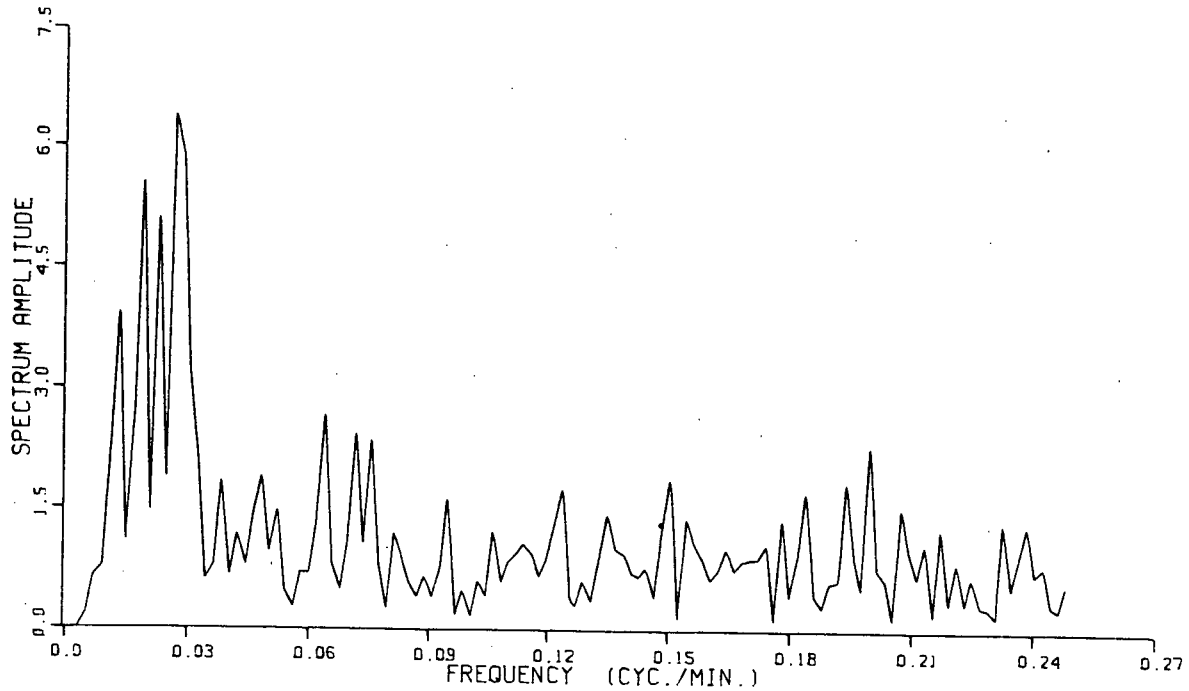

Figure 4 Spectral density of polynomial-filtered data.

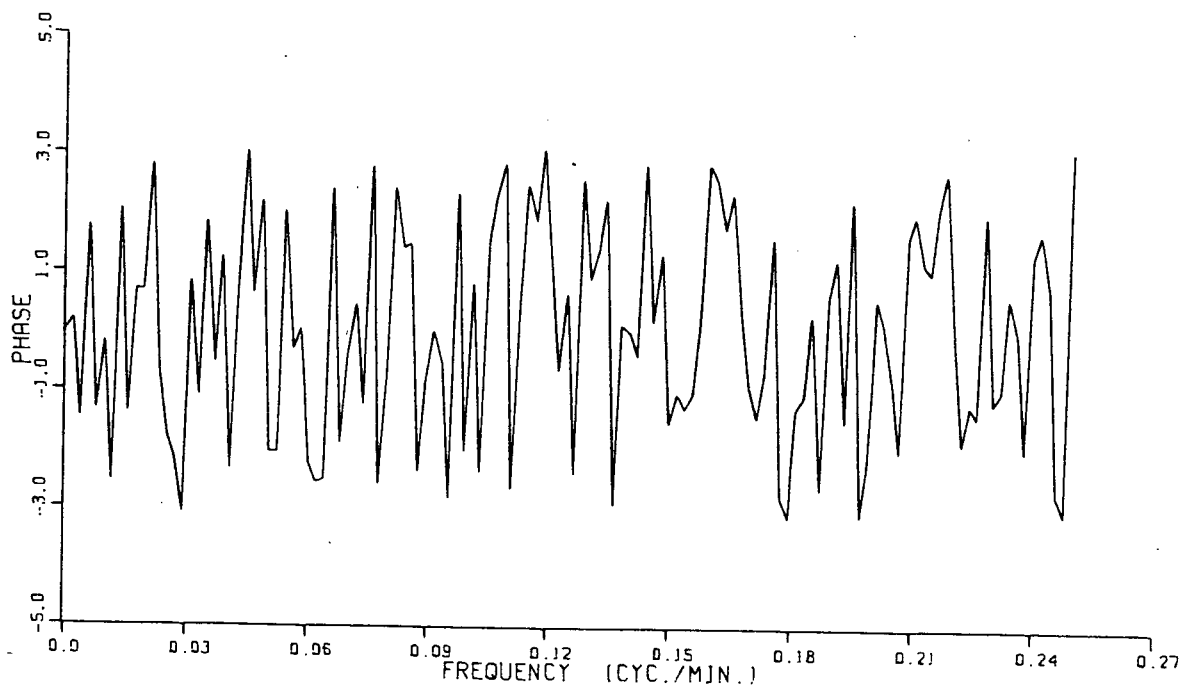

Figure 5 The phases of Fourier coefficients of polynomial-filtered data.

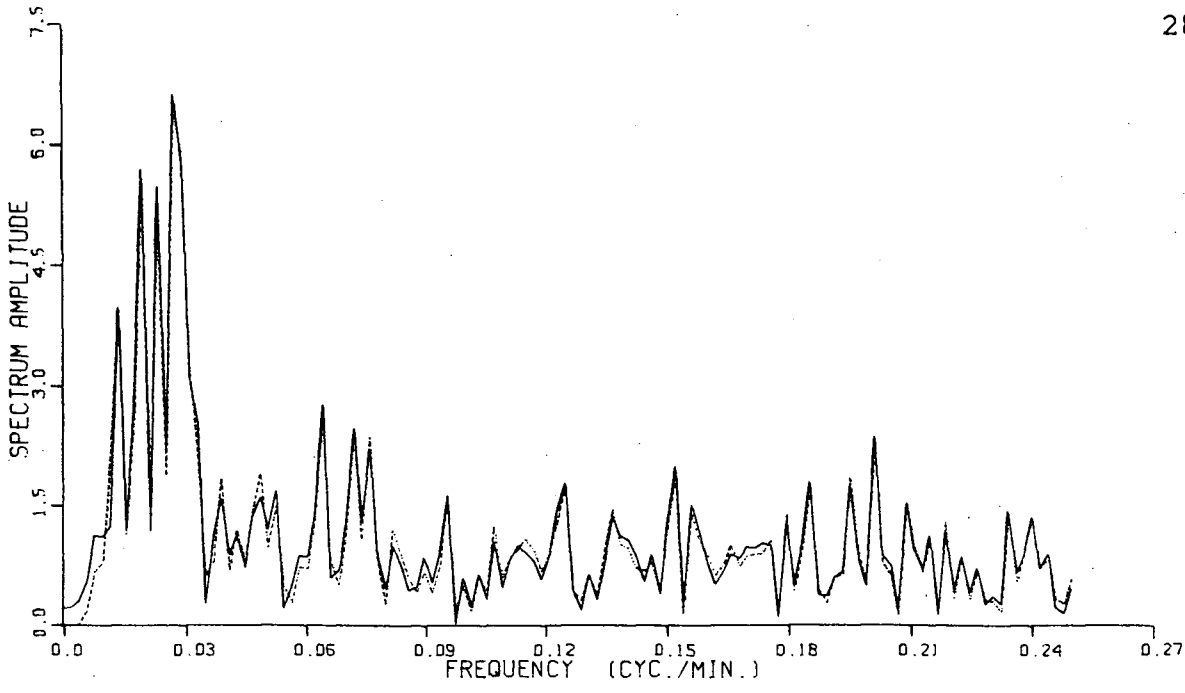

Figure 6 Comparison of spectra of Polynomial and Butterworth filtered data.
Dashed curve : polynomial filtered.
Solid curve : Butterworth filtered.

frequency components.

Digital filters are widely applied in communication technology, geophysical reseach, etc. . The advantages of these filters are that they can be applied and studied in both time and frequency domains, and the characteristics of time series can be interpreted in term of statistics by fully developed theories. The filtered data used in this research work were obtained from a 7th order Butterworth filter. This hierarchy of filters is defined in the frequency domain by the equality

$$|H_B(\omega)|^2 = \frac{1}{1 + \left(\frac{\omega}{\omega_c}\right)^{2n}} \qquad (3.3\text{-}1)$$

where

ω_c is the specified cut off frequency

n is the order of filter

Figure 7 shows the frequency response of the 7th order Butterworth filter with cut off period 2 hours. The mathematical formulation, design, characteristics and application of this filter to tidal time series are fully described by Thomson and Chow (1980).

D. METHOD OF SPECTRAL ANALYSIS

Spectral Analysis is a very common method. There is much literature about this field. Only few points need to be mentioned in this thesis.

The averaged power spectrum, or the estimator of power spectrum, may be obtained from ensemble average or frequency band average of spectra. These two procedures make the estimates consistent. Futhermore, if in the first case the time series is divided into l subseries and in the second case the spectrum is smoothed over l frequencies, both of them will yield same degrees of freedom $n=2l$ (Bendat and Piersol, 1971). The procedure to compute the 95% confidence intervals of power spectra was adopted from Jenkins and Watts (1968, p239); the values of chi-square distribution, used for computation of confidence intervals, came from a chi-square plot (Jenkins and Watts 1968. p82) and a

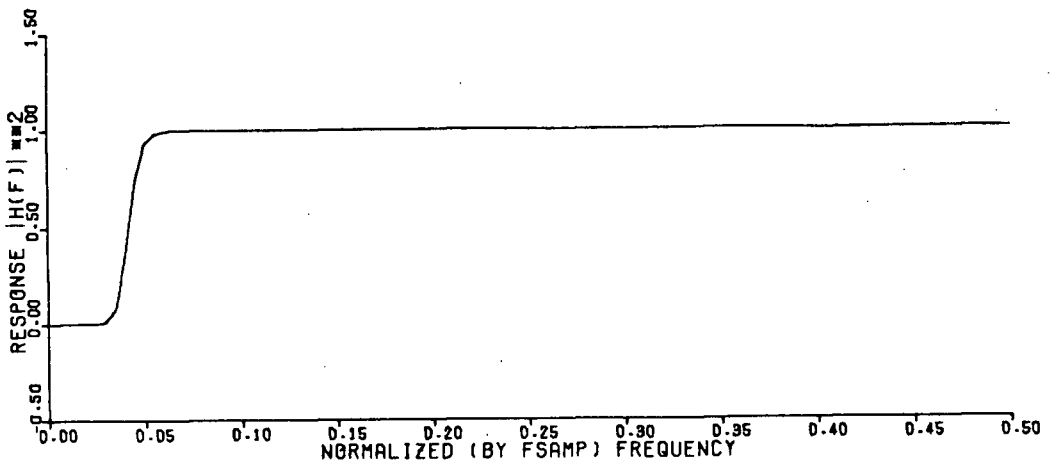

Figure 7 The frequency response of the 7th order Butterworth filter.

chi-square Table (Bendat and Piersol, 1971. p388).

The coherence estimators suggested by Bendat and Piersol (1971, p193) are frequency band averaged; those of Jenkins and Watts (1968, p374) and Bloomfield (1976, p214) are spectral window smoothed. This research mainly uses the former. The confidence intervals were computed according to Jenkins and Watts (1968, p379) and indicated by a vertical bar in each graph. A dashed horizontal line appears in the graph of coherence too. It is the 95% level of the null hypothesis. It refers to that value exceeded with 5% probability by randomly related records (Groves and Hannan, 1968). The calculation of these values follows Bloomfield (1976, p227); the observed values of coherence less than those lines should be regarded as not significantly

different from zero, and confidence interval should be used only if the coherences exceed those lines. Examples of the computation could be found in Chang's thesis (1976). This procedure to obtain 95% significance levels and confidence intervals were performed throughout this thesis. Dashed lines in the graphs of phase are zero phase lines.

The coherence definition given by Godin (1972) is:

$$\gamma^2(\sigma) = \frac{|<Z(\sigma)V(\sigma)>|^2}{<|Z(\sigma)|^2><|V(\sigma)|^2>} \qquad (3.4\text{-}1)$$

where < > indicates ensemble averaging. $Z(\sigma)V(\sigma)$ is the cross-spectrum of the observations Z(t) with the values of V(t) at various times. $|Z(\sigma)|^2$ and $|V(\sigma)|^2$ are power spectra. This method may be used for discontinuous time series, and performed in the following section to study seiches in different tidal levels. As far as I know, there is no way to estimate the significance level and confidence interval in this case.

E. SPECTRAL ANALYSIS (FIRST DATA SET)

The Butterworth-filtered time series were analysed in order to investigate the seiche activities. The sampling period of these data is two minutes, so the cut-off frequency (highest frequency obtainable by Fourier analysis) is corresponding to a period of four minutes.

First I analysed the first data set, including the data from Becher Bay and Port San Juan. The measured time series

starts from 15:10 Jan. 15 , 1980. The data were input to a computer program with 256 points per set which stands for a 8 hours 32 minutes time interval, and fed into a Fast Fourier Transform to get power spectra. Every next calculation started at a data point 8 hours later, so there is a 32 minute overlap between successive input data sets. Each power spectrum represents the frequency characteristics of sea surface fluctuation within the corresponding 8 hours. Altogether 33 sets of data were processed to look into the seiche activities of 11 days in these two bays.

Figure 8 and Figure 9 illustrate the successive 33 power spectra of Becher Bay and Port San Juan. In the spectra of Becher Bay two columns of peaks are in periods about 100 minutes and 13 minutes respectively. The 13 minutes period fluctuation is identified with excited resonant waves in the bay by numerical result in Chapter 4. The highest energy was found on Jan. 20. The 100 minutes period fluctuation may be caused by external forcing or data processing procedure. For some spectra the 100 minutes period peaks are absent which supports the first hypothesis. The spectra of Port San Juan give us a much more random picture, especially in the high frequency band. Large peaks can be seen at periods of about 30 to 45 minutes.

It is interesting to note that the high frequency band oscillations only appears in Port San Juan. Some explanations may be invoked. One is the filter function of bays, that means the geometry and bottom topography of Port

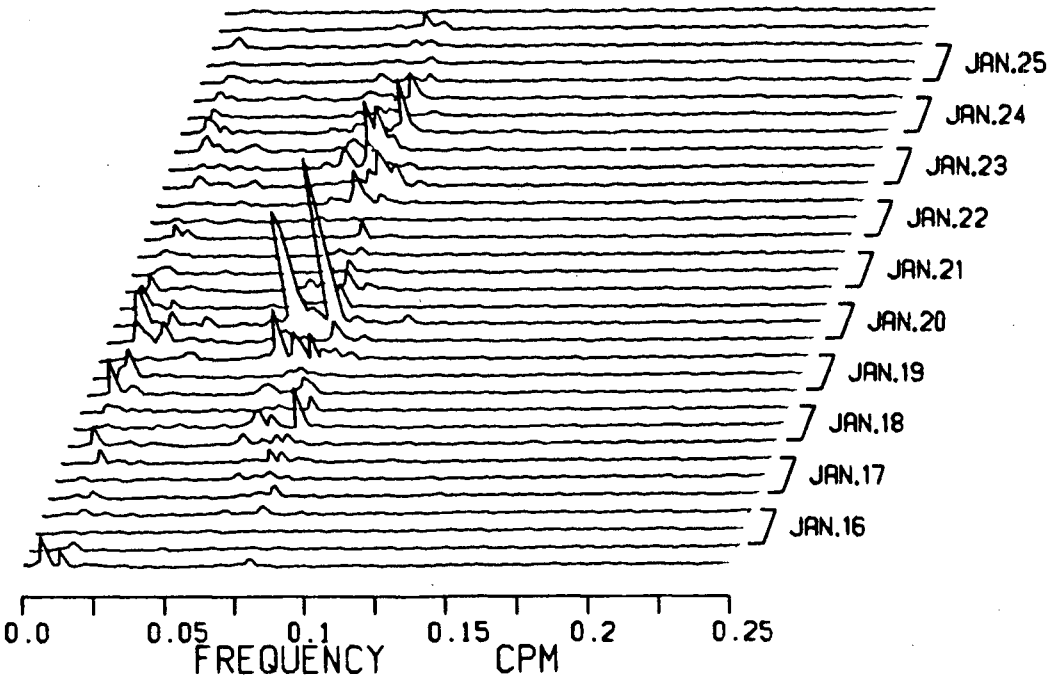

Figure 8 8-hour wave spectra of Becher Bay, January.

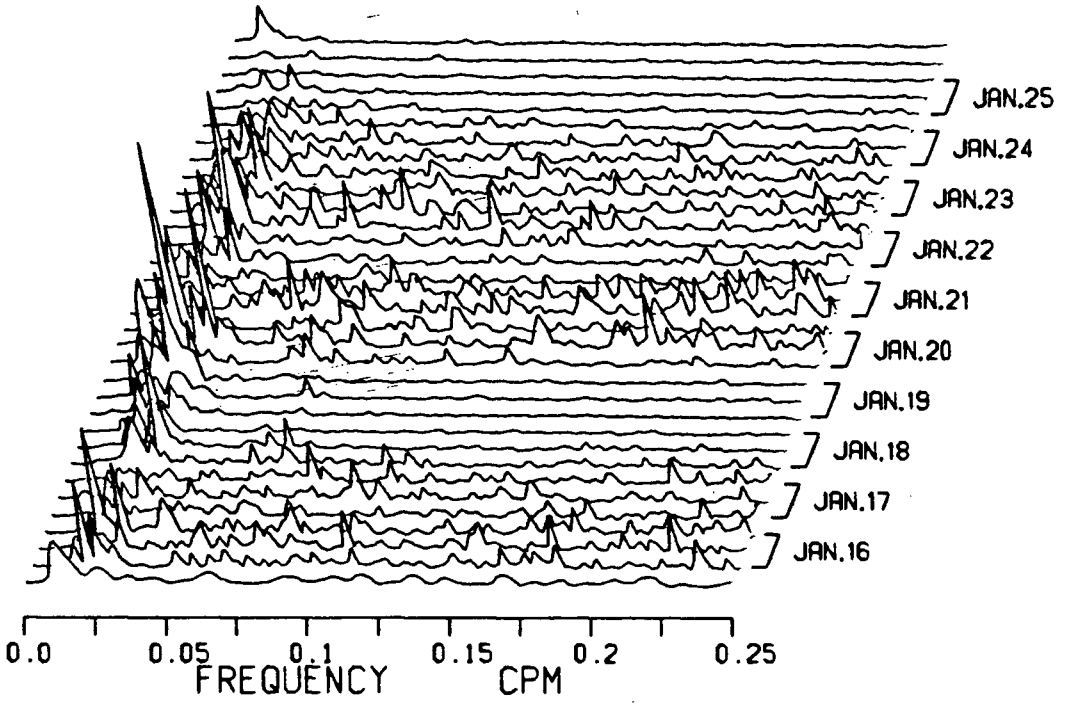

Figure 9 8-hour wave spectra of Port San Juan, January.

San Juan amplify or maintain the high frequency incoming waves inside the bay, but those of Becher Bay do not. The others are the wind momentum input through air-sea interaction and the swells from Pacific Ocean. The wind patterns are different in the vicinity of Port San Juan from that of Pedder Bay and Becher Bay. The latter is an area of calm airs. The swells of ocean could not maintain their energy to travel to as far as the vicinity of Becher Bay.

The ensemble averages of 33 power spectra of Becher Bay and Port San Juan are shown in Figure 10 and Figure 11 respectively. The main features of the spectra discussed above are made clear in these two graphs. Figure 12 shows the frequency band-averaged coherence of these two sets of time series; the main peak occurs at period range about 30 to 70 minutes, other peaks above confidence level have period 5 to 6 minutes, which implies that these two time series were correlated in this range of periods, furthermore that common sources excited seiches with these periods in the two bays.

F. SPECTRAL ANALYSIS (SECOND DATA SET)

The measurement of second data set started at 10:40 Jan. 27 , 1980 and lasted a little more than 24 days. The time series in the three bays beginning from 16:00 Jan. 27 , 1980 were inputed to a computer program to draw seventy 8-hour power spectra for every bay. The perspective views of these successive spectra are shown in Figure 13 to Figure 15

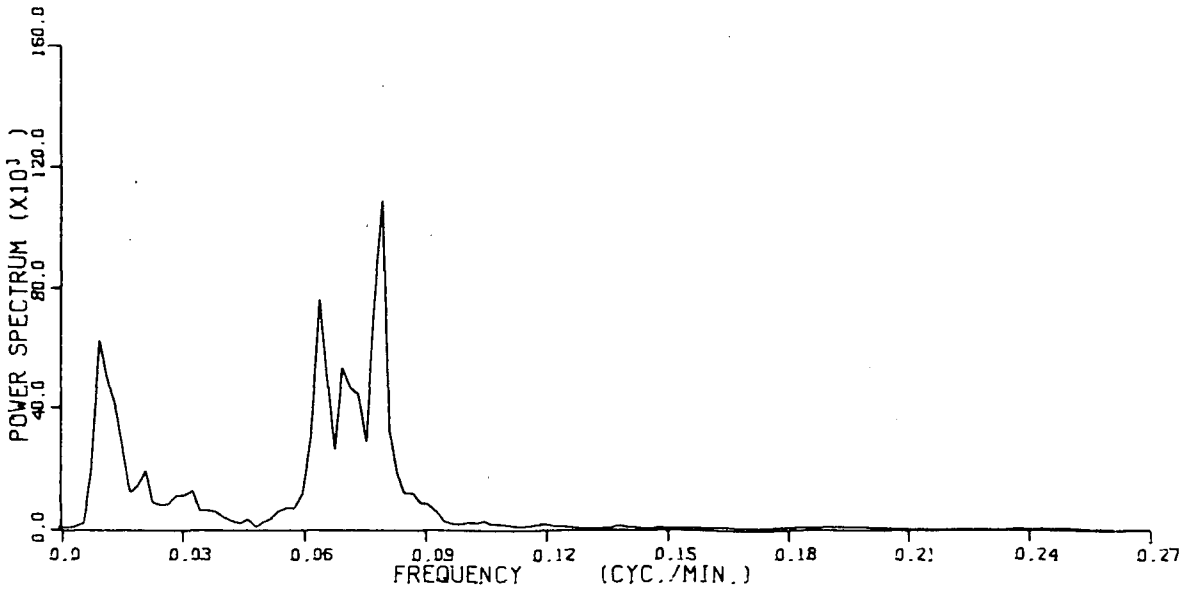

Figure 10 Power spectra of Becher Bay, January.
95% confidence interval: (0.72,1.45)*P(f)

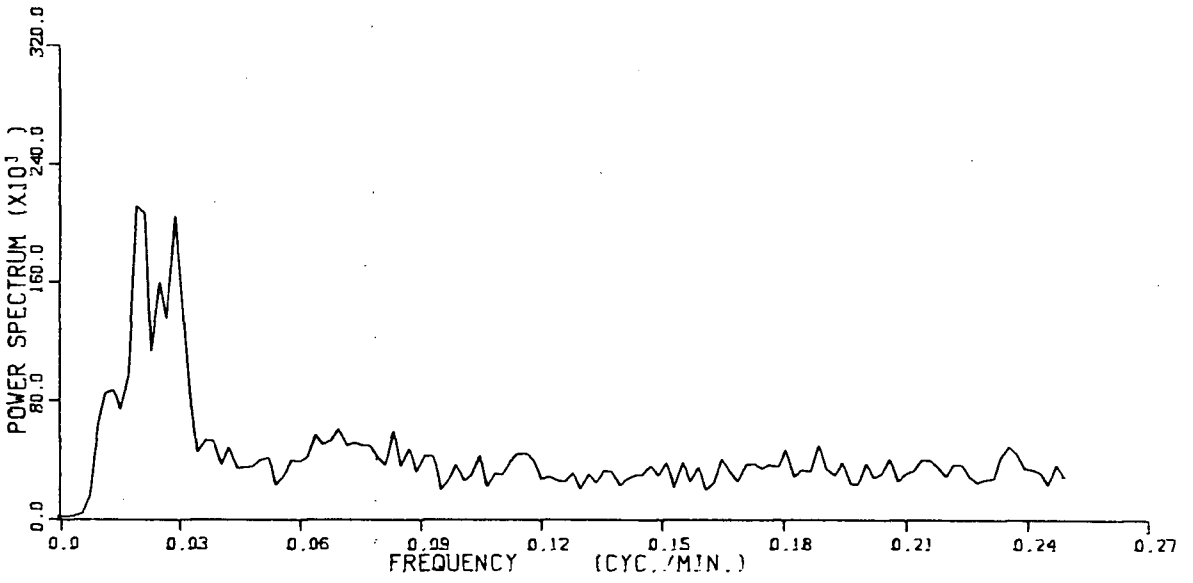

Figure 11 Power spectra of Port San Juan, January.
95% confidence interval: (0.72,1.45)*P(f)

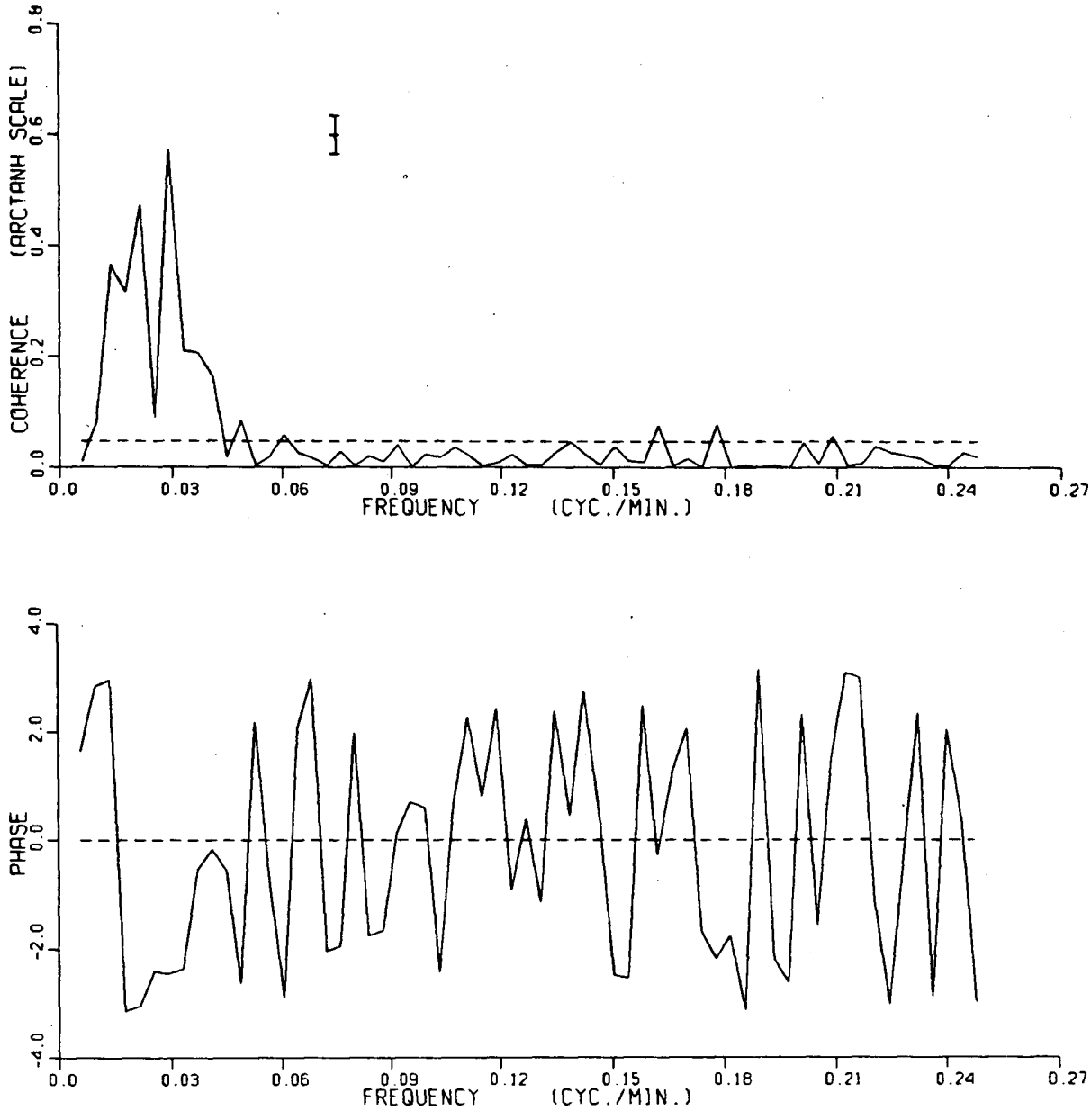

Figure 12 Coherence and phase of wave time series between Becher Bay and Port San Juan, January.
Error bars: 95% confidence intervals.
Dashed line: 95% significance level

for the three bays. The one-day ensemble-averaged spectra beginning from Jan. 28, 1980 are shown in Figure 16 to Figure 18. The spectral series of Pedder Bay and Becher Bay have obvious peaks at the resonant frequencies (confirmed by numerical model in Chapter 4), the corresponding period ranges are centered at 11 and 13 minutes, The spectral series of Port San Juan displays more disorder; only in the first and last three daily spectra does the energy appear concentrated in well-defined peaks within the period range about 30 to 40 minutes. There were several days centered on Feb. 2 when the spectra of all three bays were much more energetic than during the relatively calmer days, but high frequency band peaks could be seen only in Port San Juan. Figure 19 to Figure 21 show the ensemble averages of spectra for the complete 20-day period, i.e. the averages of 60 spectra of every bay respectively, with the corresponding 60 time series beginning Jan. 28, 1980 and lasting 20 days, every set contains 256 data points representing 8 hours 32 minutes, In Pedder Bay and Becher Bay the 11 minutes and 13 minutes period peaks are very remarkable, in Port San Juan the frequency band over 0,04 cycle per minute (25 minutes period) contains a large quantity of energy. Figure 22 shows the coherence and phase of time series of Pedder Bay and Becher Bay, Figure 23, Pedder Bay and Port San Juan, Figure 24, Becher Bay and Port San Juan. The coherences were estimated by taking frequency band-average. Figure 22 reveals that the correlated periods are more than one hour

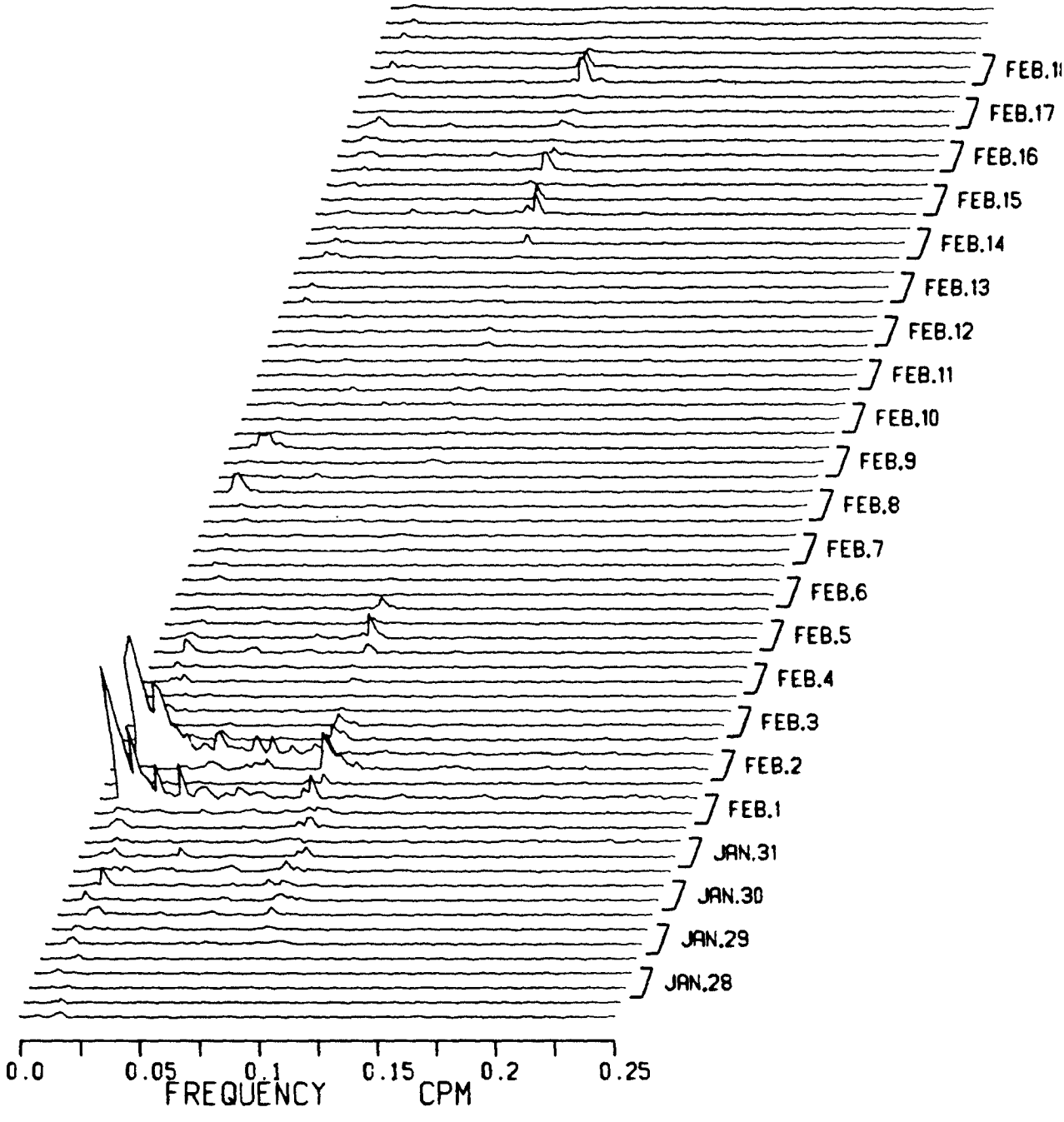

Figure 13 8-hour wave spectra of Pedder Bay, February.

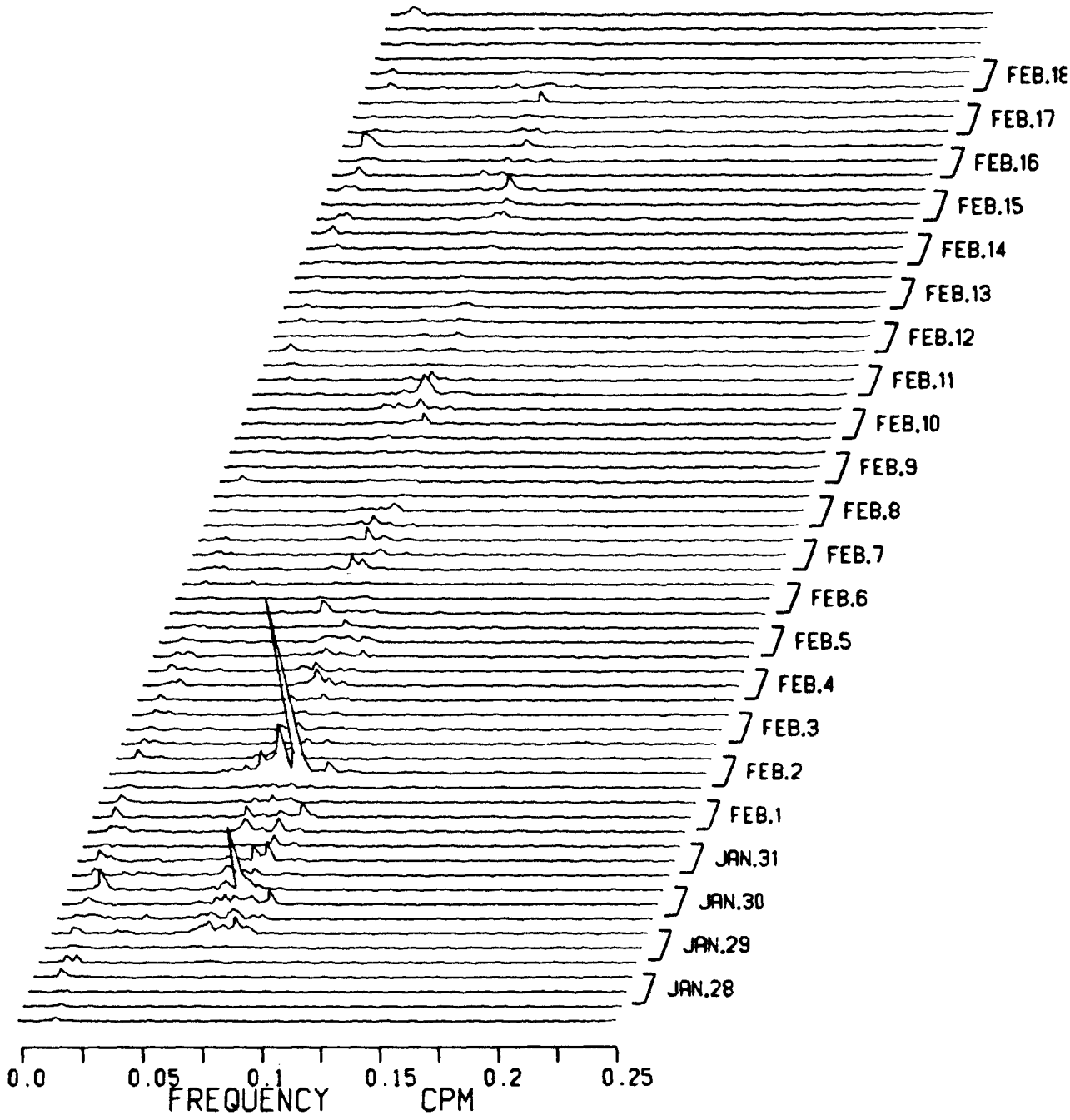

Figure 14 8-hour wave spectra of Becher Bay, February.

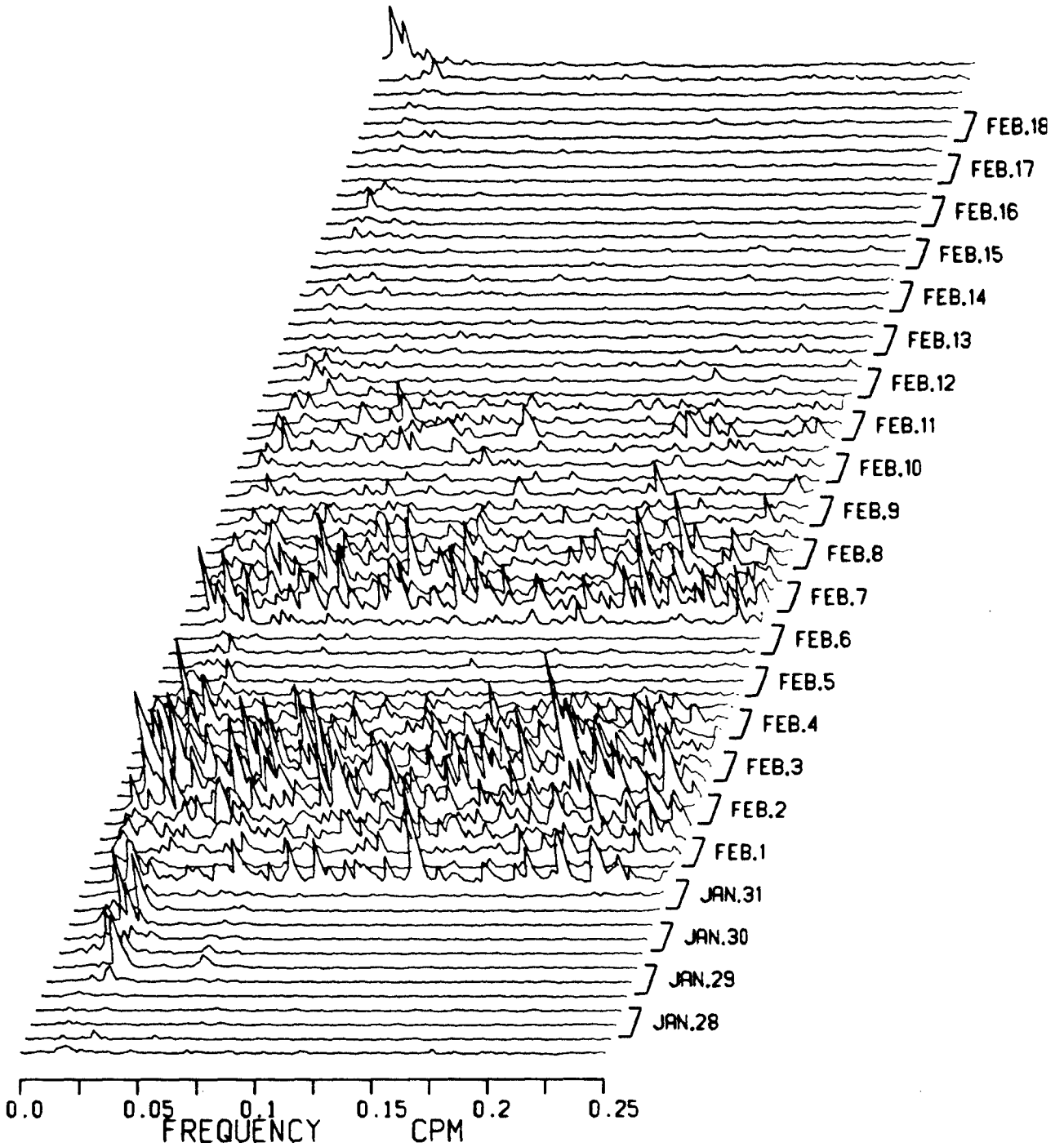

Figure 15 8-hour wave spectra of Port San Juan, February.

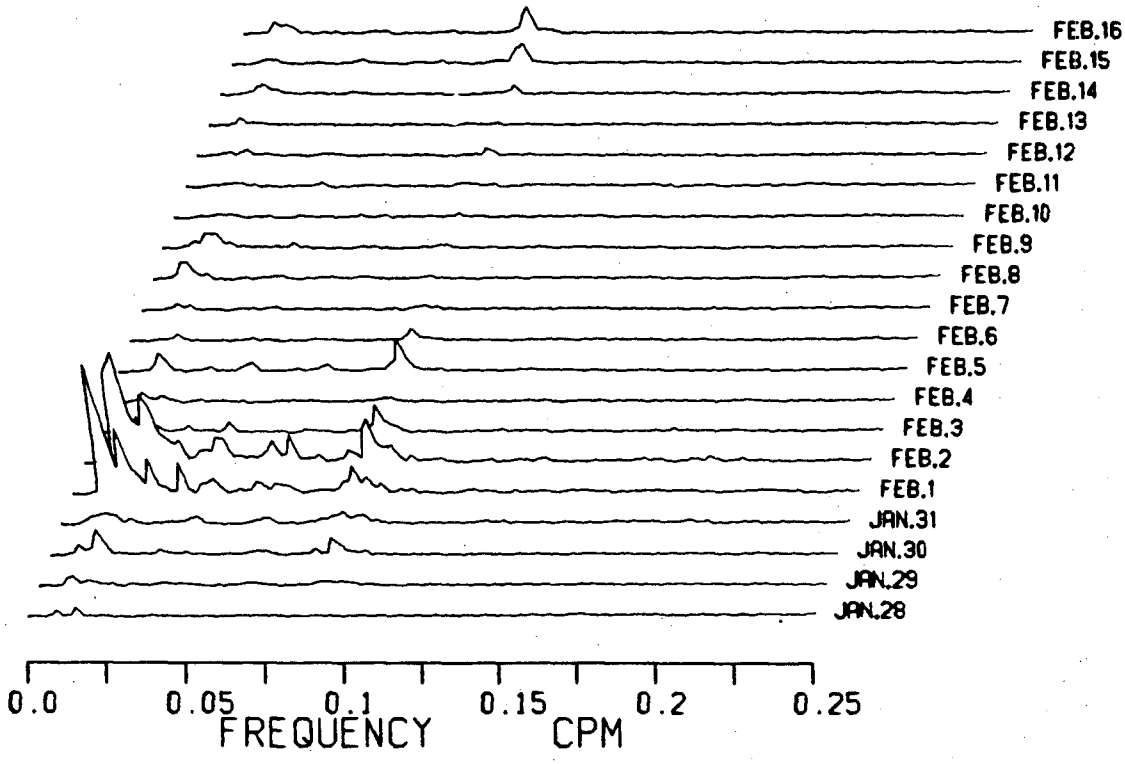

Figure 16 Daily spectra of Pedder Bay, February.

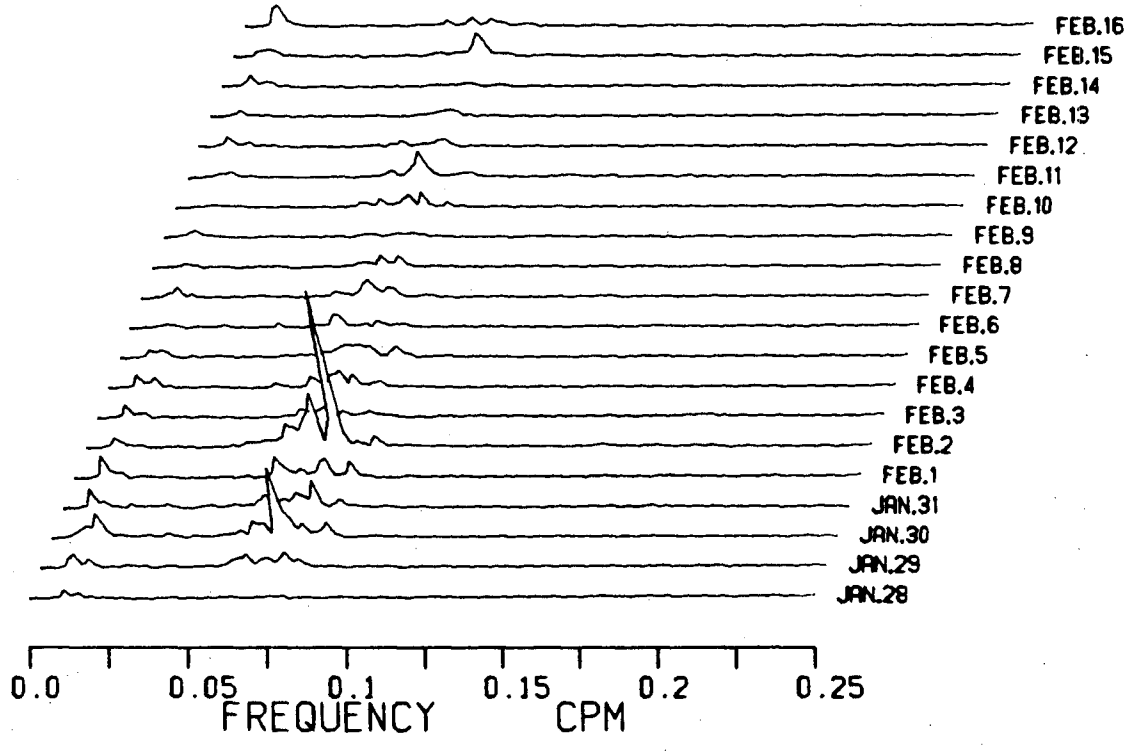

Figure 17 Daily spectra of Becher Bay, February.

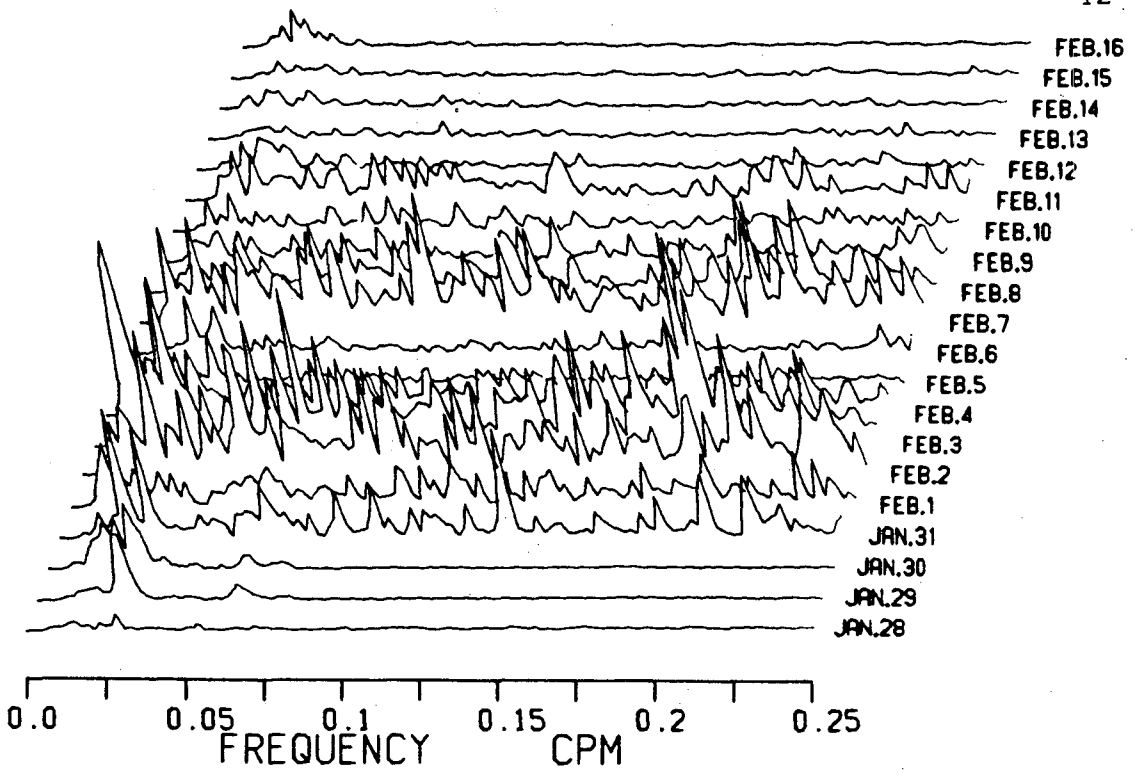

Figure 18 Daily spectra of Port San Juan, February.

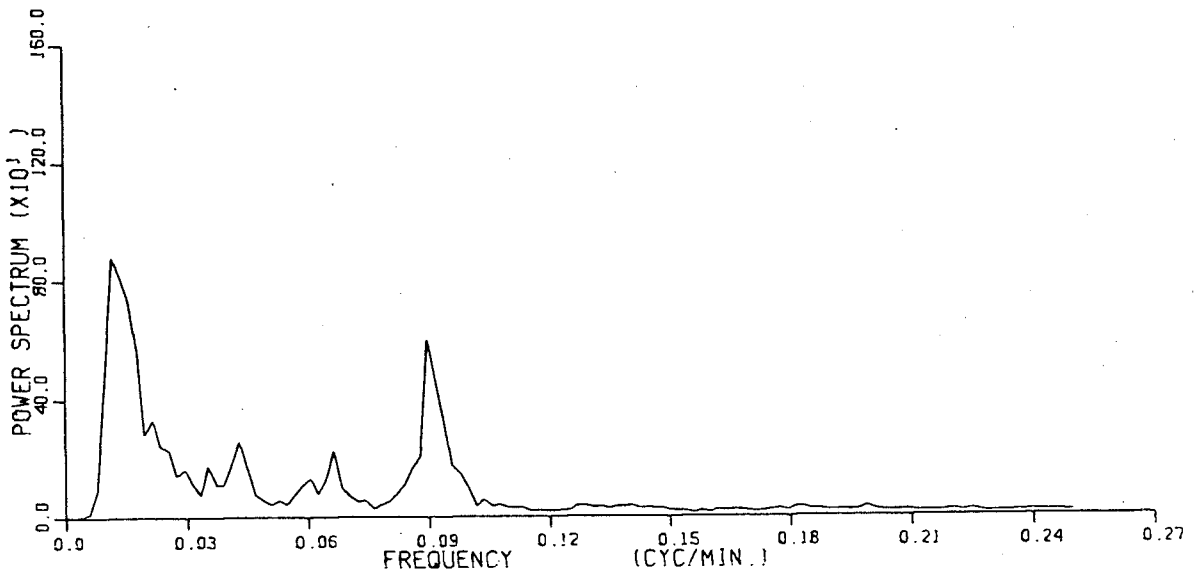

Figure 19 20-day averaged power spectra of Pedder Bay.
95% confidence interval: (0.79,1.31)*P(f)

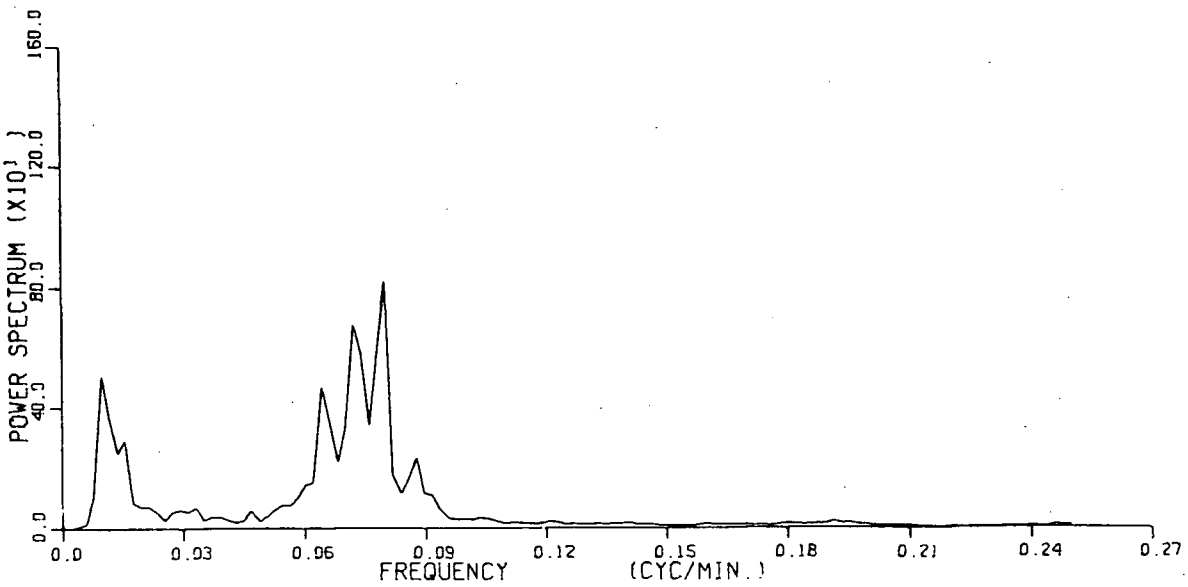

Figure 20 20-day averaged power spectra of Becher Bay.
95% confidence interval: (0.79,1.31)*P(f)

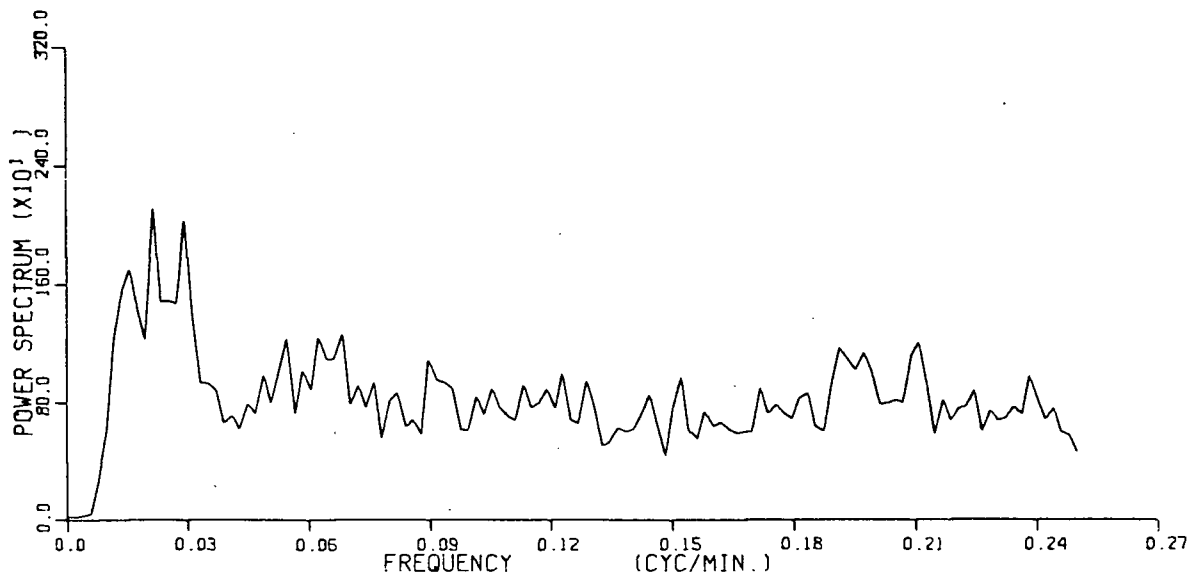

Figure 21 20-day averaged power spectra of Port San Juan.
95% confidence interval: (0.79,1.31)*P(f)

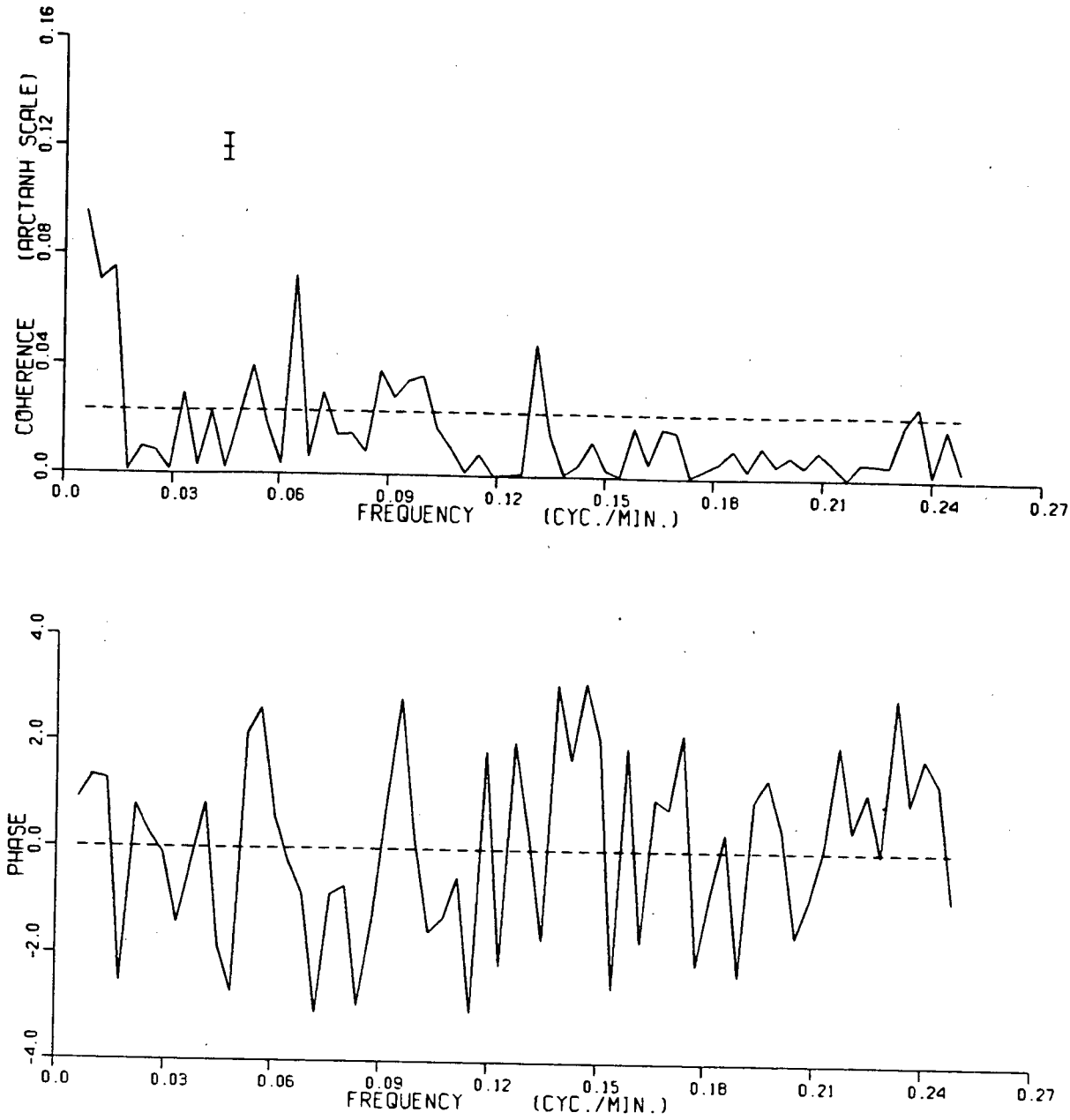

Figure 22 Coherence and phase of wave time series between Pedder Bay and Becher Bay, February.
Error bars: 95% confidence intervals.
Dashed line: 95% significance level

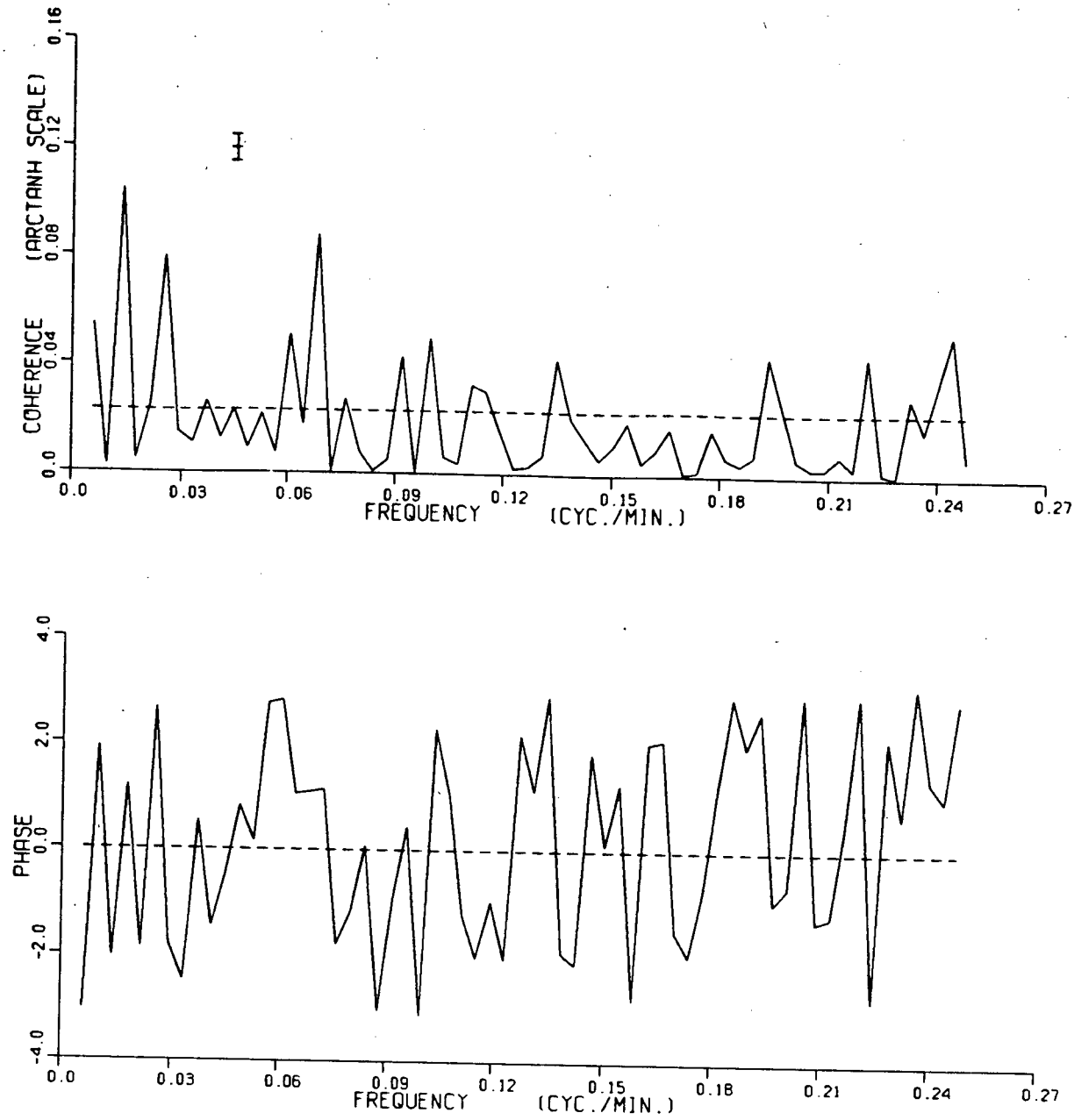

Figure 23 Coherence and phase of wave time series between Pedder Bay and Port San Juan, February.
Error bars: 95% confidence intervals.
Dashed line: 95% significance level

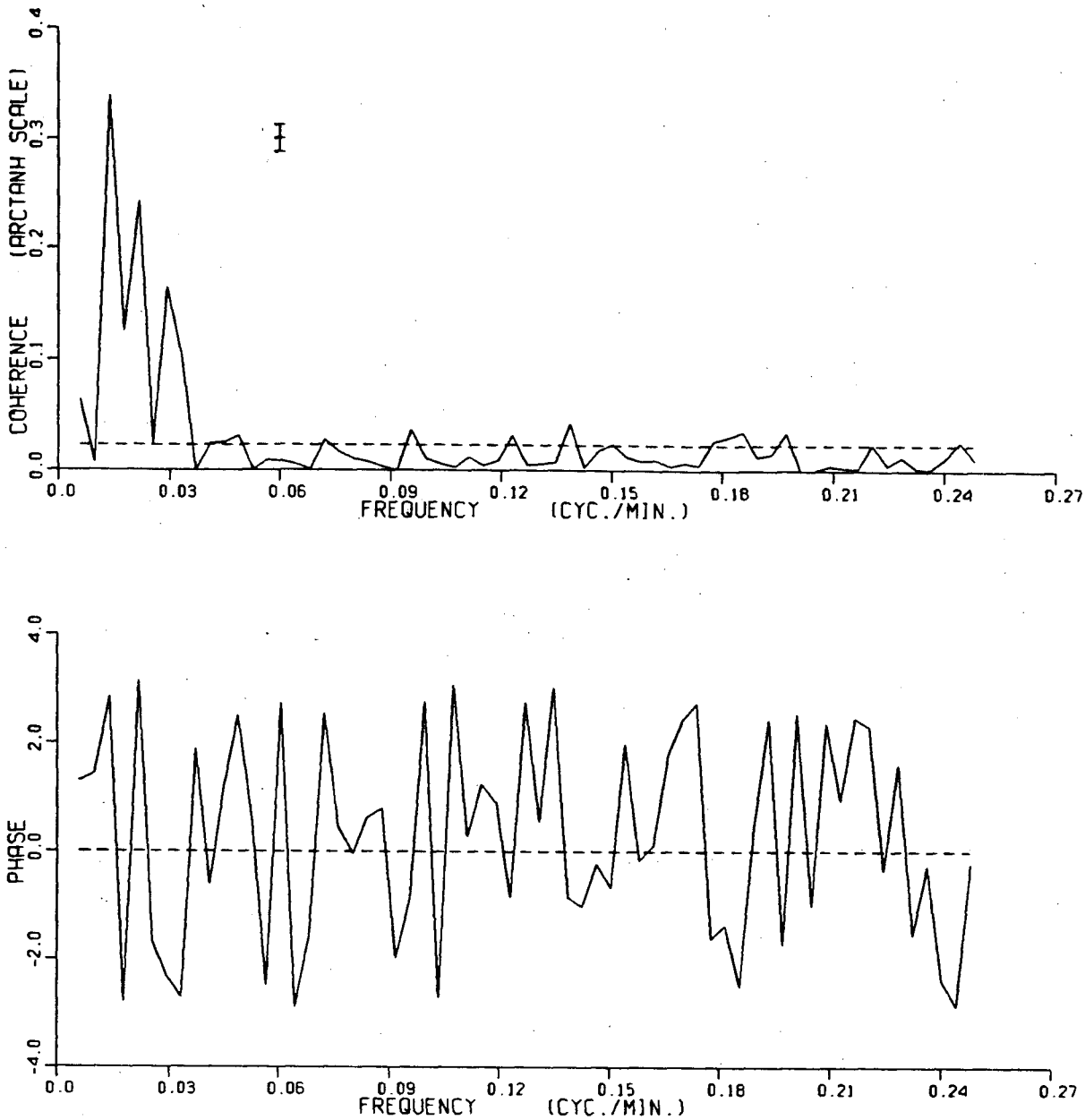

Figure 24 Coherence and phase of wave time series between Becher Bay and Port San Juan, February.
Error bars: 95% confidence intervals.
Dashed line: 95% significance level

and 15, 10-12, 7.5 minutes, the range of periods 10 to 15 covers the resonant periods of the two bays. Figure 23 shows that the correlated periods cover a wide range. Figure 24 shows predominant peaks at low frequency band with corresponding periods 30 to 80 minutes; it may be compared with Figure 21: the peaks occur at same frequency band in the power spectrum of Port San Juan as in the coherence between Becher Bay and Port San Juan, there is random noise throughout high frequency band in power spectrum, meanwhile it is greatly reduced in coherence. Keeping it in mind that the mouths of these two bays open on the same strait at the same coast line, it is logical to assume that the low frequency fluctuations of the two bays may be excited by common external forcing sources, such as edge waves, travelling along the coast line and passing across the mouths. The high frequency fluctuation of the two bays are not correlated.

The above analysis describes the general features of the spectra in those three bays. The ensemble averages throw light on these general features. The coherences imply common exciting sources, which will be discussed in Chapter 6.

G. DETAILED EXAMINATION OF TYPICAL SEICHES

By visual examination of all the data it was found that the seiche occurs at any stage of tide cycle; sometimes it is very strong, sometimes it disappears. The typical seiches had well defined frequencies and often observed in these

three bays, which revealed the different resonant frequencies of these three bays.

The typical seiches were found in all the three bays. These oscillations are typical to reveal the wave response characteristics of every bay. Four sets of 500 minutes time series were selected to look into this feature; they are described in Table 2

Table 2 Data of Typical Seiches (500 min.)

	start time and date	bays	typical period
1st set	00:00 18 Feb., 1980	Pedder	11
2nd set	09:20 2 Feb., 1980	Becher	13
3rd set	18:40 29 Jan., 1980	San Juan	33
4th set	10:40 11 Feb., 1980	San Juan	13-15

Figure 25 to Figure 28 are these unfiltered time series. The time series were chosen from stages of both high tide and low tide . Figure 29 to Figure 32 are the same time series, from which the low frequency components associated with tides were removed by a Butterworth filter. Figure 29 shows the typical seiche in Pedder Bay with period about 11 minutes. Figure 30 shows the typical seiche in Becher Bay with period about 13 minutes. Figure 31 and Figure 32 show the typical seiche in Port San Juan. The first to sixth peaks in Figure 31 have average period about 33 to 34 minutes, the other peaks have roughly same periods. Figure 32 shows seiches with period range about 8 to 15 minutes.

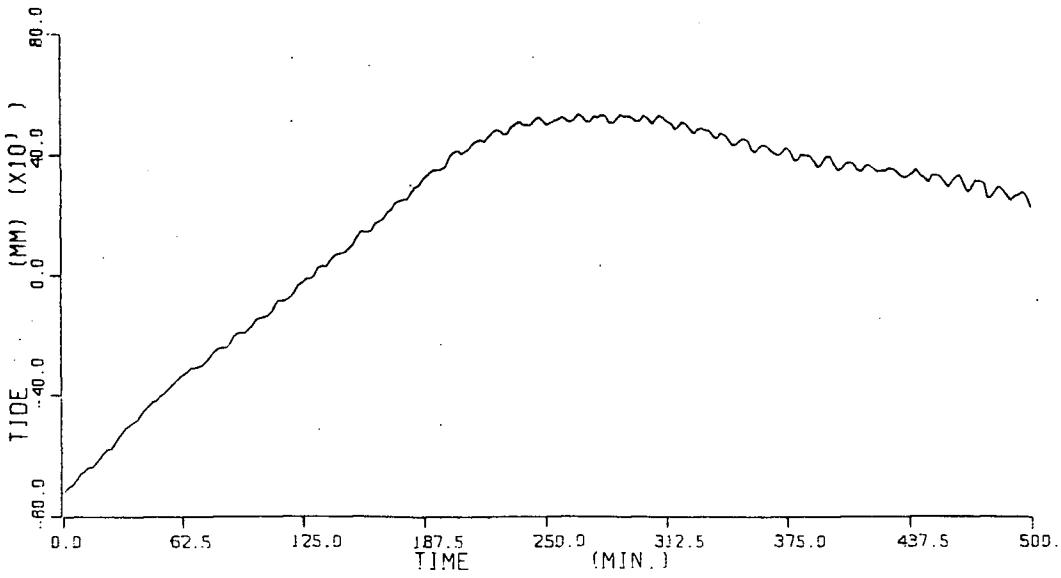

Figure 25 Wave time series beginning at 00:00 Feb. 18, 1980 in Pedder Bay.

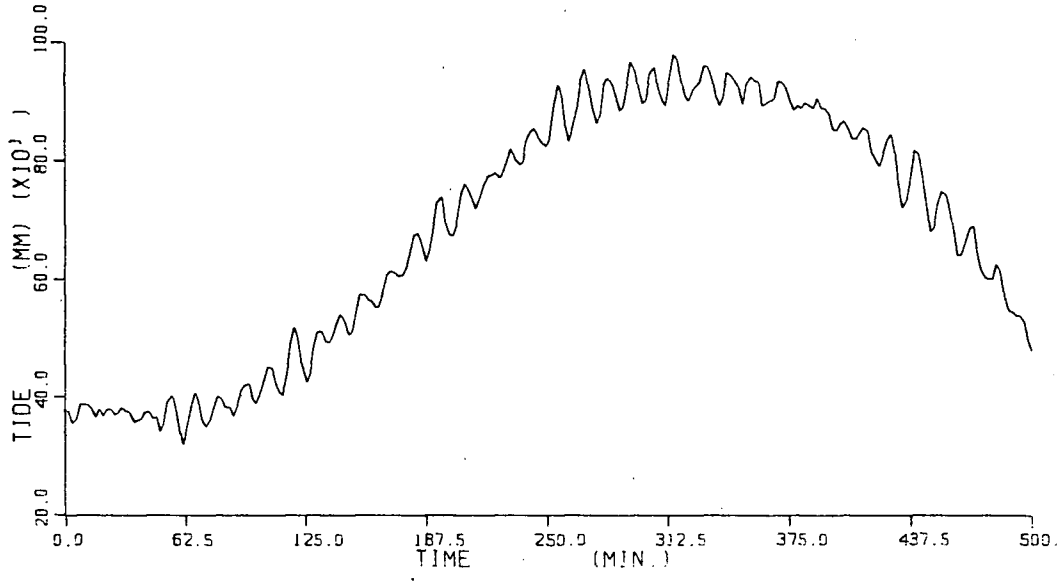

Figure 26 Wave time series beginning at 09:20 Feb. 2, 1980 in Becher Bay.

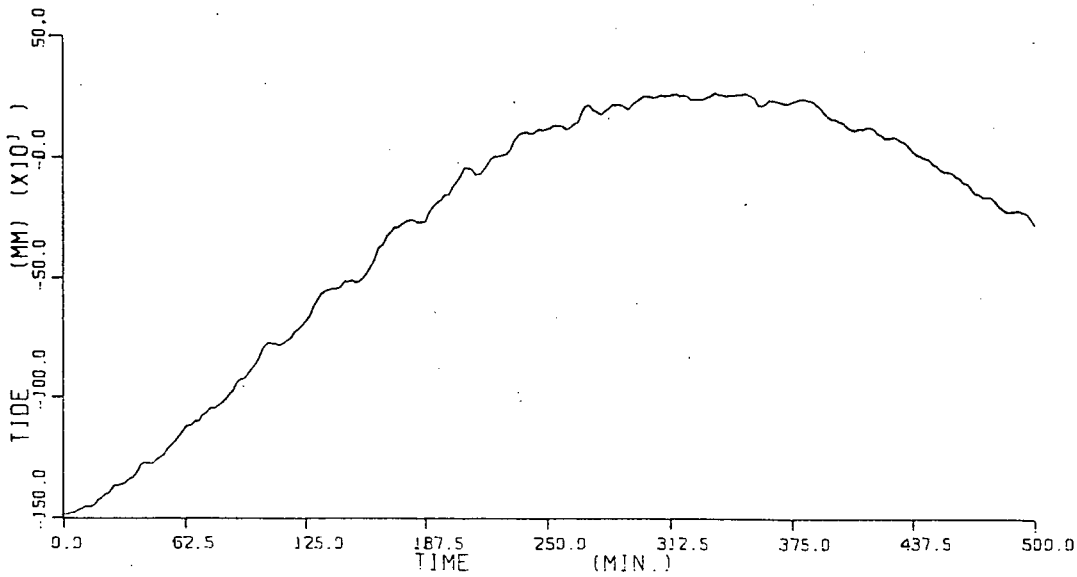

Figure 27 Wave time series beginning at 18:40 Jan. 29, 1980 in Port San Juan.

Figure 28 Wave time series beginning at 10:40 Feb. 11, 1980 in Port San Juan.

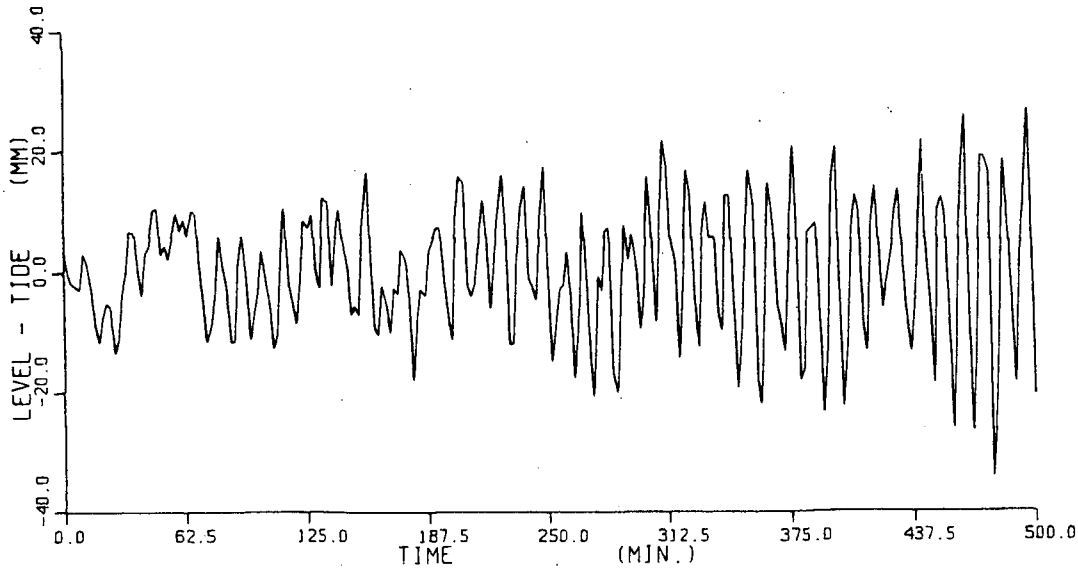

Figure 29 High frequency components of wave time series beginning at 00:00 Feb. 18, 1980 in Pedder Bay.

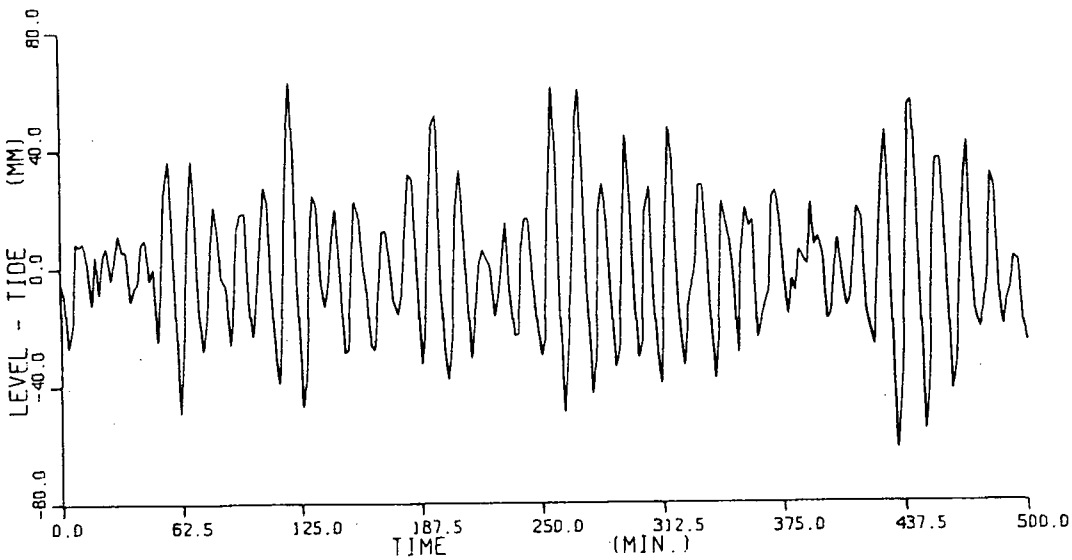

Figure 30 High frequency components of wave time series beginning at 09:20 Feb. 2, 1980 in Becher Bay.

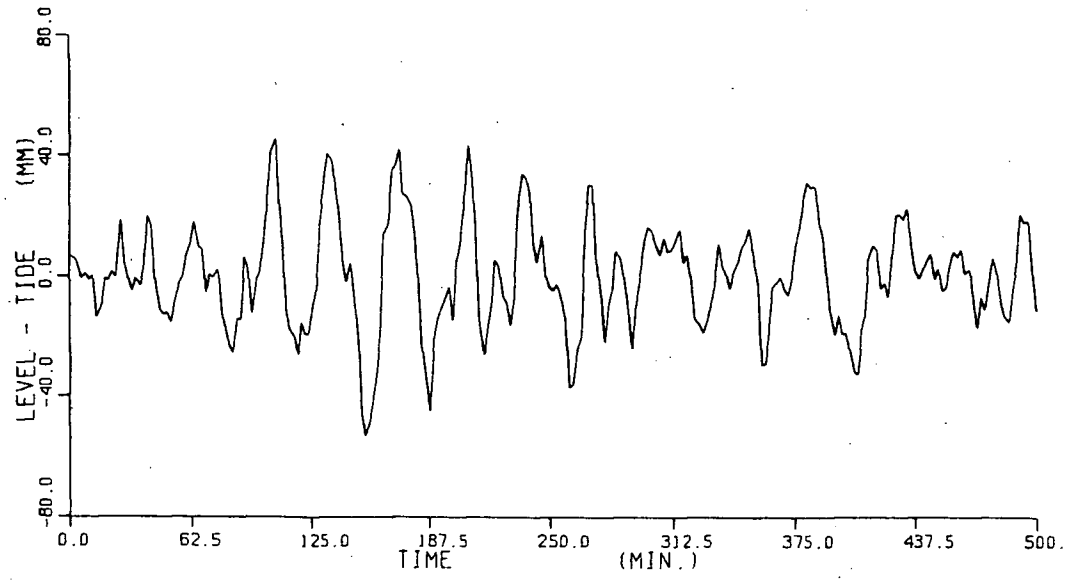

Figure 31 High frequency components of wave time series beginning at 18:40 Jan. 29, 1980 in Port San Juan.

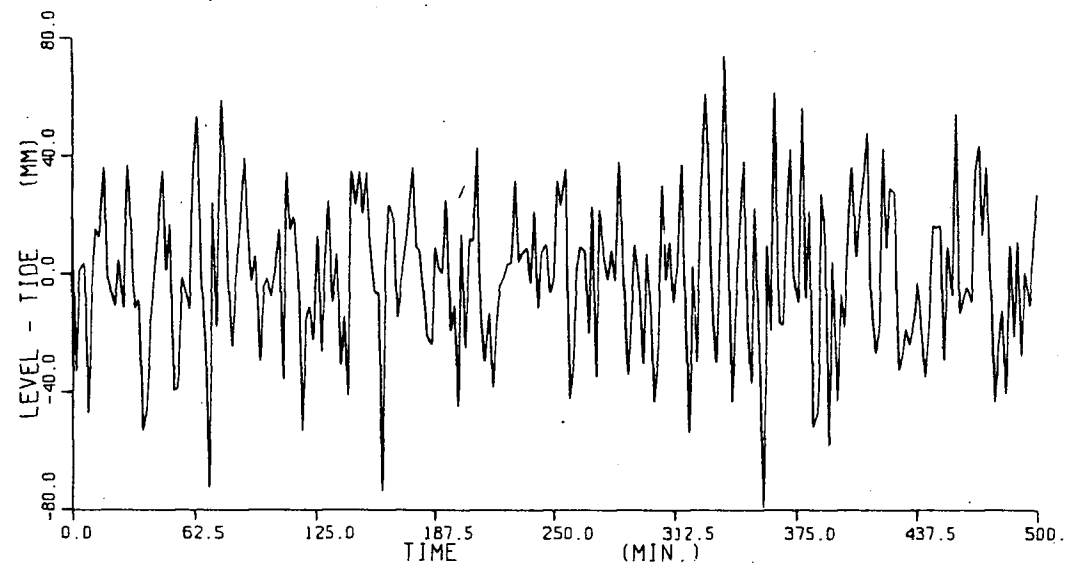

Figure 32 High frequency components of wave time series beginning at 10:40 Feb. 11, 1980 in Port San Juan.

Longer time series around those of table 2 were subject to spectral analysis to inspect the frequency signature of the strong seiches. Four sets of time series from three bays which contain the strong seiches of table 2 were selected. Each time series consists of continuous 2,048 sampling points, or 68 hours 16 minutes, and includes the time series shown in Figure 29 to Figure 32 which illustrate the typical feature of the 68-hour time series. These 68-hour data are described in Table 3

Table 3 Data of Typical Seiches (4096 min.)

	start time and date	bays	typical period
1st set	00:00 16 Feb., 1980	Pedder	11
2nd set	00:00 31 Jan., 1980	Becher	13
3rd set	00:00 28 Jan., 1980	San Juan	33
4th set	00:00 9 Feb., 1980	San Juan	13-15

The four selected time series were processed as follows. First, power spectra were calculated by Fast Fourier Transformation and 1,025 spectral coefficients were obtained for each series at the frequencies:

$$F_n = \frac{n}{4,096} \qquad n=0,1,2, \ldots\ldots, 1,024$$

Then from F_1 to F_{1024} every 8 successive coefficients were averaged and set to the central frequency, i.e. the coefficient

$$\tilde{F}_k = \frac{1}{8} \sum_{i=8k-7}^{8k} F_i$$

was attributed to the frequency

$$f_k = \frac{k}{512} - \frac{3.5}{8.0} \cdot \frac{1}{512}$$

These band-averaged frequencies give equivalent result to the ensemble averaging method (Bendat and Piersol, 1971).

Figure 33 to Figure 36 show the four band-averaged frequency spectra.

H. THE SHIFT OF RESONANT PERIOD BETWEEN HIGH AND LOW TIDE STAGES

According to Merian's formula (LeBlond and Mysak, 1978. p.293) the resonant frequency changes with the variation of water depth of a bay, namely with the stage of tide levels. Therefore I examined seiche activity at high and low tides respectively. Twelve time series were chosen from high and low tide levels respectively in each bay. Figure 37 to Figure 39 show at what tidal stage the time series were picked up for analysis. Each time series lasts four hours and 16 minutes. The origin of the X-axis stands for the time 00:00 Jan. 27, 1980. At high tide levels the selected data sets in Becher Bay are 16 minutes earlier than those in Pedder Bay; in Port San Juan, 32 minutes earlier than those in Pedder bay. At low tide levels the data sets in Becher Bay are 32 minutes earlier than those in Pedder Bay; in Port

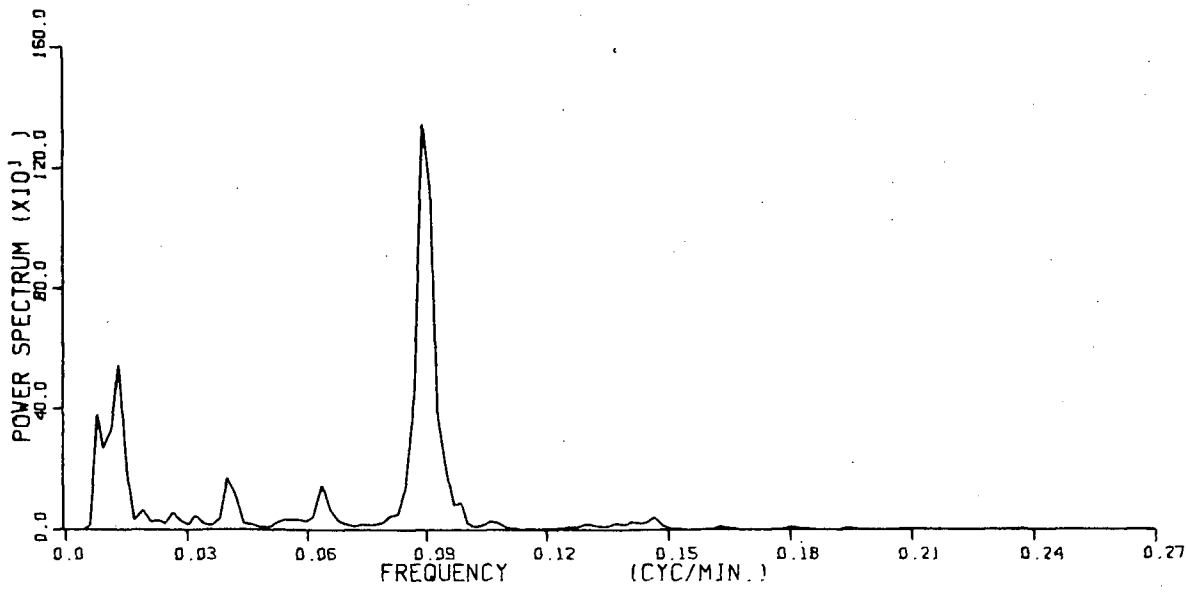

Figure 33 Power spectrum of strong seiche of Pedder Bay.
95% confidence interval: (0.55,2.32)*P(f)

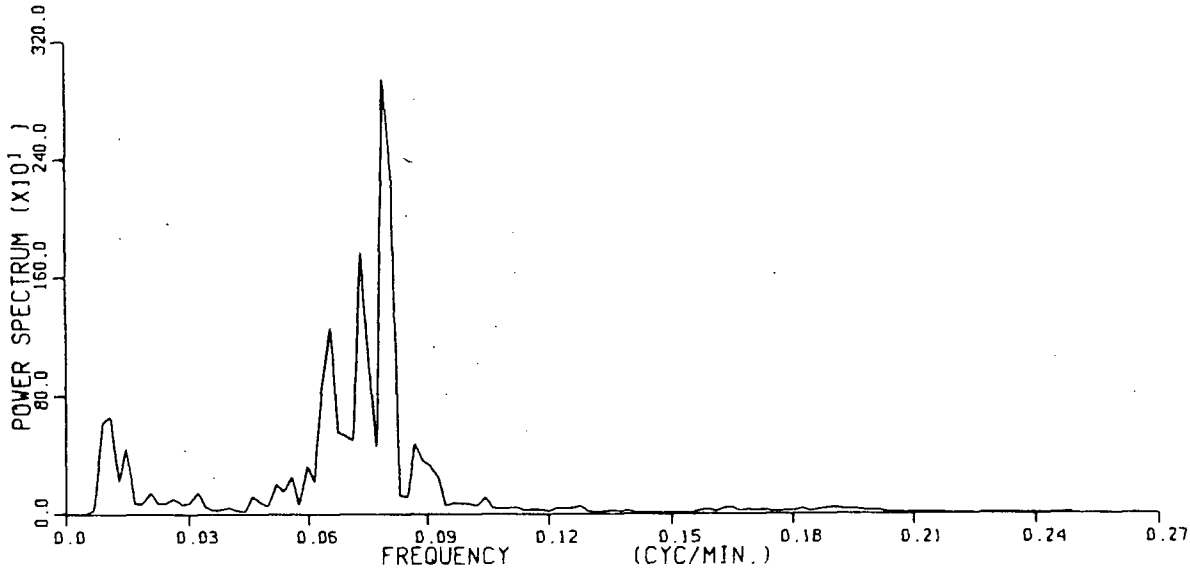

Figure 34 Power spectrum of strong seiche of Becher Bay.
95% confidence interval: (0.55,2.32)*P(f)

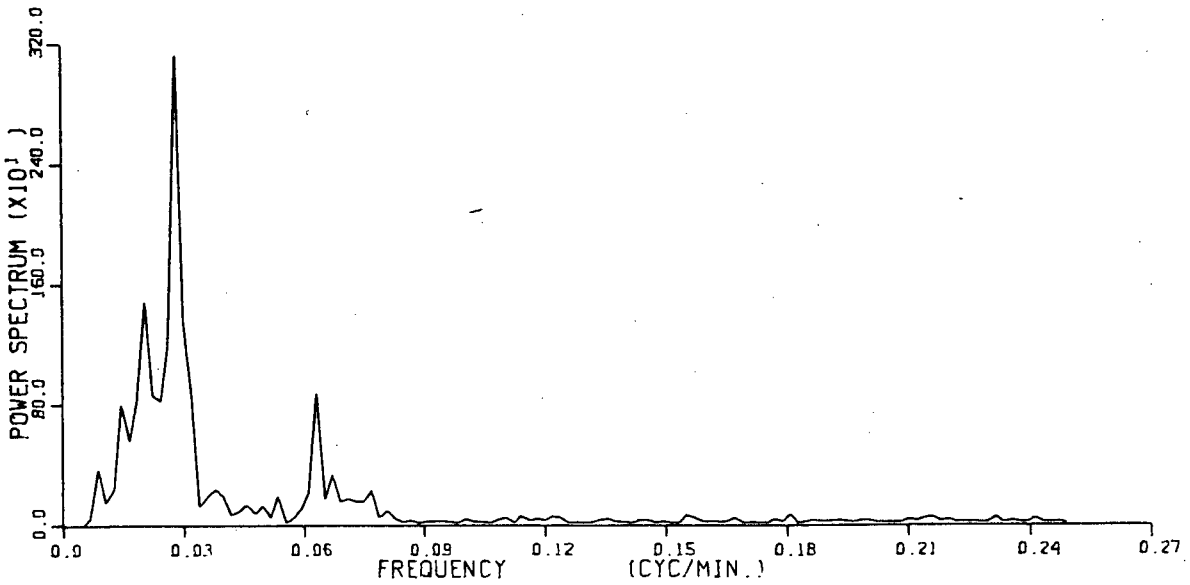

Figure 35 Power spectrum of strong seiche of Port San Juan (1).
95% confidence interval: (0.55,2.32)*P(f)

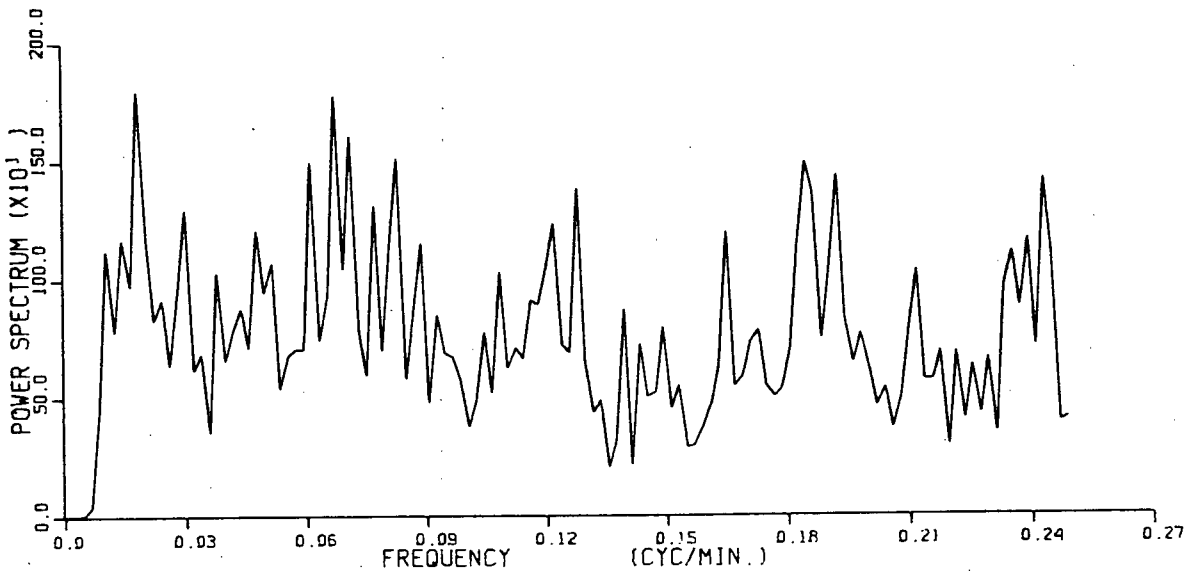

Figure 36 Power spectrum of strong seiche of Port San Juan (2).
95% confidence interval: (0.55,2.32)*P(f)

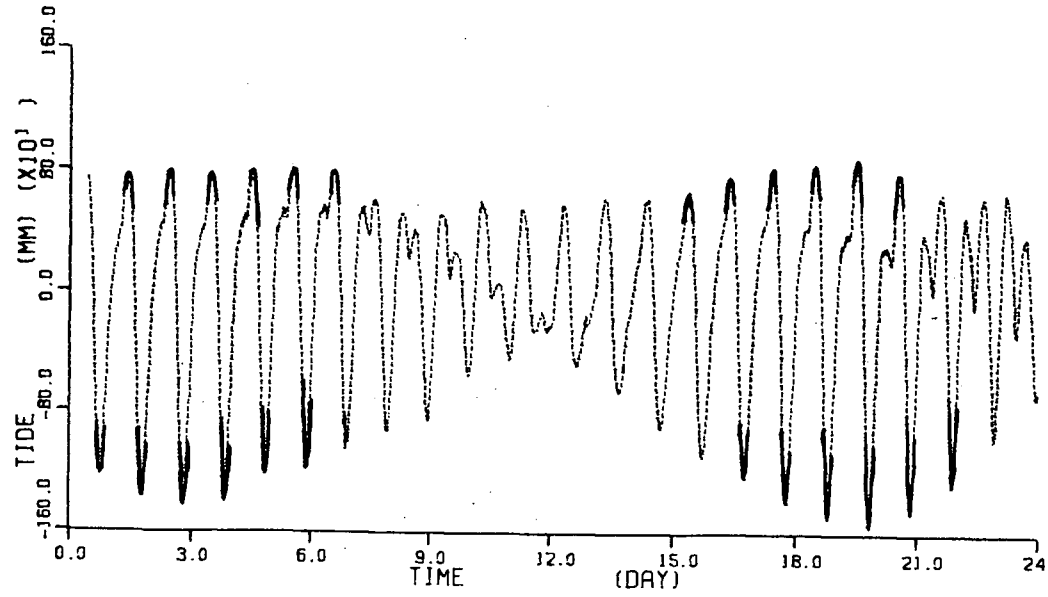

Figure 37 Tides in Pedder Bay, dotted line: whole tidal data; thick line: selected time series.

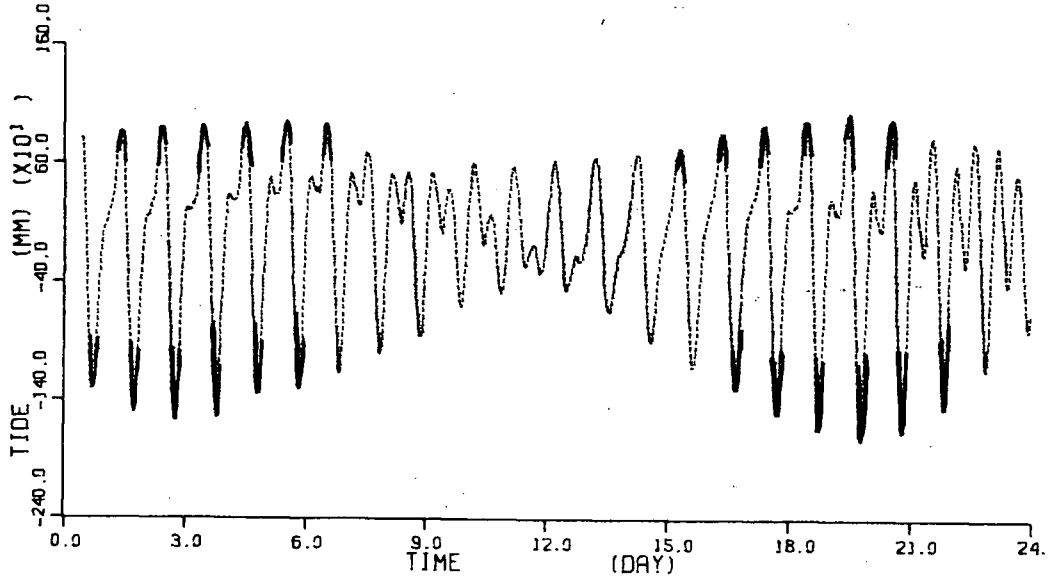

Figure 38 Tides in Becher Bay, dotted line: whole tidal data; thick line: selected time series.

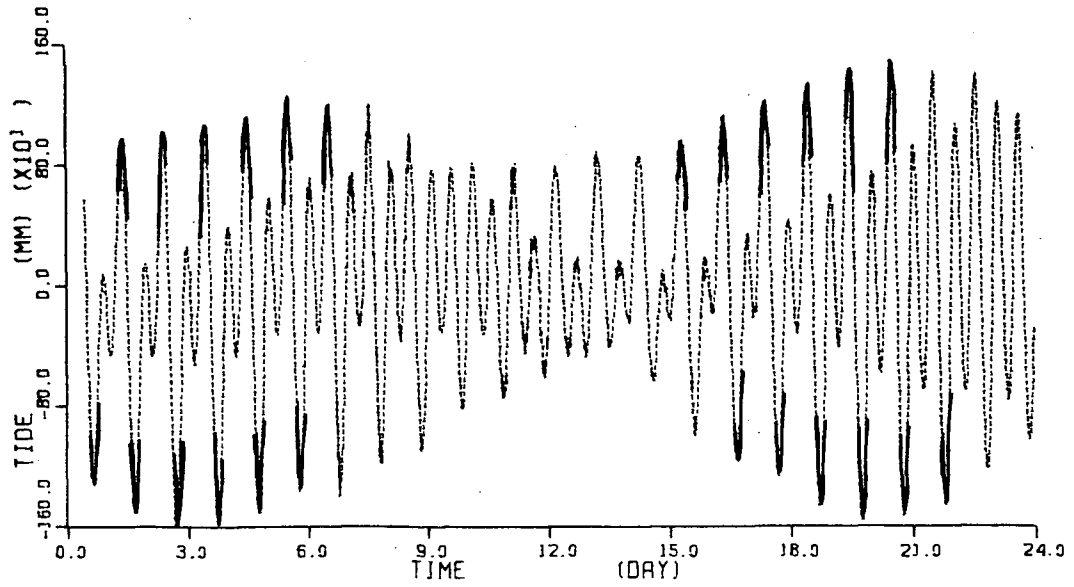

Figure 39 Tides in Port San Juan, dotted line: whole tidal data; thick line: selected time series.

San Juan, 80 minutes earlier than those in Pedder bay. This treatment could position the individual time series at central high or low tide levels and maintain constant time lags in different bays at high and low tide levels respectively. The time differences are the rough estimates of time interval for tide to travel from one bay to the other, which were obtained from visual examination of original time series in Figure 37 to Figure 39.

Figure 40 shows the power spectra of each time series at low tide level in the three bays. Figure 41 to Figure 43 show ensemble averages of 12 time series in the three bays. In Pedder Bay the 11 minutes period peak of Figure 33 is not prominent in Figure 41; rather, a low frequency peak predominates. Looking back to Figure 40 a large low

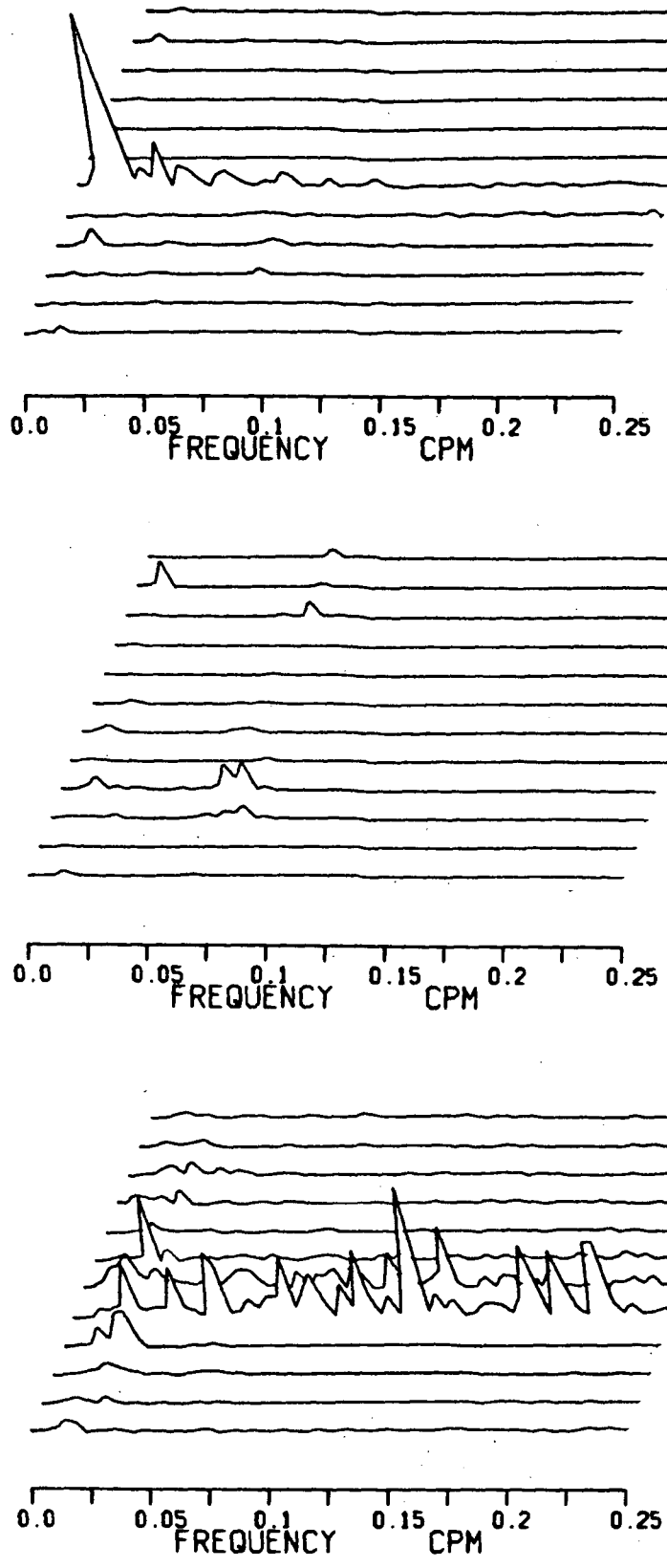

Figure 40 Power spectra of selected low tides of Pedder Bay (upper), Becher Bay (middle) and Port San Juan (lower).

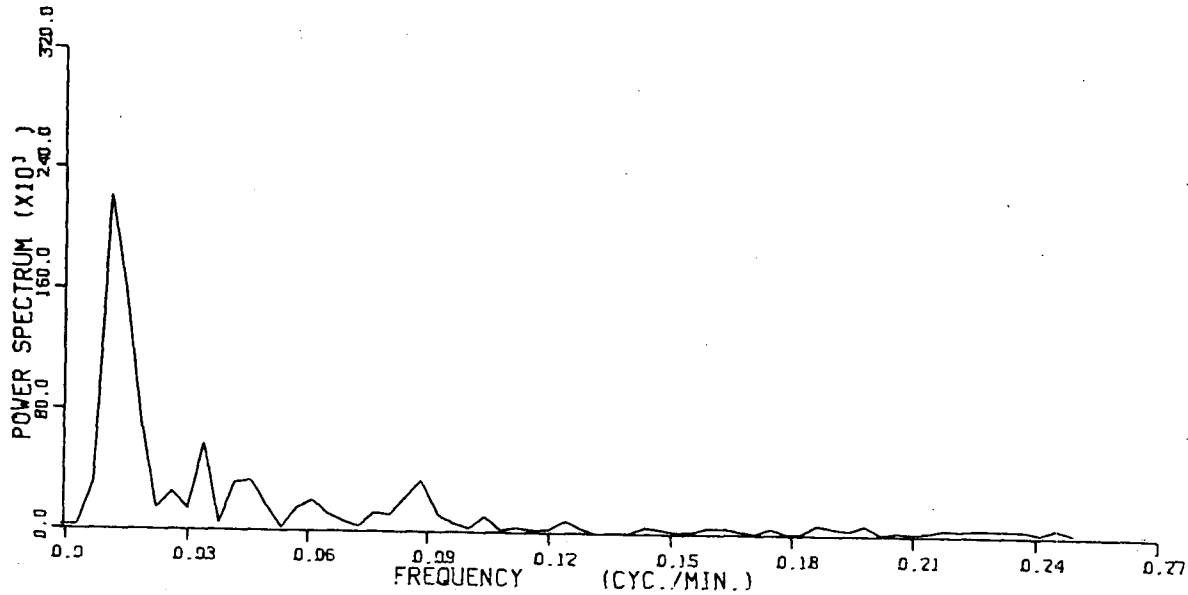

Figure 41 Averaged power spectrum of selected low tides of Pedder Bay.
95% confidence interval: (0.61,1.94)*P(f)

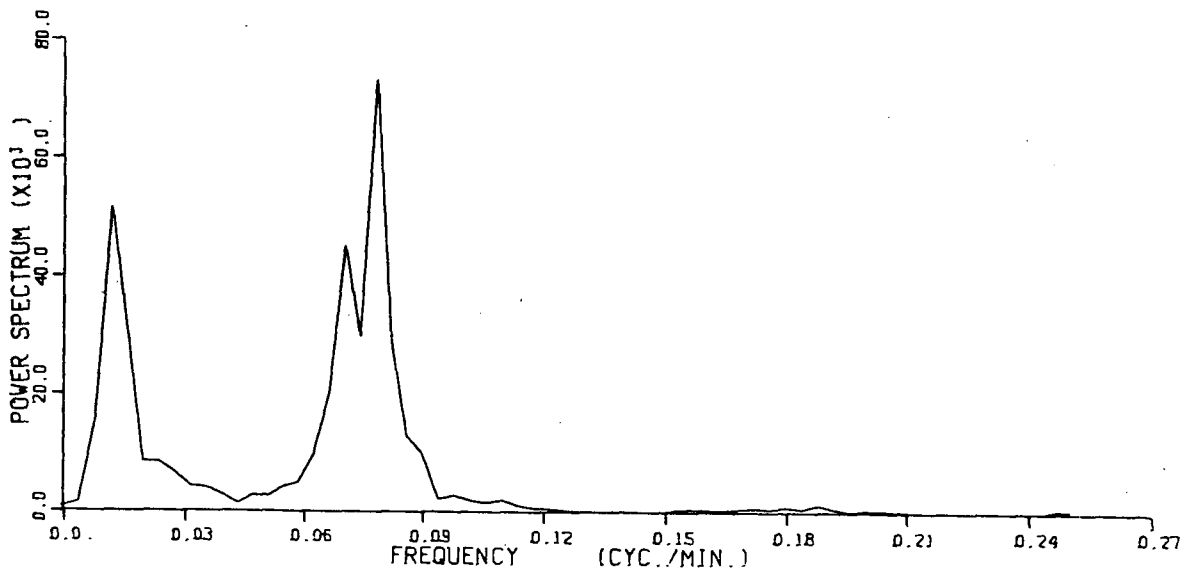

Figure 42 Averaged power spectrum of selected low tides of Becher Bay.
95% confidence interval: (0.61,1.94)*P(f)

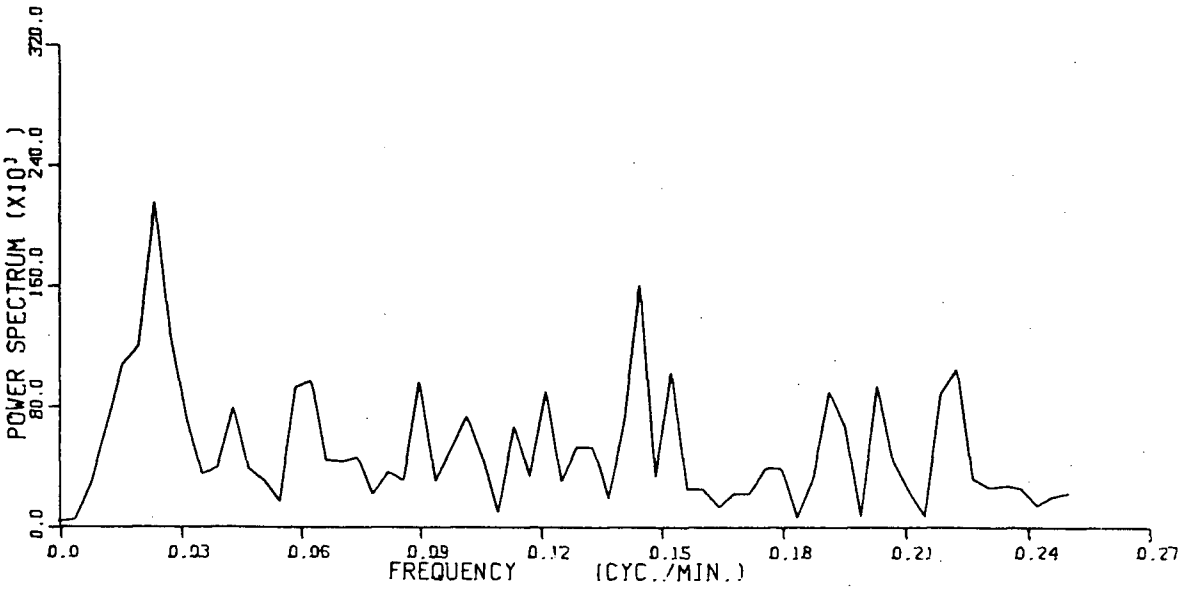

Figure 43 Averaged power spectrum of selected low tides of Port San Juan.
95% confidence interval: (0.61,1.94)*P(f)

frequency peak appears in spectra of Pedder Bay in the sixth spectum, which may be excited by external forcing. Figure 42 shows a predominant peak at about 13 minutes period. Figure 43 shows a somewhat random spectrum in Port San Juan, similar to the spectra of this bay we dealt with before. Figure 44 to Figure 46 show the coherences of Pedder Bay versus Becher Bay, Pedder Bay versus Port San Juan and Becher Bay versus Port San Juan respectively. Some large peaks appear in high frequency band which may be caused by same high frequency external forcing.

At high tides, the perspective view of spectral series is shown in Figure 47. Comparing with Figure 40 the peaks at the resonant frequencies of Pedder Bay and Becher Bay are much more obvious. Figures 48 to 50 show ensemble averaged

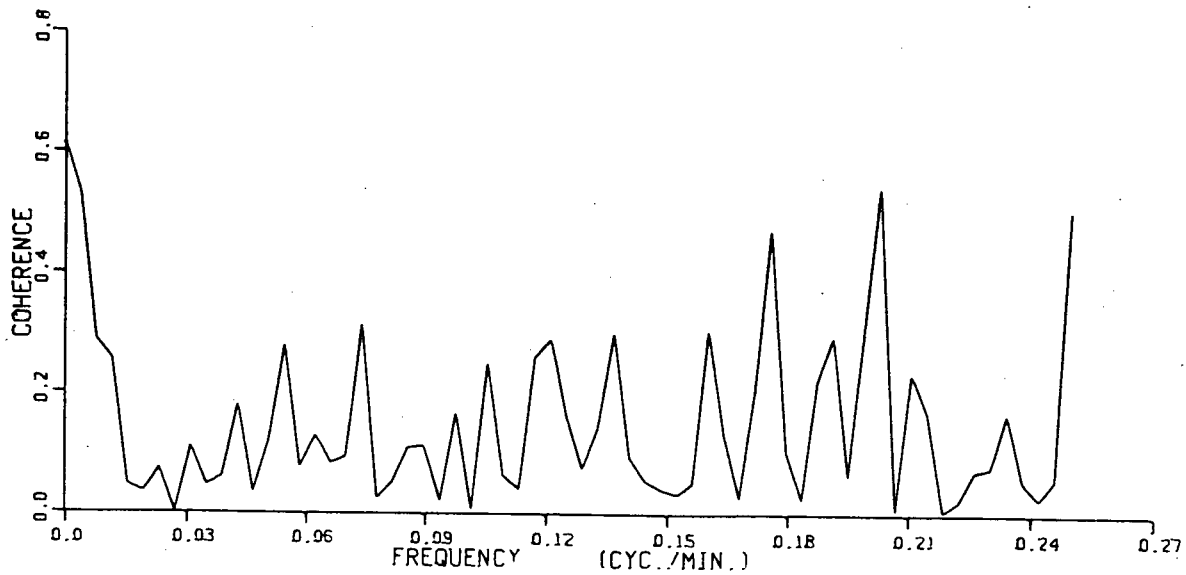

Figure 44 Coherence of selected low tides, Pedder Bay versus Becher Bay.

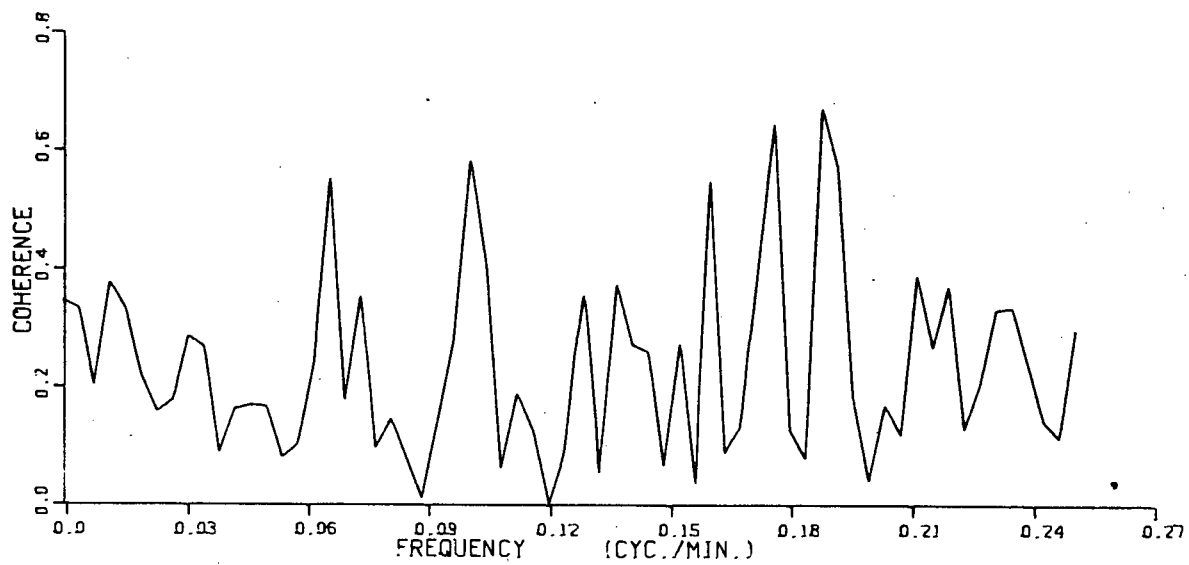

Figure 45 Coherence of selected low tides, Pedder Bay versus Port San Juan.

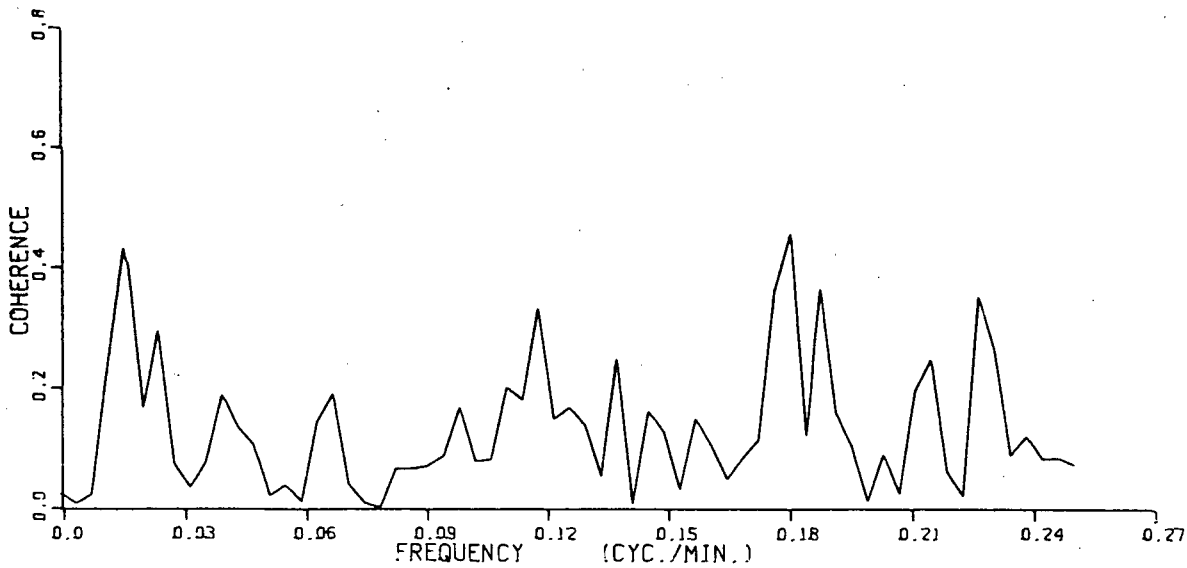

Figure 46 Coherence of selected low tides, Becher Bay versus Port San Juan.

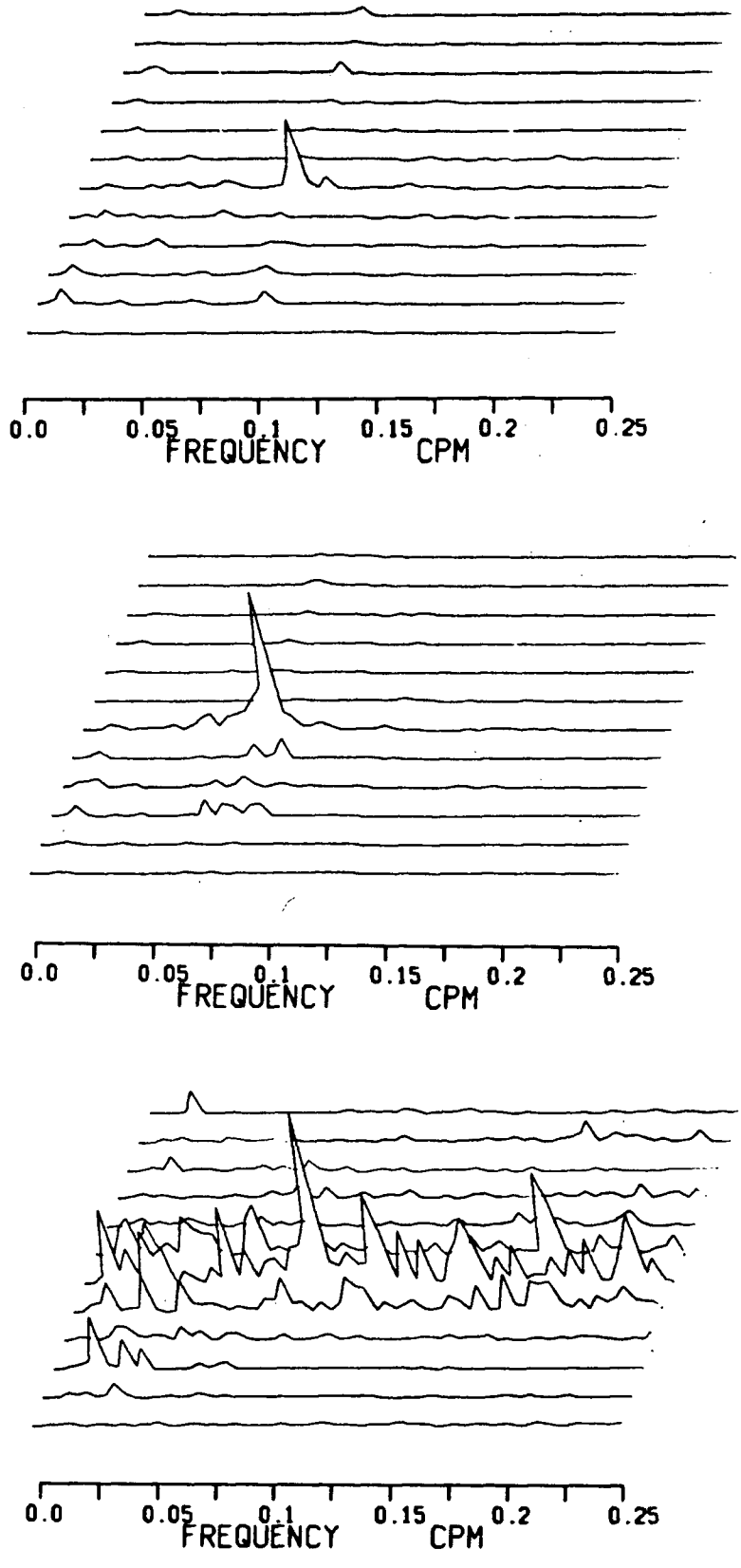

Figure 47 Power spectra of selected high tides of Pedder Bay (upper), becher Bay (middle) and Port San Juan (lower).

spectra of the 12 time series in the three bays respectively. The large peaks at the resonant frequencies of Pedder Bay and Becher Bay are pretty noticeable. Figure 51 to Figure 53 show the coherences of Pedder-Becher, Pedder-San Juan and Becher-San Juan.

Figure 54 to Figure 56 show the comparisons of ensemble averaged power spectra between low and high tide levels in the three bays respectively. In Pedder Bay and Becher Bay the peaks at resonant frequencies in high tide levels are much larger than those in low tide levels. The logical conjecture is that seiches are more easily excited at high tides; in other words, the resonant amplification factors at high tides may be larger than those at low tides.

Figures 57 to 59 compare the coherences between low and high tides of Pedder-Becher, Pedder-San Juan and Becher-San Juan. Figure 57 show a wide peak at high tides in frequency range 0.08 to 0.105 cpm or periods 12.5 to 9.5 minutes, which generally covers the range of resonant frequencies of Pedder Bay and Becher Bay. This peak suggests a common source of resonant oscillations in these two bays. But at low tides coherence is very low in same frequency range. A general feature is that low frequencies seem to be correlated at high tides, high frequencies, at low tides. Figure 58 shows several peaks at low tides, two of them are at periods 10 and 14 minutes. Figure 59 shows many sharp peaks at high tides. The oscillations at these frequencies may be generated by waves propagating in Juan de Fuca

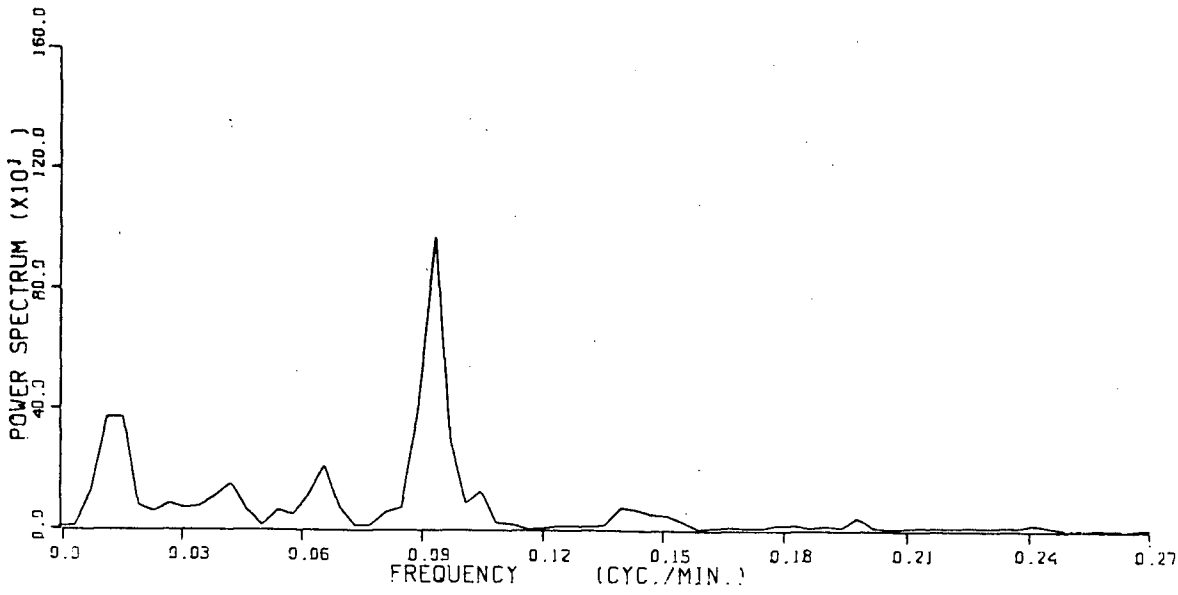

Figure 48 Averaged power spectrum of selected high tides of Pedder Bay.
95% confidence interval: (0.61,1.94)*P(f)

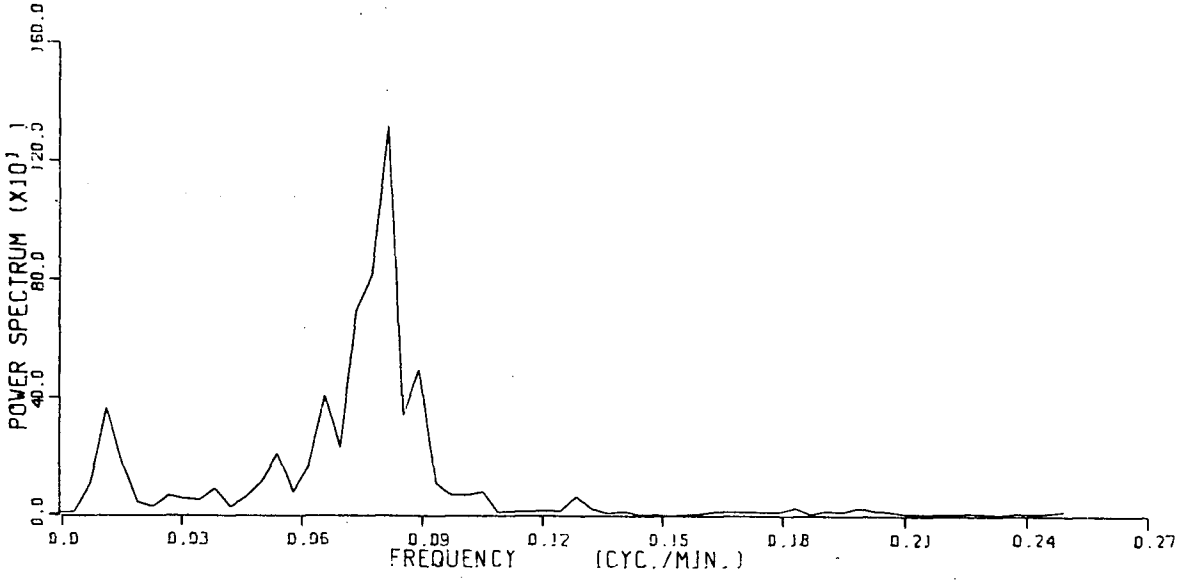

Figure 49 Averaged power spectrum of selected high tides of Becher Bay.
95% confidence interval: (0.61,1.94)*P(f)

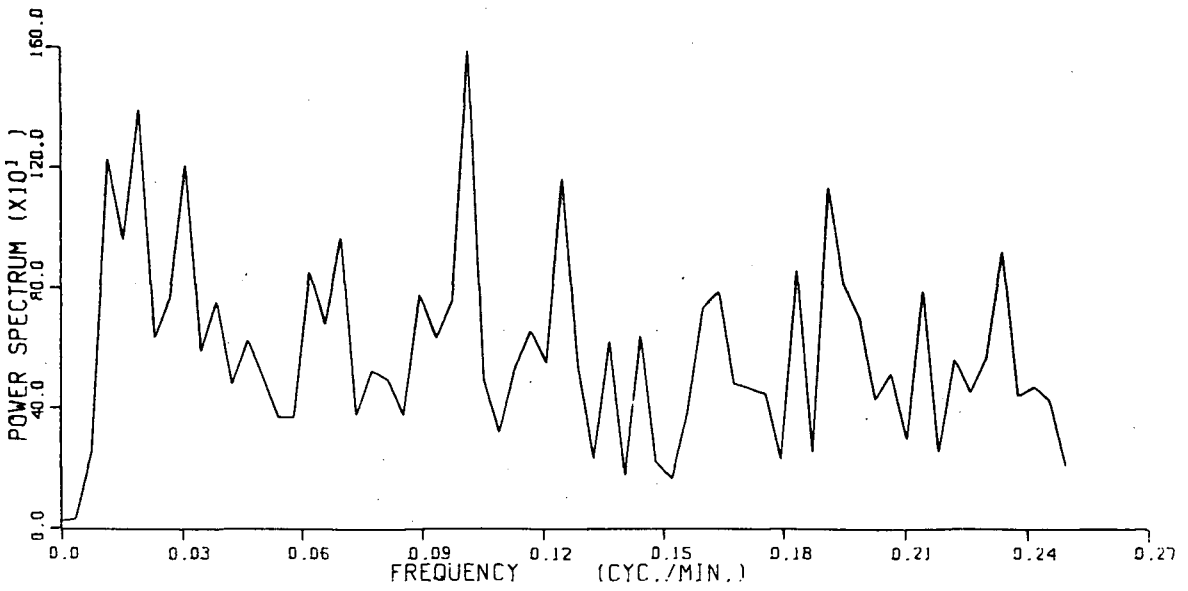

Figure 50 Averaged power spectrum of selected high tides of Port San Juan.
95% confidence interval: (0.61,1.94)*P(f)

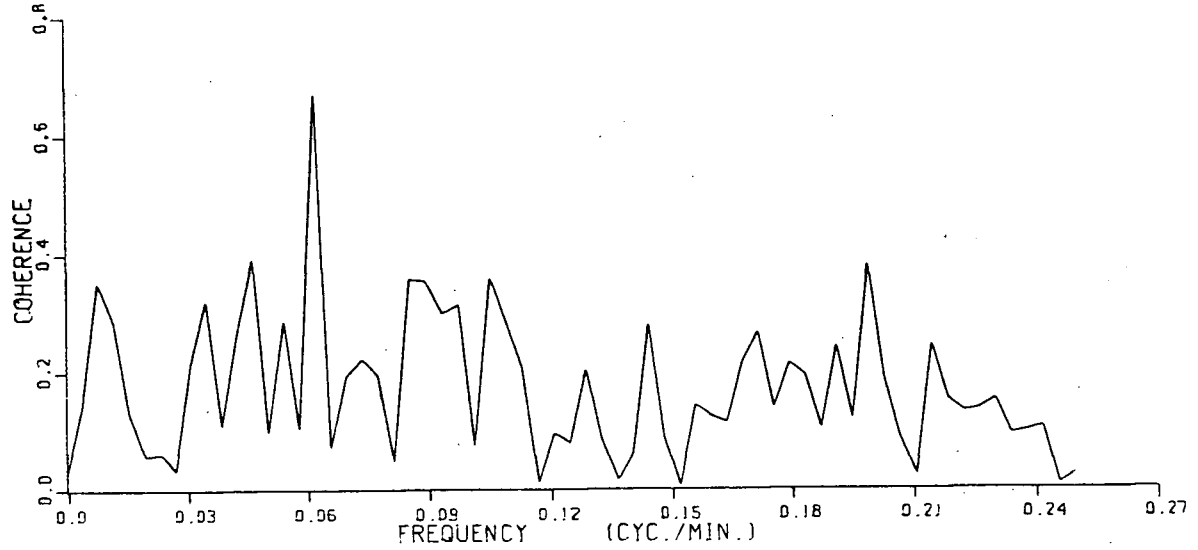

Figure 51 Coherence of selected high tides, Pedder Bay versus Becher Bay.

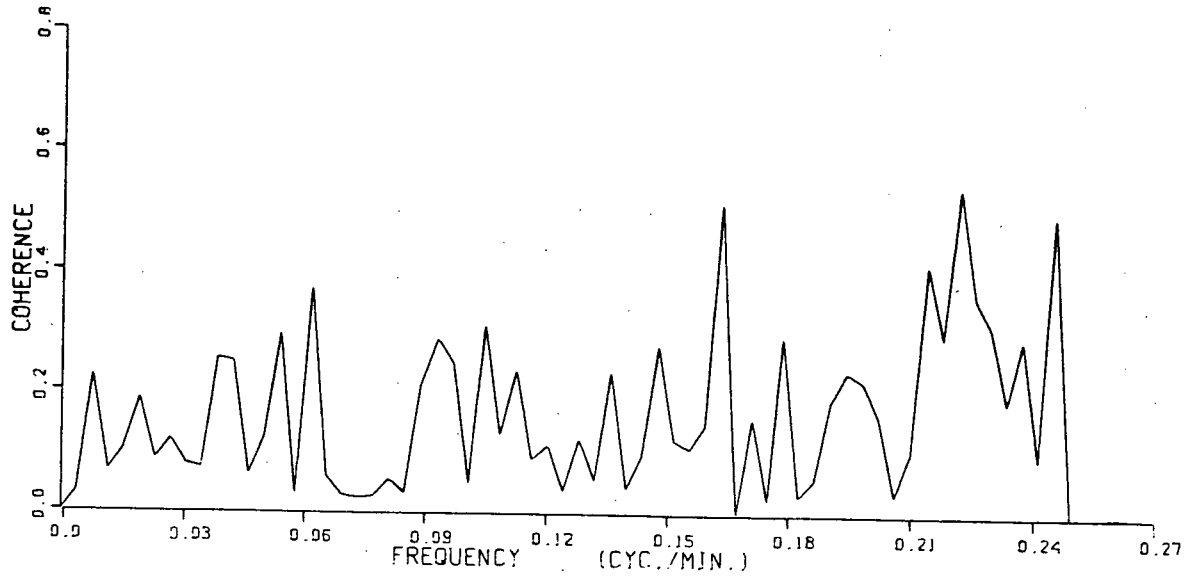

Figure 52 Coherence of selected high tides, Pedder Bay versus Port San Juan.

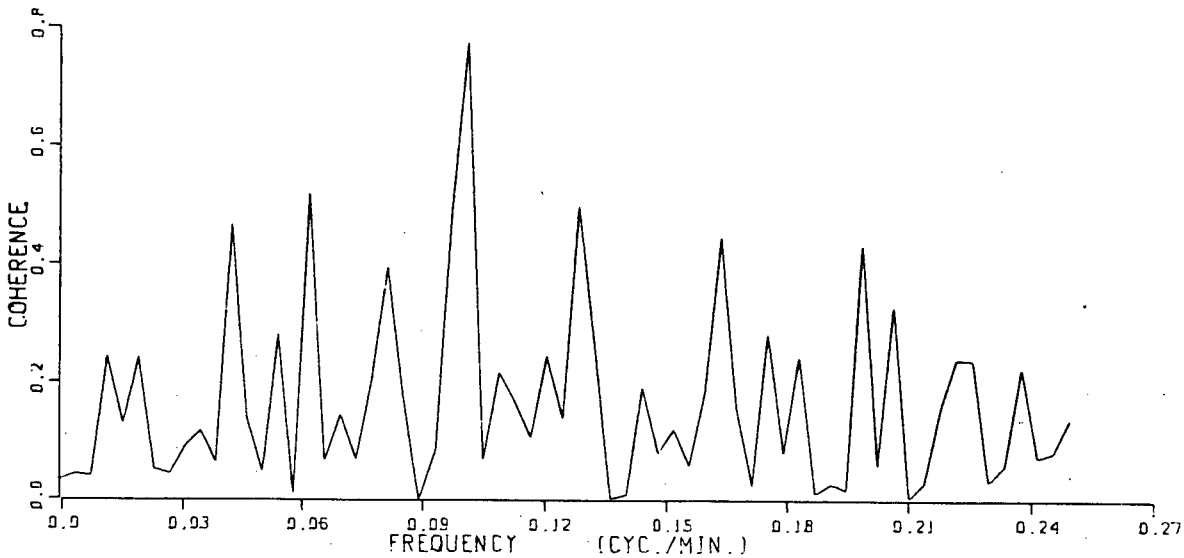

Figure 53 Coherence of selected high tides, Becher Bay versus Port San Juan.

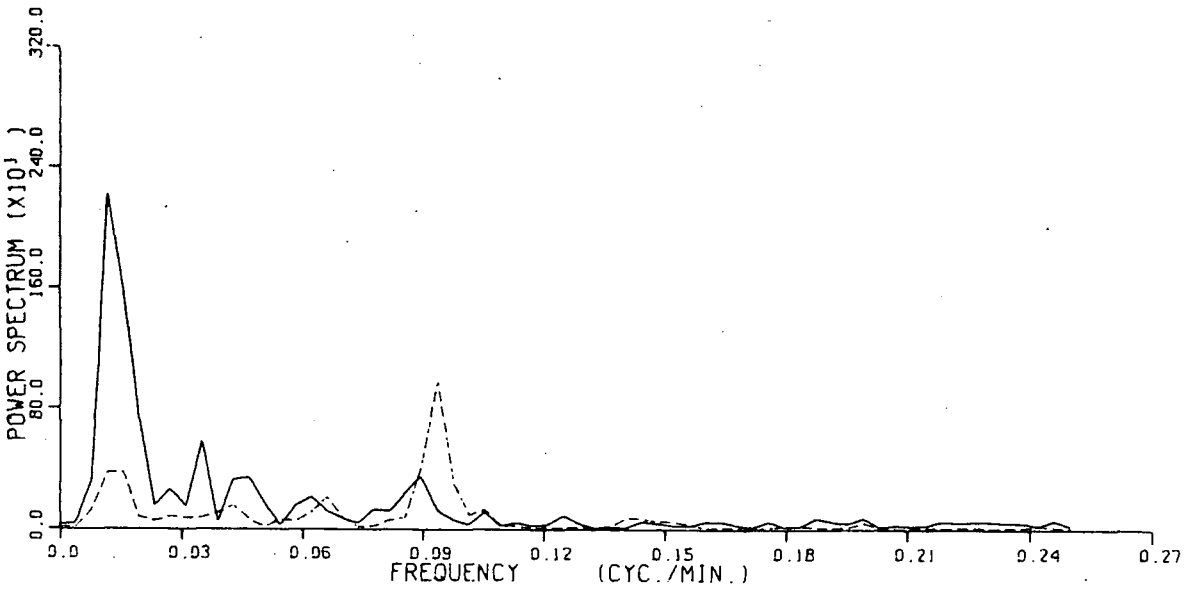

Figure 54 Comparison of averaged power spectra between low (solid line) and high (dashed line) tides of Pedder Bay.

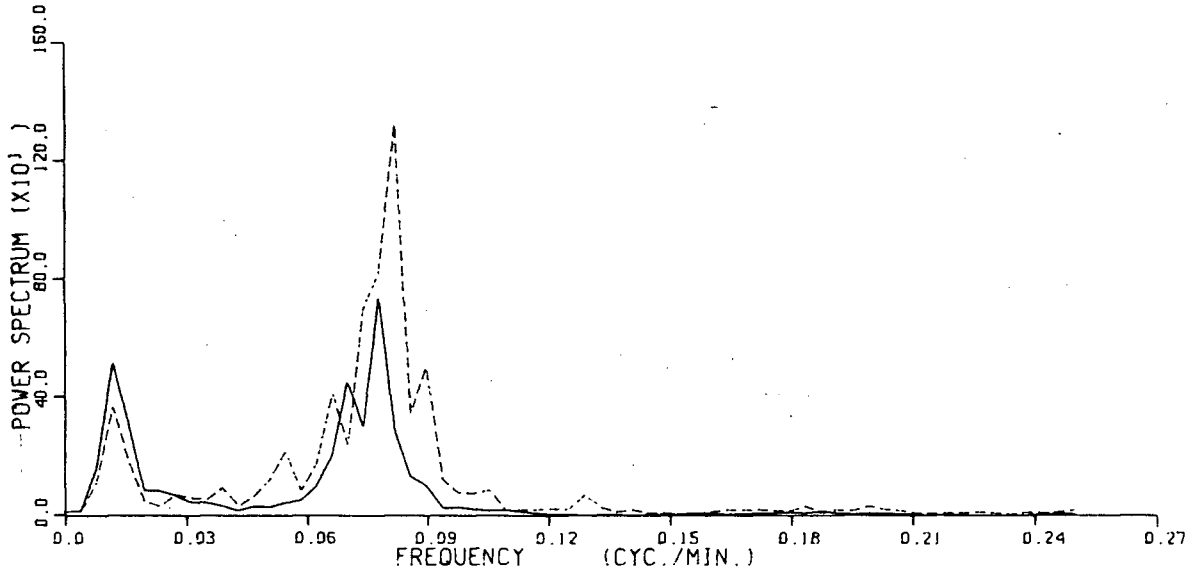

Figure 55 Comparison of averaged power spectra between low (solid line) and high (dashed line) tides of Becher Bay.

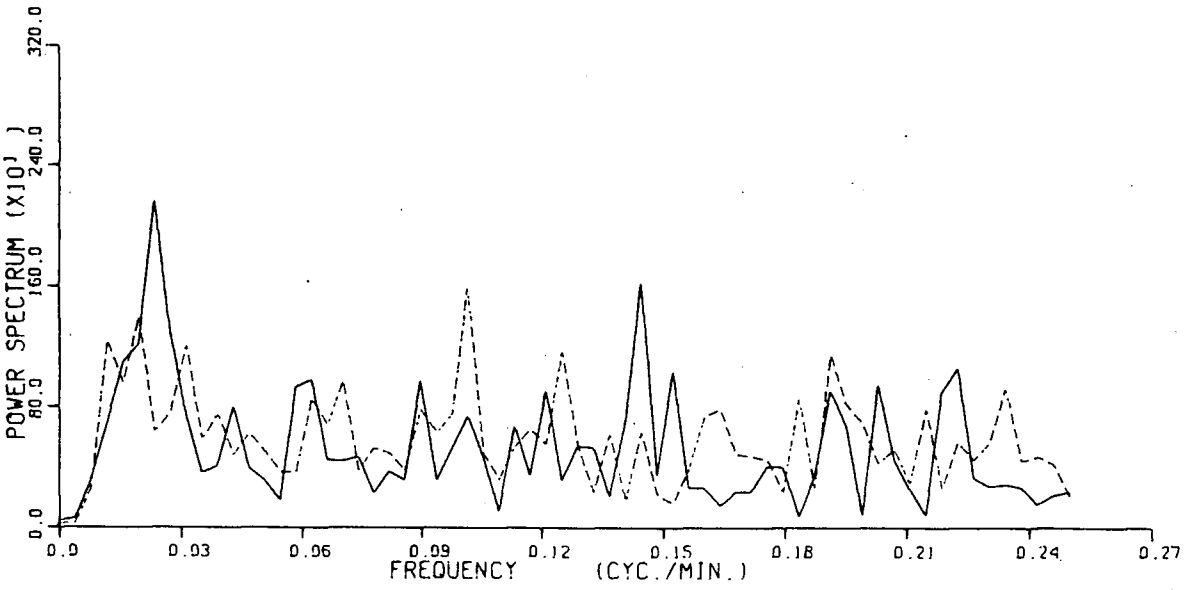

Figure 56 Comparison of averaged power spectra between low (solid line) and high (dashed line) tides of Port San Juan.

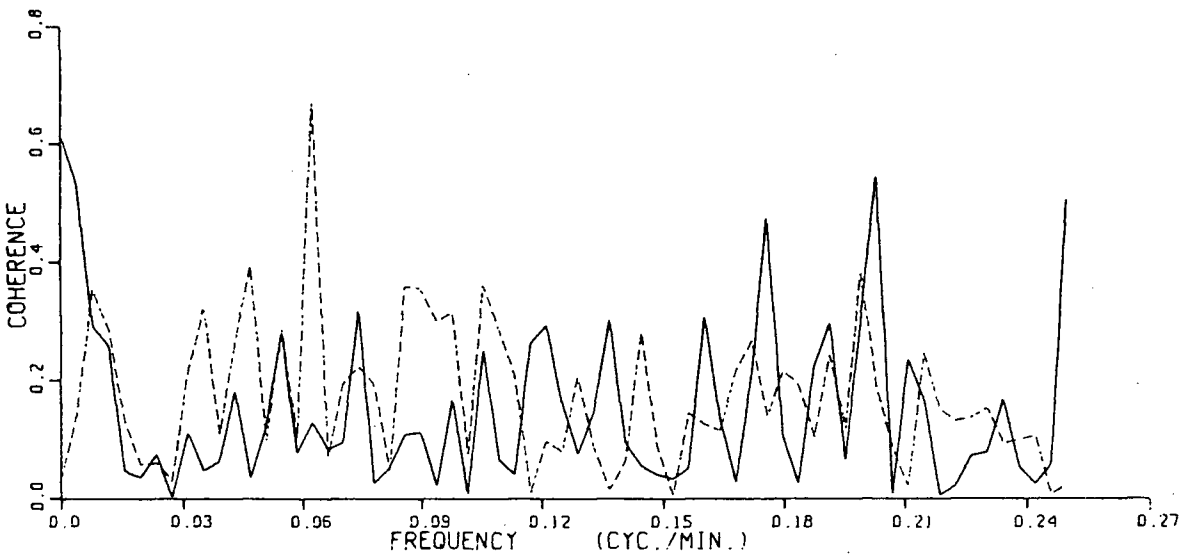

Figure 57 Comparison of coherences between low (solid line) and high (dashed line) tides, Pedder-Becher.

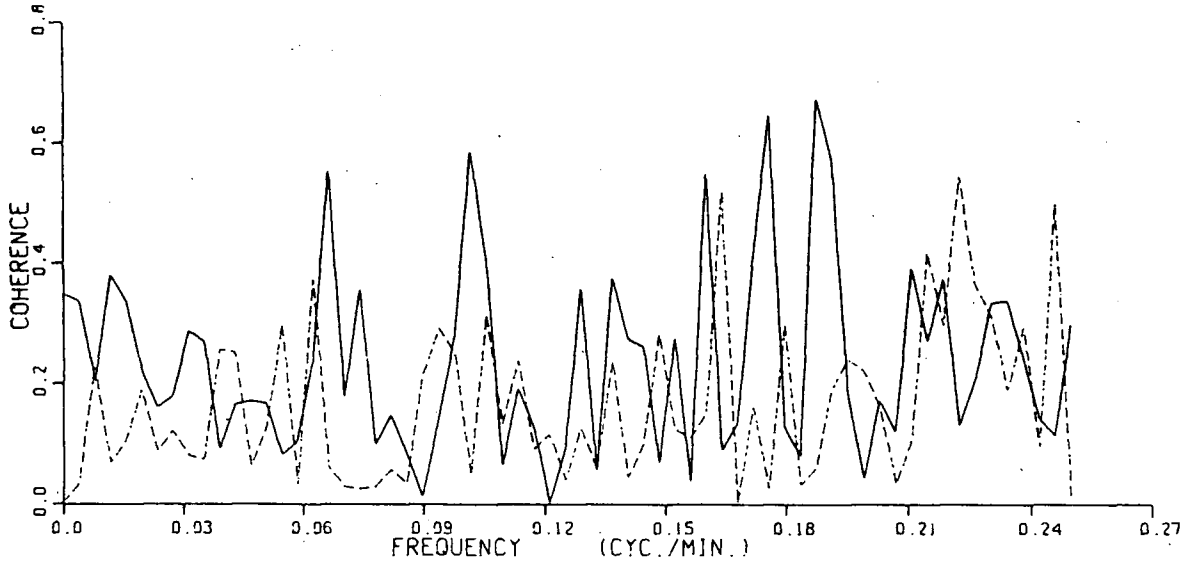

Figure 58 Comparison of coherences between low (solid line) and high (dashed line) tides, Pedder-San Juan.

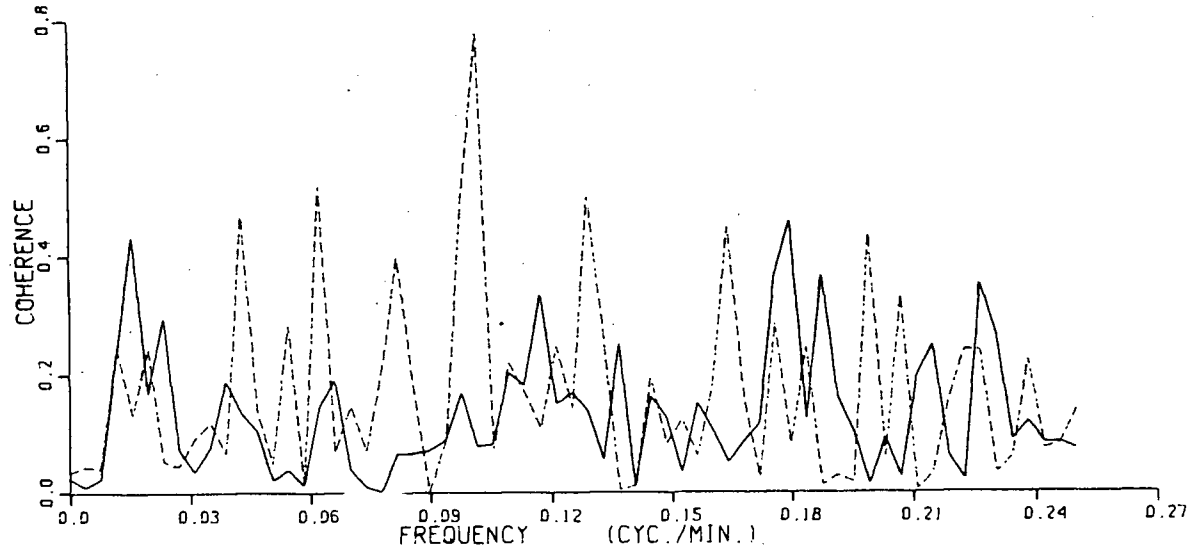

Figure 59 Comparison of coherences between low (solid line) and high (dashed line) tides, Becher-San Juan.

Strait. The above three Figures describe an interesting feature. It seems that Pedder Bay and Becher Bay are correlated at both low and high tides for different frequency bands, Pedder Bay and Port San Juan are more correlated at low tides, Becher Bay and Port San Juan are more correlated at high tides.

IV. NUMERICAL MODELLING OF SEICHES IN COASTAL BAYS

As a direct result of rapid progress of computer techniques in last decade, physical oceanographers move their attention from seeking special functions satisfying the fluid dynamical equations to numerical modelling, which is a more powerful tool in solving challenging problems.

The work described in this chapter tries to find a simple method to model the seiche activity in coastal bays. Due to the consideration of further extending the model, the simplicity and computing cost of this basic model has been a sensitive factor in its development.

A. THE FORMULATION OF THE BASIC NUMERICAL MODEL

To describe the characteristics of the wave response of a bay, we start from the shallow water equations:

$$\frac{D\mathbf{U}}{Dt} + 2\Omega\chi\mathbf{U} + g\nabla\eta + g\mathbf{U}\frac{|\mathbf{U}|}{C^2(H+\eta)} = 0$$

$$\frac{\partial\eta}{\partial t} + \nabla\cdot(H+\eta)\mathbf{U} = 0 \qquad (4.1\text{-}1)$$

where

- $\mathbf{U}$: horizontal velocity vector
- Ω : local vertical component of angular velocity of the earth
- g : gravitational acceleration
- η : elevation of sea surface above mean sea level
- H : depth of sea

C : Chezy coefficient

For simplicity the non-linear effect is ignored. For seiche studies of this project we confine our attention to small bays which are much smaller than the dimension of the earth and to high frequencies which are much higher than the angular velocity of the earth, so that the Coriolis force may be ignored. First in the numerical model, the friction term is dropped in this section. Since the ratio η/H is normally of the order 0.001 to 0.01, we replace $H+\eta$ by H. Then we get the simplified shallow water equations:

$$\frac{\partial u}{\partial t} + g\frac{\partial \eta}{\partial x} = 0$$

$$\frac{\partial v}{\partial t} + g\frac{\partial \eta}{\partial y} = 0 \qquad (4.1\text{-}2)$$

$$\frac{\partial}{\partial x}Hu + \frac{\partial}{\partial y}Hv + \frac{\partial \eta}{\partial t} = 0$$

Assuming the time harmonic factor $e^{i\omega t}$ for the variables u,v and η, after differentiating with respect to t and cancelling the factor $e^{i\omega t}$, equations (4.1-2) may be written in the form of

$$i\omega u + g\eta_x = 0$$

$$i\omega v + g\eta_y = 0 \qquad (4.1\text{-}3)$$

$$(Hu)_x + (Hv)_y + i\omega\eta = 0$$

Substituting u,v from the first two equations into the last, we get an equation for the single variable η:

$$\nabla H \cdot \nabla \eta + H \nabla^2 \eta + \frac{\omega^2}{g} \eta = 0 \qquad (4.1\text{-}4)$$

This equation governs the spatial distribution of the sea surface within a bay. The sea surface behaves as a field of standing waves when the input source to the mouth boundary of the bay is periodic.

The land boundary of the bay is treated as a rigid vertical wall. Then the normal velocity at that boundary vanishes; from equation (4.1-3) we get $\nabla\eta=0$ at the land boundary. For sinusoidal solutions, at the land boundary the amplitude of the velocity reaches its minimum and the elevation of sea surface reaches its local maximum because of the $\pi/2$ phase difference between the velocity and the elevation of sea surface.

The sea surface fluctuation at the mouth of the bay is treated as a periodic function which is represented by $\eta_m e^{i\omega t}$, where η_m is constant. Assuming the solution in the bay is $\eta_b (x,y) e^{i\omega t}$, the amplification factor is

$$A = \frac{\eta_b e^{i\omega t}}{\eta_m e^{i\omega t}} = \frac{\eta_b}{\eta_m} \qquad (4.1\text{-}5)$$

Because of the linearity of equation (4.1-4), A is the solution of the equation with boundary condition A=1 at the mouth. Then we set boundary condition at mouth to be 1 and

solve equation (4.1-4) to construct the amplification field. It should be pointed out that η in equation (4.1-4) is treated as a complex variable, the amplitude and phase of η represent respectively the amplitude amplification and phase shift between waves in the bay and at its mouth. There is no imaginary sign 'i' in equation (4.1-4) in the absence of friction, so that the real and imaginary parts of the equation are identical. Due to the zero boundary condition at the mouth in the imaginary part of the equation, which leads to a homogeneous linear equation system in a numerical model, only zero solutions exist for the imaginary part of equation. Based on the analysis above we can thus treat η as a real variable.

The method of finite difference leads to a system of linear algebraic equations. The order of the matrix of this system is the number of grid points. The computing time increases cubically with the number. This work restricts the number of grid points to less than 200 generally. In consideration of the same order variation, both in x-direction and y-direction, of the bottom topography in the concerned bays, square grids are adopted.

The simplified shallow water equation (4.1-4) is discretized to the difference equation

$$\frac{H_{i+1,j} - H_{i-1,j}}{2\Delta} \cdot \frac{\eta_{i+1,j} - \eta_{i-1,j}}{2\Delta}$$

$$+ \frac{H_{i,j+1} - H_{i,j-1}}{2\Delta} \cdot \frac{\eta_{i,j+1} - \eta_{i,j-1}}{2\Delta}$$

$$+ H_{i,j} \cdot \frac{\eta_{i+1,j} - 2\eta_{i,j} + \eta_{i-1,j}}{\Delta^2} \qquad (4.1\text{-}6)$$

$$+ H_{i,j} \cdot \frac{\eta_{i,j+1} - 2\eta_{i,j} + \eta_{i,j-1}}{\Delta^2}$$

$$+ \frac{\omega^2}{g} \eta_{i,j} = 0$$

The subscript (i,j) indicate the position (x_i , y_j),

$x_i = i\Delta$ $\qquad 0 \le i \le N$

$y_j = j\Delta$ $\qquad 0 \le j \le M$

Δ is the grid length.

In this discretization procedure, first order central differences and second order central differences are adopted to replace the corresponding derivatives, which introduce only second order errors, i.e. $O(\Delta^2)$. The first order central difference could be written in the form of $(H_{i+1/2,j} - H_{i-1/2,j})/\Delta$ etc., but considering that the values $H_{i+1/2,j}$ and $H_{i-1/2,j}$ are linear interpolations, we have

$$\frac{H_{i+1,j} - H_{i-1,j}}{2\Delta} = \frac{H_{i+1/2,j} - H_{i-1/2,j}}{\Delta}$$

so the discretization procedure is only operated at the actual grid points. Another method to discretize equation (4.1-4) was used by Olsen and Hwang (1971); their method took the difference forms of $H\nabla\eta$ first through both forward and backward differences, then took central differences to estimate $\nabla\cdot(H\nabla\eta)$. This method introduces first order error $O(\Delta)$, and performs the discretizing procedure twice. In

spite of the consideration above, it is still difficult to judge which one is more reasonable.

Using the notations

$$HX = \frac{H_{i+1,j} - H_{i-1,j}}{4\Delta^2}$$

$$HY = \frac{H_{i,j+1} - H_{i,j-1}}{4\Delta^2} \qquad (4.1\text{-}7)$$

$$H = \frac{H_{i,j}}{\Delta^2} ,$$

the difference equation (4.1-6) has the form

$$(H+HX)\eta_{i+1,j} + (H+HY)\eta_{i,j+1} + (H-HX)\eta_{i-1,j} + (H-HY)\eta_{i,j-1}$$

$$+ \left(\frac{\omega^2}{g} - 4H \right)\eta_{i,j} = 0 \qquad (4.1\text{-}8)$$

At the land boundary the bay shore is approximated by segments of straight line in the grid system; thus the normal derivatives $\partial\eta/\partial n$ are taken in either the x or y directions. If a point (i,j) has a right boundary, we have

$$\frac{\partial \eta_{i,j}}{\partial n} \simeq \frac{\eta_{i+1,j} - \eta_{i,j}}{\Delta} = 0$$

so $\eta_{i+1,j} = \eta_{i,j}$

at the boundary, the term $\eta_{i+1,j}$ in (4.1-8) disappears and its coefficient is added to that of $\eta_{i,j}$. The boundaries at

other sides can be dealt with in the same way.

If (i,j) is adjacent to a mouth point (i,j-1) , the term $\eta_{i,j-1}$ is replaced by 1 ; then the constant (H-HY) is moved to the right hand side of the algebraic equation system.

Through the procedure described above the corresponding algebraic equation could be constructed at every grid point, which formed an algebraic equation system. For convenience the equation system is written in matrix notation

$$\mathbf{A}\tilde{\eta}=\mathbf{b} \qquad (4.1\text{-}9)$$

Throughout this thesis the bold Roman letters and greek letters with tilde denote matrix or vector without further notation. Examples: **A**, **b**, **D**, **U**, $\tilde{\eta}$, $\tilde{\eta}_r$ and $\tilde{\eta}_i$.

The coefficient matrix **A** and the right hand side column vector **b** are formed through the procedure mentioned above. In order to apply this to arbitrary shaped bays, the computer program has a special treatment to detect the relative position between a current grid point and land boundary and mouth points. Equation (4.1-8) indicates that ω only appears in the diagonal of matrix **A**, which needs to be calculated only once at ω=0; when ω is changed, the value ω^2/g is added to the diagonal of **A** to obtain the amplitude field for the specified frequency ω.

For this program the main computing cost is related to the subroutine SLE which solves the linear algebraical

equation system. To guarantee the accuracy of the numerical model output the double precision subroutine SLE was chosen instead of single precision subroutine FSLE (See "UBC Matrix" ,Computing Center, UBC, for description of these two subroutines SLE and FSLE).

Double precision computing uses double storage space and much more computing time; the major drawback is the limitation in the number of grid points; as a compromise, double precision was declared only for the variables directly used in the subroutine SLE.

Let x be the calculated value in SLE or FSLE and δx be the difference of calculated and true values. The fractional error is

$$\frac{||\delta x||}{||x||} \leq n \cdot C \cdot 10^{-t} \qquad (4.1\text{-}10)$$

where n and C are the order and condition number of coefficient matrix **A** and

$$t \simeq \begin{cases} 15 \sim 16 & \text{double precision SLE} \\ 6 \sim 7 & \text{single precision FSLE} \end{cases} \qquad (4.1\text{-}11)$$

The estimation (4.1-10) was given by Conte and Boor (1972).

B. APPLICATION OF THE BASIC MODEL AND PREDICTION OF RESONANT FREQUENCIES IN COASTAL BAYS

We first describe the grids used in Pedder Bay, Becher Bay and Port San Juan respectively.

Pedder Bay is a triangular bay with a wide mouth (Figure 60). It is difficult to decide exactly where the mouth is. The resonant frequencies are dominated by the geometry and bottom topography, so that the position of the mouth affects the values of these frequencies. Under rough estimation the main resonant period is the time within which the wave travels a quarter of wave length, i.e.,

$$T = \int_l \frac{4dl}{\sqrt{gh(x,y)}} \qquad (4.2\text{-}1)$$

l is the the integral path from mouth to the head of bay. In Pedder Bay the value of h at mouth is much larger than that at the head, so that the resonant period shift is not very sensitive to the position of the mouth adopted by the numerical grid. For this work the mouth is chosen as a straight line from Cape Calver to William Hd (Figure 60). Numerical results for other mouth positions have been compared and confirm the insensitivity of the resonant periods to a change of mouth position.

Becher Bay is a roughly square bay with islands inside it (Figure 61). The grid mouth is chosen as a straight line from Alldridge Pt. to Church Pt.. Two islands are drawn in the grid (Figure 62).

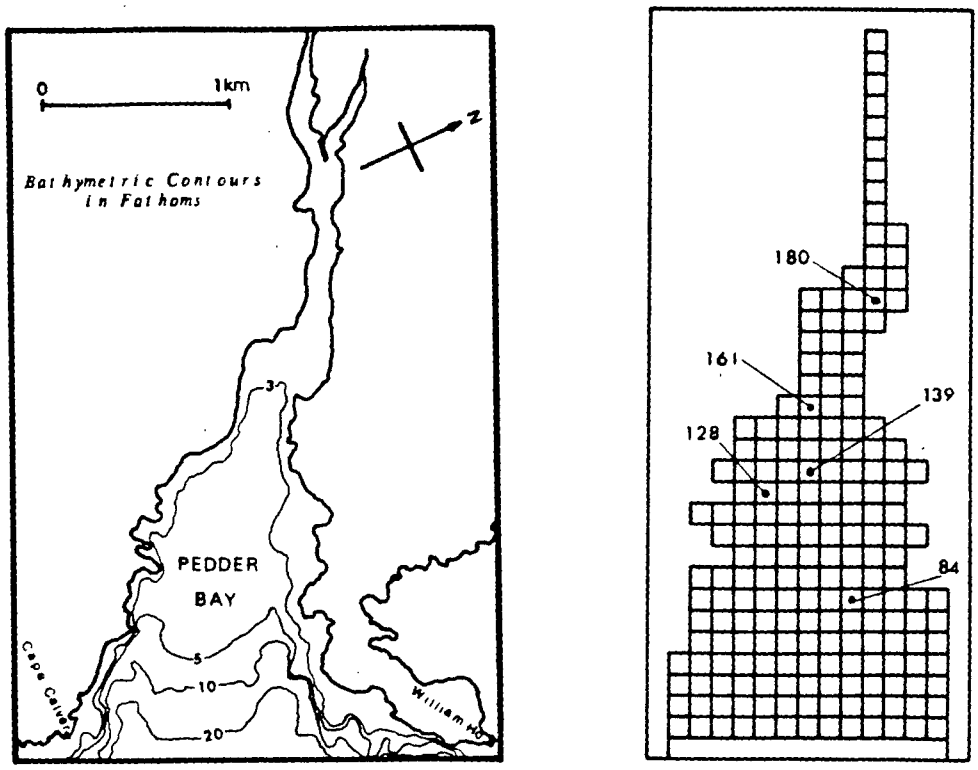

Figure 60 The shape of Pedder Bay and its numerical grid.

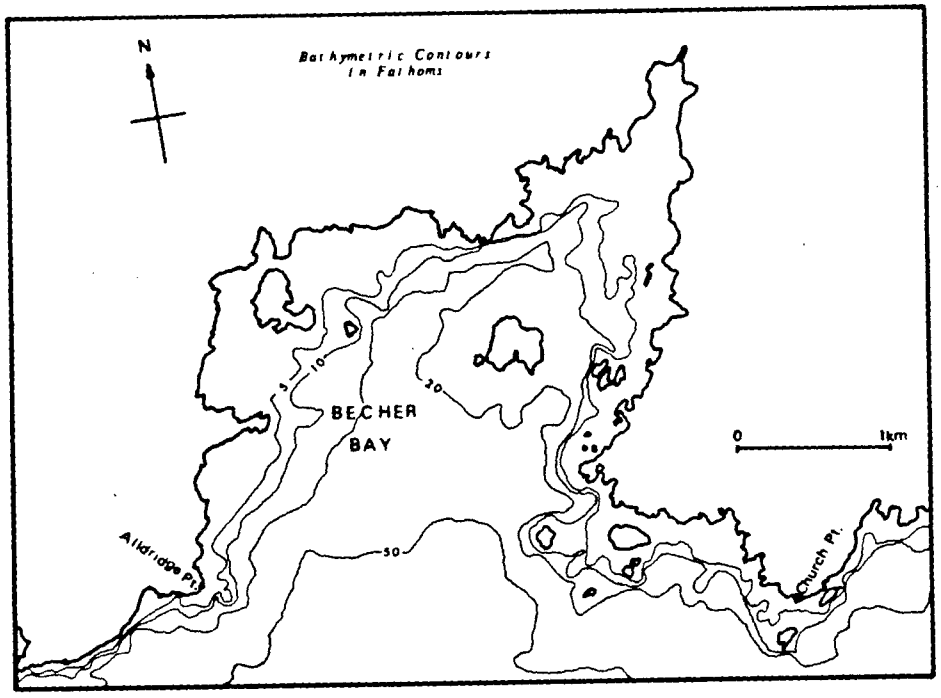

Figure 61 The shape of Becher Bay.

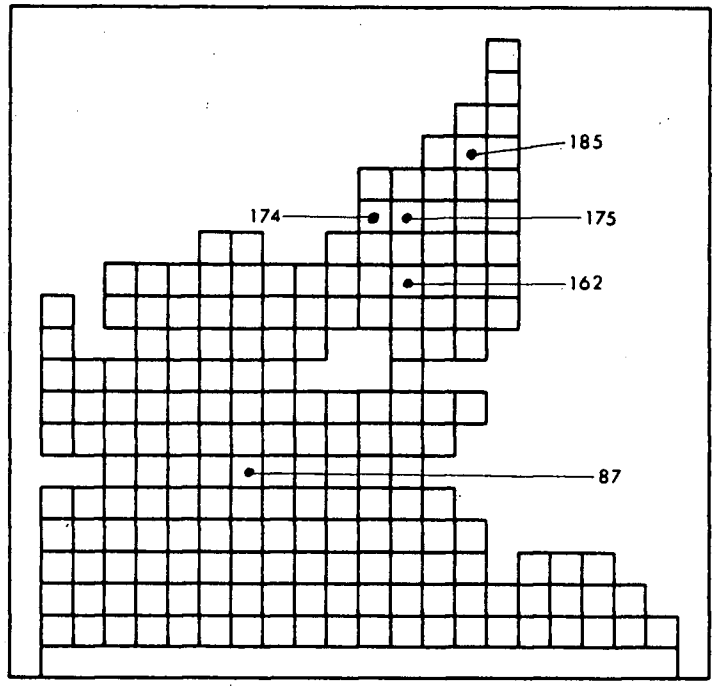

Figure 62 The numerical grid of Becher Bay.

The case of Port San Juan is a little troublesome. This port is roughly rectangular, but the central line is not perpendicular to the coast line (Figure 63). First I took the extended coast line as its mouth which resulted in a ragged land boundary (Figure 64). At the sharp convex corners the variables should be single-valued as anywhere else, but actually multi-valuedness is introduced by the boundary condition $\partial\eta/\partial n=0$ which leading to the equalities $\eta_{i,j} = \eta_{i+1,j}$ and $\eta_{i,j} = \eta_{i,j-1}$ in the case that η is at the land boundary (Roache, 1976). Numerical results from the grid shown in Figure 64 were chaotic instead of showing resonance modes. Then I changed to the grid shown in Figure 65. The shortcoming of this grid is that the mouth line does not line up with the coast line. But the numerical result

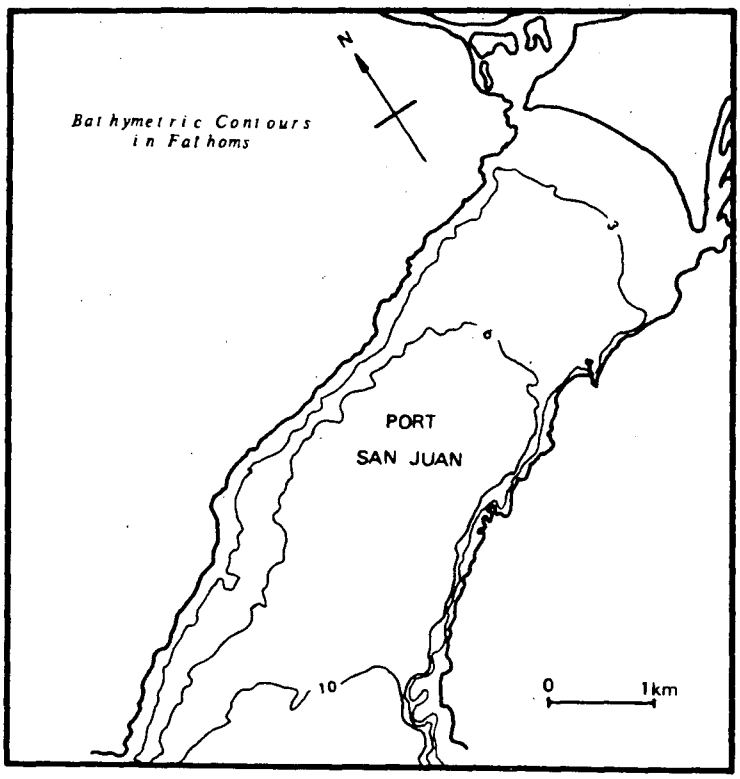

Figure 63 The shape of Port San Juan.

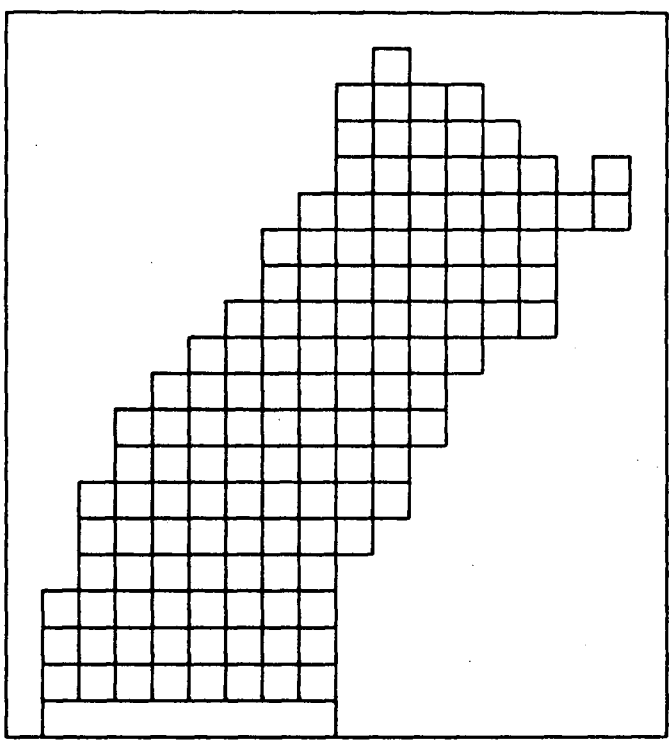

Figure 64 The numerical grid of Port San Juan.

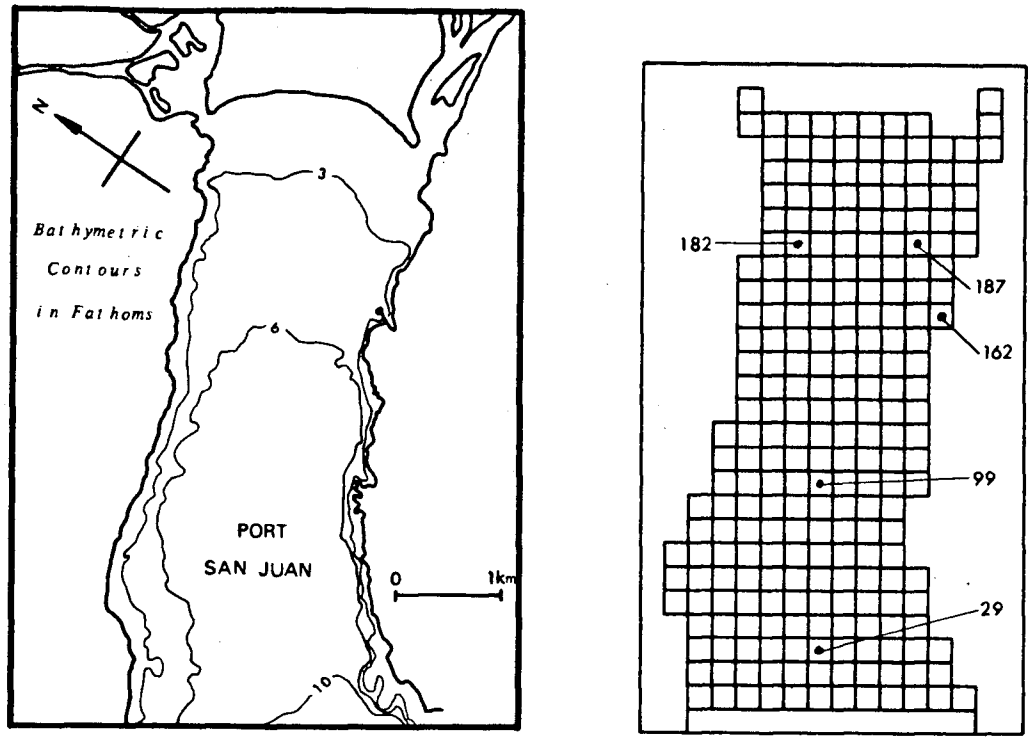

Figure 65 The modified numerical grid of Port San Juan.

from this grid is more acceptable after comparison with the spectral analysis of measured data.

Interpolations of chart depths were directly adopted as input to the numerical model; these are water depths at lower low water of large tides. The ideal input depth should be that at mean sea level. At mean tides, the rims of the bays will be drowned by incoming tides, resulting in changes of area, and in the representation of the bays' geometry.

The output of the numerical model applied to the three bays is a function of 3-dimensional variable: $\eta(x,y,\omega)$, For convenience of presentation in 2-dimensional graphs, only 5 grid points were selected at selected positions in each bay (Figure 60 , Figure 62 and Figure 65).

Figure 66 shows the amplification factor versus period at grid point #161 of Pedder Bay (pressure gauge position) from the output of numerical model. Here we use absolute values of the amplification factors in the graph and will do so in subsequent graphs if there is no special explanation. In this Figure there are three obvious peaks at periods 18, 11 and 7 minutes. Figure 67 shows the amplification factor at all 5 points in Pedder Bay. At all 5 points the same resonant periods are revealed, but the values of the factors have some differences. Generally speaking, for the first mode the closer to the head of the bay the larger the amplification factors are. Figure 68 shows the curve of amplification factor at grid point #175 in Becher Bay (pressure gauge position). Two peaks are revealed: the periods at 13 and 7 minutes. Figure 69 shows the amplification factors at all of the 5 points in Becher Bay. The same peaks are revealed; the grid points closer to the head have larger amplification factors. Figure 70 and Figure 71 show the amplification factors in Port San Juan. A large resonant peak appears at period 33 minutes, and there is also a small resonant peak at period 11 minutes.

For a more detailed presentation, contour graphs are used to describe the distributions of the amplification factors in different bays at different typical resonant periods.

Figures 72 to 74 show the amplification factor fields in Pedder Bay. Figure 72 gives the factor field at period 18

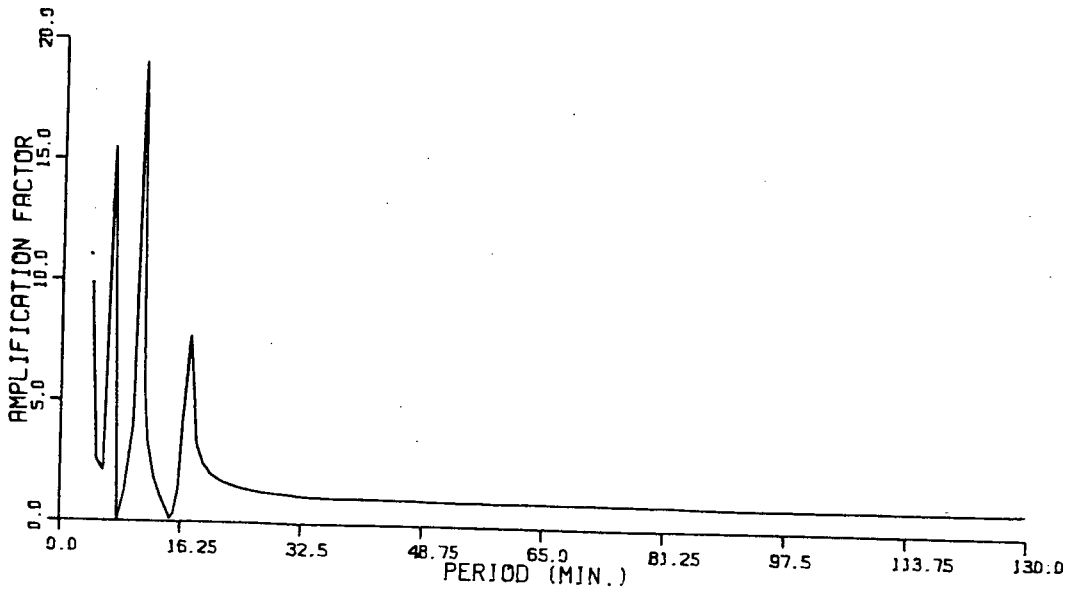

Figure 66 Amplification factor of grid 161 in Pedder Bay.

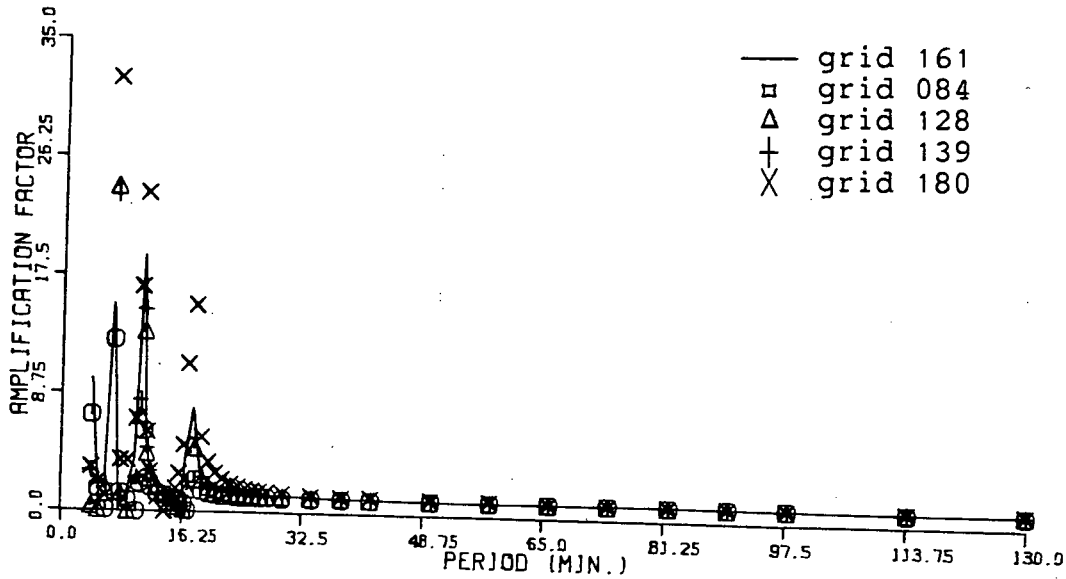

Figure 67 Amplification factor at 5 points of Pedder Bay.

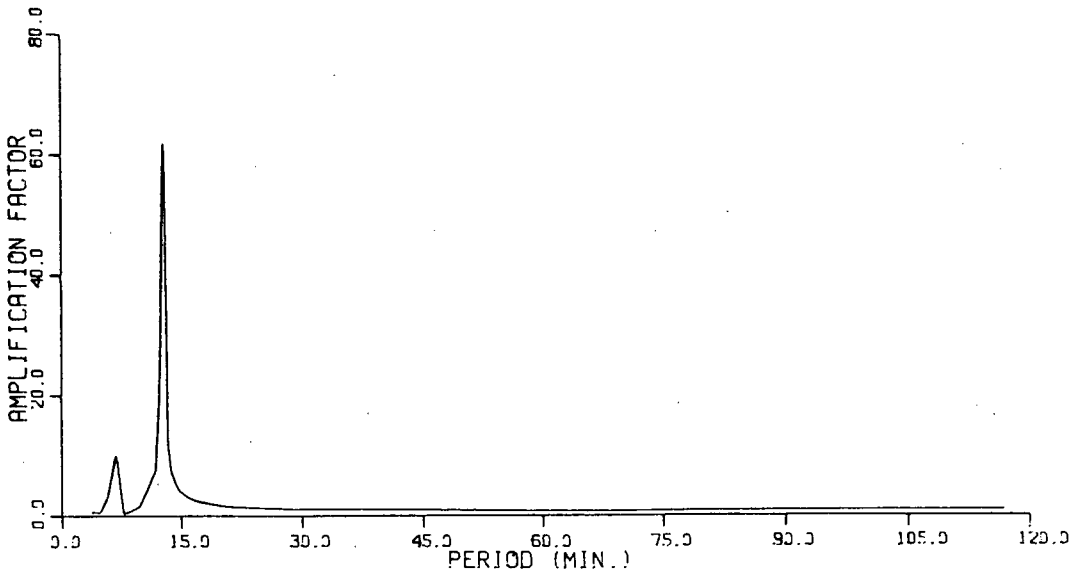

Figure 68 Amplification factor at grid 175 in Becher Bay.

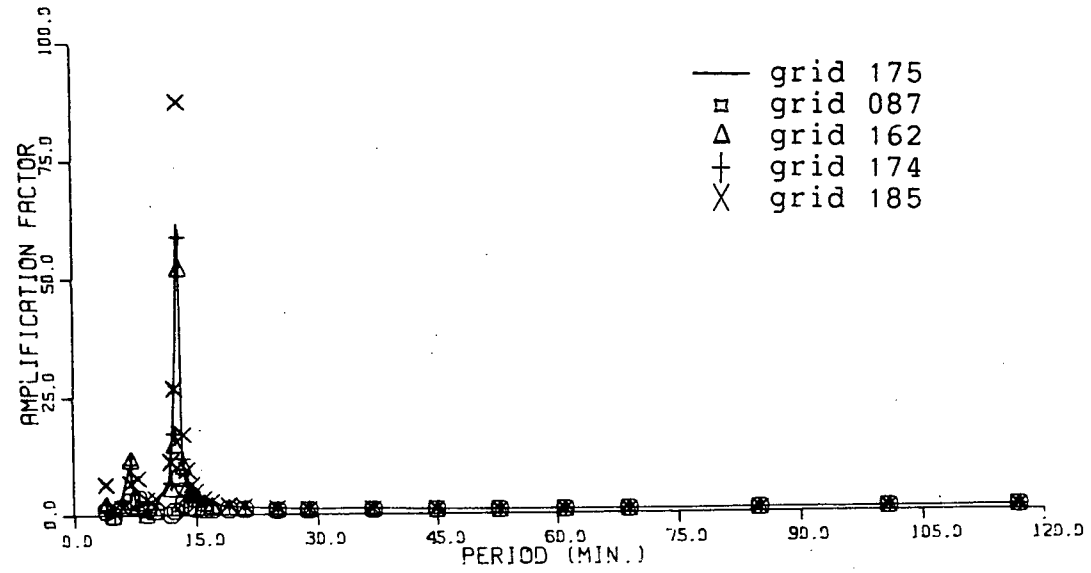

Figure 69 Amplification factor at 5 points of Becher Bay.

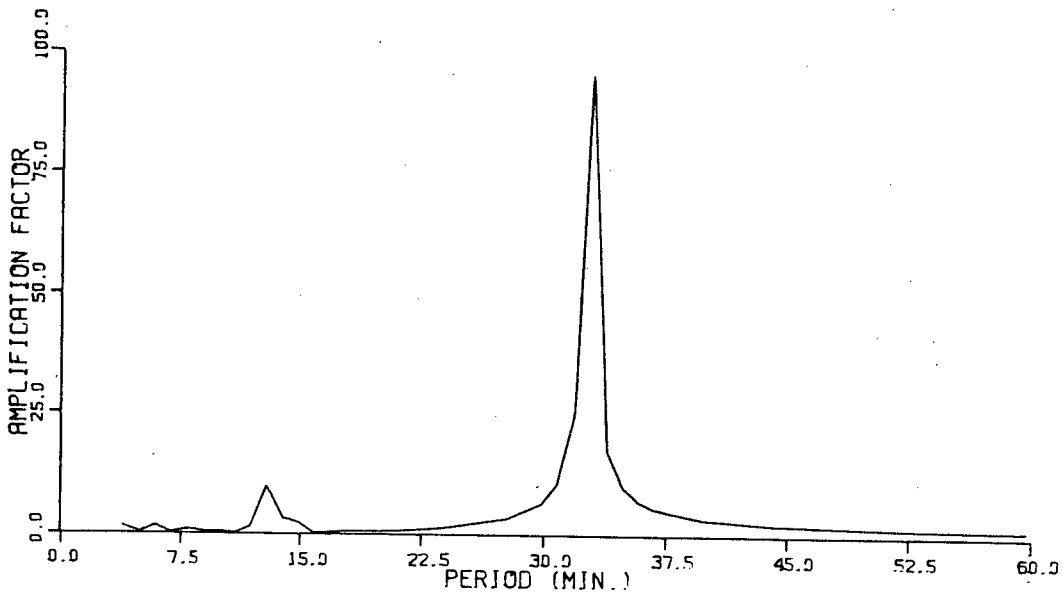

Figure 70 Amplification factor at grid 187 of Port San Juan.

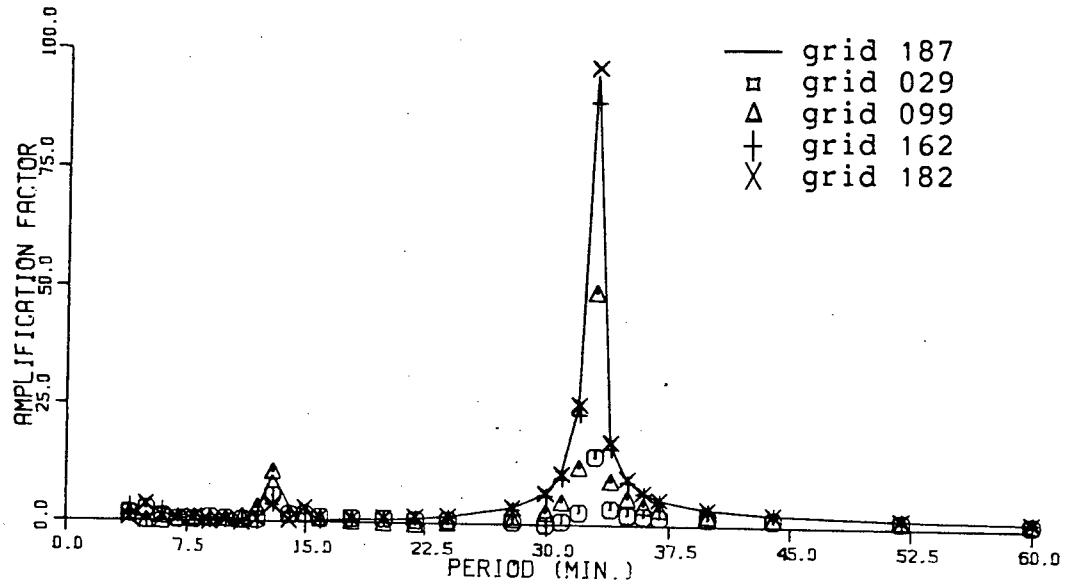

Figure 71 Amplification factor at 5 points of Port San Juan.

minutes which is the resonant period of first mode. There is no nodal line across the bay, the amplification factor gets larger from mouth to head. The amplification factor values increase greatly along the inlet to the head of the bay. Figure 73 shows the amplification field at period 11 minutes, it indicates that this period is a second mode resonant period with a single nodal line across the bay; the values of amplification in the inner part become negative, which means that the fluctuation of sea surface in this area has inverse phase. Figure 74 shows the distribution of amplification factor at the third mode, with resonant period 7 minutes. Two nodal lines can be seen from the contour graph.

Figure 75 and Figure 76 are amplification factor fields in Becher Bay, representing a first mode with resonant period 13 minutes and a second mode with resonant period 7 minutes respectively.

Figure 77 to Figure 79 show amplification fields in Port San Juan, the corresponding periods are 33,13 and 11 minutes successively. Periods 33 and 13 minutes are resonant periods. The amplification is small at period 11 minutes, this period is chosen to show the different nodal lines.

C. INFLUENCE OF TIDAL LEVEL

To inspect the effects of a change of water depth the calculation was done at mean sea level in Pedder Bay, i.e. adding 1.8 meters to chart depth. Figure 80 shows the

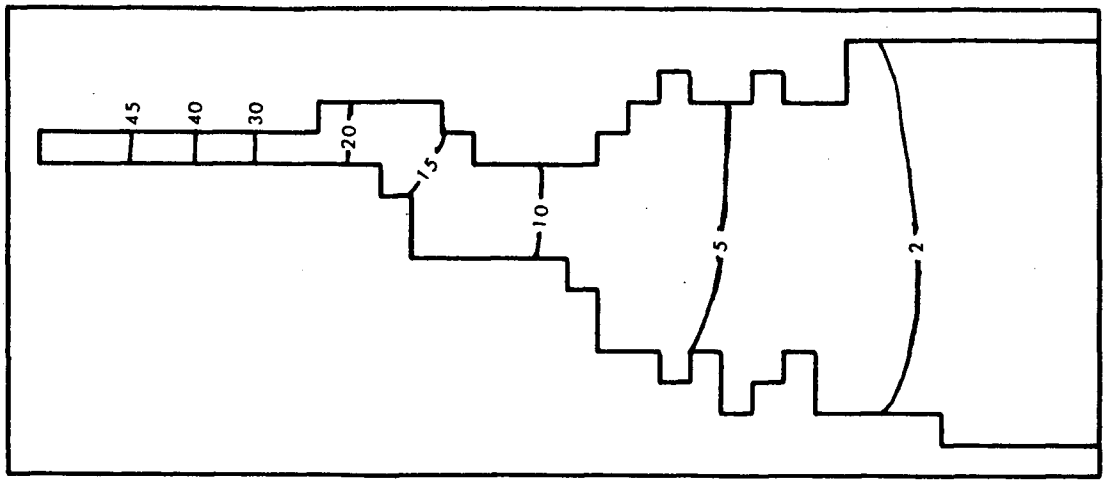

Figure 72 Contour map of amplification factor: first mode of Pedder Bay.

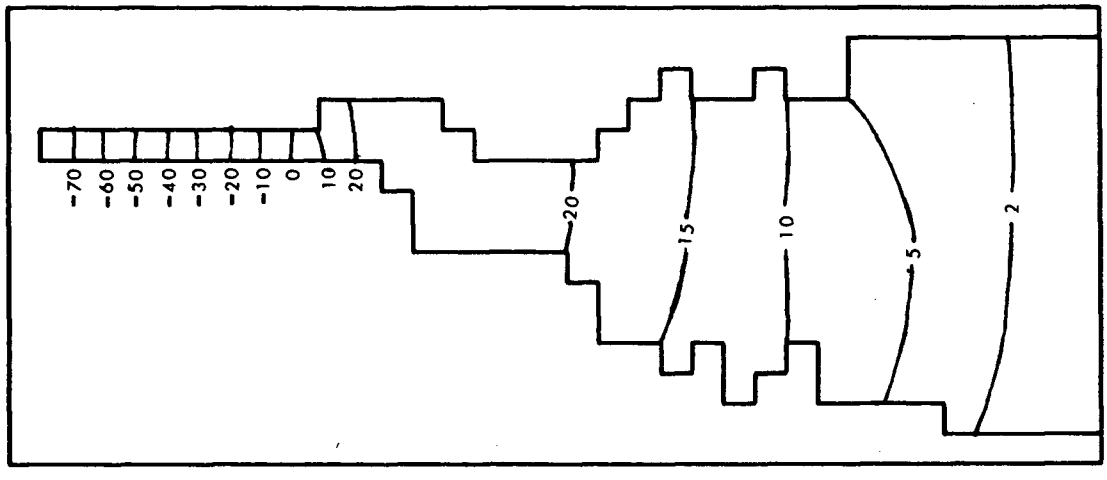

Figure 73 Contour map of amplification factor: second mode of Pedder Bay.

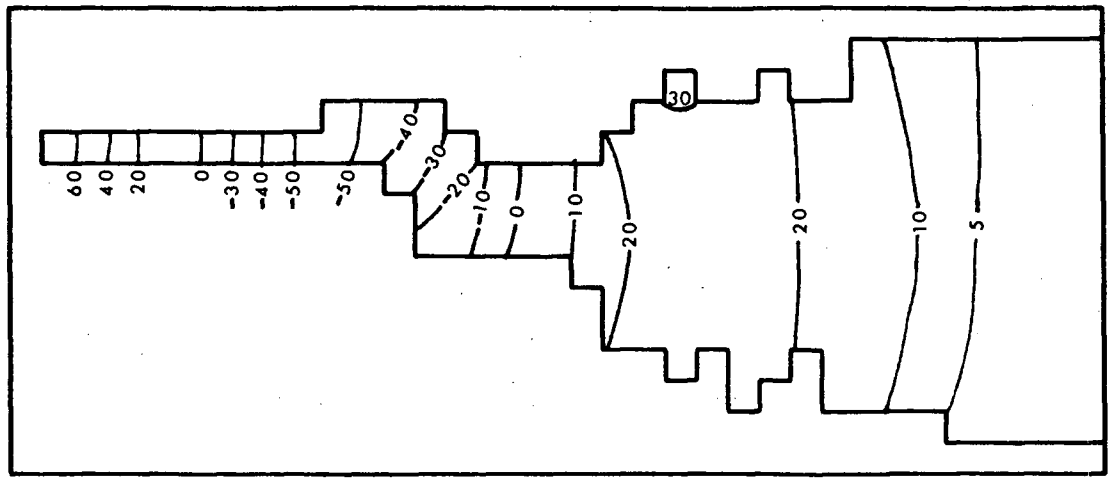

Figure 74 Contour map of amplification factor: third mode of Pedder Bay.

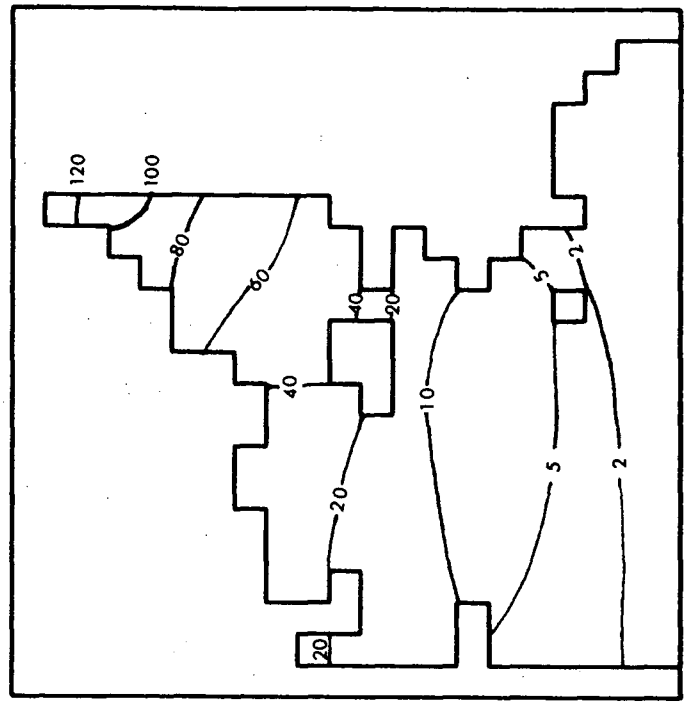

Figure 75 Contour map of amplification factor: first mode of Becher Bay.

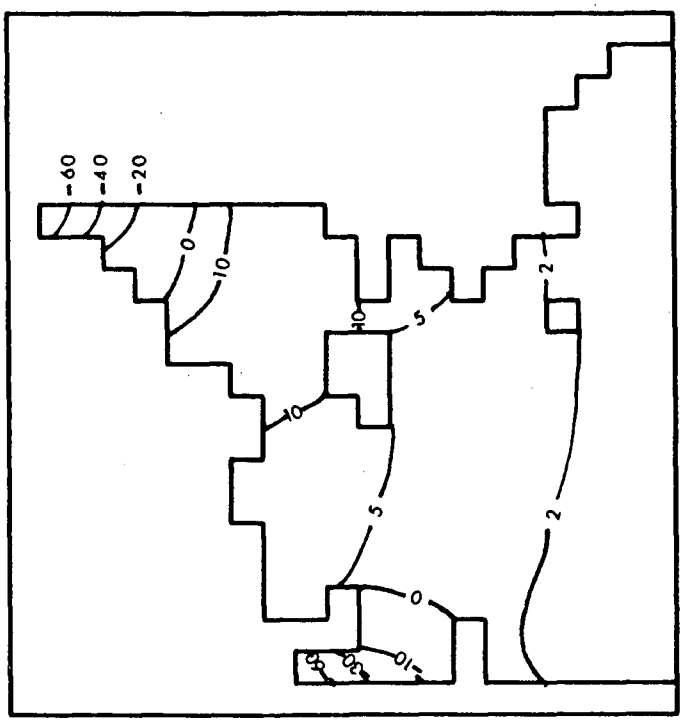

Figure 76 Contour map of amplification factor: second mode of Becher Bay.

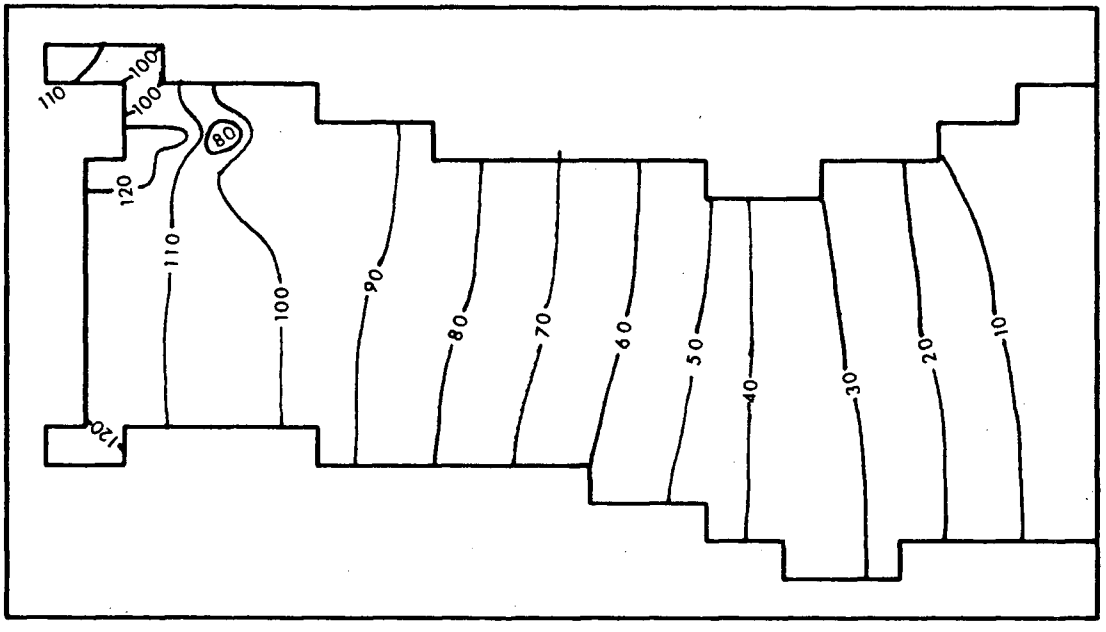

Figure 77 Contour map of amplification factor: first mode of Port San Jaun.

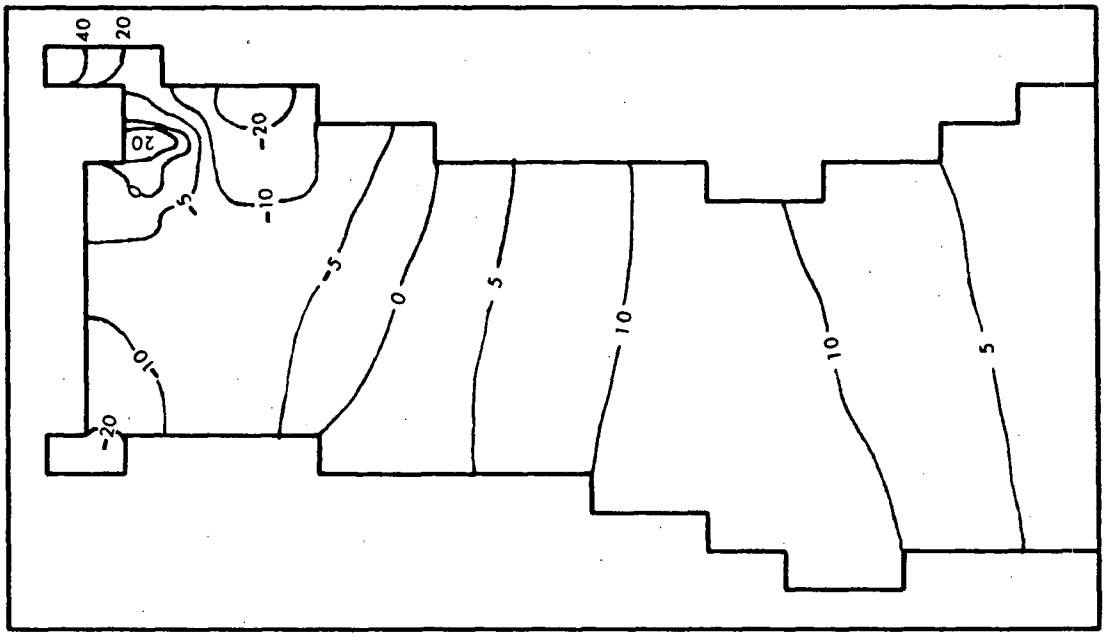

Figure 78 Contour map of amplification factor: second mode of Port San Juan.

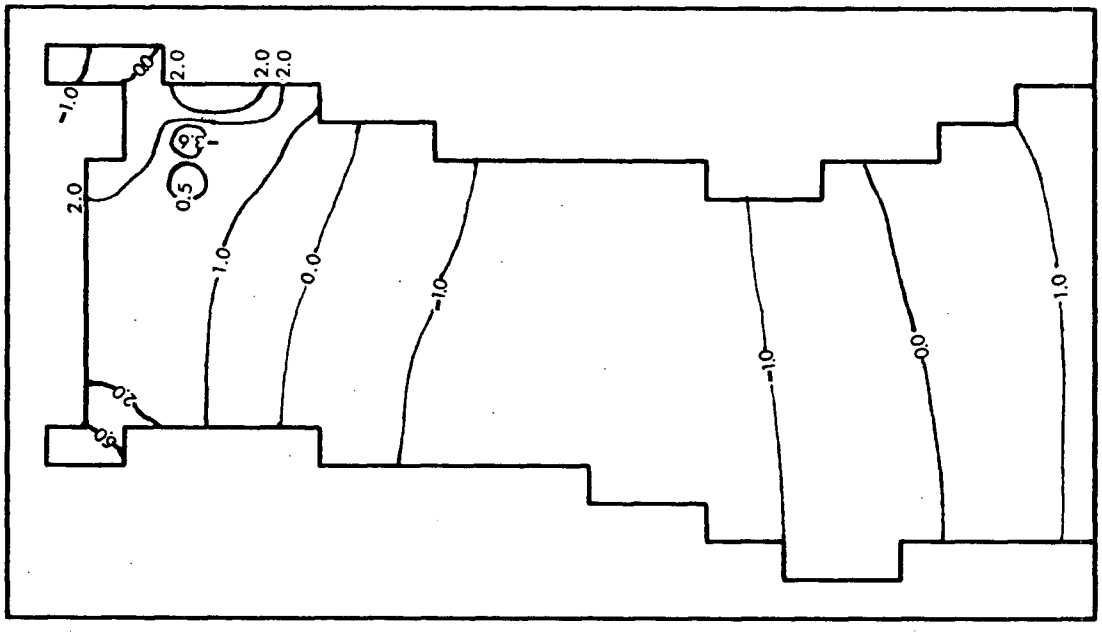

Figure 79 Contour map of amplification factor: third mode of Port San Juan.

comparison in the 5 grid points of Pedder Bay. The solid lines represent amplification factor at chart depth, the dashed lines represent the factor at mean sea level. When the depth is increased, the peaks of the dashed lines shift left, i.e. the corresponding resonant frequencies become higher. This phenomenon agrees with the rough estimation of resonant frequencies in an open-ended rectangular bay of uniform depth:

$$f_{res} = \frac{4\sqrt{gh}}{(2n-1)l} \qquad n = 1 , 2 , ... \qquad (4.3\text{-}1)$$

where l is the length of the bay. After adding 1.8 meters, the third mode peaks become smaller. The result represented by dashed lines could not be treated as the actual amplification factor at mean sea level, because the area of the real bay changes due to the rising tide. Generally speaking, the position of land boundary plays a significant role in governing the resonant frequencies. The water depth of the rim of bays is much shallower than that of bays' centers or bay mouths, so waves travel very slowly, which increases the wave period greatly. Therefore the position of the land boundary has a significant influence to the resonant period. This feature is not considered above.

The reasonableness of adopting chart depth may be explained by rough estimation. Based on (4.2-1)

$$T = \int_l \frac{4dl}{\sqrt{gh(x,y)}}$$

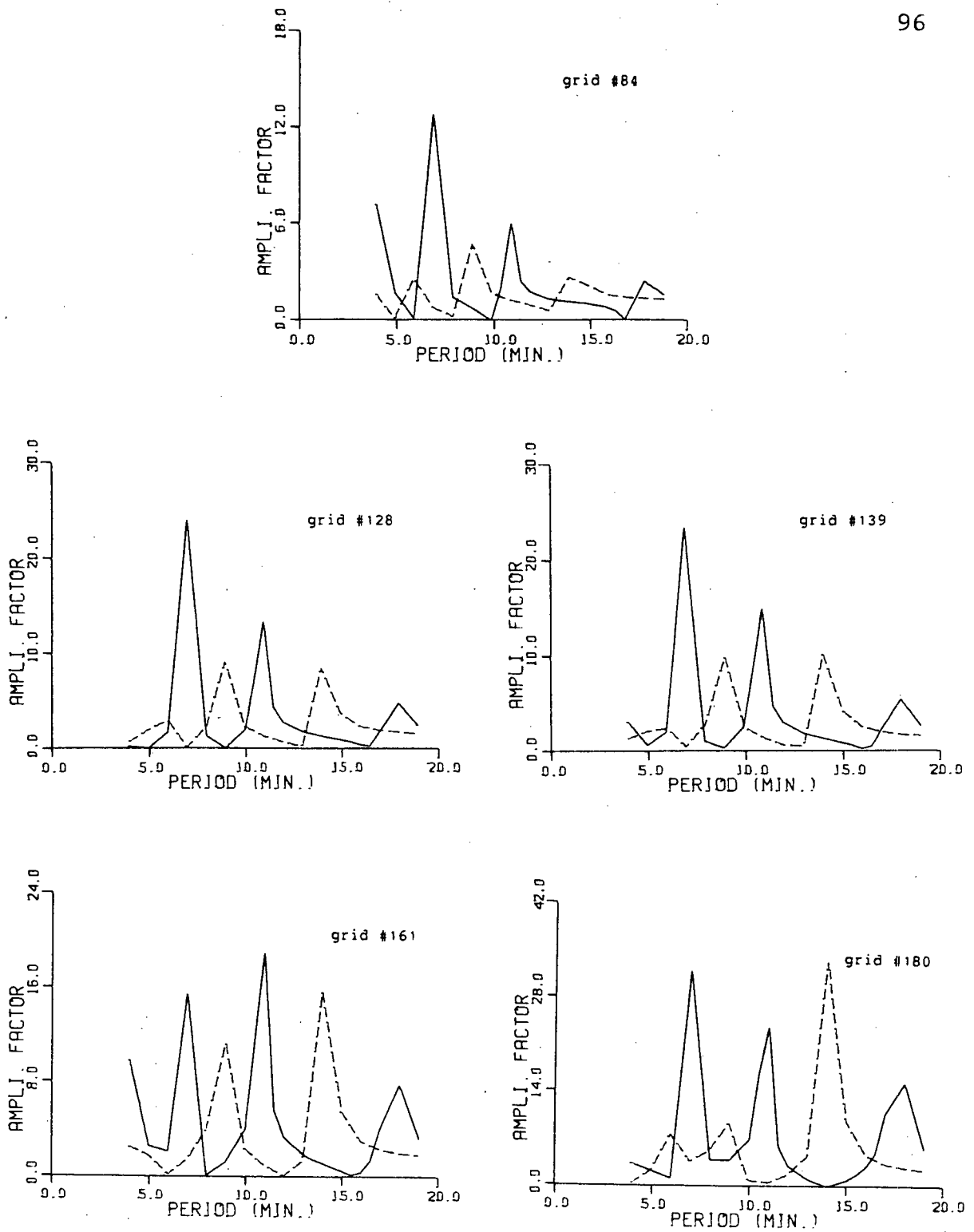

Figure 80 Comparison of amplification factors of Pedder Bay.
Solid line: chart depth.
Dashed line: mean sea level.

we have

$$\frac{\partial T}{\partial h} < 0 \qquad \text{and} \qquad \frac{\partial T}{\partial l} > 0 \qquad (4.3\text{-}2)$$

so when the tide rises, both h and l increase, and their effect on the resonant frequency of bay is to offset each other. We will use the output of the numerical model at chart depth for comparison purposes in further work.

The real situation is much more complicated because of the arbitrary shape of a bay which may not be simplified to one-dimensional. In order to test the effect of the change of a bay's area, the grid of Port San Juan was augmented as shown in Figure 81, where the water depths of augmented area are assumed to be 0.5 meter. Using the basic numerical model the amplifications from the augmented grid are shown in Figure 82. We see the resonant peaks of augmented grid shift to shorter periods instead of longer periods.

The amplifications in Figure 82 are absolute values as mentioned before. Figure 83 show values of these amplifications themselves. We may notice the changes of signs of amplifications, which implies that the dominant peaks from basic grid and augmented grid belong to different modes. There is no way to separate longitudinal modes and transversal modes in arbitrary domain, therefore there is no way to identify explicitly the same order modes of different grids. The further exploration of this problem is beyond the scope of this research.

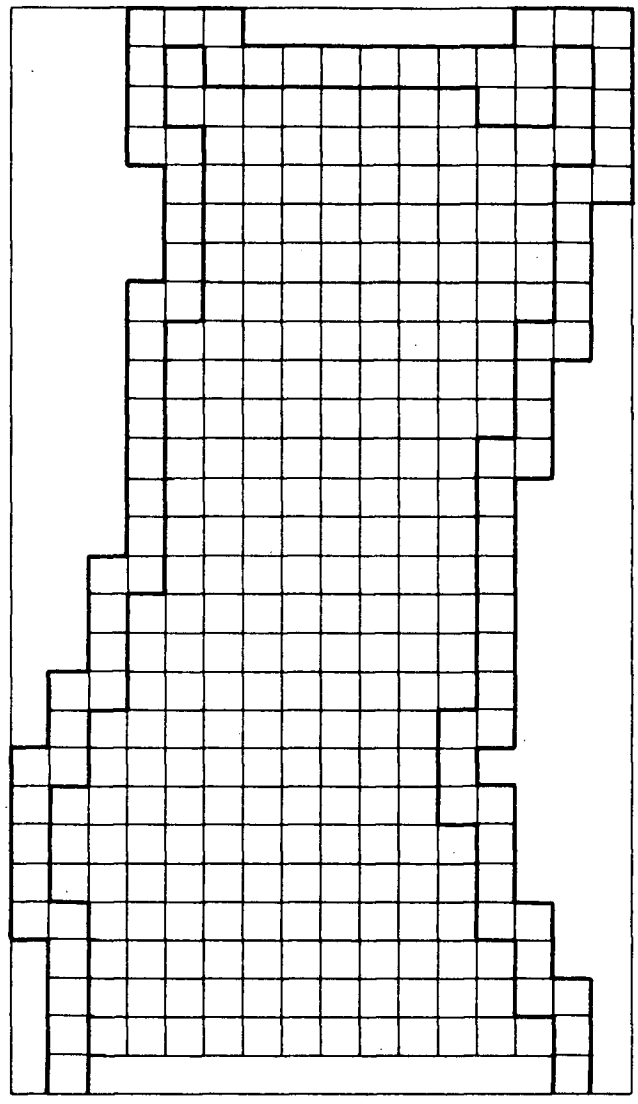

Figure 81 Augmented grid of Port San Juan. Thick lines are primitive and augmented boundaries.

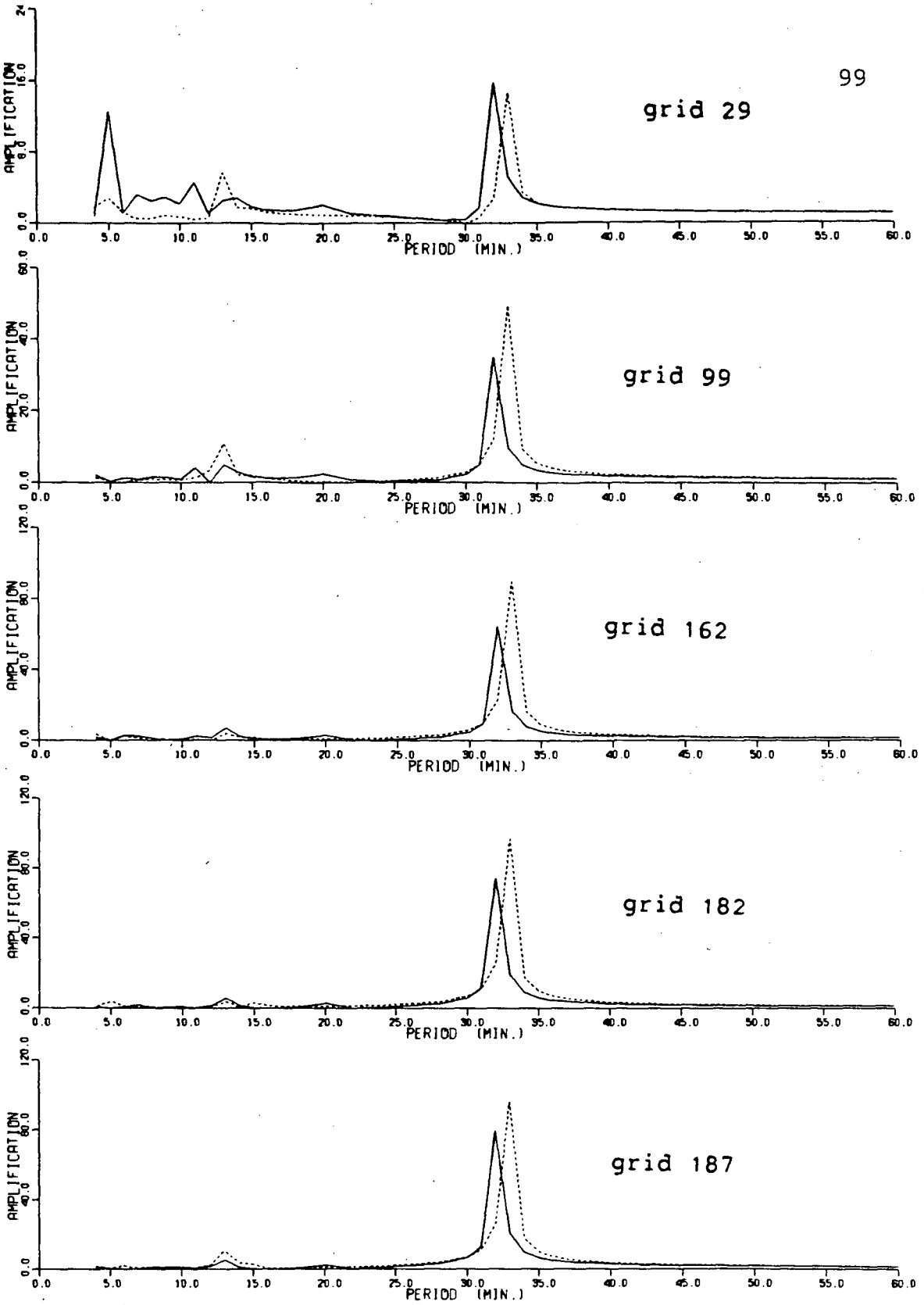

Figure 82 Comparison of amplifications (absolute values) between basic grid and augmented grid, Port San Juan.
Solid line: augmented grid.
Dashed line: basic grid.

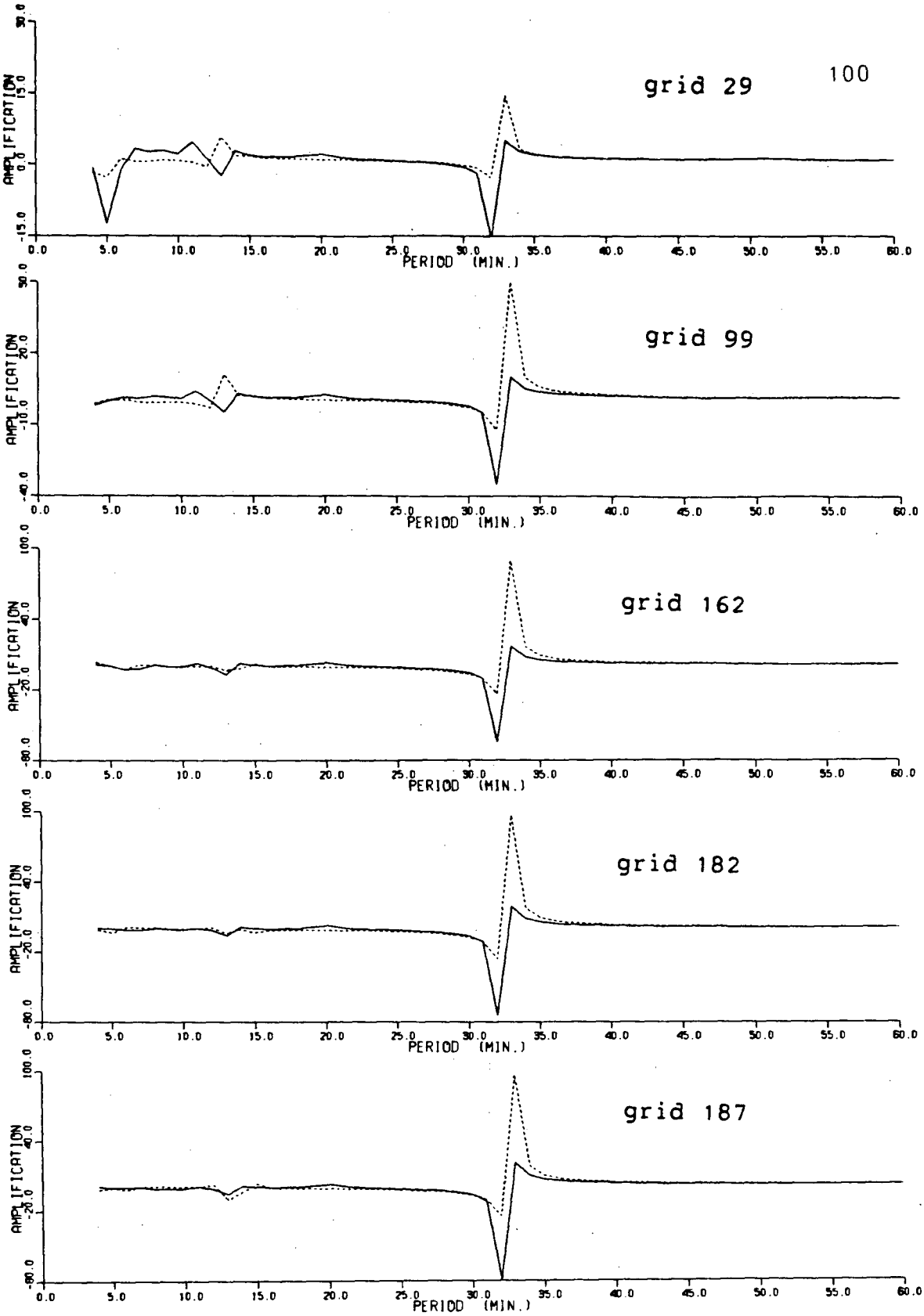

Figure 83 Comparison of amplifications (true values) between basic grid and augmented grid, Port San Juan.
Solid line: augmented grid.
Dashed line: basic grid.

D. THE EFFECT OF BOTTOM FRICTION

To consider the effect of friction we still start from the linearized shallow water equations, for simplicity, adopting the linear friction terms λu and λv :

$$u_t + g\eta_x + \lambda u = 0$$

$$v_t + g\eta_y + \lambda v = 0 \qquad (4.4\text{-}1)$$

$$(Hu)_x + (Hv)_y + \eta_t = 0$$

Time harmonic dependence $e^{i\omega t}$ is assumed to eliminate the variable t in equation (4.4-1) ; thus $u=u_0(x,y)e^{i\omega t}$, $v=v_0(x,y)e^{i\omega t}$, $\eta=\eta_0(x,y)e^{i\omega t}$. After the $e^{i\omega t}$ is cancelled and dropping the '$_0$' we obtain

$$i\omega u + g\eta_x + \lambda u = 0$$

$$i\omega v + g\eta_y + \lambda v = 0 \qquad (4.4\text{-}2)$$

$$(Hu)_x + (Hv)_y + i\omega\eta = 0$$

From the first two equations of (4.4-2) we have

$$u = -\frac{g\eta_x}{i\omega+\lambda}$$

$$v = -\frac{g\eta_y}{i\omega+\lambda}$$

substituting into the third equation of (4.4-2)

$$\left[\frac{Hg}{i\omega+\lambda} \eta_x \right]_x + \left[\frac{Hg}{i\omega+\lambda} \eta_y \right]_y - i\omega\eta = 0$$

which may also be written, after multiplication by $(i\omega+\lambda)$

$$[\nabla H\cdot\nabla + H\nabla^2 + \frac{\omega^2}{g} - i\frac{\omega\lambda}{g}]\eta = 0$$

Introducing $L = \nabla H\cdot\nabla+H\nabla^2+\omega^2/g-i\omega\lambda/g$ as a linear operator, then we have

$$L\eta = 0 \qquad (4.4-3)$$

The result we are interested in is only the ratio of η at a specified point in the bay to the η at mouth :

$$A(x,y,\omega) = \frac{\eta_b^*(x,y,\omega)}{\eta_m^*(x,y,\omega)} \qquad (4.4-4)$$

where η_b^* stands for η in the bay

η_m^* stands for η at the mouth

We set boundary condition at mouth $\eta_m^* = \eta_m e^{i\phi_m}$ as a uniform periodic oscillation with maximum amplitude η_m and phase ϕ_m , and assume the solution of boundary value problem (4.4-3) is $\eta_b^* = \eta_b e^{i\phi_b}$, i.e. standing wave with maximum amplitude η_b (x,y,ω) and phase ϕ_b (x,y,ω).

Therefore we get

$$A = \frac{\eta_b}{\eta_m} e^{i(\phi_b - \phi_m)} \tag{4.4-5}$$

substituting (4.4-5) into (4.4-3), we have

$$\begin{aligned} L\,A &= L\left[\frac{\eta_b}{\eta_m} e^{i(\phi_b - \phi_m)}\right] \\ &= L\left[\eta_b(x,y,\omega) e^{i\phi(x,y,\omega)} \cdot (\eta_m e^{i\phi_m})^{-1}\right] \qquad (4.4\text{-}6) \\ &= (\eta_m e^{i\phi_m})^{-1} L\left[\eta_b(x,y,\omega) e^{i\phi(x,y,\omega)}\right] = 0 \end{aligned}$$

Then the boundary value problem becomes

$$LA = 0 \qquad \text{inside the bay} \tag{4.4-7}$$

$$A = 1 \qquad \text{at the mouth} \tag{4.4-8}$$

For the following work we just consider equation (4.4-3) plus open boundary condition η=1 at mouth. This is equivalent to the problem for the amplification factor A.

Notating $\eta = \eta_r + i\eta_i$ where

η_r real part of η

η_i imaginary part of η ,

equation (4.4-3) is divided into two parts:

$$\begin{aligned} A\eta_r + D\eta_i &= 0 \\ -D\eta_r + A\eta_i &= 0 \end{aligned} \tag{4.4-9}$$

with the operators

$$A = \nabla H \cdot \nabla + H\nabla^2 + \frac{\omega^2}{g}$$

$$D = \frac{\omega\lambda}{g}$$

The open boundary condition is $\eta_r = 1$ and $\eta_i = 0$, i.e. $\phi_b = 1$ and $\phi_m = 0$.

A is an operator of the frictionless shallow water equation (4.1-4) leading to matrix **A** in (4.1-9), D represents the effect of friction.

To obtain numerical solution of [(4.4-7)+(4.4-8)], I considered four possible methods.

The first method is identical to that used in frictionless model, for which we had (4.1-9) from

$$\begin{aligned} A\eta &= 0 \qquad \text{inside the bay} \\ \eta &= 1 \qquad \text{at the mouth} \end{aligned} \tag{4.4-10}$$

The discrete finite difference form of (4.4-10) leads to a system of linear algebraic equations

$$\mathbf{A}\tilde{\eta}_o = \mathbf{b}_o \tag{4.4-11}$$

here **A** is the matrix of coefficients, identical to the **A** in (4.1-9), $\tilde{\eta}_o$ is the vector of solution and $\mathbf{b}_o$ is the vector

introduced by the open boundary value. The open boundary value is a constant factor of $\mathbf{b}_o$; it doesn't contribute anything to matrix **A**.

Now $\tilde{\eta}$ denotes a column vector formed by $\tilde{\eta}_r$ and $\tilde{\eta}_i$, **b**, a column vector formed by $\mathbf{b}_o$ and a same size zero vector and **D** is the product of $\frac{\omega\lambda}{g}$ and an identity matrix:

$$\left[\tilde{\eta}\right]_{2n\times 1} = \begin{bmatrix}\left[\tilde{\eta}_r\right]_{n\times 1} \\ \left[\tilde{\eta}_i\right]_{n\times 1}\end{bmatrix} \tag{4.4-12.1}$$

$$\left[\mathbf{b}\right]_{2n\times 1} = \begin{bmatrix}\left[\mathbf{b}_o\right]_{n\times 1} \\ \left[\mathbf{0}\right]_{n\times 1}\end{bmatrix} \tag{4.4-12.2}$$

$$\mathbf{D} = \begin{bmatrix} \frac{\omega\lambda}{g} & & 0 & 0 \\ & \ddots & & \\ & & \ddots & \\ & & & \ddots \\ 0 & & & \frac{\omega\lambda}{g} \\ 0 & 0 & & \end{bmatrix}_{n\times n} \tag{4.4-12.3}$$

The equation system [(4.4-7)+(4.4-8)] leads to a system of linear algebraic equations:

$$\begin{bmatrix} A & D \\ -D & A \end{bmatrix} \begin{bmatrix} \\ \tilde{\eta} \\ \\ \end{bmatrix} = \begin{bmatrix} \\ b \\ \\ \end{bmatrix} \qquad (4.4\text{-}13)$$

With this method we have to deal with large size matrix, it not only increases computing expenses, but also decreases the accuracy.

From the handling of the equation system it is obvious that the bottom friction not only changes the amplitude of the amplification factor, but also causes a phase shift. System (4.4-13) can be solved by subroutine SLE as described before.

A second method starts from (4.4-13), which we split into real and imaginary parts:

$$A\tilde{\eta}_r + D\tilde{\eta}_i = b_o \qquad (4.4\text{-}14)$$

$$A\tilde{\eta}_i - D\tilde{\eta}_r = 0 \qquad (4.4\text{-}15)$$

from (4.4-14)

$$\tilde{\eta}_i = D^{-1}b_o - D^{-1}A\tilde{\eta}_r = D^{-1}(b_o - A\tilde{\eta}_r) \ .$$

Substituting into (4.4-15)

$$AD^{-1}b_o - AD^{-1}A\tilde{\eta}_r - D\tilde{\eta}_r = 0$$

i.e.

$$\mathbf{D}^{-1}(\mathbf{A}\mathbf{b}_0-\mathbf{A}^2\tilde{\eta}_r-\mathbf{D}^2\tilde{\eta}_r)=0$$

$$\mathbf{A}\mathbf{b}_0-\mathbf{A}^2\tilde{\eta}_r-\mathbf{D}^2\tilde{\eta}_r=0$$

$$\tilde{\eta}_r=(\mathbf{A}^2+\mathbf{D}^2)^{-1}\mathbf{A}\mathbf{b}_0$$

Because **D** is the product of a constant and the identity matrix, we need only one matrix multiplication to get

$$\mathbf{A}^*=\mathbf{A}^2+\mathbf{D}^2$$

and one multiplication of a matrix and a vector to get

$$\mathbf{b}^*=\mathbf{A}\mathbf{b}_0$$

In order to obtain $\tilde{\eta}_r$, we solve the algebraic equation system

$$\mathbf{A}^*\tilde{\eta}_r=\mathbf{b}^*$$

instead of calculating the inverse matrix $(\mathbf{A}^*)^{-1}$ in consideration of saving computing time.

Table 4 shows the comparison of computing times of linear algebraic equation system and inverse matrix, where N is the order of matrix, namely the number of grid points.

Table 4 CPU Time for subroutines SLE and INV

N	System of Linear Equations (SLE)	Inverse Matrix (INV)
20	0.003	0.012
50	0.013	0.154
100	0.051	1.177
150	0.114	3.973
200	0.201	9.355

From Table 4 we know that computing time increases greatly along with the order of matrix, and the computing of inverse matrix should be replaced by solving the corresponding system of linear equations.

The third method starts from (4.4-14) and (4.4-15). From (4.4-15),

$$\tilde{\eta}_r = \mathbf{D}^{-1}\mathbf{A}\tilde{\eta}_i \ ;$$

substituting into (4.4-14), we get

$$(\mathbf{A}\mathbf{D}^{-1}\mathbf{A}+\mathbf{D})\tilde{\eta}_i = \mathbf{b}$$

To proceed this way, we have to calculate $\tilde{\eta}_i$ first, but $\tilde{\eta}_i$ is smaller than $\tilde{\eta}_r$, and as a result small round off errors in $\tilde{\eta}_i$ maybe causes large errors in $\tilde{\eta}_r$.

A fourth method was considered. From (4.4-15)

$$\tilde{\eta}_i = \mathbf{A}^{-1}\mathbf{D}\tilde{\eta}_r \ ;$$

substituting into (4.4-14), we get

$$\mathbf{A}\tilde{\eta}_r + \mathbf{D}\mathbf{A}^{-1}\mathbf{D}\tilde{\eta}_r = \mathbf{b}_o$$

$$(\mathbf{A} + \mathbf{D}\mathbf{A}^{-1}\mathbf{D})\tilde{\eta}_r = \mathbf{b}_o$$

But the calculation of $\mathbf{A}^{-1}$ costs much more computing time as shown in Table 4.

After performing computation with the first three methods with one value of λ in Pedder Bay, I found that methods 2 and 3 saved about 3/4 computer storage space and 1/3 computing time compared with method 1. There was no substantial difference of computed results among the 3 methods when double precision was invoked, but for single precision the difference reached up to 10% in some cases.

Taking $\lambda=3.0\times10^{-5}\cdot s^{-1}$ (Proudman 1953; Jamart and Winter 1978) and computing with method 3, the result shows that the bottom friction doesn't cause any meaningful change in the amplification factors. Two other values, $\lambda=3.0\times10^{-4}$ and $\lambda=1.0\times10^{-3}$ were taken into the same computing procedure in the three bays. The results are shown in Figure 84 to Figure 86, where the solid lines are frictionless output of numerical model, "Δ" for $\lambda=3.0\times10^{-5}$, "+" for $\lambda=3.0\times10^{-4}$, "$\times$" for $\lambda=1.0\times10^{-3}$.

For the larger amplification factor, Isozaki (1979) pointed out that the linear model produced a slightly larger amplitude of sea level oscillations than the nonlinear

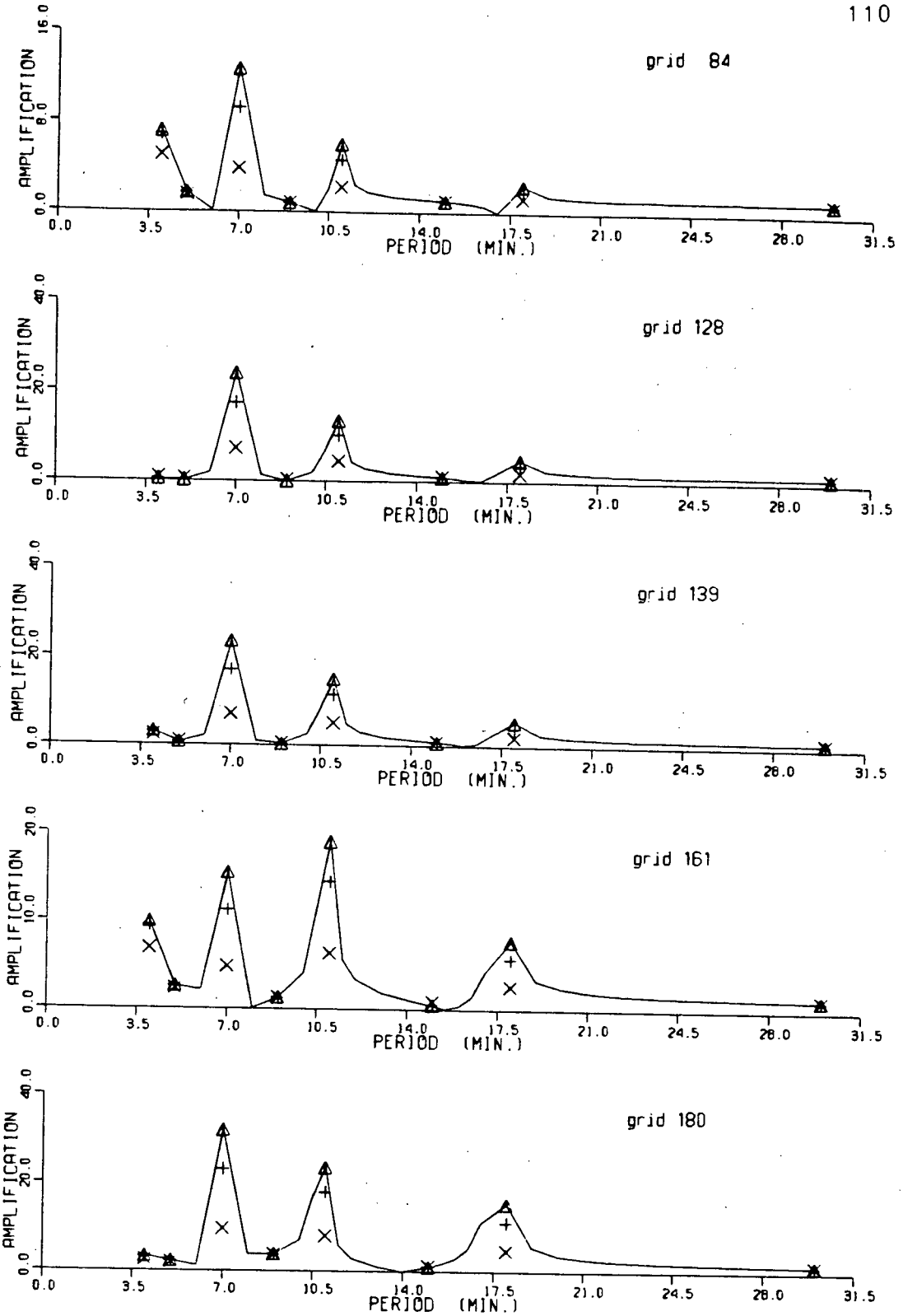

Figure 84 The effect of friction coefficients in the numerical model of Pedder Bay.

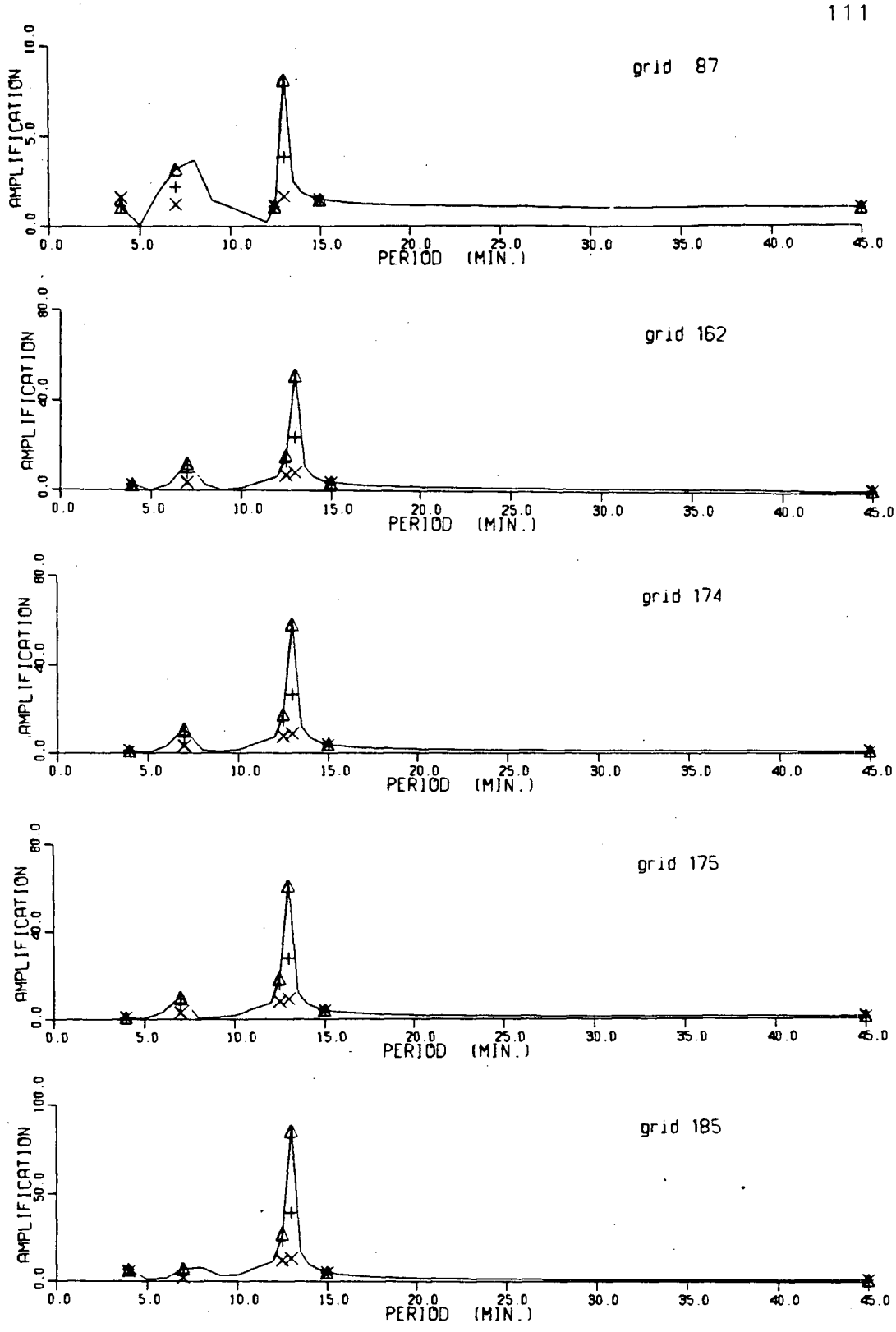

Figure 85 The effect of friction coefficients in the numerical model of Becher Bay.

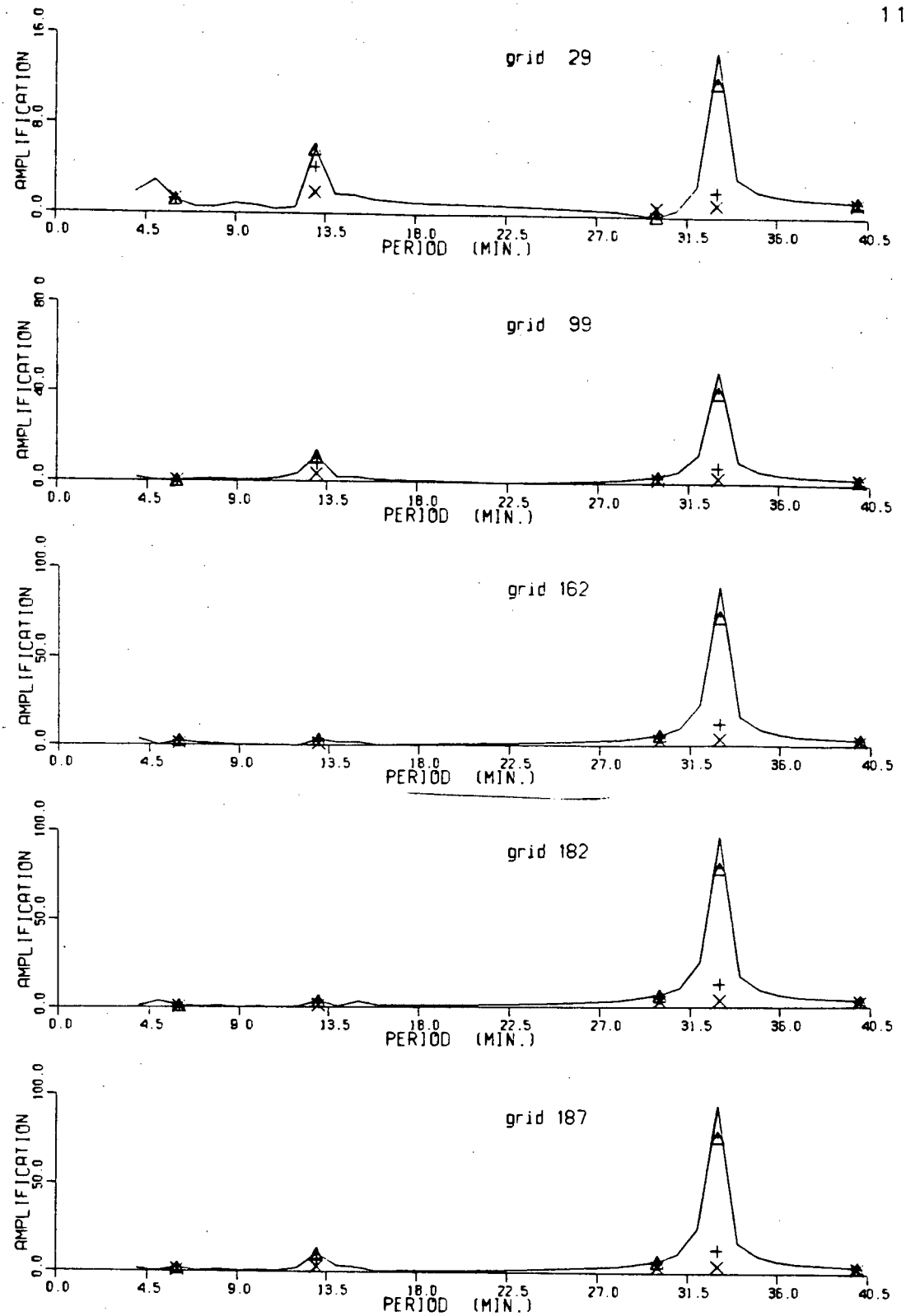

Figure 86 The effect of friction coefficients in the numerical model of Port San Juan.

model, but the differences are not significant. Another possible damping factor is the effect of ocean impedance through the boundary condition. In the case of large amplification the water communication between open ocean and a bay becomes an important factor, the ocean impedance could not be ignored.

In spite of the reasons given above the range of amplification is still an argueable problem. Olsen and Hwang (1971) reported the simultaneously measured wave data inside and outside Keauhou Bay, Hawaii, which do show amplications of as much as 33 at selected frequencies.

V. COMPARISON OF THE RESULTS BETWEEN NUMERICAL MODEL AND SPECTRAL ANALYSIS

The amplification factors predicted by the numerical model are compared here with the power spectra of measured data.

The seiche does not always occur due to the absence of exciting sources, so first I compared the numerical results with the typical resonant spectra, i.e. with band averaged spectra described in Chapter 3 and presented in Figure 33 to Figure 35. These spectra were calculated from selected time series when typical seiche fluctuation occured.

Figure 87 shows the comparison in Pedder Bay. The solid line is the measured spectrum, the symbol □ represents the amplification factor in grid #161, where the pressure gauge was installed to measure the sea level fluctuations. The amplification factors were multiplied by 80 to make the maxima of spectrum and the factors have the same scale. The peaks at 11 minutes period agree very well with each other. The numerically predicted resonant periods at 18 and 7 minutes peaks, or 0.06 and 0.14 cpm in frequency, are not present in the observed spectrum. The low frequency peaks of spectra may not be due to resonance.

Figure 88 shows the comparison in Becher Bay at grid #175 which is the gauge position. The amplification factors were enlarged 50 times. The peaks at period 13 minutes (0.077 cpm in frequency) agree very well. In the observed spectra there is no peak at the predicted second resonant

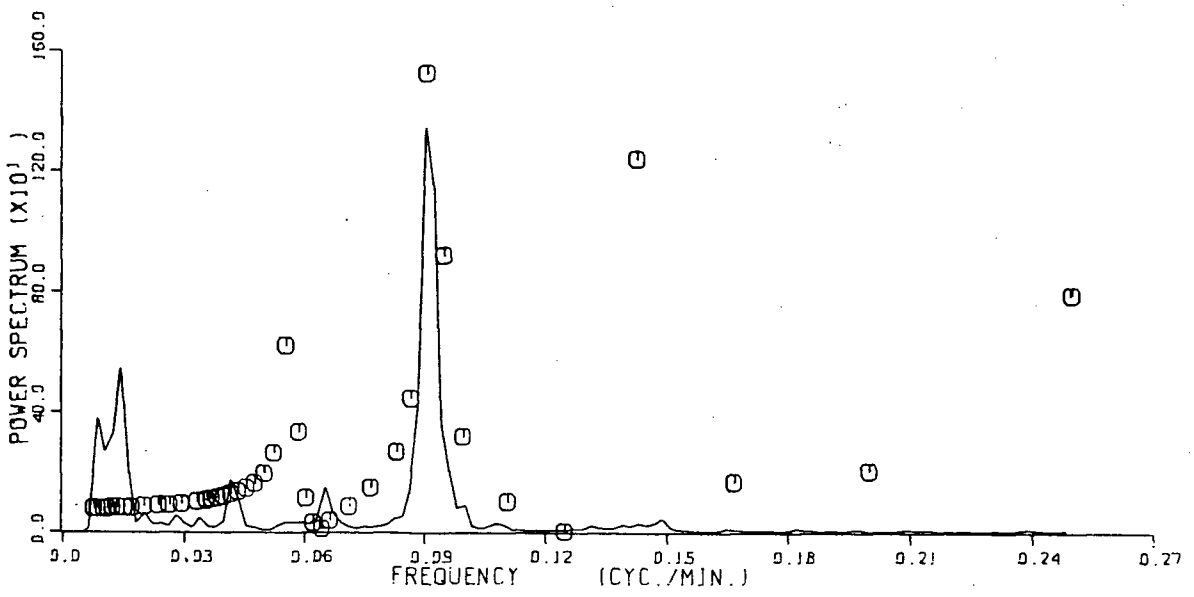

Figure 87 Comparison between observed spectrum (solid line) and amplification factors (□) in Pedder Bay.

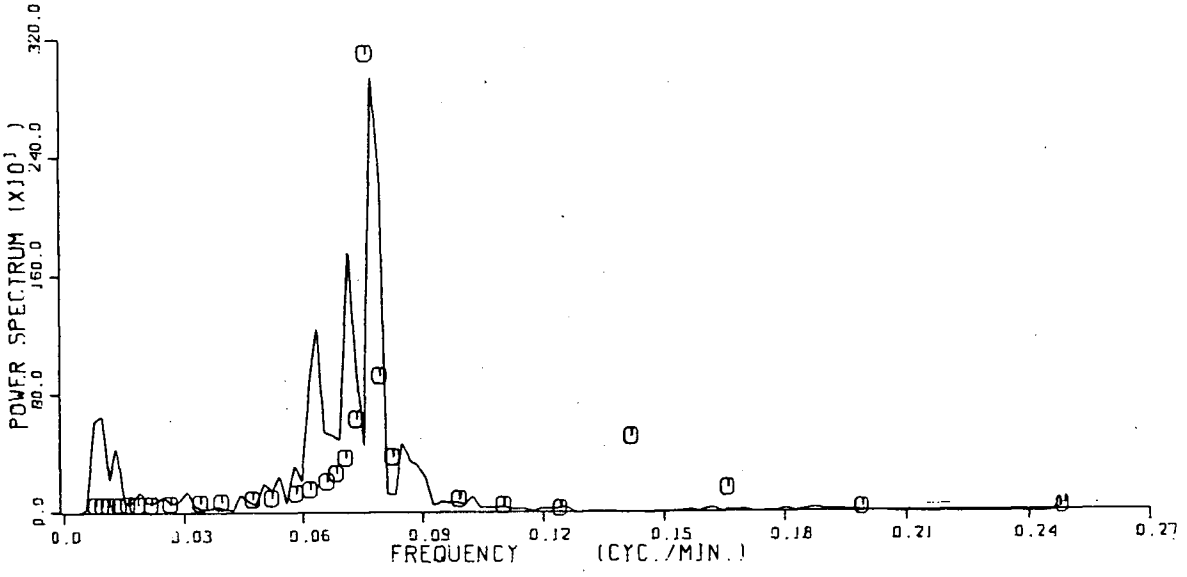

Figure 88 Comparison between observed spectrum (solid line) and amplification factors (□) in Becher Bay.

period 7 minutes. The low frequency peak of the spectrum at period about 100 minutes should be attributed to external forcing.

Figure 89 shows the comparison in Port San Juan at grid #187 (pressure gauge position). The resonant period for the predicted first mode (33 minutes) agrees very well with the observed spectrum. Another peak of spectrum is in period about 15 minutes which may be attributed to the second mode with period 13 minutes.

Summarizing the above comparisons we could conclude that the main amplification factors of numerical model are always identified in the observed spectra, even though the numerical model is constructed on the basis of a very simplified equation system. In other words, the resonant frequencies of a bay are controlled only by gravitational acceleration, pressure gradient and water mass continuity. Therefore it is practical and realistic to predict the resonant frequencies of these bays by the numerical model on the basis of only these three terms.

Figure 90 to Figure 92 show the same comparisons in Pedder Bay, Becher Bay and Port San Juan respectively, but the observed spectra are the 20-day ensemble averaged spectra shown in Chapter 3 Figure 19 to figure 21. Features similar to those seen in the last three figures are observed. It is worth pointing out that in Port San Juan there is substantial high frequency energy which is not related to the amplification factor predicted by numerical

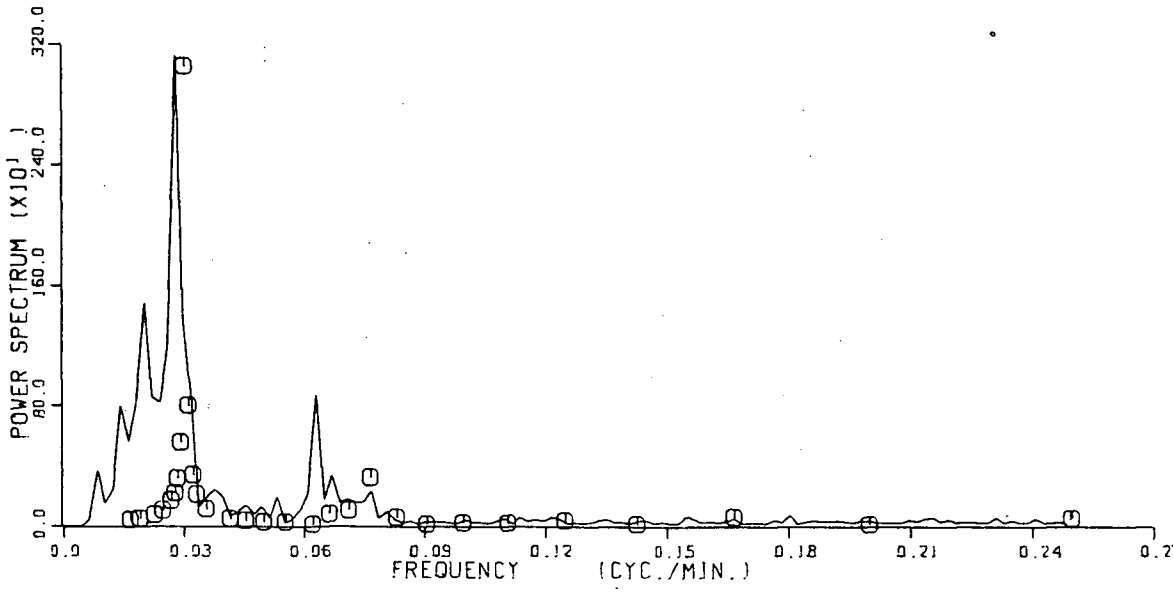

Figure 89 Comparison between observed spectrum (solid line) and amplification factors (□) in Port San Juan.

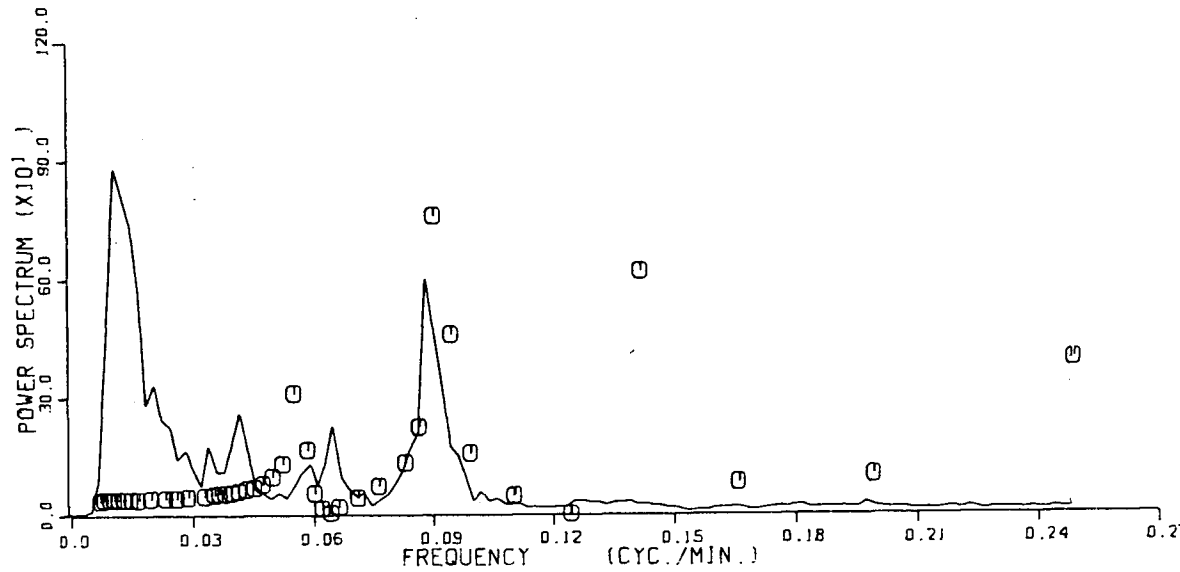

Figure 90 Comparison between 20-day averaged observed spectrum (solid line) and amplification factors (□) in Pedder Bay.

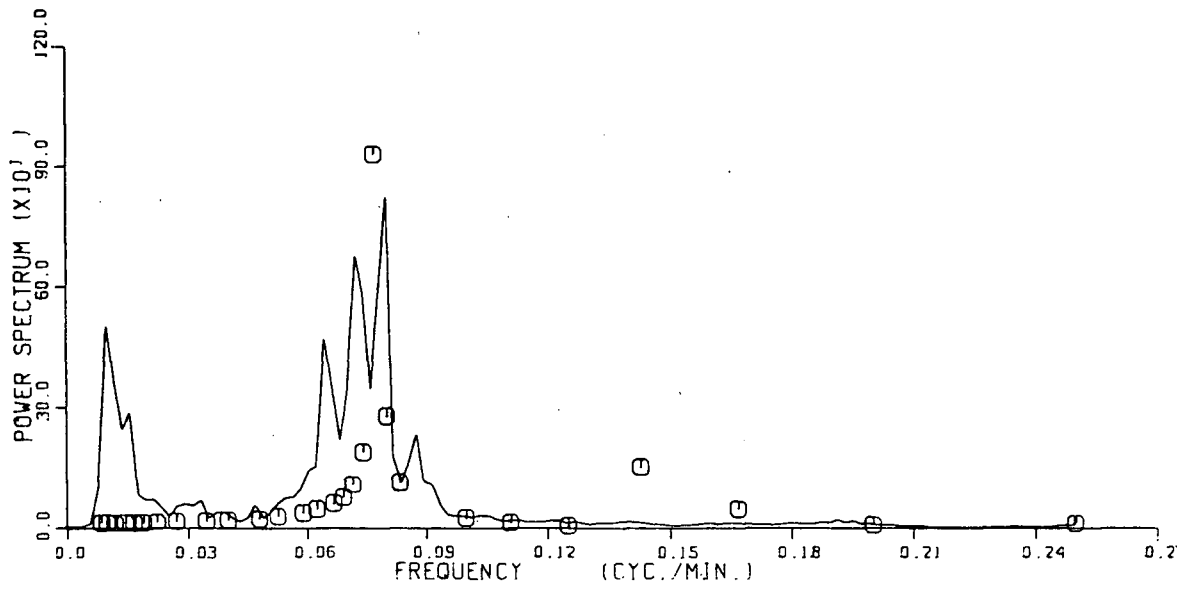

Figure 91 Comparison between 20-day averaged observed spectrum (solid line) and amplification factors (□) in Becher Bay.

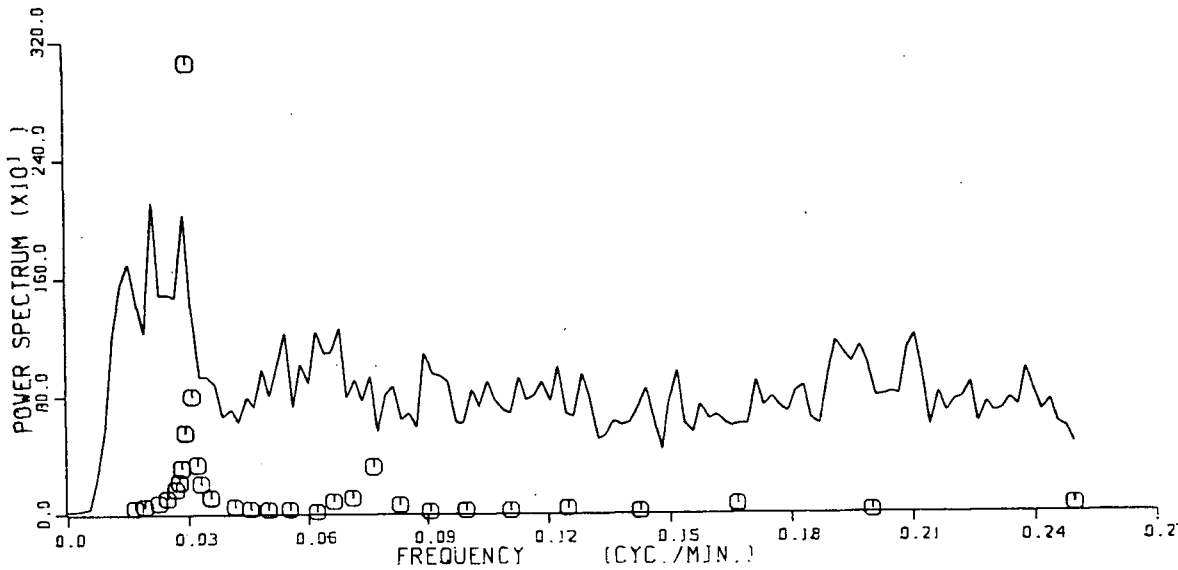

Figure 92 Comparison between 20-day averaged observed spectrum (solid line) and amplification factors (□) in Port San Juan.

model.

Figure 93 compares the numerical model and the observed spectrum in Pedder Bay under the circumstance of deeper water. The dashed line is the amplification factor when a depth of 1.8 meters was added to chart depth at grid #161 shown in Chapter 4 Figure 80 fourth graph by a dashed line. The solid line is the high tide level spectrum of Pedder Bay shown in Chapter 3 Figure 48. Because of the reason discussed in Chapter 4 the depth-added numerical prediction is not really reliable, therefore the comparison shows poor agreement.

In the spectra of Port San Juan large peaks are often seen at periods of about 30 to 45 minutes, the mean of this period range being a little larger than the resonant period of 33 minutes predicted by the numerical model. This discrepancy could be interpreted by the grid of Port San Juan: part of the bay close to the mouth is not included in the grid of numerical model because of the limitation of the chart used in this work, which undoubtedly reduces the predicted resonant period of the numerical model.

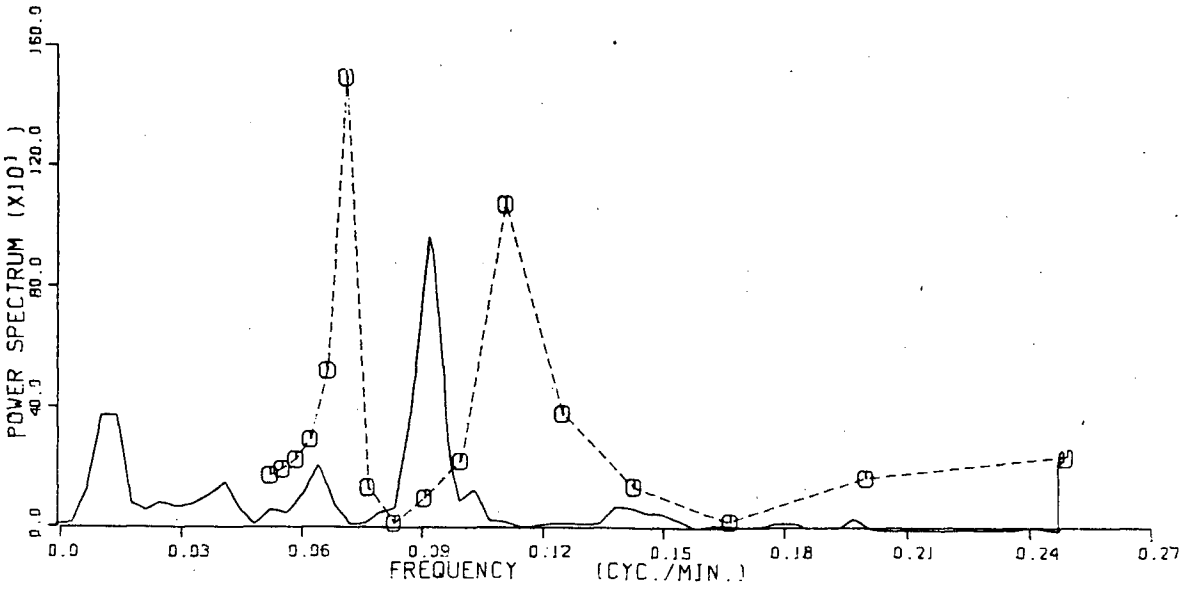

Figure 93 Comparison of observed spectrum (solid line) and amplification factors (□) for deep water in Pedder Bay.

VI. INVESTIGATION OF EXCITING SOURCES FOR OBSERVED SEICHES

In my summary of seiche exciting sources in Chapter 2, I concluded that the most probable causes of seiches are seismic activity on the ocean bottom, incoming waves from adjacent waters and wind stress or barometric jump. In the other words, seiching could be excited through the invasion from "army, navy and airforce". This Chapter discusses these possibilities.

The coherences from first data set and second data set showd very obvious correlation within the range of periods 30 minutes to about 1 hour between Becher Bay and Port San Juan. The coherence peaks within this range are well above confidence levels. We may conclude that those oscillations were excited by sources which traveled along Juan de Fuca Strait. From the coherences of second data set we have found that the oscillations of Pedder Bay were correlated with those of other bays at period more than 30 minutes and many shorter periods, including its resonant period 11 minutes,. which suggests the common exciting sources had wide range of periods.

Looking back to Figures 8 to 9 and Figures 13 to 18 in Chapter 3, we may find that around Jan. 20 and Feb. 2 there were obviously strong seiches whose detail is shown in Figure 94.

In order to reveal the common sources of these strong seiches, coherences and phases were computed and shown in Figures 95 to 98. The data used span one day and ten hours,

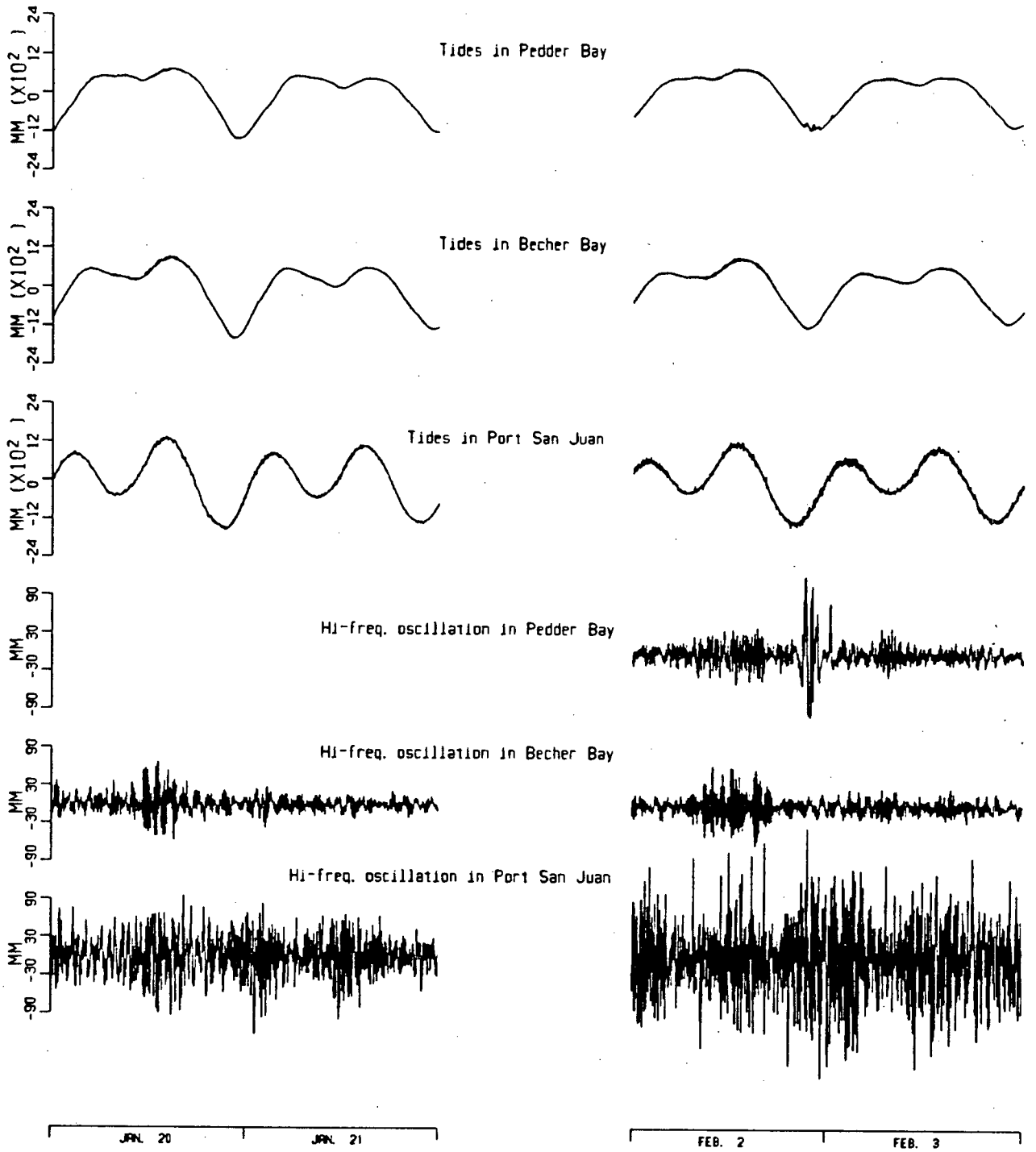

Figure 94 Strong seiches and corresponding tides.

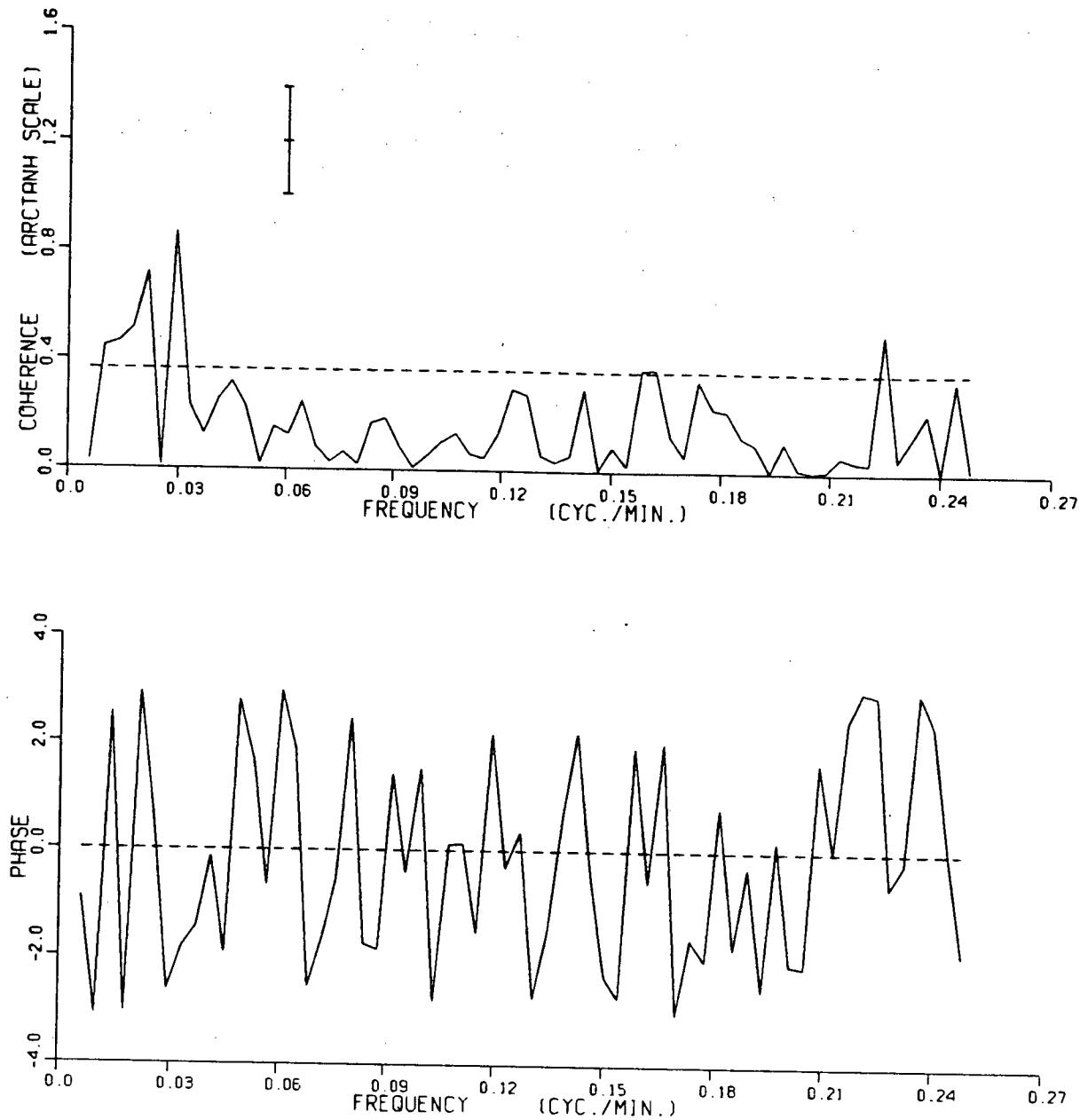

Figure 95 Coherence and phase between Becher Bay and Port San Juan, January.
Error bars: 95% confidence intervals.
Dashed line: 95% significance level

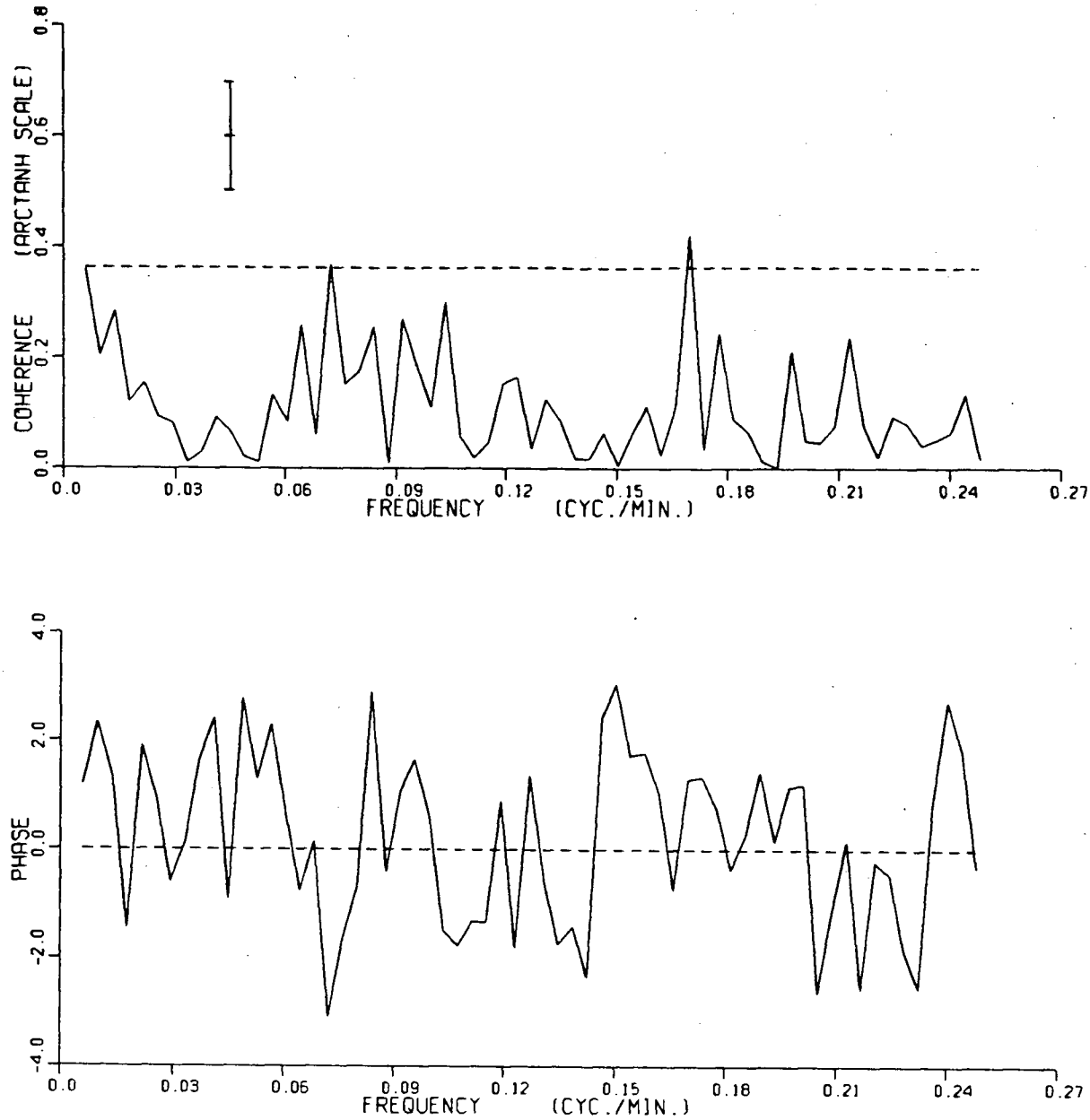

Figure 96 Coherence and phase between Pedder Bay and Becher Bay, February.
Error bars: 95% confidence intervals.
Dashed line: 95% significance level

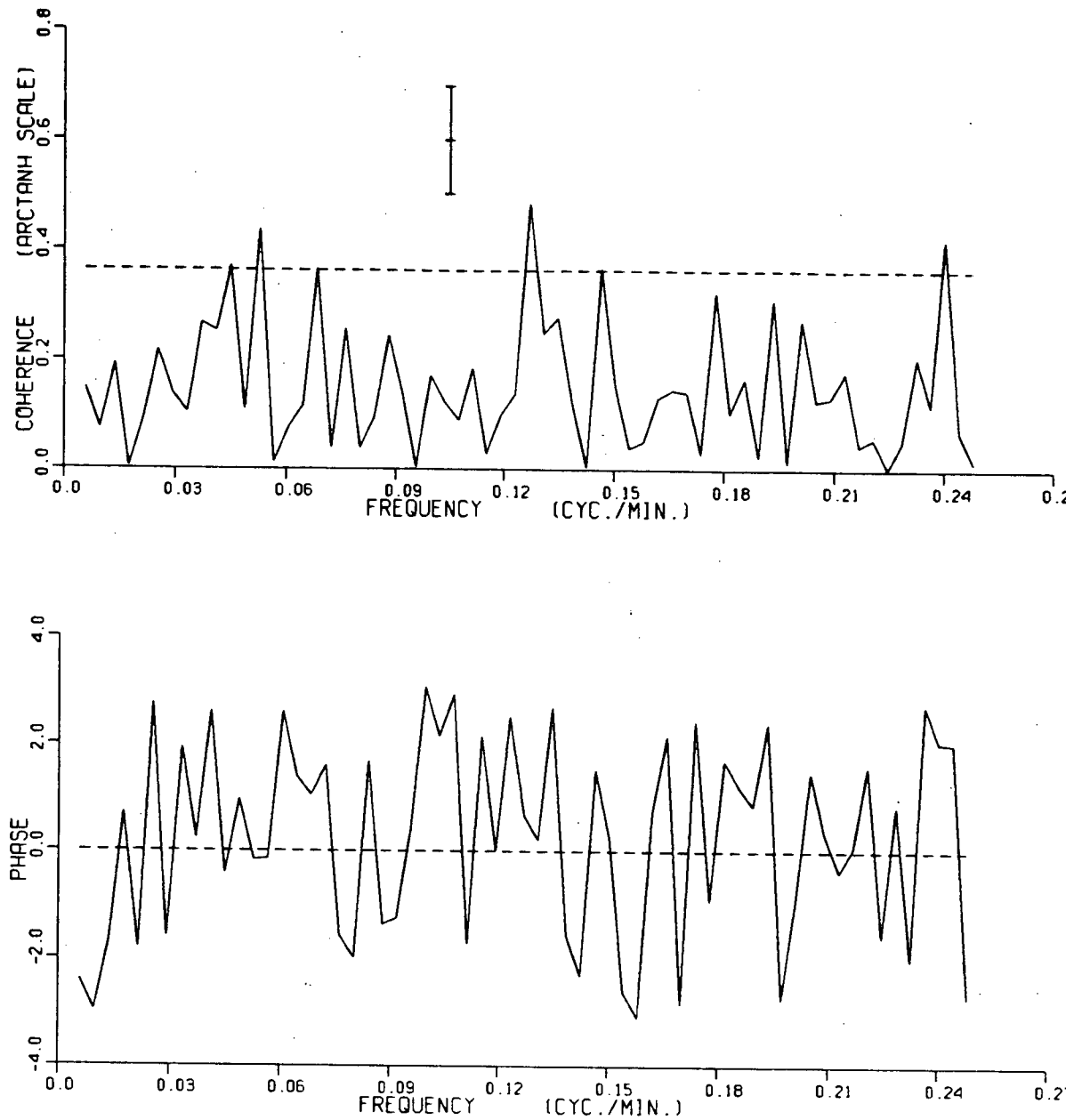

Figure 97 Coherence and phase between Pedder Bay and Port San Juan, February.
Error bars: 95% confidence intervals.
Dashed line: 95% significance level

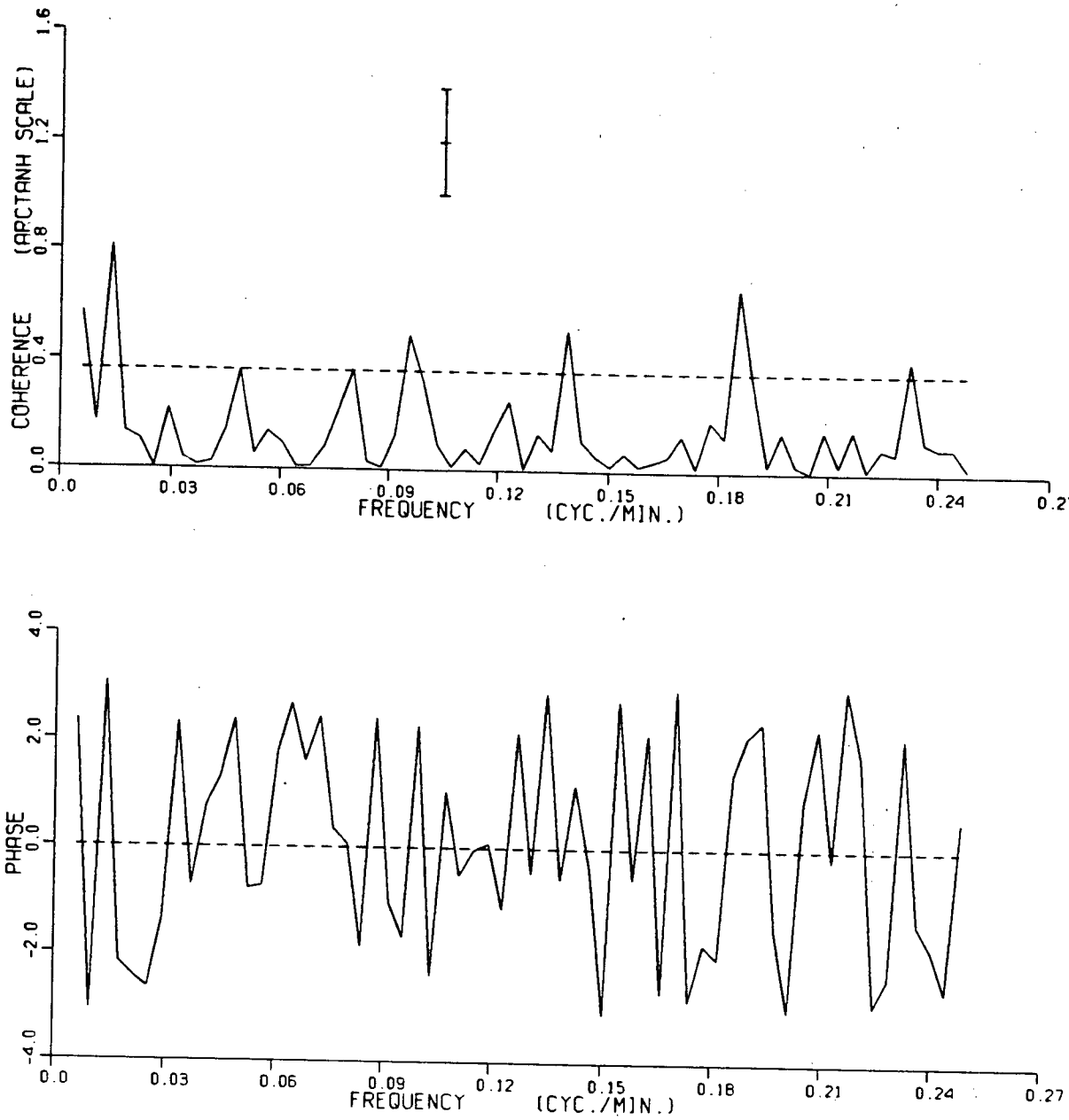

Figure 98 Coherence and phase between Becher Bay and Port San Juan, February.
Error bars: 95% confidence intervals.
Dashed line: 95% significance level

beginning from 00:00 Jan. 20 and 00:00 Feb. 2 respectively. The oscillations of Becher Bay and Port San Juan were correlated on both Jan. 20 and Feb. 2 at low frequency band. But Pedder Bay shows poor coherences with others.

We now concentrate on these dates to reveal the seiche-exciting sources.

A. SEISMIC ACTIVITY

By careful reading of the "Canadian Earthquakes National Summary", there was no recorded seismic activity on January 18 and 19, 1980. The recorded earthquakes of January 20 are described in Table 5:

Table 5 Seismic Activities, Jan. 20, 1980

DATE(1980)	H-TIME(UT)	LATITUDE (NORTH)	LONGITUDE (WEST)	MAGNITUDE
JAN. 20	11:33 (1)	59.40	134.65	ML=3.5
JAN. 20	13:01 (2)	59.45	134.61	ML=2.0

From Jan. 25 to Feb. 4, 1980, all earthquake records are shown in Table 6:

Table 6 Seismic Activities, Jan. 25 to Feb.4, 1980

DATE(1980)	H-TIME(UT)	LATITUDE (NORTH)	LONGITUDE (WEST)	MAGNITUDE
JAN. 28	00:41 (3)	46.67	122.20	ML=2.9
JAN. 29	00:41 (1)	46.68	122.09	ML=2.8

JAN. 29	06:07 (1)	47.92	122.49	ML=1.3
JAN. 31	00:00 (2)	49.35	115.18	ML=2.9
JAN. 31	01:41 (2)	48.72	122.06	ML=1.2

The above earthquakes occured inland far from Juan de Fuca Strait. The magnitudes are comparatively small. Therefore we conclude that the observed seiches are not related to the seismic activity.

B. INCOMING WAVES

The possible incoming waves which excite seiches in coastal bays are edge waves, swell and internal waves.

1. EDGE WAVES

The first candidate of seiche-exciting waves is edge waves passing along the coast by the mouths of bays.

The bottom profile of Juan de Fuca Strait just off the three bays may be represented by exponential curve. Then we select parameters H_0 and α to fit the exponential functions in the form of $H=H_0[1-\exp(-\alpha x)]$ to estimate the section of the Strait. Afterwards we could exactly follow Ball's method (1967) to calculate the dispersion relation of edge waves in term of hypergeometric function (Abramowitz and Stegun, 1970).

Figure 99 shows the selected exponential function by the solid curve and sounding depths by the circles for the bottom profile off Pedder Bay. Figure 100 is the resulting

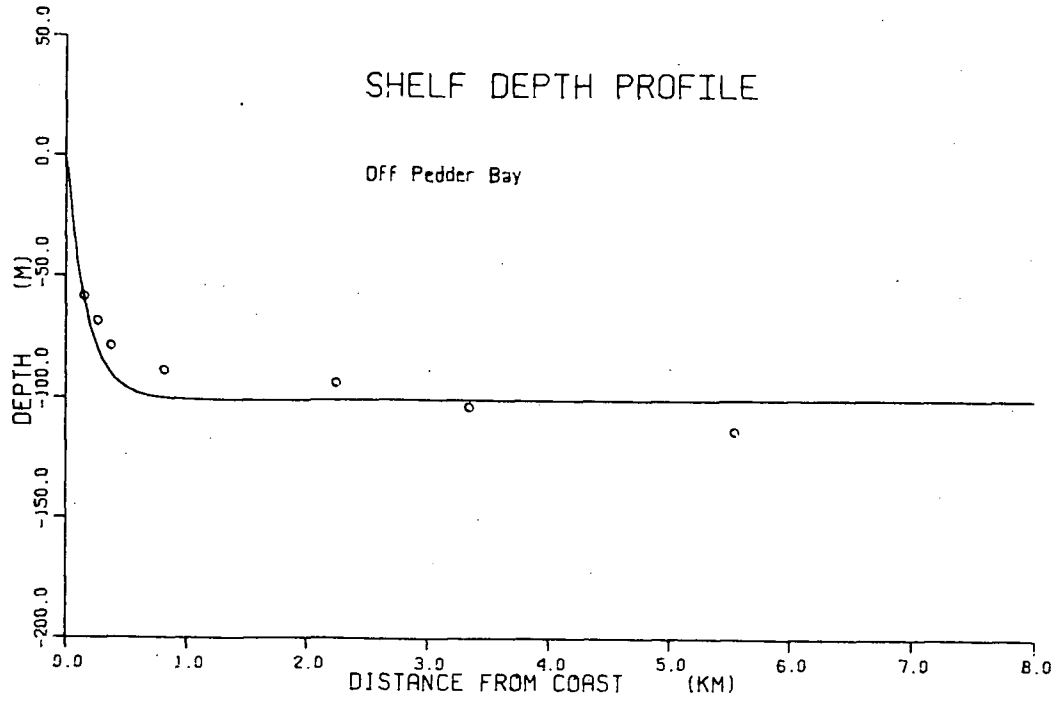

Figure 99 Exponential fitting for bottom profile off Pedder Bay.Circles are sounding depths.

dispersion relation from Ball's method. The dashed lines indicate modes which do not satisfy the boundedness conditions as x goes to ∞ imposed by Ball's theory. Bottom profiles and dispersion relations are shown in Figure 101 and Figure 102 for Becher Bay, Figure 103 and Figure 104 for Port San Juan.

Based on the calculated modes the corresponding sea surfaces are shown in Figure 105 for Pedder Bay, where the maximum wave amplitude at coast is assumed to be 1. Figure 106 for Becher Bay, Figure 107 and Figure 108 for Port San Juan for different periods. The width of the Strait of Juan de Fuca is only about 20 km, but the sea surface displacement does not change significantly within a distance of the same order. Ball's theory assumes an infinite shelf,

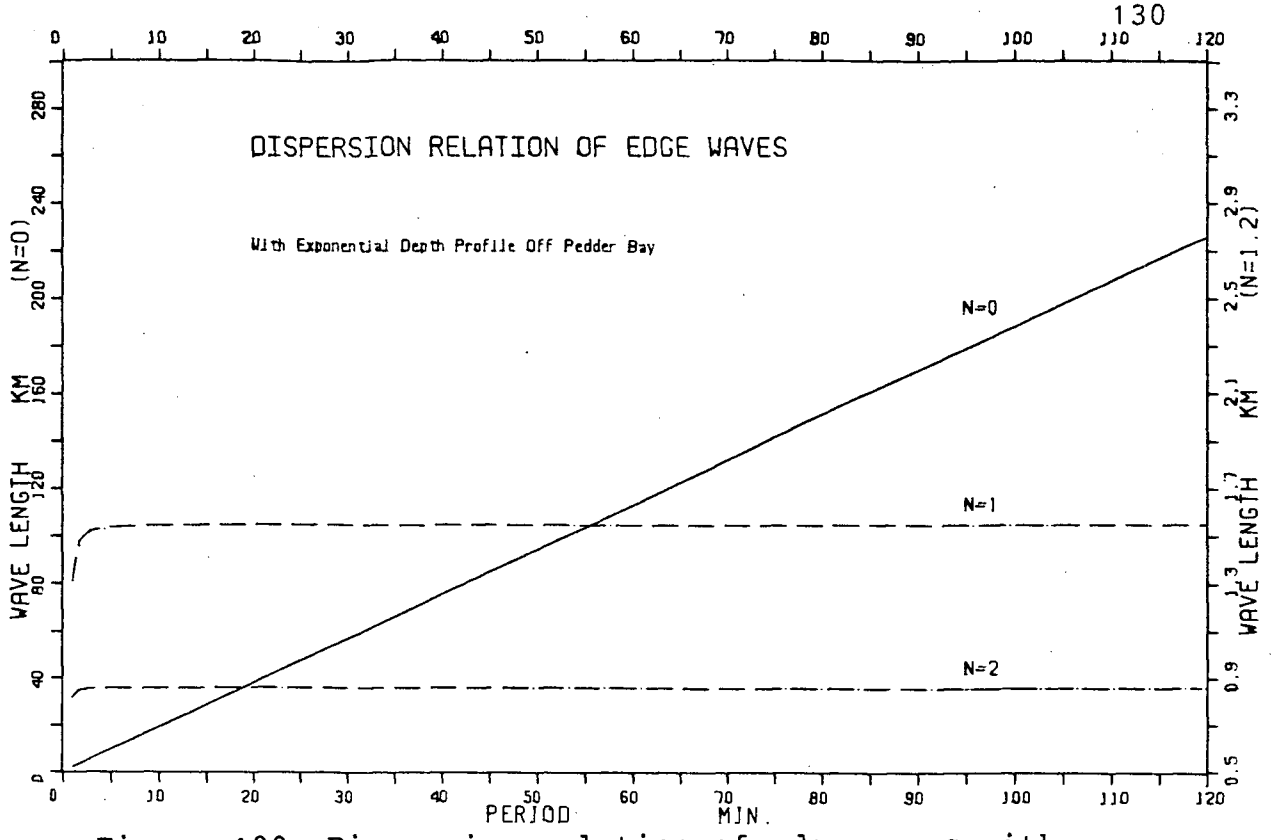

Figure 100 Dispersion relation of edge waves with exponential depth profile off Pedder Bay.

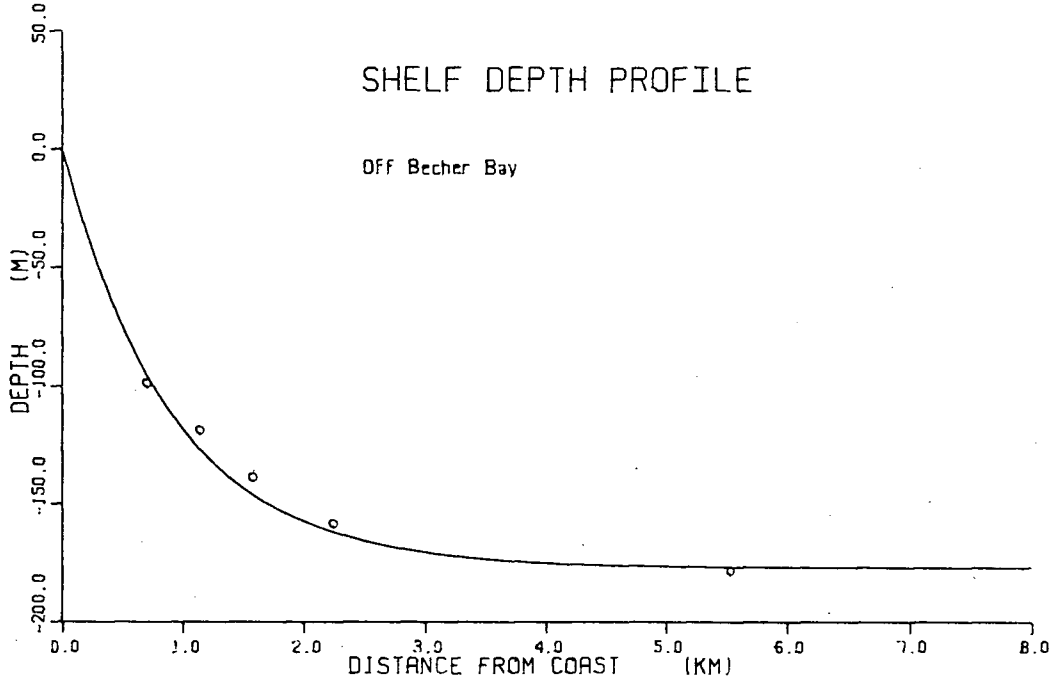

Figure 101 Exponential fitting for bottom profile off Becher Bay.Circles are sounding depths.

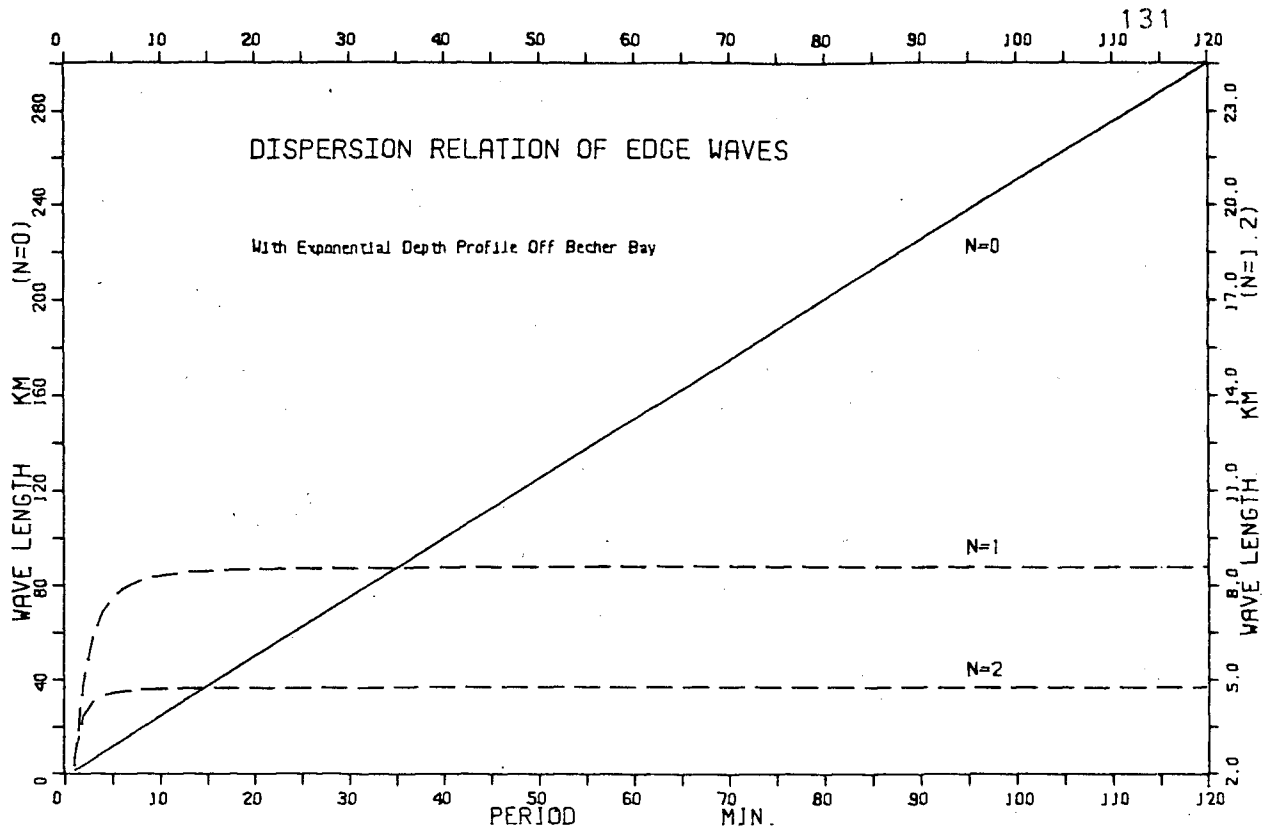

Figure 102 Dispersion relation of edge waves with exponential depth profile off Becher Bay.

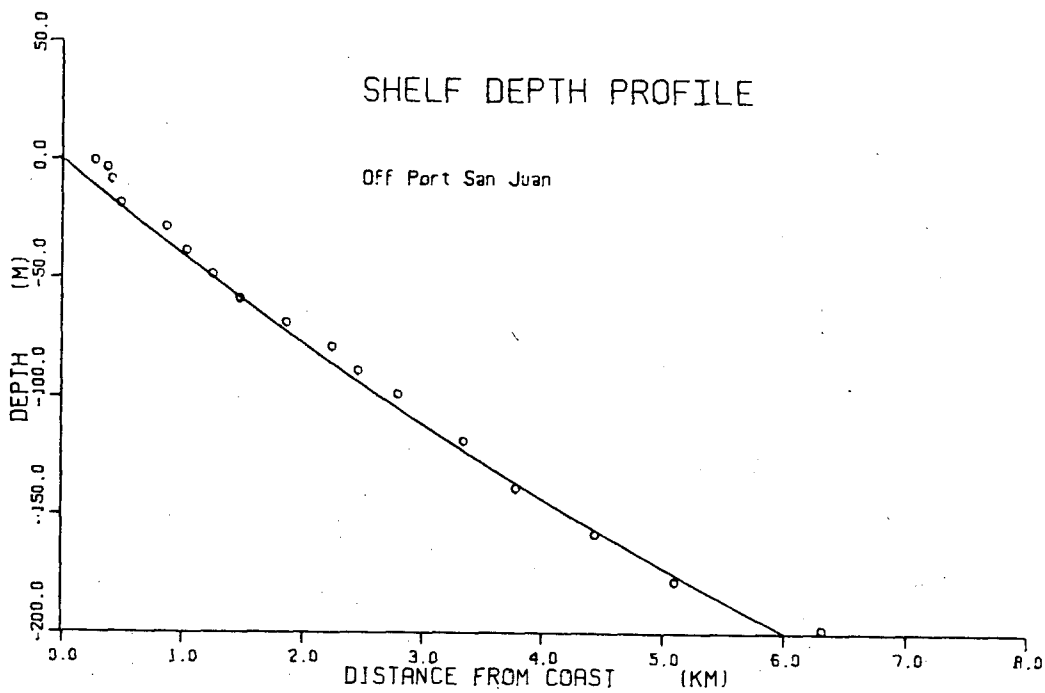

Figure 103 Exponential fitting for bottom profile off Port San Juan.Circles are sounding depths.

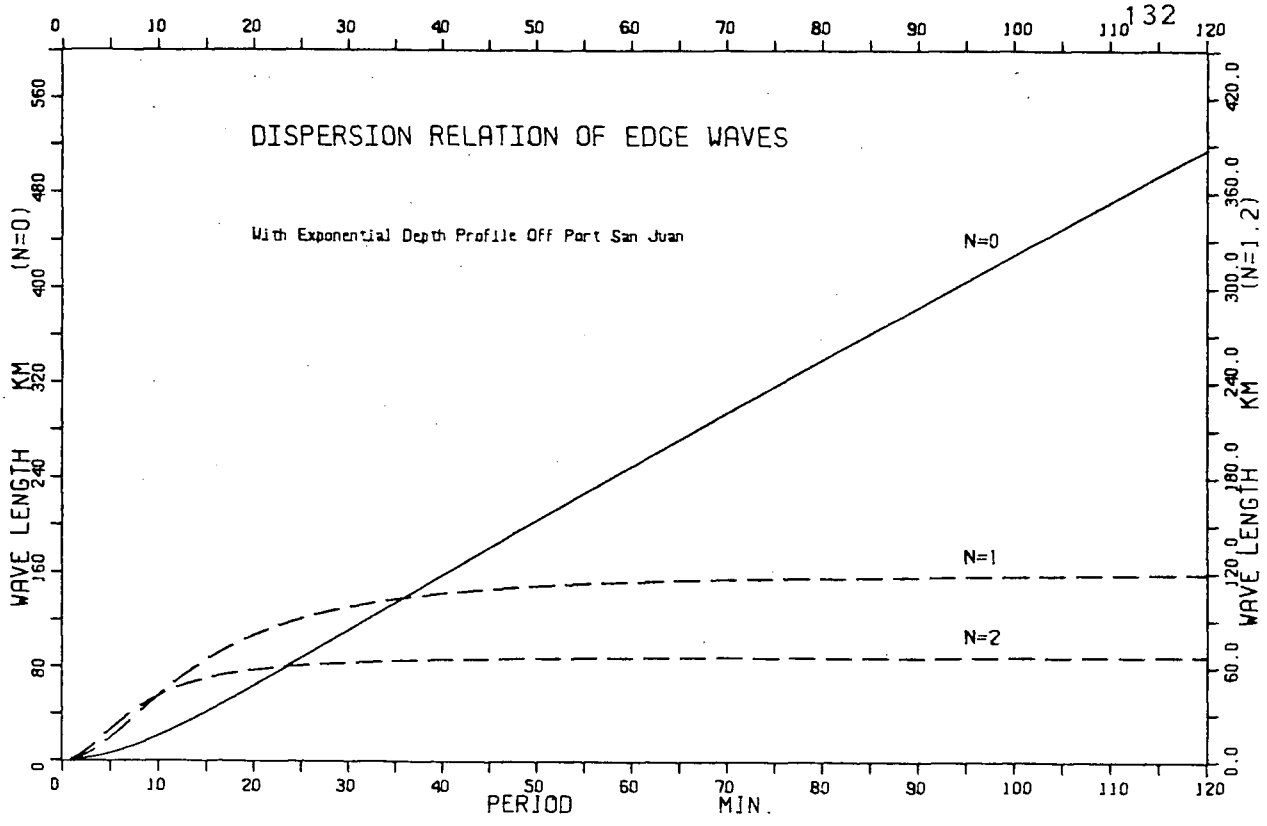

Figure 104 Dispersion relation of edge waves with exponential depth profile off Port San Juan.

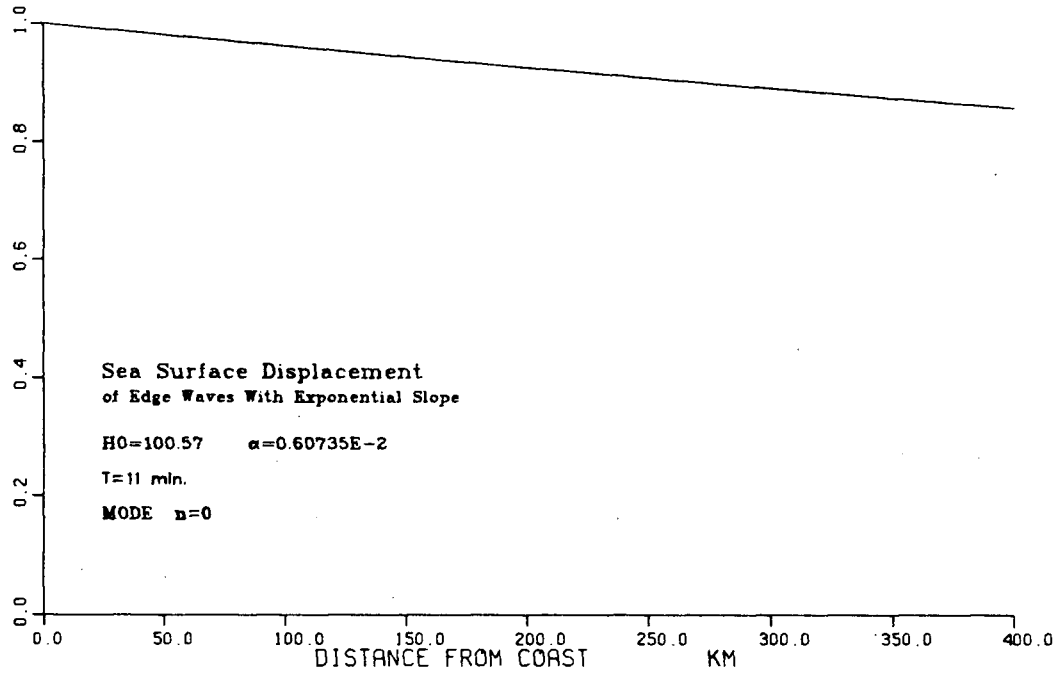

Figure 105 Sea surface displacement in period 11 min. off Pedder Bay.

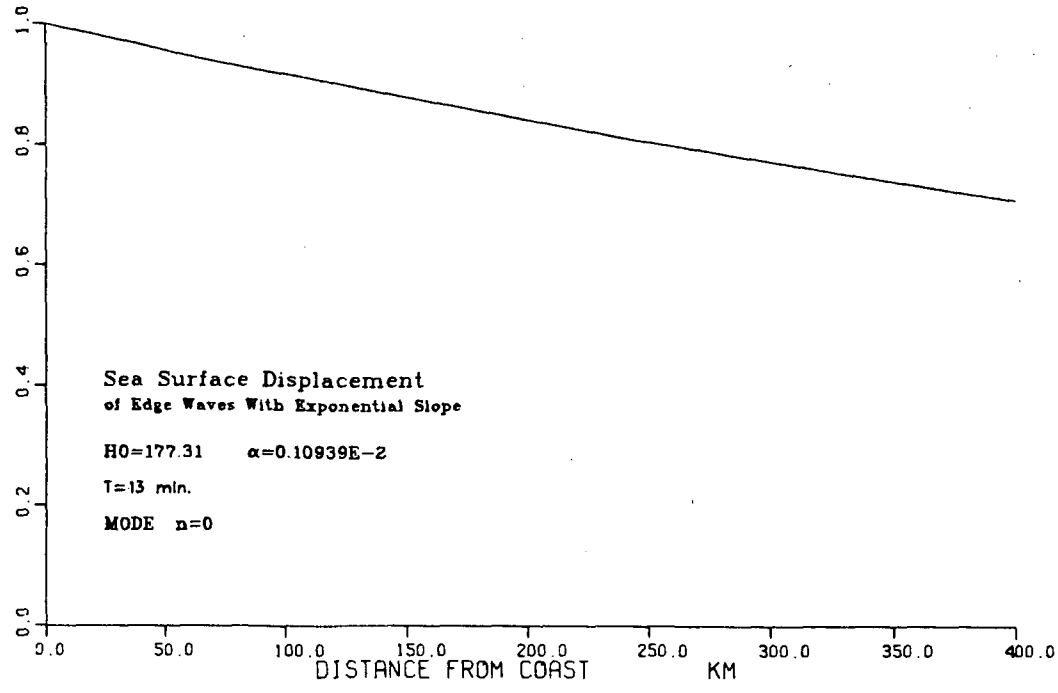

Figure 106 Sea surface displacement in period 13 min. off Becher Bay.

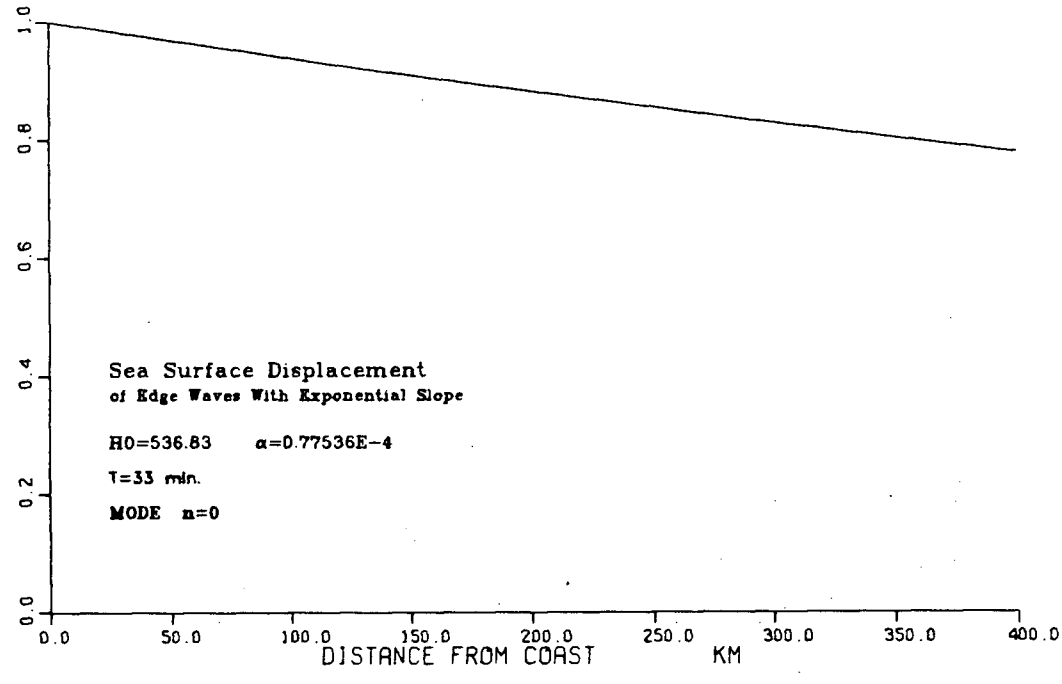

Figure 107 Sea surface displacement in period 33 min. off Port San Juan (exponential profile).

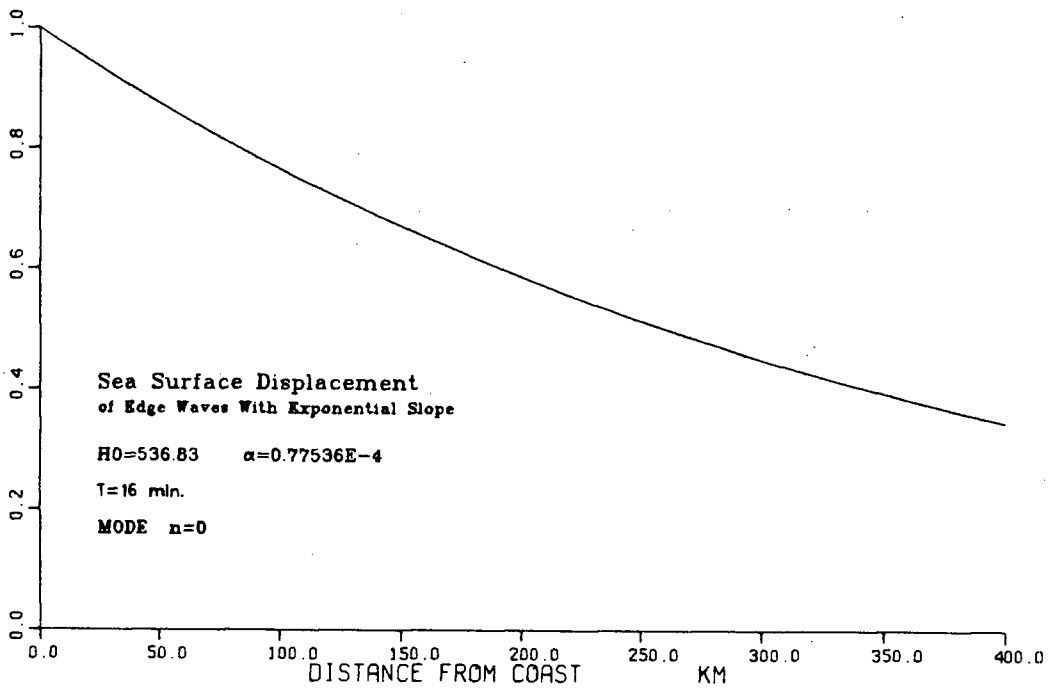

Figure 108 Sea surface displacement in period 16 min. off Port San Juan (exponential profile).

therefore the calculated modes do not decay rapidly enough to fit into the Strait of Juan de Fuca.

More attempts were made in Port San Juan. The bottom profile was set as a straight line $H=-\alpha x$ off the Port as shown in Figure 109, where the circles indicate sounding depths. The modes of dispersion relations were calculated in term of Laguerre function (LeBlond and Mysak, 1978. p.231). Figure 110 shows the first four modes. Figure 111 and Figure 112 are the sea surface displacement with wave periods 33 and 16 minutes. Figure 113 shows the sea surface displacement at 6,000 meters off the coast against different periods.

The analysis mentioned above is not satisfactory for theoretical or practical considerations. These edge wave

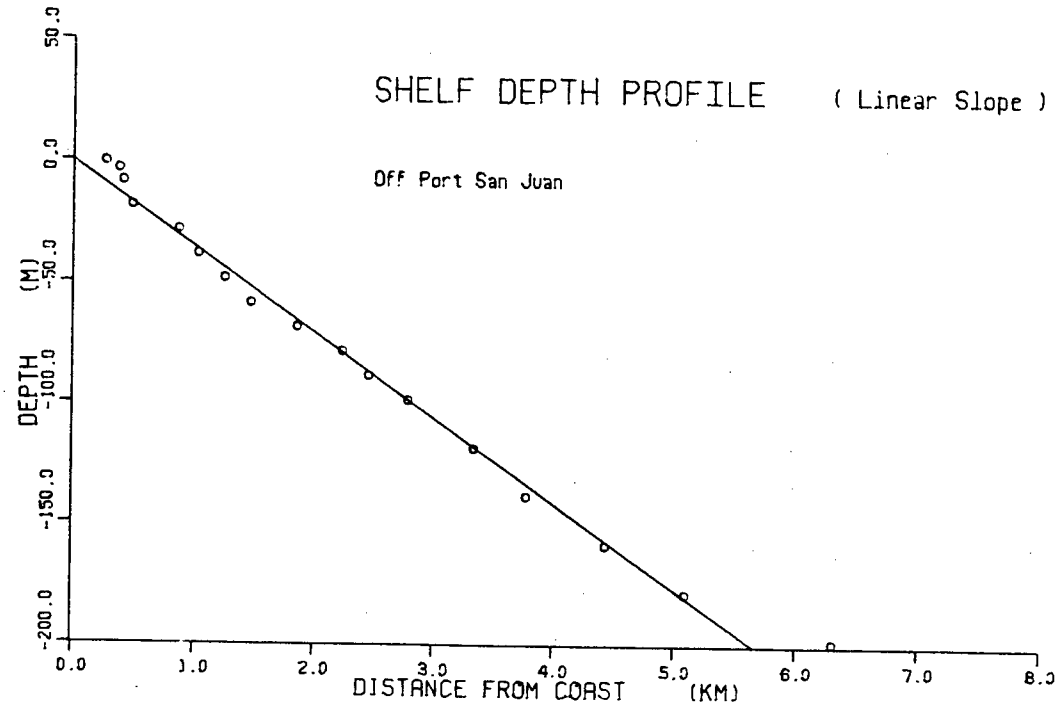

Figure 109 Linear fitting for bottom profile of Port San Juan.Circles are sounding depth.

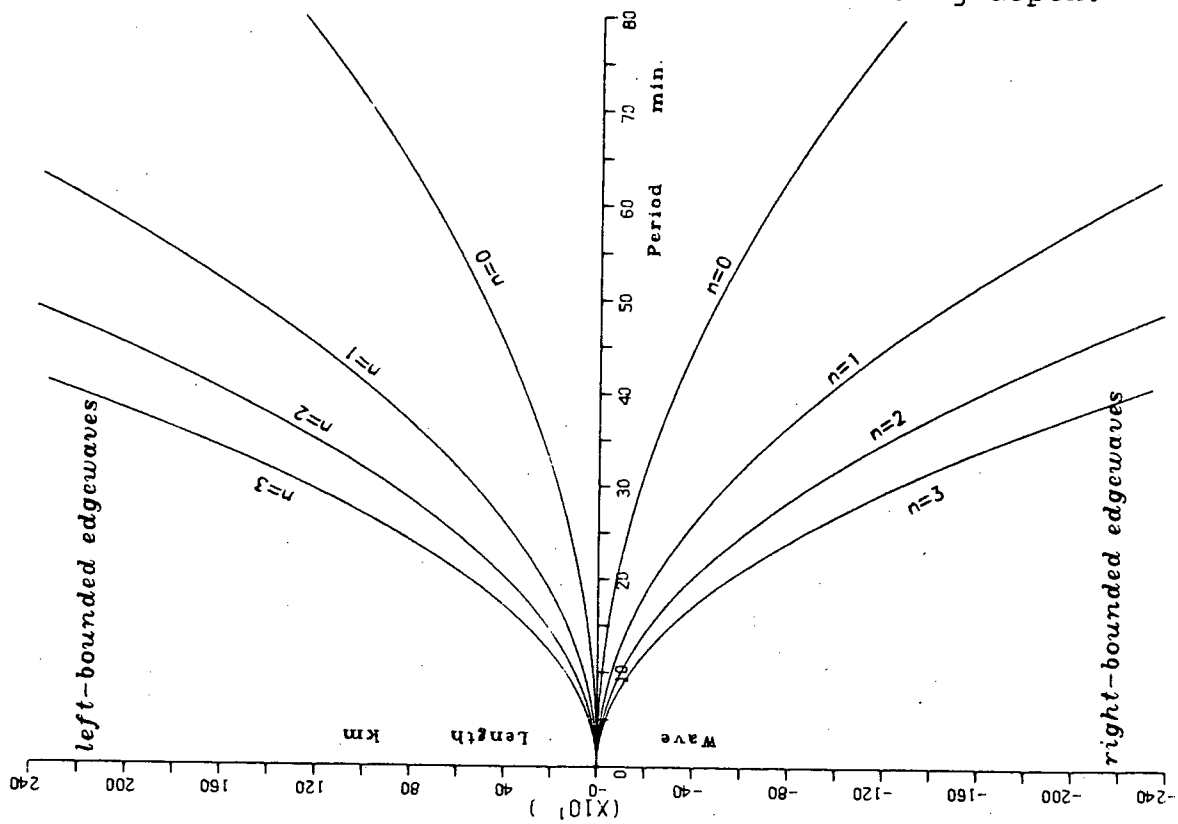

Figure 110 Dispersion relation of edge waves with linear depth profile off Port San Juan.

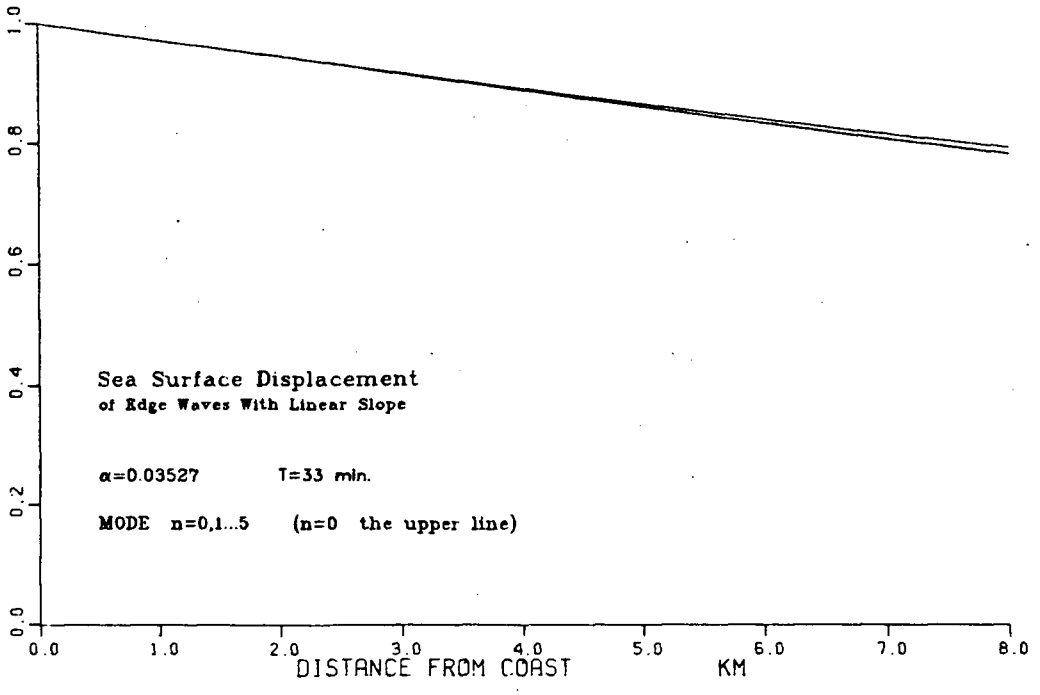

Figure 111 Sea surface displacement in period 33 min. off Port San Juan (linear profile).

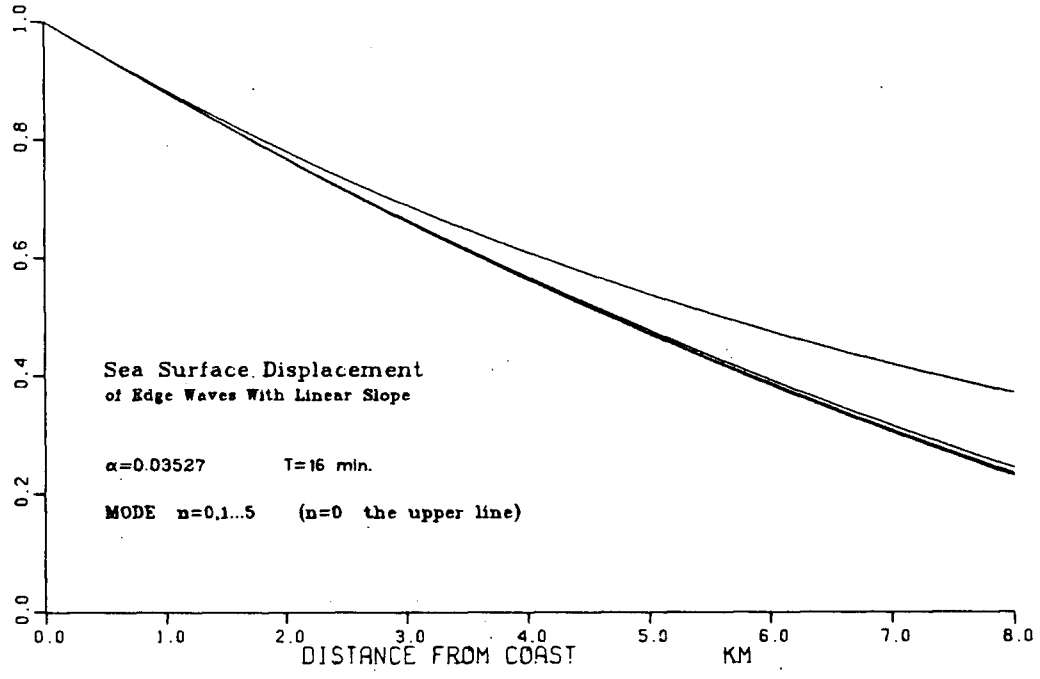

Figure 112 Sea surface displacement in period 16 min. off Port San Juan (linear profile).

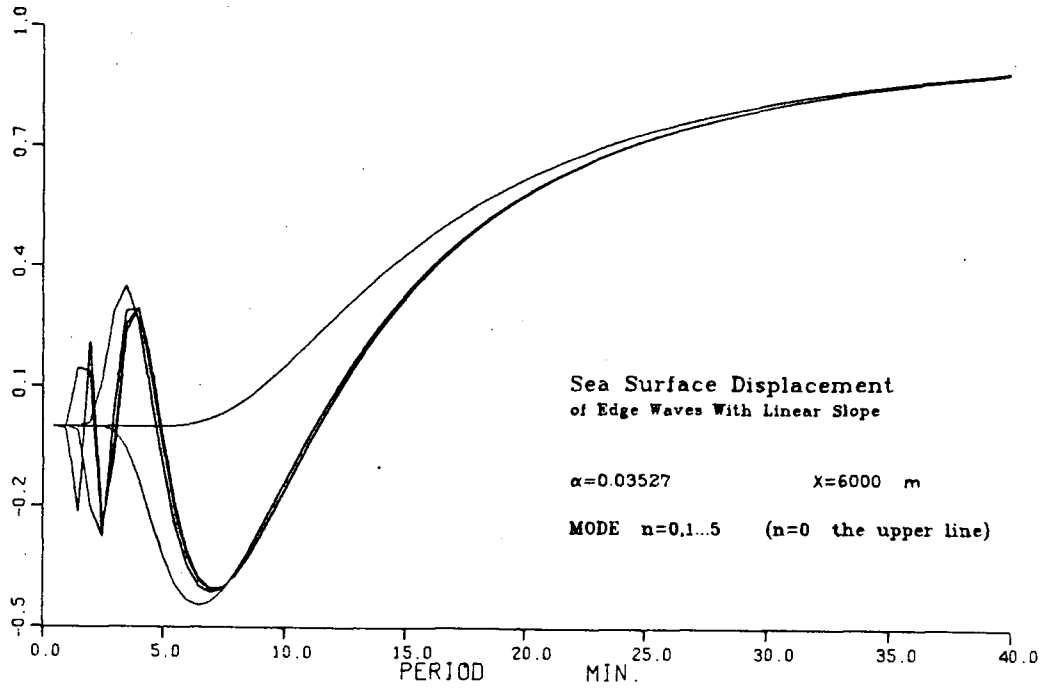

Figure 113 Surface displacement at 6,000 m off Port San Juan (linear profile).

theories can only be applied in the case of a single side boundary. For our problem we need to obtain solutions from both sides of the strait and match the solutions (sea surface displacement and its derivative) at one point of the strait. From the computing results presented above it seems futile to try to match the solutions. Thereby numerical modeling was invoked again to seek the acceptable modes of dispersion relation in the Strait of Juan de Fuca.

We start from the equation (4.1-4) for the single variable η as shown in the derivation of basic model:

$$\nabla H \cdot \nabla \eta + H\nabla^2 \eta + \frac{\omega^2}{g}\eta = 0$$

The depth H changes only in the cross-strait direction and

the plane waves propagate along the strait, i.e. H=H(x) and $\eta=\eta^*(x)e^{i(\omega t-ky)}$. After differentiation with respect to y and dropping the "*", we get

$$gH\eta_{xx} + gH_x\,\eta_x + (\omega^2 - gHk^2)\eta = 0$$

substituting $u=\eta_x$ the second order equation becomes two first order equations:

$$\eta_x = u$$

$$u_x = -\frac{H_x}{H}\,u - \left(\frac{\omega^2}{gH} - k^2\right)\eta$$

with u=0 on both boundaries.

Figure 114 is a spline fit of the bottom profile off Port San Juan. The variables H, u and η take 100 values respectively at equal intervals along the x direction, i.e. H_i , u_i and η_i , i=1,2,...100. Using the corresponding difference equations we are able to calculate the H_{i+1} , u_{i+1} and η_{i+1} from H_i , u_i and η_i , i=1,2,...99. The H_1 and H_{100} take the value 0.5 m instead of 0 to avoid singularities on both boundaries. The u_1 takes the value of 0 and η_1 takes the value of 0.1. The ω's take values corresponding to periods of every half minute from 1 minute to 40 minutes. The k's take values corresponding to wave lengths of every half km from 1 km to 120 km. After computation we get the values of u_{100} on the grid of ω-k. In

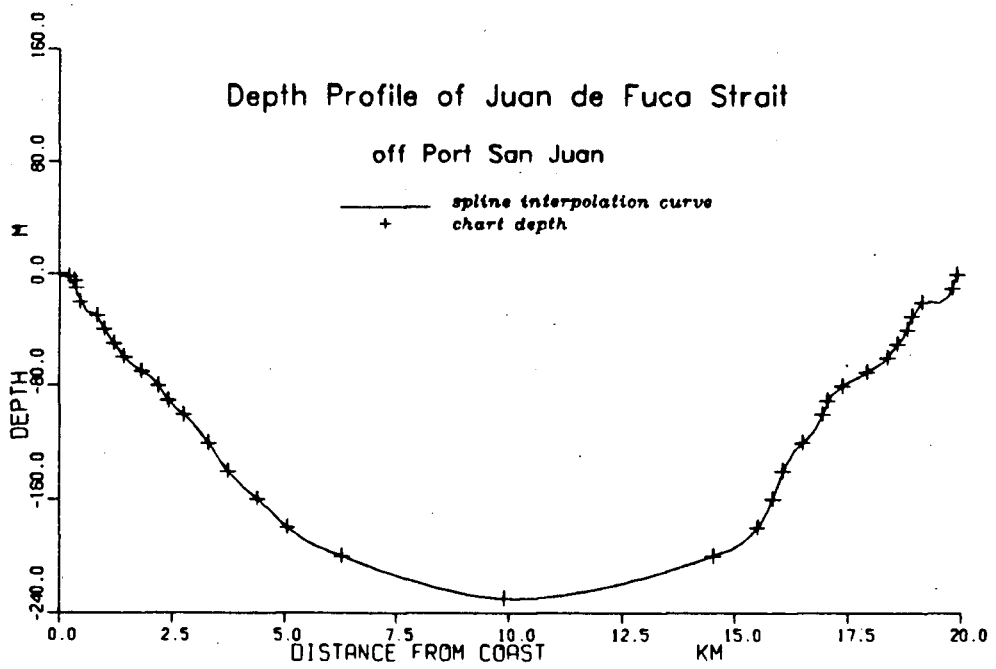

Figure 114 Spline fit of the depth profile off Port San Juan.

consideration of continuity of u as a function of ω and k, the 0-contours are drawn on this grid which is shown in Figure 115. These 0-contours are treated as the dispersion relation curves of the along strait propagating waves.

For comparison purpose the analytical dispersion relation is calculated in the case of flat bottom. The analytical dispersion relation is

$$\frac{\omega^2}{gH} - \frac{n^2\pi^2}{L^2} = k^2$$

where L is the width of the strait and n is the mode number. Taking the averaged depth of the strait as H, the calculated dispersion relation curves are shown in Figure 116. These two sets of curves are quite resemblant and confirm the

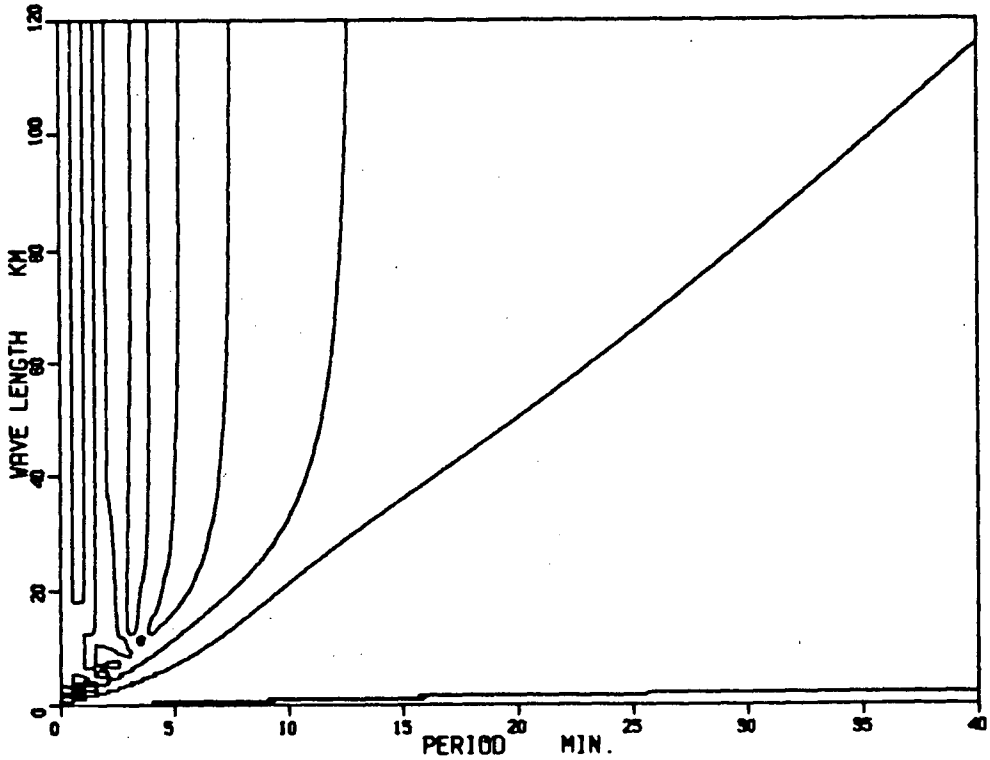

Figure 115 Dispersion relation of edge waves from numerical model (off Port San Juan).

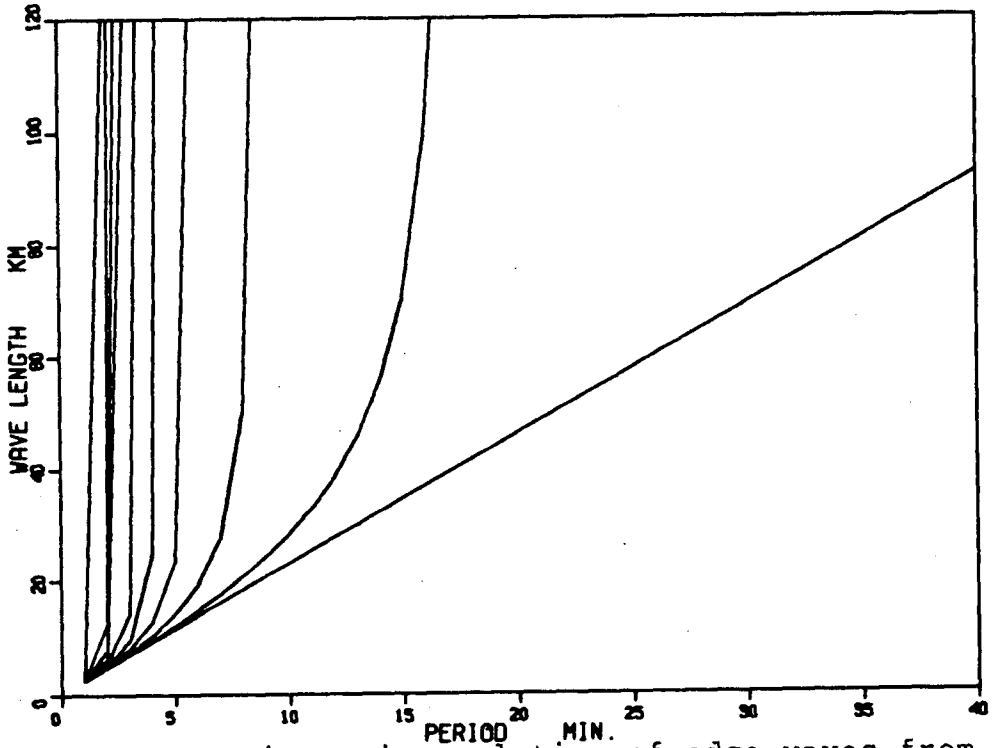

Figure 116 Dispersion relation of edge waves from analytic model with flat bottom (off Port San Juan).

correctness of the numerical results.

The corresponding results of the strait off Becher Bay are shown in Figure 117 to Figure 119. When these edge waves with periods close to the eigen-periods of bays propagate by the mouths of the bays, seiches inside the bays will be excited.

Looking back to Figure 12 and Figure 24 we find that at low frequency band (corresponding periods 20 to 60 minutes) the coherences are well above the confidence levels. It suggests that the oscillations of Becher Bay and Port San Juan are highly correlated within this range of periods, furthermore these oscillations may be excited by common source. We hypothesize that the common source is in the form of plane waves travelling along the Strait and the phase differences continuously change with frequencies. After adding 2π to certain values of phases in the period range of 20 to 60 minutes, we find that the phases $\Delta\phi$'s increase approximately linearly with frequencies. The approximate value of $C=\Delta\phi/f$ is 160 minutes. The distance between Port San Juan and Becher Bay is L=68km. The source at the mouths of these two bays may be written as $e^{i(kx-\omega t)}$ and $e^{i[k(x+L)-\omega t]}$, so that $\Delta\phi=kL=\omega L/c$, and the phase speed c may be calculated:

$$c = \frac{\omega L}{\Delta\phi} = \frac{2\pi f L}{\Delta\phi} = \frac{2\pi L}{C} \simeq 2.67 \text{ km/min.} \simeq 160 \text{ km/hr.}$$

From the calculated dispersion relations of edge waves we

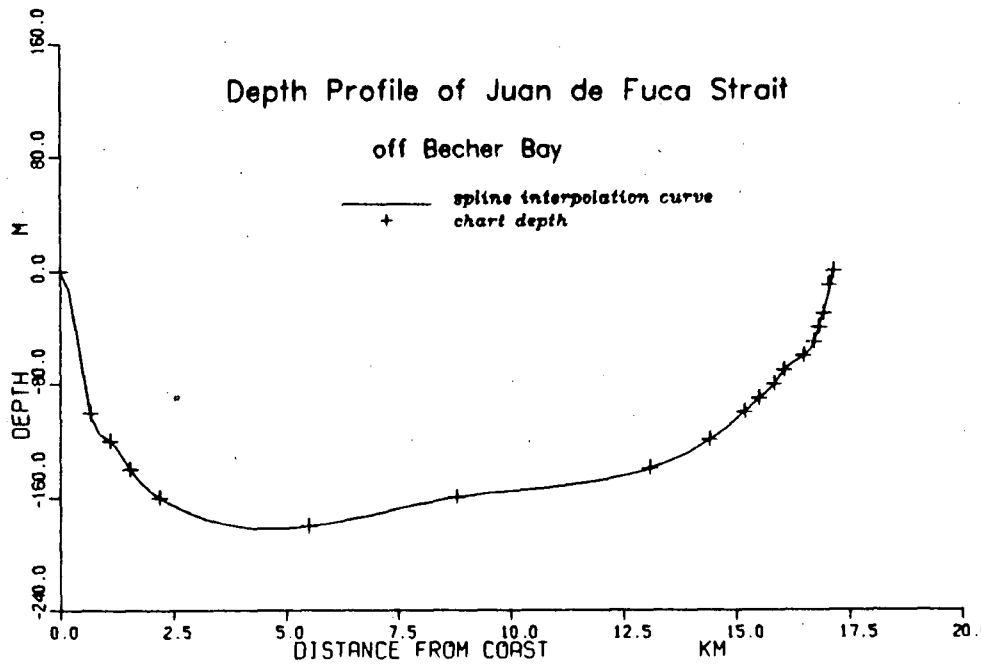

Figure 117 Spline fitting of depth profile off Becher Bay.
Symbols + are sounding depth.

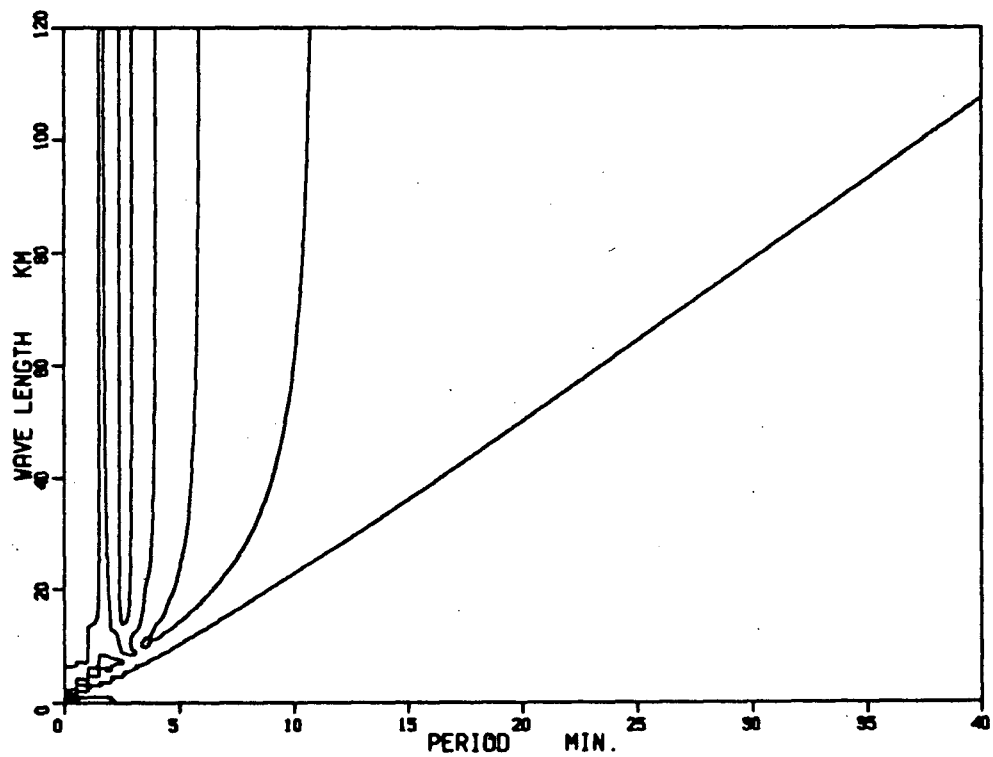

Figure 118 Dispersion relation of edge waves from numerical model (off Becher Bay).

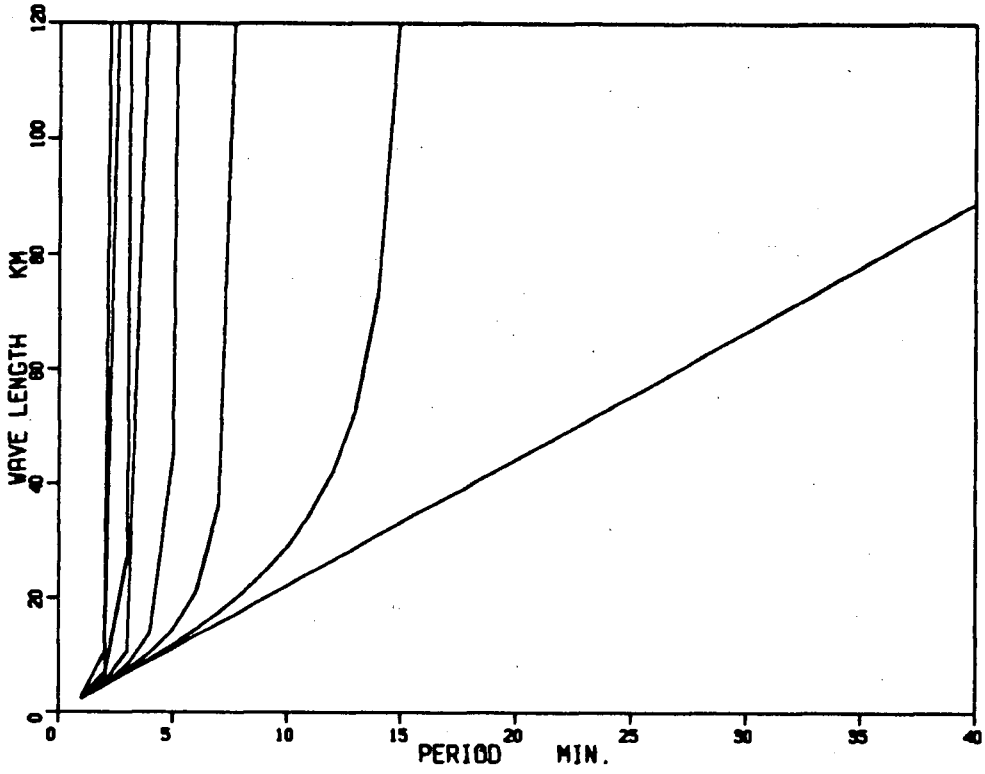

Figure 119 Dispersion relation of edge waves from analytic model with flat bottom (off Becher Bay).

know that the phase speed of edge waves is approximastely 160 km/hr. within the period range of 20 to 40 minutes. This result verifies the above hypothesis. Based on this analysis we conclude that the common source was edge waves. These edge waves often occur in Juan de Fuca Strait and are most important common sources throughout the observed seiches in this research. This thesis only revealed a little of this fact, mainly at low frequency band. The calculated dispersion relations of edge waves, coherences and phases of observed oscillations imply that the oscillations in three bays were often generated by edge waves with wide range of periods. The further analysis, especially the analysis of phases, has not been completed in this thesis.

2. SWELL

Data of waves at Tofino (west coast of Vancouver Island) are available and presented in Figure 120 and Figure 121. In January the peak period of waves reaches its maximum (about 20 seconds) on the 20th. On February the 2nd, peak period reaches its local maximum. On the other days of February the longer peak periods appeared again, but the corresponding significant wave heights are low. During these two days intensive seiche energy was found. The longer peak periods (15 to 20 seconds) associated with larger significant height of waves seem to be correlated with occurrences of seiches.

Within the days Jan. 16 to Feb. 18, the high frequency band of power spectra in Port San Juan contained more energy on Jan. 16 to 17, Jan. 20 to 24, Jan. 31 to Feb. 4 and Feb. 7 to 8 than that on the other days. The corresponding significant height of swells were obviously high. We may conclude that the high frequency peaks in the spectra of Port San Juan were related to large swells observed at Tofino. The frequencies of those swells (periods 10 to 20 seconds) were much higher than the cut off frequency of the power spectra, they contributed power to the spectra through aliasing. Those swells were not related to the oscillations in Pedder Bay and Becher Bay.

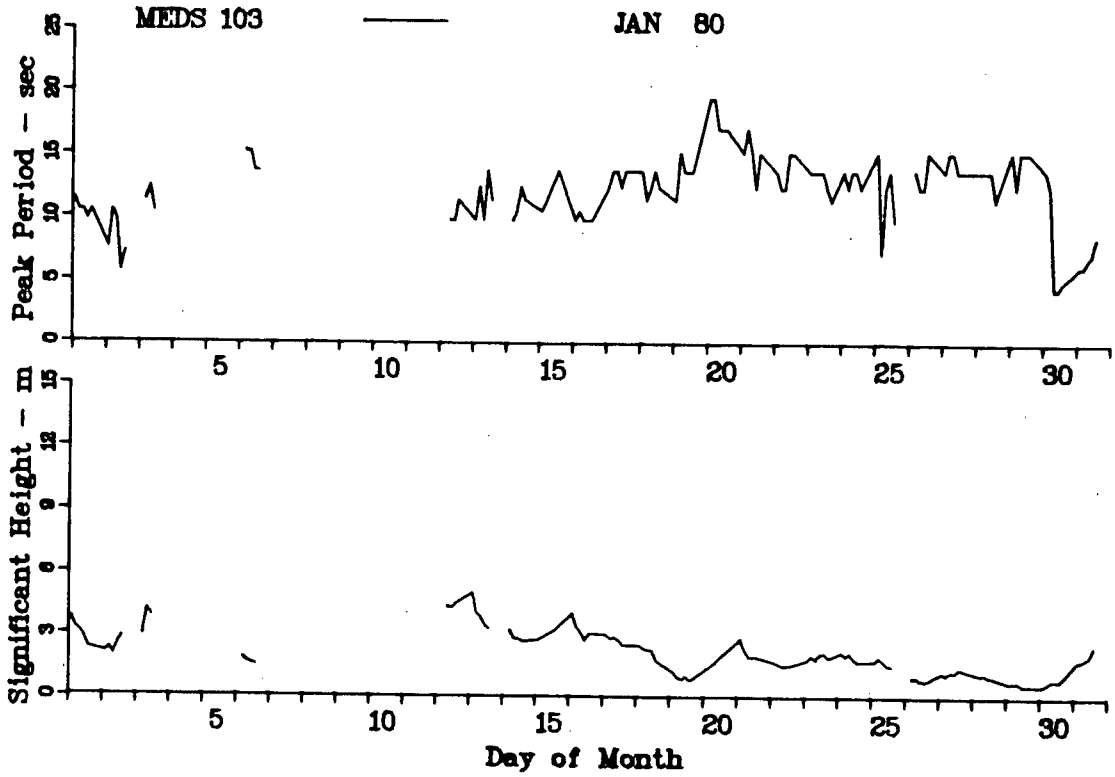

Figure 120 Wave data at Tofino, Jan. 1980.

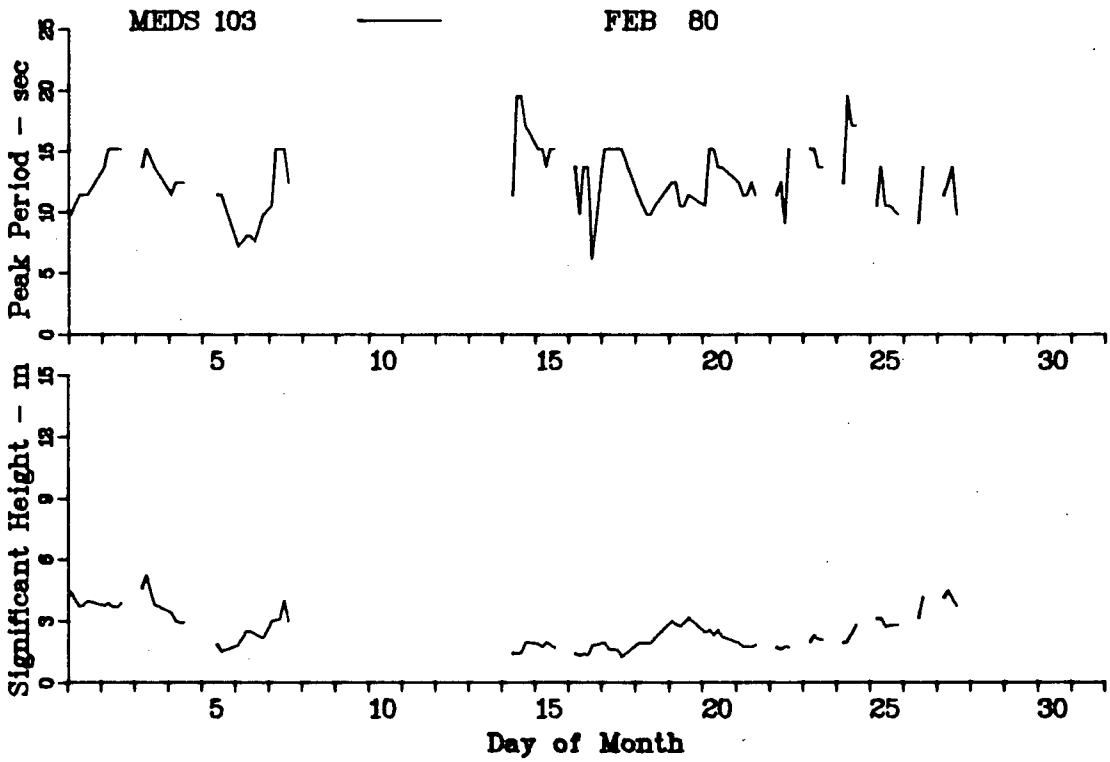

Figure 121 Wave data at Tofino, Feb. 1980.

3. INTERNAL WAVES

Internal waves may be one of the sources of the excited seiches. Deep ocean internal waves commonly originate from the interaction between tidal currents and bottom topography, such as abyssal hills, submarine mountains, or other sea bottom discontinuities. It is generally accepted that oceanic internal tides are generated at the edge of a continental shelf. Recently Baines (1983) estimated the global internal tide energy generation at all continental shelf-slope junctions for M_2 and S_2 frequencies. Observations have shown that internal tides have large amplitudes in the vicinity of continental slopes, and contribute a significant fraction of the horizontal velocity field at tidal frequencies (LeBlond and Mysak, 1978. p60). A portion of the waves travel onto the shelf.

Observations off the coast of British Columbia and Washington verify the existence of large internal oscillations. Measurement of bottom pressure and temperature variation off the B.C. coast suggest that internal tides originate with tidal flow over seamounts, abyssal hills and rough seafloor terrain. Within certain B.C. coastal waters groups of internal waves cover a wide range of periods and amplitudes. (Thomson, 1981)

Figure 122 shows a satellite image of surface slick bands at the mouth of Juan de Fuca Strait, which illustrates the internal waves in this region. Figure 123 is a tracing of part of this image. The troughs of internal waves produce

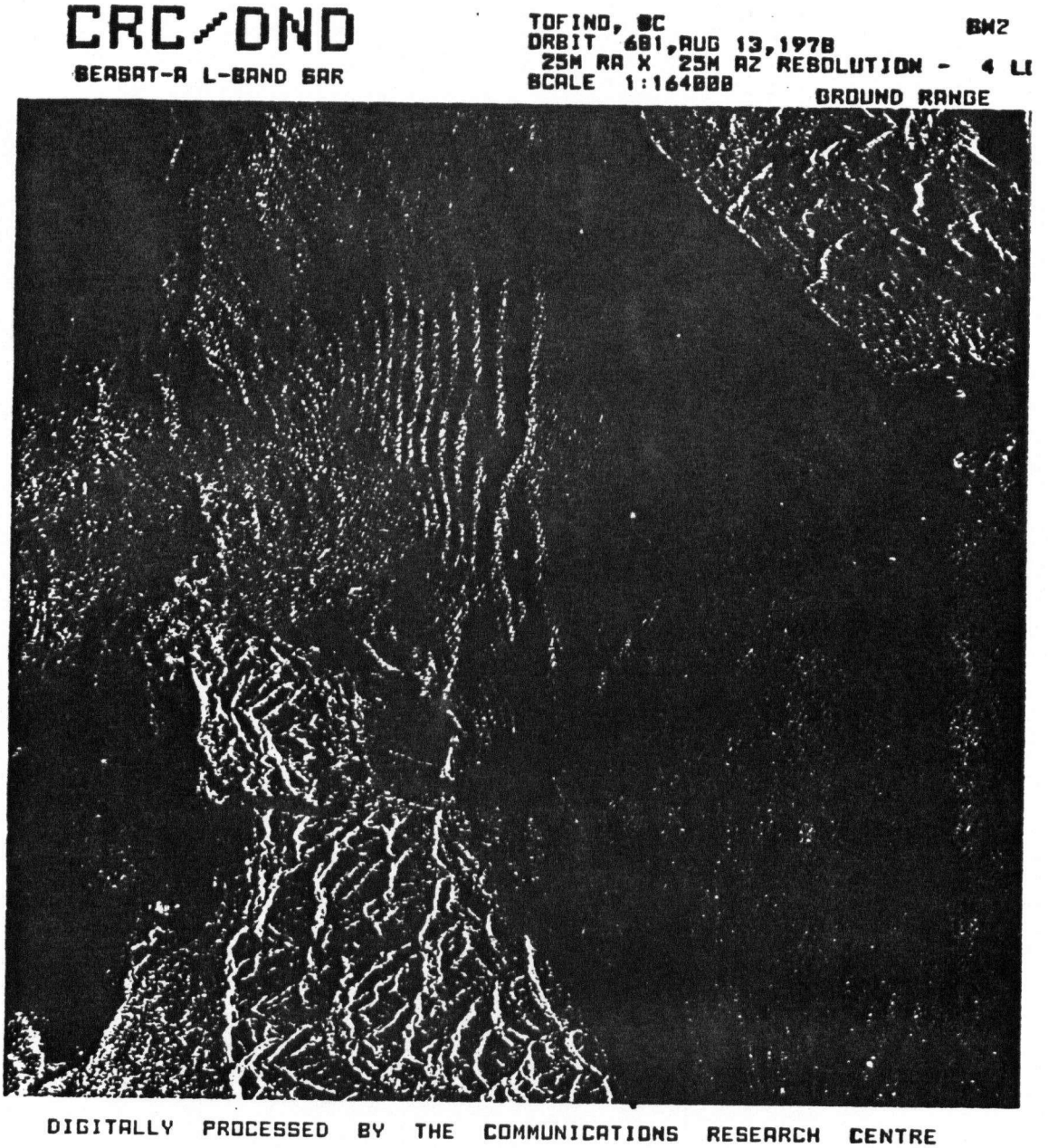

Figure 122 Internal waves from satellite.

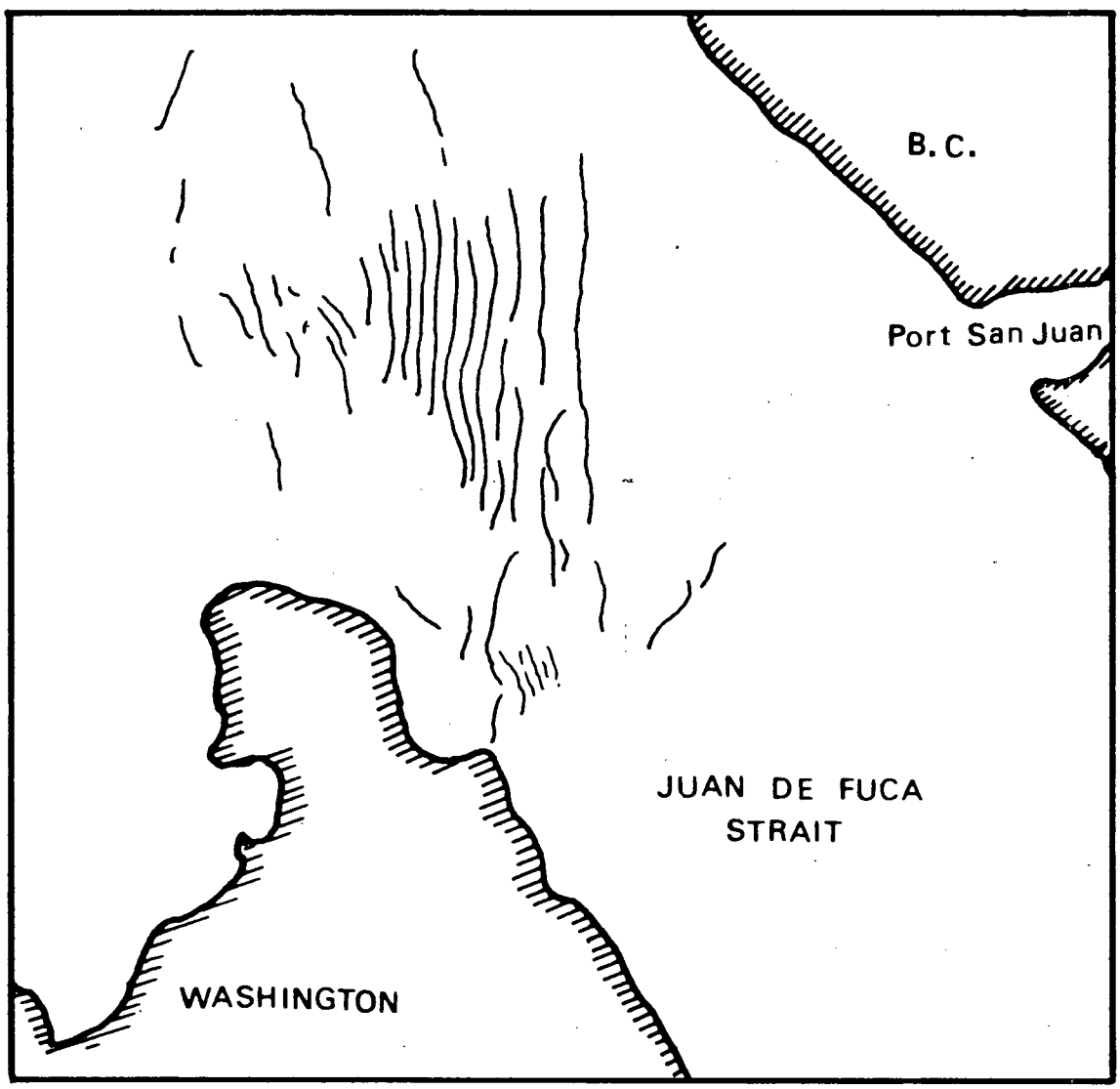

Figure 123 A tracing of part of the satellite image.

convergences of surface waters over them, the crests produce divergences. When these waves approach the mouth of a bay, the convergences and divergences work as a pump to discharge and charge the bay. In a two-layer system, for example, where the upper layer offshore is thicker than the depth of the bay, the horizontal flow in the upper layer within the bay may not be completely balanced by an opposite flow in the lower layer, and sea level oscillations will result. This procedure may transfer energy from internal waves to seiches.

Giese *et al* (1982) put forward an hypothesis about the relationship between coastal seiches and oceanic internal tides. They examined tide records from 1955 through 1971 at Magueyes Island, Puerto Rico, and found that the seiche activity was highly correlated with lunar phase. The maximum activity occured approximately 7 days after new and full moon; the mean number of oscillations per fortnight varied inversely with the absolute difference in time between the preceding new and full moon and the perigee nearest to it, i.e. the degree of seiche activity depended upon the magnitude of the preceding spring tides. The authors concluded that the internal waves were formed by tidal currents along the southeastern margin of the Caribbean Sea where the semidiurnal tide reached its greatest range; it took five days for these waves to travel to Puerto Rico. Since the age of the tide in the southeastern Caribbean was about two days, the largest internal waves would reach

Puerto Rico approximately 7 days after new and full moon. This hypothesis was verified again by the observed internal waves and seiches in the Sulu Sea. The observation of internal waves in Sulu Sea was carried out by Apel *et al* (1980).

In this research the available data cover the days from Jan. 15 to Feb. 20. Within this period there were two prominent seiche activities around Jan. 20 and Feb. 2, on Feb. 15 to 18 small seiches were observed in the three bays. The time interval between these seiche activities was a fortnight which suggests a possible correlation between seiches and lunar phase.

Figure 124 shows the tide record at Port San Juan, which is the smoothed curve of the original data of this research. Time lags between spring tides and the following strong seiches were approximately one to two days. If we assume these strong seiches were generated by tide-induced internal waves, these one to two days were the time difference between the surface tides and the tide-induced internal waves travelling from the place where the internal waves were generated by tides (probably at the edge of a continental shelf) to Juan de Fuca Strait.

We may estimate the speed of internal waves (Pond and Pickard, 1983. p238):

$$c^2 \simeq g \frac{\Delta\rho}{\rho_2} \cdot \frac{h_1 \cdot h_2}{h_1 + h_2}$$

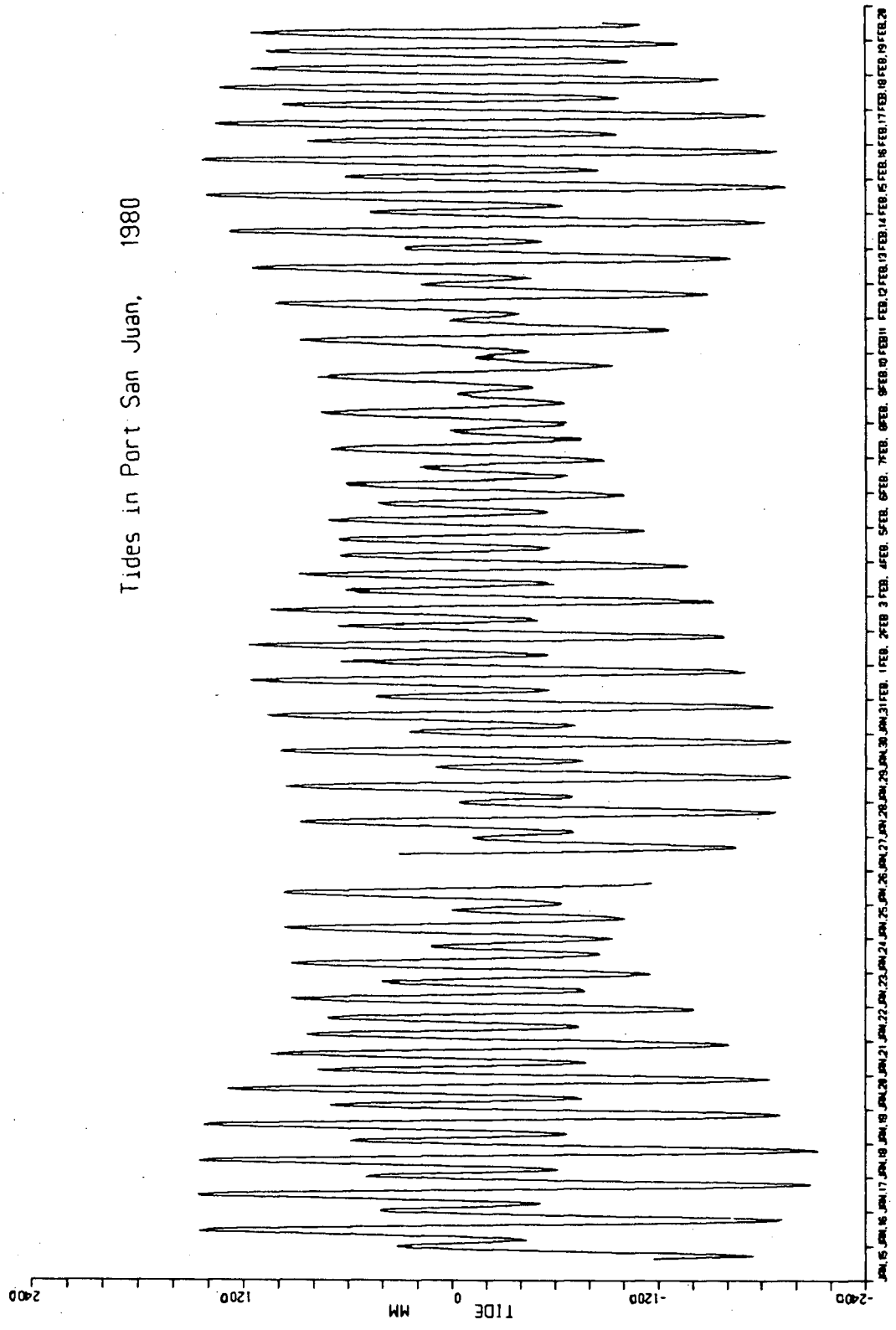

Figure 124 Tides in Port San Juan.

and take values of the water depths of continental shelf off Juan de Fuca Strait, and of the winter density profile in that area (Werner and Hickey, 1982): h_1=50m, h_2=150m, ρ_1=1.025, ρ_2=1.026. The estimated speed c=2.16 km/hr.. The width of the continental shelf off Juan de Fuca Strait is about 100 km; if internal waves were generated at the edge of the continental shelf, it would take them 46 hours to travel to Juan de Fuca Strait. Thus the internal waves would arrive in Juan de Fuca Strait a little less than two days after the preceding spring tides. If the internal waves were generated at the edges of banks 40 to 80 km from Juan de Fuca Strait on the continental shelf, it would take them about 19 to 37 hours to travel to Juan de Fuca Strait.

From Figure 124 we may see the spring tide of middle January was larger than that of late January, but degrees of succedent seiches were inverse, especially in Port San Juan (looking back to Figure 94). On the other hand the observed seiches after spring tide of mid-February were small (see Figures 13 to 18). The above facts may not disprove the hypothesis that tide-induced internal waves were responsible for the observed strong seiches, since the generation of internal waves not only depends upon the producing forces, but also upon the stratification of sea water. The source which may have enhanced the seiches of Feb. 2 will be discussed in following section.

It is suggested that long-term (eg. more than one year) observation of sea surface oscillation should be carried out

to test the fortnightly pattern, which may improve our understanding not only of seiches, but also of internal waves off B.C. coast.

C. WINDS

Prevailing oceanic winds off the outer British Columbia-Washington coast are from the southwest in winter. The flow of air within Juan de Fuca Strait is strongly influenced by the adjoining mountainous terrain; the corresponding wind directions are easterly in winter. Because of the funneling effect of the topography, these easterly winds undergo a seaward acceleration along the Strait. Wind patterns in the eastern sector of the Strait are further complicated by the inertia of local air flow. In the lee of the mountains the winds overshoot and leave an area of calm airs in the vicinity of Port Angeles (Thomson, 1981).

From the spectral analysis we found energy at high frequency only in Port San Juan. Besides the swells discussed before, the strong winds in the eastern sector of Juan de Fuca Strait may also contribute energy to the high frequency oscillations of Port San Juan. Pedder Bay and Becher Bay are located in an area of calm airs, therefore it's very rare to find high-frequency oscillations.

The wind data are available at Race Rocks (close to Pedder Bay and Becher Bay) and Cape Beale (close to Port San Juan, see Figure 1). These data are presented by stick

diagrams in Figure 125 and Figure 126. The same data are presented by speed-direction time series and compared with seiche energy in Figure 127 and Figure 128. The winds at Race Rocks may affect Pedder Bay and Becher Bay. The winds at Cape Beale may affect Port San Juan; within Juan de Fuca Strait the winds are influenced by mountainous terrain.

For the peak of seiche energy on Jan. 20 the wind speeds are generally small at both stations. The direction of winds does not change sharply. Therefore it is hard to find any obvious correlation between the seiche energy peak and wind data. For the peak of wave energy on Feb. 2 the wind speeds are comparatively large at both stations.

By visual examination of these wind data Figures, the seiche activities observed in the three bays were neither related to strong winds, nor certain directions of winds. It is fairly obvious that the observed seiches were not caused directly by winds.

D. BAROMETRIC VARIATION

The other possible source of the large amplitude seiches is the barometric pressure variations. The atmospheric pressure data within that period are given in Figure 129. Figure 130 is the rate of change of the pressure. There was no significant pressure jump on Jan. 20. On Feb. 1 to Feb. 2 there was peak on the pressure curves and the rate of change of the pressure dropped abruptly. Similar barometric jumps could be found Feb. 3 through 8.

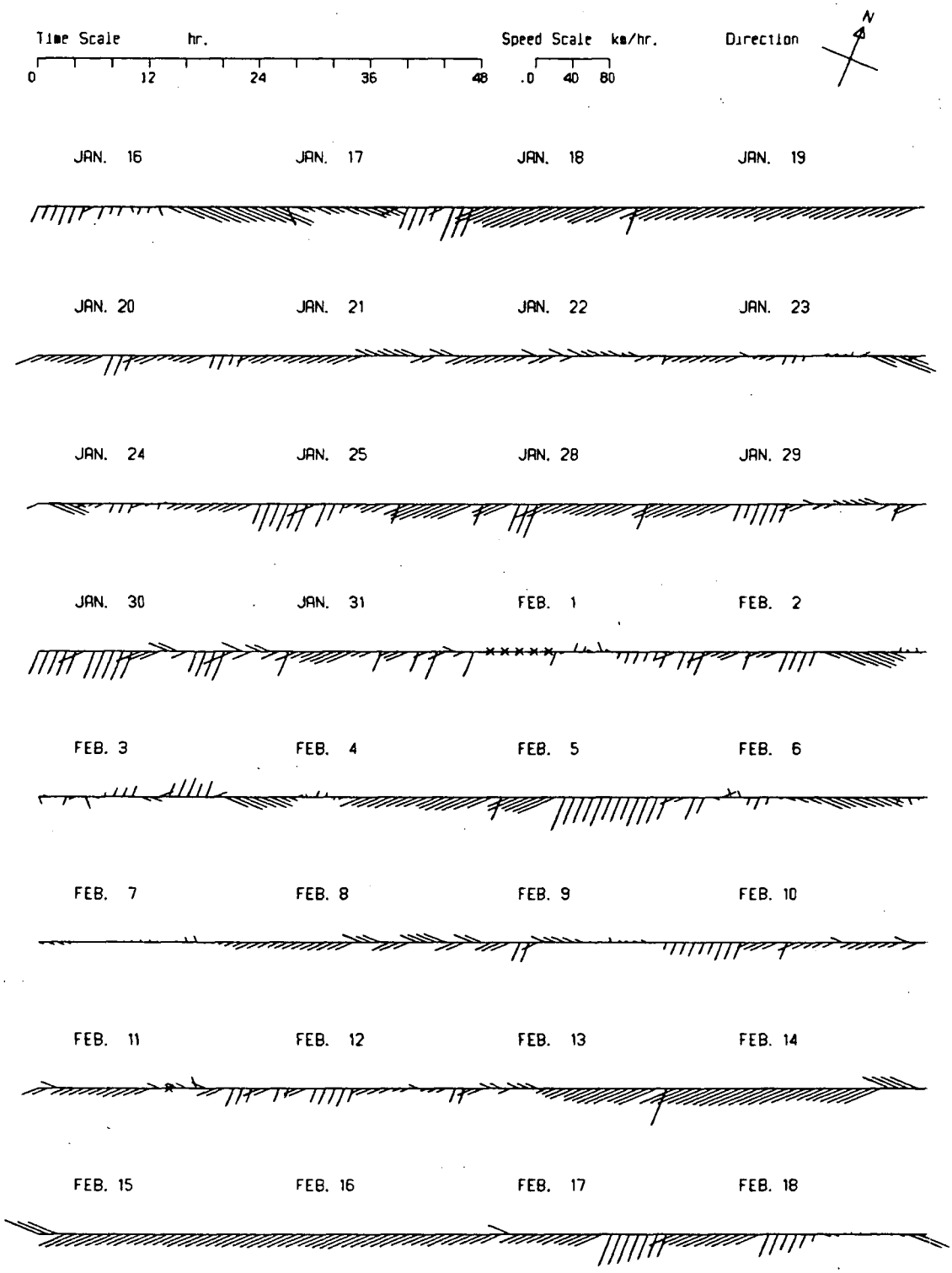

Figure 125 Stick diagram of the winds at Race Rocks.
X : data missing.

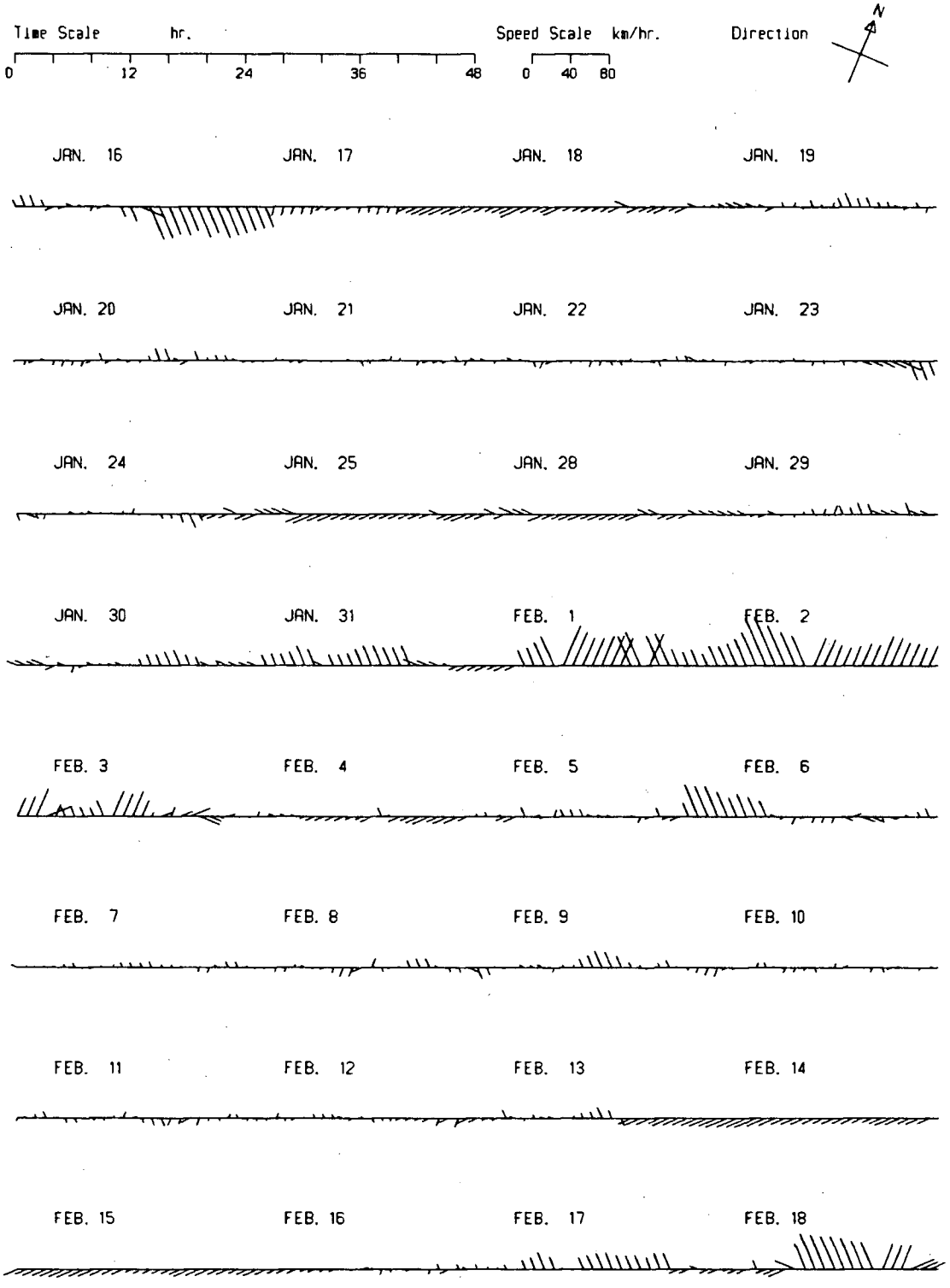

Figure 126 Stick diagram of the winds at Cape Beale.

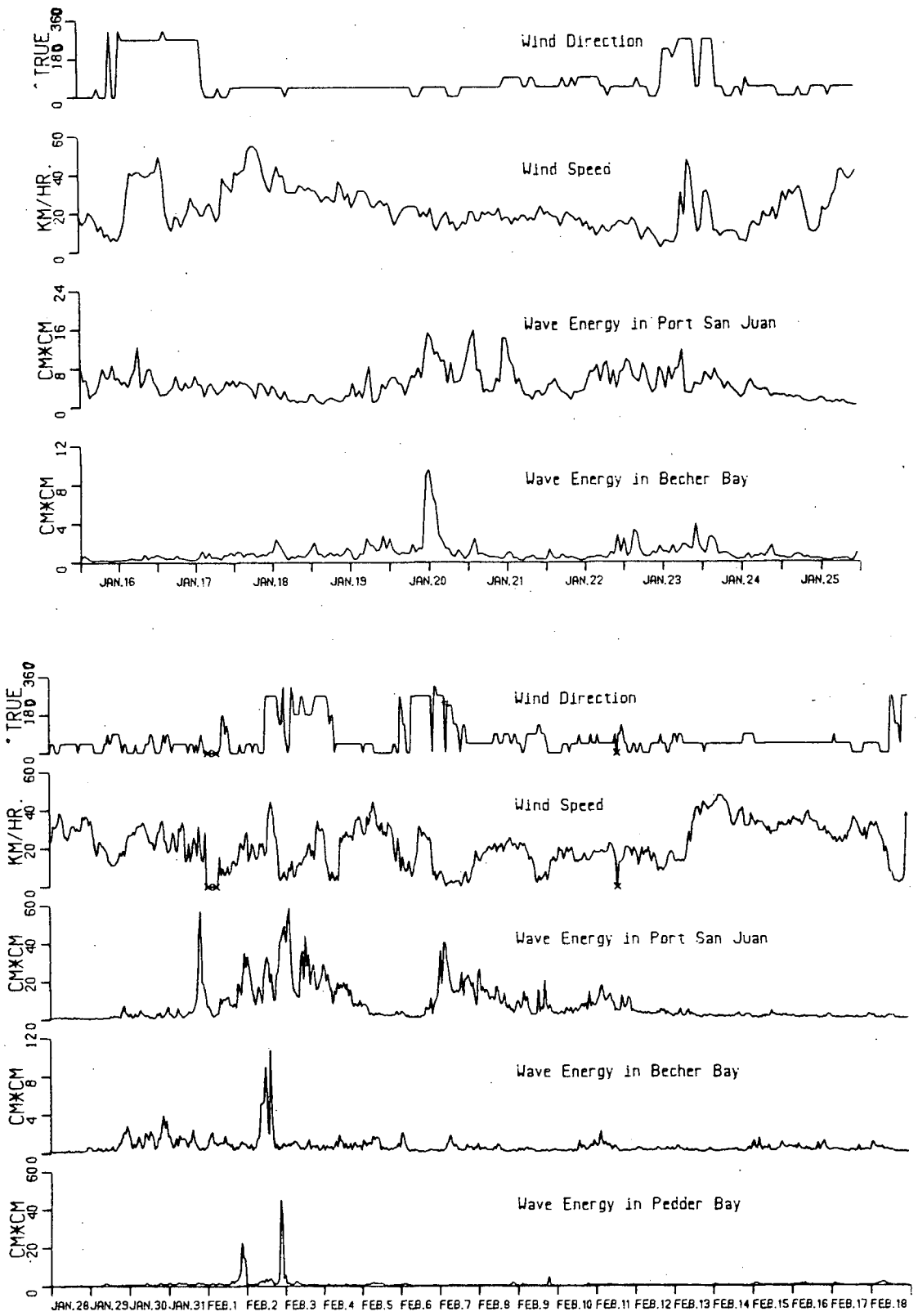

Figure 127 The comparison of seiche energy and wind data at Race Rocks.
X : data missing.

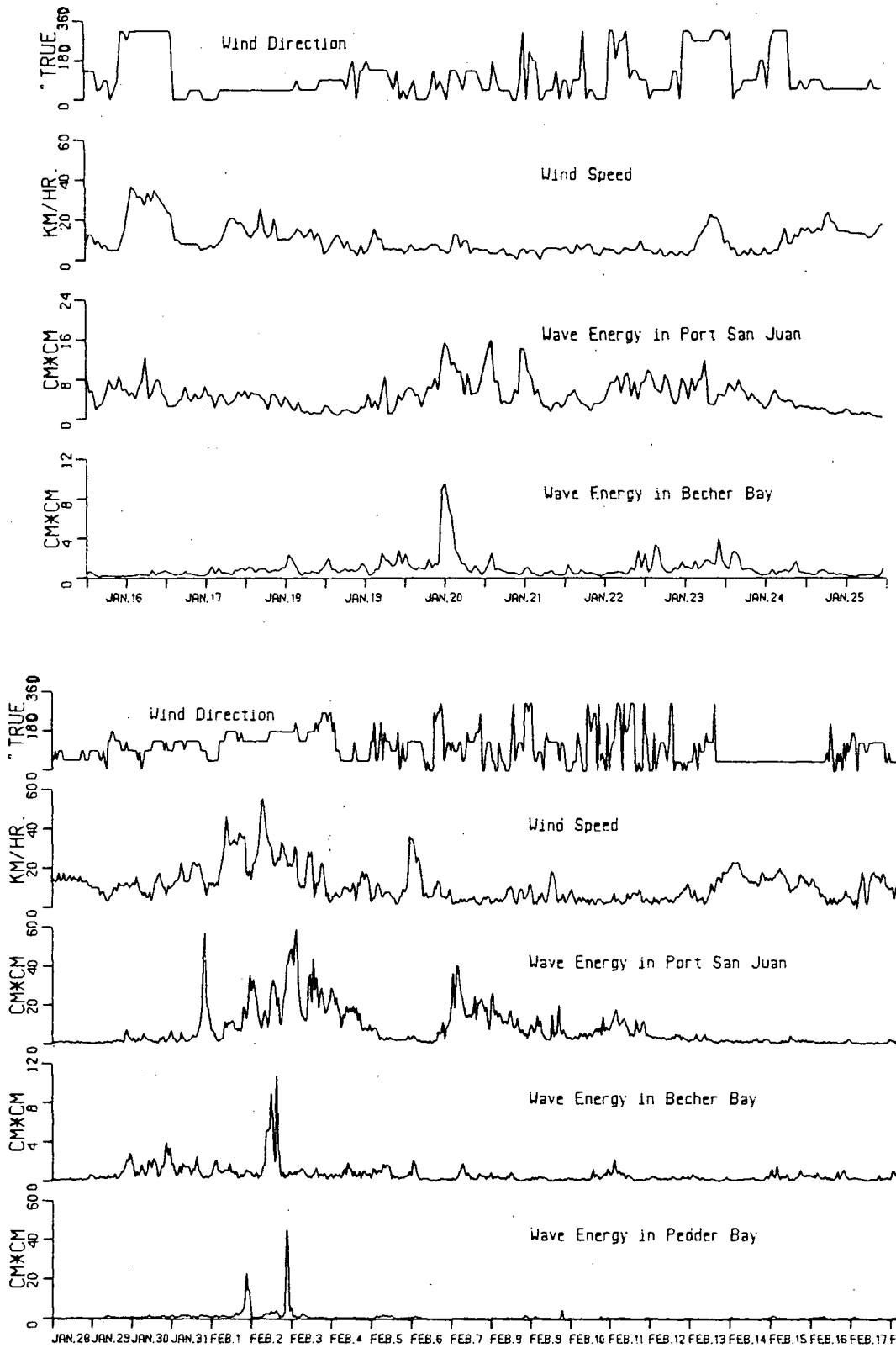

Figure 128 The comparison of seiche energy and wind data at Cape Beale.

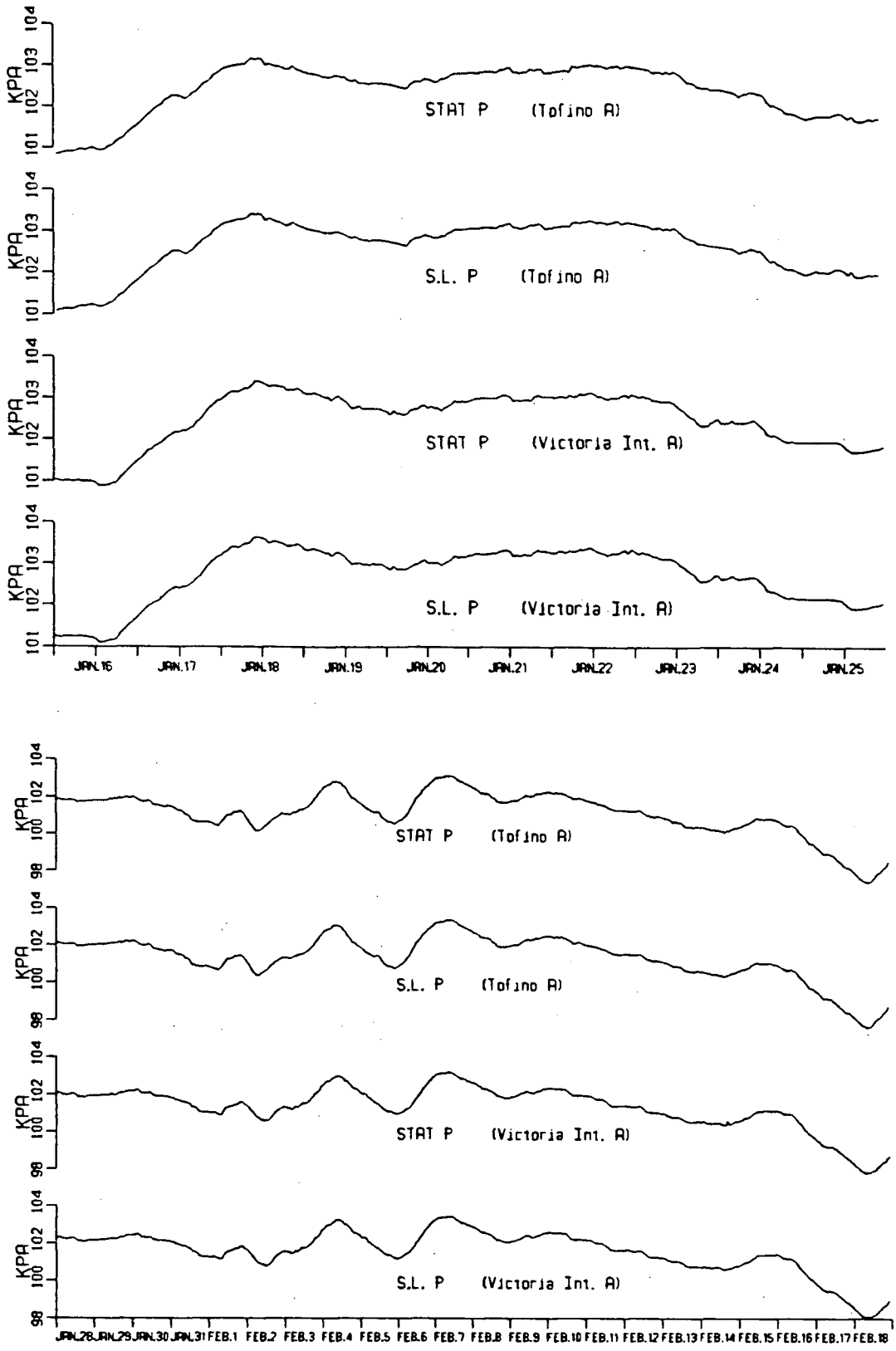

Figure 129 Atmospheric pressure data at stations Tofino and Victoria.

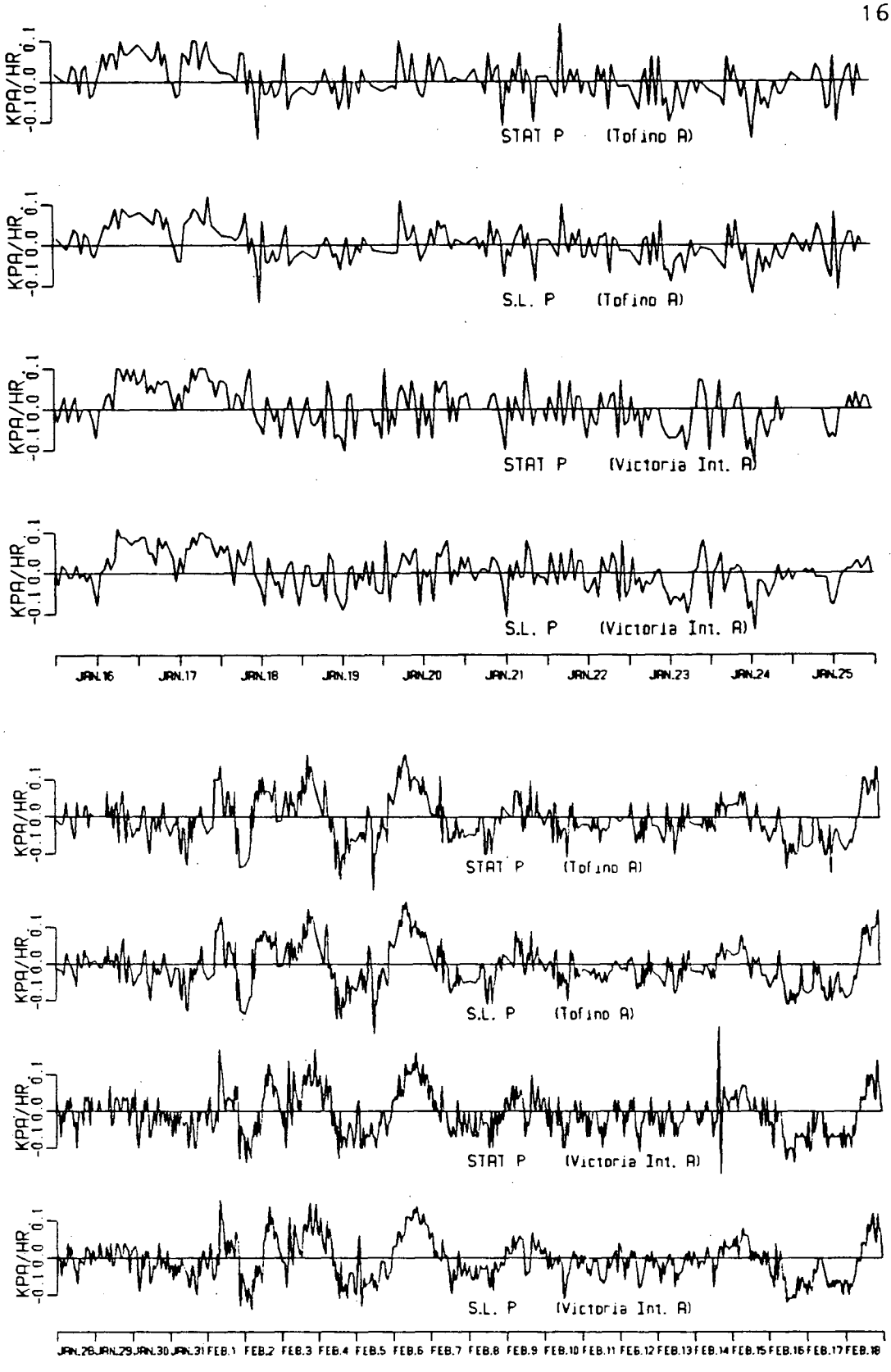

Figure 130 Rate of change of pressure at stations Tofino and Victoria.

The notable feature of the pressure on Feb. 1 to Feb. 2 is that the pressure increased to the maximum and dropped to minimum within about one day, but the similar process on Feb. 3 to 8 took four days.

Figure 131 shows the sea-level pressure maps of Jan. 20. The time on these maps is Greenwich time. On Jan. 20 the pressure gradient is not along the Strait of Juan de Fuca. The 1028 mb contour moved about 50 km from 00:20 to 15:00 along the Strait at speed less than 5 km. Figure 132 shows the sea-level pressure maps of Feb. 2. On Feb. 2 the pressure contours are perpendicular to the middle line of the strait, so that the pressure gradient is along the strait. Taking 1008 mb contour as an example, on Feb. 2, 9 o'clock across northern end of Vancouver Island, 15 o'clock across the southern end, 21 o'clock still across the southern end, then back to northern end at 3 o'clock of Feb. 3. Then we estimate that the pressure front moved at a speed about 100 km/hr. on the first half day of Feb. 2 in direction SSE and on the second half day of Feb. 2 in the opposite direction.

Proudman (1953) discussed the problem of coupling between moving air-pressure disturbances and sea level variation. Platzman (1958) performed a numerical simulation of the surge of 26 June 1954 on Lake Michigan caused by an intense and fast-moving squal-line. Orlić (1980) and Hibiya (1982) explained the cause of observed seiches by Proudman coupling. Our problem is to find a quantitative relation

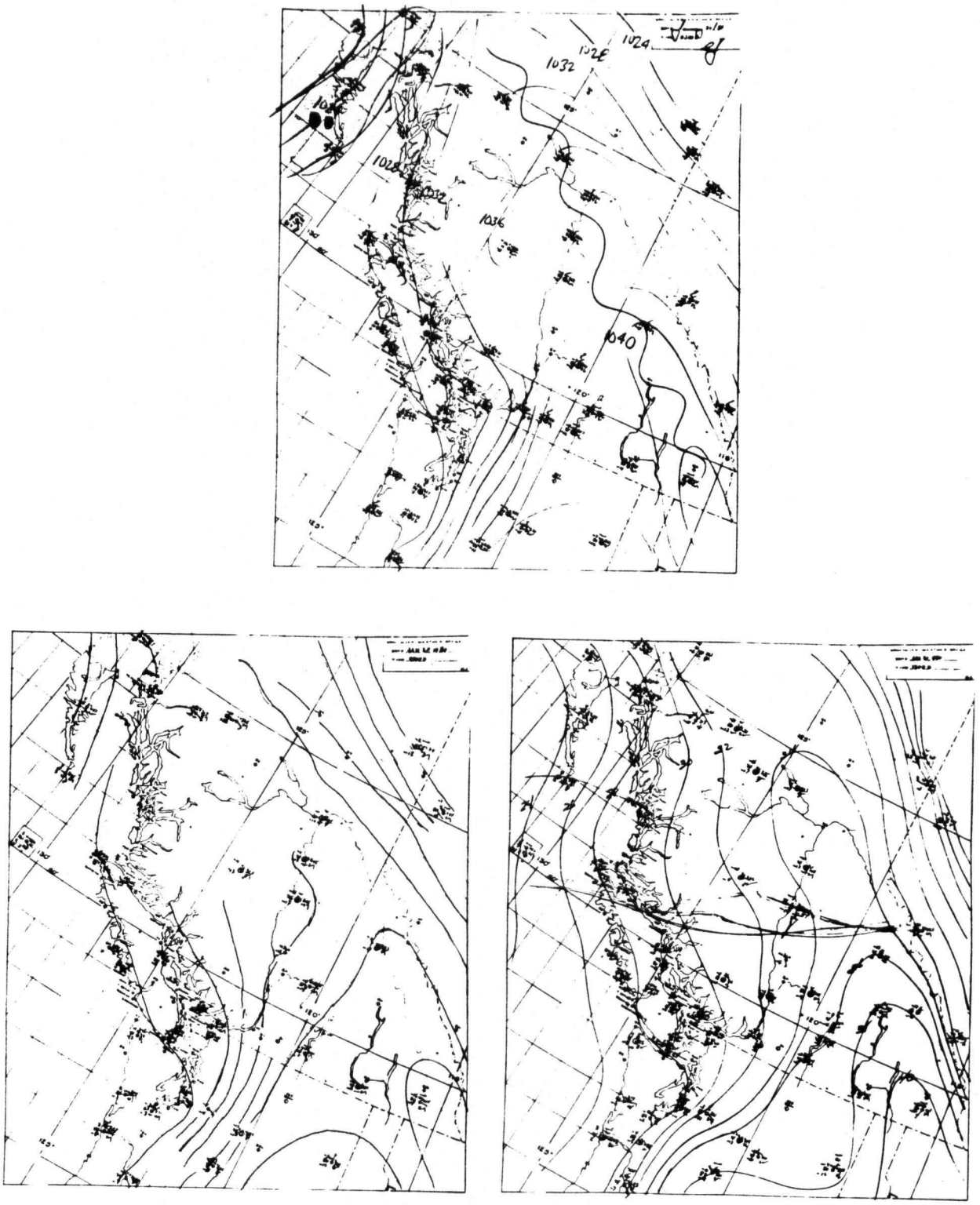

Figure 131 Barometric maps (1).
Upper: Jan. 20 0200.
Lower-left: Jan. 20 0900.
Lower-right: Jan. 20 1500.

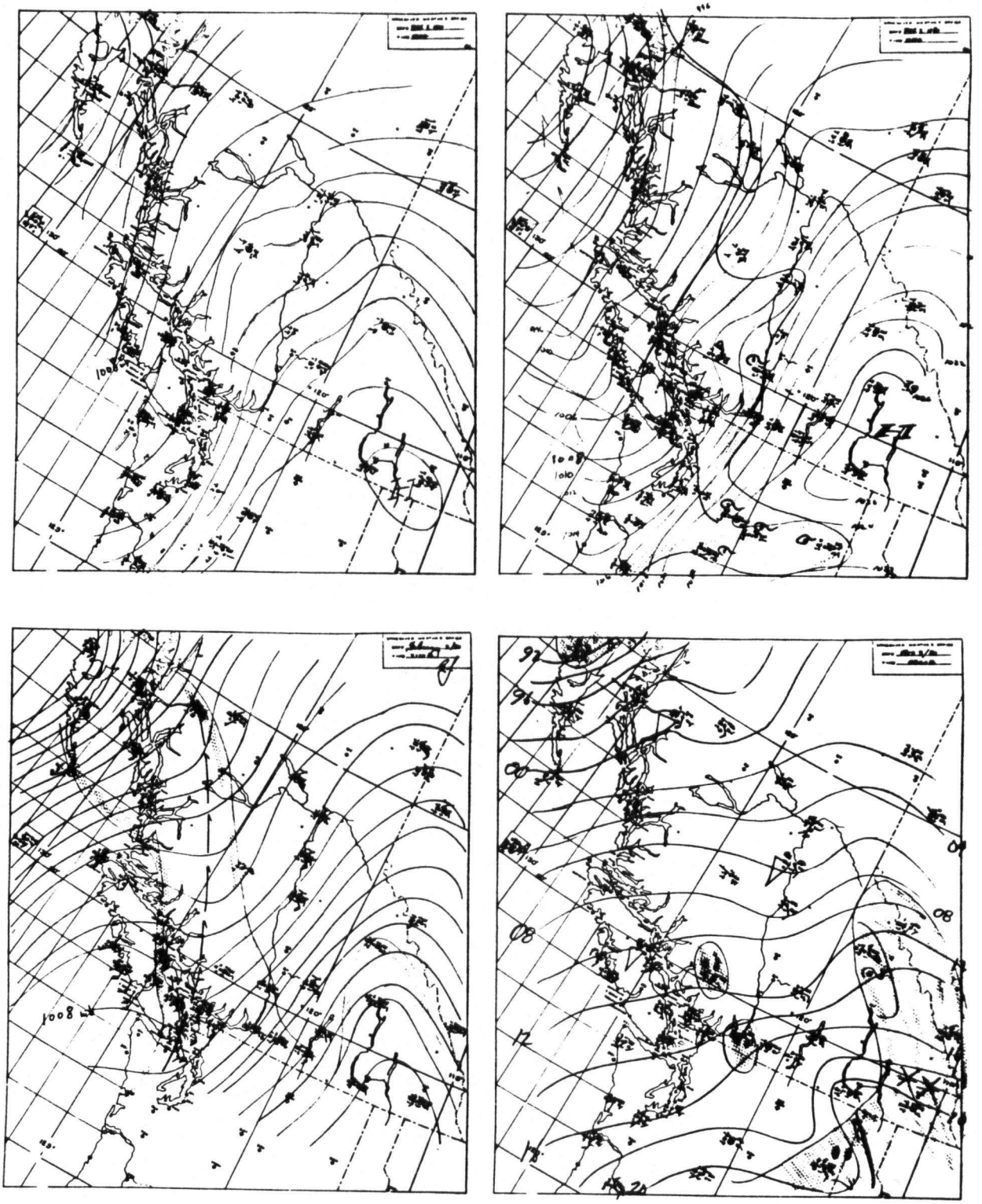

Figure 132 Barometric maps (2).
Upper-left: Feb. 2 0900.
Upper-right: Feb. 2 1500.
Lower-left: Feb. 2 2100.
Lower-right: Feb. 3 0200.

between the travelling atmospheric pressure disturbance and the generated water waves, and then how the generated water waves excited seiches in the coastal bays.

In the case of wave propagation in x-direction, a forced wave $\eta(x-vt)$ with phase velocity v could be generated by a traveling atmospheric pressure disturbance with the velocity v of the form $\eta^*(x-vt)$. If η is the water surface elevation relative to mean sea level, then $\eta^*=-p/(\rho \cdot g)$ represents the barometric response, where p is the atmospheric pressure deviation at sea surface, g the gravity acceleration and ρ the mean density of sea water. Then η is given by $\eta=\eta^*/(1-v^2/c^2)$ where c is the phase speed of shallow water waves (Proudman, 1953). For example, if $c\simeq120$ km/hr. and $v\simeq100$ km/hr., $c > v$, the water wave travels in phase with the pressure disturbance. The surface elevation is amplified by $\eta/\eta^*\simeq3.3$. When v approaches c, the resonance will generate large amplitude propagating waves. A singularity v=c indicates a maximum amplification. Taking $v=80\sim120$ km/hr, i.e. $v=22\sim33$ m/s, if $v=c=\sqrt{gh}$, we have $h\simeq50\sim110$ m. Therefore for the occurrence of Proudman resonance the depths from 50 to 110 m are needed. These depths can be found in front of those coastal bays. The speed of the pressure disturbance changes within some range, and the speed of shallow water waves changes due to water depth in different regions. The averaged c and v were close enough to make sure this resonance would probably happen.

The calculated dispersion relation of edge waves in Juan de Fuca Strait shows that the water waves with period 10 to 40 minutes have speed about 120 to 170 km/hr., which is comparable to the speed of the barometric front. In the vicinity of resonant condition v=c, we have to treat the problem as an initial value problem, in which the amplitude of the water waves increase linearly with time t. Thus edge waves along the Strait may be generated by the transient forcing of the impulsive pressure disturbance, then excite the seiches inside the bays.

In contrast for the case of a pure forced wave, the maximum elevation $\Delta\eta$ of water level appears in the front part of the forcing region, and is given by

$$\Delta\eta=-(\Delta\eta^*/L)\cdot x/2$$

where x is the distance travelled by the front, L is the distance from the pressure maximum to the front (Hibiya and Kajiura, 1983). It is noted that $\Delta\eta$ is proportional to x and inversely proportional to L. So the high pressure gradient and long distance travelled by the pressure disturbance could excite large amplitude forced water waves. This situation can be found on the barometric maps of Feb. 2.

E. CONCLUSION

After examining every possibility of seiche-exciting sources, we may approach our preliminary conclusion.

Edge waves in Juan de Fuca Strait are the major source of seiches in these three bays. The study of coherences and

phases reveals the phase speed of the exciting source with different periods, which agrees very well with the computed speed of edge waves in the Strait.

The strongest seiches on Feb. 2 may be explained by Proudman resonance of the observed traveling atmospheric pressure wave. The pressure wave may have generated long waves in Juan de Fuca Strait. When these waves passed by the mouths of the coastal bays, the seiches were excited at the resonant frequencies of the corresponding bays. Looking back to Figures 96 to 98 we may find that oscillations in Becher Bay and Port San Juan were correlated at different frequencies, which supports the hypothesis that these oscillations were excited by waves with wide range of periods traveling in the Strait. The oscillations of Pedder Bay showed poor coherences with those of other two bays, the strong seiches in Pedder Bay may not be generated by the same traveling waves, but by same barometric disturbance through Proudman resonance.

As for the exciting source of seiches of Jan. 20, it is fairly obvious that those seiches were not related to seismic activity or wind and barometric pressure, as shown by the available data. Figure 95 shows that oscillations of Becher Bay and Port San Juan were correlated at low frequency band. A possible candidate is waves (surface or internal) propagating from the ocean, traveling into the Strait and exciting the seiches in the bays.

Tide-induced internal waves may play the leading role in the generation of these seiches. This hypothesis may explain the fortnight pattern of strong seiches observed on January 20 and February 2. The satellite image shows that internal waves reach only the mouth of Juan de Fuca Strait, which may explain why Port San Juan always possessed more wave energy. Unfortunately the necessary data of displacement of isopycnals are unavailable, we could not reach our conclusion through an analysis of tidal data whose duration was not greatly longer than a lunar month.

The swell data of Tofino were obviously correlated with the high frequency oscillations of Port San Juan, they contributed power to spectra through aliasing.

Internal waves and edge waves damped when they travelled to the east end of Juan de Fuca Strait, and winds were generally strong in the vicinity of Port San Juan, that is why oscillations in Port San Juan possessed more energy.

BIBLIOGRAPHY

Abramowitz,M. and Stegun,I.E., 1970. **Handbook of mathematical functions.** *7th ed., Dover, New York, N.Y. 1046p.*

Akamatsu,Hideo, 1982. **Seiche in Nagasaki Bay.** *Pap.Met.Geophys., Tokyo, 33(2):95-115. (In Japanese)*

Apel,J.R., Holbrook,J.R. and Tsai,J., 1980. **The Sulu Sea internal soliton experiment, part A: background and overview (abs.).** *EOS, Trans.Am.Geophy.Un., 61,1009, 1980.*

Ball,F.K., 1967. **Edge waves in an ocean of finite depth.** *Deep-sea Res. 14:79-88.*

Barber,F.G. and Taylor,J., 1977. **A note on free oscillation of Chedabucto Bay.** *Manuscript report series No.47, Published by Fisheries and Environment Canada, Ottawa, Ont..*

Bendat,J.S. and Piersol,A.G., 1971. **Ramdom Data: Analysis and Measurement Procedure.** *New York, Wiley-Interscience; 407 pps.*

Ben-Menahem,A. and Vered,M. 1982. **Seiches in the eastern Mediterranean at Haifa Bay(Israel).** *Boll.Geofis.teor.appl., 24(93):17-29.*

Bergsten,F., 1926. **The seiche of Lake Vättern.** *Geogr.Ann., Stockh. 8: nos.1,2.*

Blackford,R.L., 1978. **On the generation of internal waves over a sill — a possible non-linear mechanism.** *Journal of Marine Research 36:529-549.*

Bloomfield,Peter, 1976. **Fourier analysis of time series: an introduction.** *Jhon Wiley & Sons.*

Bowers,E.C., 1977. **Harbour resonance due to set-down beneath wave groups.** *J.Fluid Mech.(1977), Vol.79, part 1, pp.71-92.*

Chang, Phillip Yit Kuen, 1976. **Subsurface currents in the Strait of Georgia, west of Sturgeon Bank.** *Master's Thesis, UBC.*

Clarke,D.J., 1968. **Seiche motions for one-dimensional flow.** *J.Mar.Res., 26:202-207.*

Conte,S.D. and Carl de Boor, 1972. **Elementary Numerical Analysis.** *McGraw-Hill, Inc. pp.153*

Crean,P.B., 1983. **Current Atlas, Juan de Fuca Strait to Strait of Geogia.** *Canadian Government Publishing Center.*

Defant,A., 1961. **Physical Oceanography. Vol.2, part 1, Chap.6.** *Pergamon Press,New York.*

Dyer,K.R., 1982. **Mixing caused by lateral internal seiching within a partially mixed estuary.** *Estuar.coast. Shelf Sci., 15(4):443-457.*

Fair,S. and Michelato,A., 1980. **Surface seiches in the Gulf of Cagliari (south Sardinia).** *Boll.Geofis.teor.appl., 22(85):69-80.*

Garrett,C., 1975. **Tides in gulfs.** *Deep-Sea Research, 1975, Vol.22, pp.23-35.*

Giese,G.S., Hollander,R.B., Fancher,J.E. and Giese,B.S., 1982. **Evidence of coastal seiche excitation by tide-generated internal solitary waves.** *Geophysical Reseach Letters, Dec. 1982, Vol.9, No.12, pp.1305-1308.*

Godin,G., 1972. **The analysis of tides.** *University of Toronto Press, 1972.*

Gotlib,V.Iu and B.A.Kagan, 1980. **Resonance periods of the World Ocean.** *Dokl.Nauk SSSR, 252(3):725-728. (In Russian)*

Groves,G.W. and Hannan,E.J., 1968.**Time series regression of sea level on weather.** *Rev.Geophys., 6:129-174.*

Heaps,N.S. and Ramsbottom,A.E., 1966. **Wind effects on the water in a narrow two-layered lake.** *Philos.Trans.R.Soc.Lond., A, 259:391-430.*

Hibiya,Toshiyuki and Kinjiro Kajiura, 1982. **Origin of the Abiki phenomenon (a kind of seiche) in Nagasaki Bay.** *J. oceanogr. Soc. Japan, 38(3): 172-182.*

Hwang,L.S. and Tuck,E.O., 1970. **On the oscillations of harbours of arbitrary shape.** *J. Fluid Mech. Vol. 42, part 3, pp. 447-464.*

Isozaki,Ichiro, 1979. **On the seiches of Habu-harbor (Oshima Island, Japan).** *Oceanogrl Mag., 30(1/2): 31-46.*

Jamart,B.M. and Winter,D.F., 1978. **A new approach to the computation of tidal motions in estuaries.** *In J. Nihoul [ed.] Hydrodynamics of estuaries and fjords, Elsevier, Amsterdam, 546p.*

Jenkins,G.M. and Watts D.G., 1968. **Spectral Analysis and Its Application.** *Holden-Day, Inc. San Francisco, Calif..*

Johns,B. and Hamzah,A.M., 1969. **On the seiche motion.** *Proc. Camb. Phil. Soc. (1969), 66, 607.*

Kosuge, Susumu and Akira Saito, 1981. **A study of harbor oscillations in Shimizu Harbor (Japan).** *J. Fac. mar. Sci. Technol., Tokai Univ., 14: 275-286 (In Japanese).*

Lanyon,J.A., Eliot,I.G. and Clarke,D.J., 1982. **Observations of shelf waves and bay seiches from tidal and beach groundwater-level records.** *Mar. Geol.,*

49(1/2): 23-42.

LeBlond,P.H. and Mysak,L.A., 1978. **Waves in the Ocean.** *Elsevier Scientific Publishing Company, 1978.*

Lee,J.J., 1971. **Wave-induced oscillation in harbours of arbitrary geometry.** *J.Fluid Mech. Vol.45, part2, pp.375-394.*

Lemon,D.D., 1975.**Seiche excitation in a coastal bay by edge waves travelling on the continental shelf.** *Master's thesis, University of British Columbia.*

Lemon,D.D., LeBlond,P.H. and Osborn,T.R., 1979. **Seiche excitation in Port San Juan, British Columbia.** *J. Fish. Res. Bd Can., 36(10): 1223-1227.*

Matuzawa, T., K.Kanbara and T. Minakami, 1933. **Horizontal movement of water in the tsunami of March 3, 1933.** *Jan. J. Astr. Geophys., 11, No.1, 1933.*

Mattioli,F and Tinti,S., 1978. **Wave-induced oscillations in large-mouthed harbours.** *Nuovo Cim., (C)1(1): 18-30.*

Mattioli,F and Tinti,S., 1979. **Discretization of the harbour resonance problem.** *J.Wat Way Port coast.Ocean Div., Am.Soc.civ.Engrs, 105(WW4): 464-469.*

Miles,J. and Munk,W., 1961. **Harbour paradox.** *Journal of the Waterways and Harbour Division, August 1961,*

pp. 111-130.

Miles,J.W., 1971. **Resonant response of harbours: an equivalent-circuit analysis.** *J.Fluid Mech. (1971), Vol.46, part 2, pp.241-165.*

Miles,J.W., 1974. **Harbour seiching.** *An. Review Fluid Mech., 6, 17-35, 1974.*

Miles,J.W., 1981. **Nonlinear Helmholtz oscillations in harbours and coupled basins.** *J.Fluid Mech. (1981), Vol.104, pp.407-418.*

Munk,W.H., 1962. **The Sea.** *Interscience Publ.1, New York*

Nakamura, Shigehisa and Shigeatsu Serizawa, 1983. **Shelf-seiches off Susami,southern Japan.** *Mer, Tokyo, 21(2):89-94 (In Japanese).*

Noiseux,C.F., 1983. **Resonance in open harbours.** *J.Fluid Mech. (1983), Vol.126, pp.219-135.*

Odamaki,Minoru, Yuko Yano and Kiyoshi Nitta, 1983. **'Abiki' the large seiche on the west coast of Kyusyu (Japan).** *Rept hydrogr.Res.,Tokyo,18:83-103 (In Japanese). Maritime Safety Agency, Tokyo, Japan.*

Olsen K. and Hwang L.S., 1971. **Oscillations in a Bay of Arbitrary Shape and Variable Depth.** *J.Geop.Res., Vol.76, No.21, 5048-5064,*

Orlić,M., 1980. **About a possible occurrence of the Proudman**

resonance in the Adriatic. *Thalassia Jugosl., 16(1):79-88.*

Papa,Lorenzo, 1981. **A numerical and statistical investigation of a seiche oscillation of the Ligurian Sea.** *Dt.hydrogr.Z., 34(1):15-25.*

Papa,Lorenzo, 1983. **A numerical computation of a seiche oscillation of the Ligurian Sea.** *Geophys.J.R.astr.Soc., (1983) 75, 659-667.*

Petrusevics,P., H.Allison and B.Carbon, 1979. **Seiches on the western Australian inner continental shelf.** *Search, 10(11):399-400.*

Pierini,S., 1981. **Tides and Seiches in Gulfs.** *IL NUOVO CIMENTO, Vol.4C, N.4, pp.458-470.*

Platzman,G.W., 1975. **Normal Modes of the Atlantic and Indian Ocean.** *Journal of Physical Oceanography, Vol.5, No.2:201-221.*

Pond, S. and Pickard,G.L. (1983). **Introductary Dynamical Oceanography.** *Pergamon Press.*

Proudman,J., 1953. **Dynamical oceanography.** *Methuen, London, 409p.*

Rao,D.B., 1966. **Free gravitational oscillations in rotating rectangular basins.** *J.Fluid Mech., 25:523-555.*

Roache,P.J., 1976. **Computational Fluid Dynamics.** *Hermosa*

Publishers, 1976. pp.195.

Stigebrandt,A., 1976. **Vertical diffusion driven by internal waves in a sill fjord.** *Journal of Physical Oceanography 6, 634-649.*

Sündermann,J., 1966. **Ein Vergleich zwischen der analytischen und der numerischen Berechnung winderzeugter Strömungen und Wasserstände in einem Modellmeer mit Anwendungen auf die Nordsee.** *Mitt. Inst. Meeresk. Univ. Hamburg. Nr.4, pp.77.*

Thomson,R.E. and Chow,K.Y., 1980. **Butterworth and Lanczos-window cosine digital filters: with application to data processing on the UNIVAC 1106 computer.** *Pacific Marine Science Report 80-9.*

Thomson,R.E., 1981. **Oceanography of the British Columbia coast.** *Ottawa , Ont. : Canada Dept. of Fisheries and Oceans, c1981.*

Ulrych,T.J. and Bishop,T.N., 1975. **Maximum entropy spectral analysis and autoregressive decomposition.** *Rev.Geophys. and Space Phys. 13(1):183-200.*

Waddell,E., 1976. **Swash-groundwater-beach profile interactions.** *In: R.A.Davies and R.L.Elhington (Editor), Beach and Nearshore Sedimentation. Soc.Econ.Palaeontol.Mineral., pp.115-125.*

Werner,F.E. and Hickey,B.M. (1982). **The Role of a Longshore Gradient in Pacific Northwest Coastal Dynamics.** *Journal of Physical Oceanography, March 1983.*

Wübber,Ch. and Krauss,W., 1979. **The two-dimensional seiches of the Baltic Sea.** *Oceanol. Acta, 2(4): 435-446.*